



UNIVERSITY OF
BIRMINGHAM

Design and Development of Rotating Membrane Emulsification for Production of Particle-stabilised Emulsions

By

Panagiotis Gerasimos Arkoumanis

A thesis submitted to
the University of Birmingham
for the degree of
DOCTOR OF PHILOSOPHY

School of Chemical Engineering
College of Engineering and Physical Sciences
University of Birmingham
May 2019

UNIVERSITY OF
BIRMINGHAM

University of Birmingham Research Archive

e-theses repository

This unpublished thesis/dissertation is copyright of the author and/or third parties. The intellectual property rights of the author or third parties in respect of this work are as defined by The Copyright Designs and Patents Act 1988 or as modified by any successor legislation.

Any use made of information contained in this thesis/dissertation must be in accordance with that legislation and must be properly acknowledged. Further distribution or reproduction in any format is prohibited without the permission of the copyright holder.

Abstract

Emulsions and emulsion-based systems constitute a great proportion of many consumer products; from milk, spreads and sauces to hand creams and paints. Current emulsification methods such as high shear mixing, colloid milling or high-pressure homogenisation are based on the dissipation of high amounts of energy to randomly disrupt emulsion droplets resulting in an emulsion product with a non-uniform microstructure that could be subject to destabilisation. Membrane emulsification has emerged as a promising, low-energy technique to manufacture emulsion droplets one at a time in a controlled manner. This is possible by introducing the dispersed phase through the pores of a membrane in the continuous phase and adjusting the transmembrane pressure and shear close to the membrane surface. Despite the positive performance of membrane emulsification on the stabilisation of conventional emulsions with emulsifiers, fabrication of stable Pickering (i.e. colloidal particle-stabilised) emulsions through this technique is restricted by the poor mixing environment in the continuous phase and the limited diffusivity and interfacial tension lowering capacity of the colloidal species.

This thesis advances the knowledge on the droplet formation mechanisms and the process limitations encountered during the production of Pickering emulsions via a rotating membrane emulsification set-up, and linking these with the stability of the subsequent emulsions produced. Extending this knowledge, particles that demonstrate poor Pickering performance are combined with a surfactant (Tween 20) or dairy protein (WPI) to exploit their synergism towards effective particle-stabilisation of emulsions. Apart from membrane rotational velocity and transmembrane pressure, the membrane properties (material and pore size/ porosity) are expected to have a profound effect on operational attributes; thus oil

throughput and energy consumption have been studied to assess the overall performance of rotating membrane emulsification towards manufacturing of stable 'Pickering' type emulsions.

To my family (Mum, Dad, Fotini, Marilia)

and to Nina

Acknowledgements

Since the journey of my PhD has come to an end, I would like to take this opportunity to thank the people who supported me and made this dissertation possible.

First and foremost, I would like to thank my supervisor Dr Fotis Spyropoulos for his continuous guidance and support all those years and for his dedication to our project. His professionalism and enthusiasm for our research field inspired me and certainly made me a better scientist. I would also like to express my sincere gratitude to him for believing in me and giving me this fantastic opportunity to conduct a PhD as a member of his team.

Besides my supervisor, I am thankful to Prof. Ian Norton for our discussions and his insightful feedback that helped me acquire a multi-facet understanding of my project.

I extend my gratitude to all the members of the Microstructure group who not only supported my work during my time at the University of Birmingham but also created a friendly atmosphere for me. I also couldn't forget my master students who contributed with their work to my project, but most importantly, they trusted me for the completion of their research projects.

I gratefully acknowledge the School of Chemical Engineering, the Engineering and Physical Sciences Research Council (EPSRC) and the Centre for Innovative Manufacturing in Food for their financial support that enabled me to pursue my PhD and enhance my skill set by taking part in multiple conferences and training opportunities.

A big thank you to the postgraduate administration team of the School of Chemical Engineering and especially to Lynn Draper for her kind support and encouragement. Not to

forget the contribution of the Chemical Engineering workshop technicians (Bob, Dave) and the effort they put in assembling and machining the membranes.

Last but not least, I would like to thank my parents, my sister and all my friends who believed in me and supported me all those years, without them this thesis would not have been completed.

A special thank you goes to my partner Nina; you have been my inspiration and my motivation, next to me at the hardest part of this journey; I could not do this without you.

Table of Contents

1. Introduction	1
1.1. Background and motivation	2
1.2. Aims and objectives	5
1.3. Thesis layout	6
1.4. Dissemination of research	7
2. Literature review	9
2.1. Emulsions and (in)stability	10
2.2. Emulsifiers	12
2.2.1. Surfactants	13
2.2.2. Biopolymers	14
2.3. Colloidal particles	16
2.3.1. Pickering stabilisation	17
2.3.2. Stability conferred by colloidal particles	19
2.3.3. Edible colloidal particles	20
2.3.4. Combination of colloidal particles and emulsifiers	24
2.3.4.1. Silica particles as co-stabilisers	24
2.3.4.2. HPMC particles as co-stabilisers	27
2.4. Emulsification	29
2.4.1. High-energy methods	30
2.4.2. Low-energy methods	35
2.4.3. Emulsification efficiency	37
2.5. Membrane emulsification	40
2.5.1. Membrane technology for emulsion production	41
2.5.2. Membrane emulsification set-ups	45
2.5.2.1. Moving continuous phase	47
2.5.2.2. Moving membrane	48
2.5.3. Factors influencing emulsion microstructure in DME	53
3. Materials and Methods	62
3.1. Materials	63
3.2. Methods	63
3.2.1. Preparation of continuous phase	63
3.2.1.1. Particle suspensions	63
3.2.1.2. Solutions of emulsifiers	64
3.2.1.3. Particle-emulsifier mixtures	64

3.2.2.	Emulsification.....	65
3.2.2.1.	Rotating Membrane Emulsification (RME)	66
3.2.2.2.	High Shear Mixer (HSM)	67
3.2.3.	Analytical techniques	68
3.2.3.1.	Particle and emulsion droplet size measurement.....	68
3.2.3.2.	Zeta-potential measurements	69
3.2.4.	Microstructure visualisation	70
3.2.5.	Viscosity measurements	71
3.2.6.	Dispersed phase rate and flux measurements	71
3.2.7.	Energy consumption measurements	72
4.	Surfactant-free Pickering emulsions produced via rotating membrane emulsification	74
4.1.	<i>Introduction</i>	76
4.2.	<i>Results and discussion</i>	77
4.2.1.	Aqueous particle suspension behaviour	77
4.2.1.1.	Effect of the pH environment	77
4.2.1.2.	Effect of shear on the viscosity of aqueous particle suspensions	81
4.2.2.	Pickering emulsions.....	86
4.2.2.1.	Formulation effects	86
4.2.2.2.	Processing effects	105
4.3.	<i>Conclusions</i>	118
5.	Pickering particle and emulsifier co-stabilised emulsions produced via rotating membrane emulsification.....	120
5.1.	<i>Introduction</i>	122
5.2.	<i>Results and discussion</i>	125
5.2.1.	Particle and mixed particle-emulsifier aqueous suspensions	125
5.2.1.1.	Effect of Tween 20	126
5.2.1.2.	Effect of WPI.....	130
5.2.2.	Co-stabilised Pickering emulsions.....	133
5.2.2.1.	Effect of Tween 20	133
5.2.2.2.	Effect of WPI.....	143
5.3.	<i>Conclusions</i>	148
6.	Processing performance of rotating membrane emulsification for production of emulsions co-stabilised by Pickering particles and emulsifiers.....	150
6.1.	<i>Introduction</i>	152
6.2.	<i>Results and discussion</i>	155
6.2.1.	Formulation effects on membrane fouling and performance	155

6.2.2.	Effect of transmembrane pressure	159
6.2.3.	Effect of membrane	168
6.2.4.	Process efficiency	174
6.3.	<i>Conclusions</i>	182
7.	Conclusions and recommendations for future work	184
7.1.	<i>Overall Conclusions</i>	185
7.2.	<i>Future Outlook</i>	192
	Supplementary data to Chapter 4	197
	Supplementary data to Chapter 5	204
	Supplementary data to Chapter 6	207

List of Figures

Fig. 2.1: Schematic representation of O/W emulsion destabilisation mechanisms (adapted from [32]).	12
Fig. 2.2: Schematic representation of colloidal particles adsorbed at a planar oil-water interface for different contact angles measured through the water phase (top). Positioning of particles at the curved oil-water interface of O/W ($\theta_w < 90^\circ$) and W/O ($\theta_w > 90^\circ$) emulsions (bottom). Adapted from [1].	18
Fig. 2.3: Chemical structures of cellulose (A), hydroxypropyl methyl cellulose (B) and rutin hydrate (C) (adopted by supplier's MSDS documentation).	21
Fig. 2.4: Schematic representation of high-energy emulsification devices and indicated droplet disruption mechanism. (A) high-shear mixer, (B) colloid mill, (C) ultrasonic probe, (D) high-pressure homogeniser, (E) microfluidizer. Adapted from [31].	31
Fig. 2.5: Schematic representation of the main low-energy emulsification methods. (A - B) microfluidic emulsification, (C) phase inversion temperature, (D) spontaneous emulsification, (E) phase inversion composition. Adapted from [31].	36
Fig. 2.6: Droplet size as function of energy density for several emulsification devices. Blue: low-energy methods, Red: high-energy methods. Adapted from [6, 91, 115].	39
Fig. 2.7: Schematic representation of the type of emulsions produced in membrane emulsification depending on the contact angle (θ) (through the water phase) formed between the membrane and the immiscible phases: (a) for hydrophilic membranes the contact angle favour formation of O/W emulsions and (b) hydrophobic membranes ($\theta > 90^\circ$) are ideal for W/O emulsion. Adapted from [127].	42
Fig. 2.8: (A-B) SEM and XMT micrographs from surface and cross-section of SPG [130], (C) SEM micrograph of cross-section of ceramic membrane [135], (D) SEM micrograph of polycarbonate membrane [136], (E) optical micrograph of laser-drilled stainless steel membrane [137], (F) optical micrograph of nickel microsieve [137].	44
Fig. 2.9: Schematic representation of membrane emulsification configurations.	46
Fig. 2.10: Factors influencing emulsion microstructure as delivered by membrane emulsification.	53
Fig. 2.11: Simplified schematic representation of forces applied on a droplet during RME. The viscous tangential drag force (F_D) points towards the paper surface.	57

Fig. 3.1: Schematic representation of rotating membrane emulsification set-up.	66
Fig. 4.1: Z-potential and particle size as a function of pH for silica (Native pH: 10), HPMC (Native pH: 6.2), Rutin (Native pH: 5.1) and CMCC (Native pH: 5.9) at a particle concentration of 1.5 wt.%, as measured by DLS. Each data point represents an average of a triplicate of measurements and error bars represent one standard deviation. Where not visible, error bars are smaller than the symbols.	79
Fig. 4.2: Apparent viscosity of suspensions as function of the shear rate for different types of particles at concentration 1.5 wt. % at 20 °C. Silica was at pH 2 and the rest particle suspensions at their native pH. Each line represents a power law fit with parameters given in Table 4.2. Each data point represents the average of a triplicate of measurements and error bars represent one standard deviation.	83
Fig. 4.3: Average droplet size and span values of fresh emulsions stabilised with a range of particles at concentration 1.5 wt. %. An SPG 6.1 µm membrane was used at 10 kPa and 2000 rpm. Symbols represent the average of a triplicate of measurements and error bars represent one standard deviation.	87
Fig. 4.4: Correlation between critical concentration (C_{cr}) as calculated by Eq. (4.3) and concentration of a range of particles in fresh emulsions. Calculations are shown in Appendix A. All emulsions were 110 g and contained 10 wt. % oil, prepared with a 6.1 µm SPG membrane at 10 kPa and 2000 rpm.	96
Fig. 4.5: Droplet size distribution of emulsions stabilised with different concentrations of HPMC and pictures of emulsions after standing for 2 hours, prepared with different concentrations of (A) HPMC and (B) CMCC at native pH. All emulsions were 10 wt. % oil made with a 6.1 µm SPG membrane at 10 kPa and 2000 rpm.	99
Fig. 4.6: Average droplet size and span values of emulsion droplets stabilised with silica particles as function of concentration, and subsequent stability over 21 days. A 6.1 µm SPG membrane was used at 10 kPa transmembrane pressure and a rotational velocity of 2000 rpm. Photos and micrographs were captured within 24h following emulsification.	101
Fig. 4.7: Average droplet size and span values of emulsions stabilised with rutin as function of concentration, and subsequent stability over 21 days. A 6.1 µm SPG membrane was used at 50 kPa transmembrane pressure and a rotational velocity of 2000 rpm.	103
Fig. 4.8: A. Rutin stabilised emulsions after standing for 2 hours at room temperature and B. 3D AFM captured image of oil droplet surface in emulsion stabilised with 1.5% Rutin	

particles. All emulsions were 10 wt. % oil made with a 6.1 μm SPG membrane at 50 kPa and 2000 rpm.....	104
Fig. 4.9: Average droplet size and span values of emulsions as function of the transmembrane pressure stabilised with 1.5 wt.% Silica (A & C) and 1.5 wt.% rutin (B & D). An SPG 6.1 μm membrane was used at 2000 rpm.	111
Fig. 4.10: Average droplet size (top) and span (bottom) of emulsions as function of rotational velocity stabilised with 1.5 wt.% particles. An SPG 6.1 μm membrane was used at 50 kPa transmembrane pressure.	114
Fig. 4.11: Rate of oil added in the continuous phase during production of emulsions stabilised with (A) 1.5 wt.% silica and (B) 1.5 wt.% rutin particles using an SPG 6.1 μm membrane at different rotating velocities at constant transmembrane pressure 50 kPa.	117
Fig. 5.1: (A) Aqueous suspensions of 3 wt.% silica particles alone, mixed with 0.05 wt.% and 3 wt.% Tween 20, 1 day after preparation, all at pH 2. (B) Schematic of the top and bottom layers of the aqueous mixtures.	128
Fig. 5.2: Particle size of aqueous suspensions of 3 wt.% silica particles mixed with Tween 20 at pH 2.	128
Fig. 5.3: Schematic representation of aqueous suspensions of 3 wt.% HPMC particles mixed with 0.05 wt.% (left) and 3 wt.% Tween 20 (right), at pH=6.5.	129
Fig. 5.4: Schematic representation of aqueous suspensions of WPI mixed with (A) silica at pH=2 and (B) HPMC particles at pH=6.5.	132
Fig. 5.5: Average droplet diameter and span values of emulsions stabilised with a fixed concentration of 3 wt.% silica and its mixtures with Tween 20 at pH 2. For co-stabilised emulsions, the average values account for droplets from all layers (see Fig. 6). An SPG 6.1 μm membrane was used at 10 kPa and 2000 rpm.	135
Fig. 5.6: Droplet size distribution of emulsion co-stabilised with 3 wt.% silica and 3 wt.% Tween 20 at pH 2 after 1 day. Micrographs were taken from the cream and the sediment layer of the emulsion. The scale is 50 μm in all cases.....	137
Fig. 5.7: Cryo-SEM micrographs of emulsion droplets stabilised by 3 wt.% silica alone with a close-up of the droplet surface (A-B), 3 wt.% Tween 20 alone (C), 3 wt.% silica mixed with 0.05 wt. % Tween 20 top and bottom layer (D-E), 3 wt.% silica mixed with 3 wt.% Tween 20 top and bottom layer (F-G). All emulsions were produced by an SPG 6.1 μm at 10 kPa and 2000 rpm. All pictures were taken 3 days following emulsification.....	138

Fig. 5.8: Average droplet diameter and span values of emulsions stabilised with 3 wt.% HPMC and its mixtures with Tween 20 at pH 6.5. An SPG 6.1 µm membrane was used at 10 kPa and 2000 rpm.	141
Fig. 5.9: Cryo-SEM micrographs of emulsion droplets stabilised by 3 wt.% HPMC mixed with (A-B) 0.05 wt.% Tween 20, (C-D) 3 wt.% Tween with a close-up of the aqueous phase gel network. All emulsions were produced by an SPG 6.1 µm at 10 kPa and 2000 rpm.	143
Fig. 5.10: Average droplet diameter and span values of emulsions stabilised with 3 wt.% silica and its mixtures with WPI at pH 2. An SPG 6.1 µm membrane was used at 10 kPa and 2000 rpm.	145
Fig. 5.11: Average droplet diameter and span values of emulsions stabilised with 3 wt.% HPMC and its mixtures with WPI at pH 6.5. An SPG 6.1 µm membrane was used at 10 kPa and 2000 rpm.	147
Fig. 6.1: Average oil flux of emulsions prepared with an SPG 6.1 µm membrane at constant transmembrane pressure 10 kPa and constant rotational velocity 2000 rpm. The dashed line represents the oil flux achieved at the same set-up for 1 wt.% Tween 20.	157
Fig. 6.2: Influence of transmembrane pressure on the oil flux through a 6.1 µm SPG membrane used at a constant rotational velocity of 2000 rpm to produce co-stabilised emulsions. Each line represents a power law fit ($y = a x^b$) with parameters given next to the legend.	160
Fig. 6.3: Effect of transmembrane pressure on average droplet diameter and span values of emulsions stabilised with 3 wt. % silica, 0.05 wt.% Tween 20 and both species at pH 2. An SPG 6.1 µm membrane was used at 2000 rpm.	163
Fig. 6.4: Effect of transmembrane pressure on average droplet diameter and span values of emulsions stabilised with 3 wt.% HPMC, 0.05 wt.% Tween 20 and both species at pH 6.5. An SPG 6.1 µm membrane was used at 2000 rpm.	166
Fig. 6.5: Particle size distribution and average span values of fresh emulsions co-stabilised by 3 wt.% silica and WPI at pH 2, produced with an SPG 6 µm and a Stainless Steel (SS) 50 µm membrane at constant transmembrane pressure of 50 kPa and constant rotational velocity of 2000 rpm.	170
Fig. 6.6: (A) Rate of oil added in the continuous phase at pH 2 and (B) number of droplets generated during production of co-stabilised emulsions (10 wt.% oil) by a Shirasu Porous	

Glass (SPG) and a Stainless Steel (SS) membrane at a constant transmembrane pressure of 50 kPa and constant rotational velocity of 2000 rpm.	172
Fig. 6.7: Effect of shear rate on the average droplet diameter of emulsions co-stabilised with 3 wt.% silica mixed and 0.05 wt.% Tween 20 at pH 2, prepared with HSM at different processing times.	176
Fig. 6.8: Droplet size (top) and span (bottom) as a function of energy density and production rate, for emulsions co-stabilised by 3 wt.% silica particles produced by RME equipped with an SPG 6.1 μm membrane at 2000 rpm, and HSM at 7000 rpm. All emulsions contained 10 wt.% oil at production rates between 0.1 and 11 kg h^{-1} . Symbols with red border indicate an unstable emulsion.	179
Fig. 6.9: Droplet size (top) and span (bottom) as a function of energy density and production rate, for co-stabilised emulsions produced by RME equipped with an SPG 6.1 μm membrane at 2000 rpm, and HSM at 7000 rpm. All emulsions contained 10 wt.% oil at production rates between 0.1 and 11 kg h^{-1}	181

List of Tables

Table 2.1: Overview of types of emulsions produced via rotating membrane emulsification.	51
Table 3.1: Composition of continuous phase and their abbreviations used in Chapters 5 & 6. Concentration of all particles was 3 wt.% in all cases. Concentrations are in wt.%: weight of individual species over the weight of the final emulsion.	65
Table 3.2: Specifications of membranes used in this study. The porosity of SPG membrane has been estimated by [130] and of SS is calculated in Appendix C.	67
Table 3.3: Operating conditions and shear rate values for all emulsification systems.....	68
Table 4.1: Average particle size D32, and span of 1.5 wt.% particle suspensions at native pH and at the Isoelectric Point (IEP).....	80
Table 4.2: Effect of concentration on the apparent viscosity of a range of particle suspensions at constant temperature 20°C. The consistency (A) and power law index (n) values are listed for each flow curve fitted to the power law model. Flow curves for all concentrations are presented in Appendix A.1.	85
Table 4.3: Average droplet diameter (D43) of emulsions stabilised with 1.5 wt. % particle suspensions prepared at native pH and IEP. A 6.1 µm membrane was used at 10 kPa and 2000 rpm. Emulsions that presented phase separation are indicated as ‘PS’	90
Table 4.4: Particle radius, interfacial tension (Appendix A.2), contact angle, adsorption free energy (calculated by Eq. (2.2) and kinetic energy of a range of particles. Contact angle values have been reported for silica [183, 184], HPMC, Rutin and CMCC [11].	92
Table 4.5: Adsorption and droplet formation time of 1.5 wt.% particles in emulsions made with a SPG 6.1 µm membrane at varied transmembrane pressure and rotational velocity of the membrane.	109
Table 4.6: Rotational velocity, shear rate, viscosity, shear stress and Taylor number (Ta) of silica and rutin suspensions at particle concentration 1.5 wt.%. Viscosity data obtained from Table 4.2.	115
Table 5.1: Z- average size, zeta potential and the corresponding span or polydispersity index (PDI) of aqueous particle suspensions and their mixtures with emulsifiers. Particle concentration was 3 wt.% in all cases. Samples annotated with a star presented more than one peaks and their particle size distribution is presented in Appendix B.....	127

Table 6.1: % change in the average droplet size (D43) of emulsions for a range of transmembrane pressures after storing at room temperature for 3 weeks. The (+) symbol indicates an increase and (-) a reduction in the droplet size. Values annotated with a star (*) refer to emulsions that showed evidence of phase separation and a cross mark (†) indicates the existence of an oil layer without phase separation. PS indicates phase separation of the samples within less than 24 h. 167

Table 6.2: List of species mixed in water to form 10 wt.% O/W emulsions and measured emulsion densities. Concentrations are in wt.%: weight of individual species over the weight of the final emulsion 175

Acronyms and abbreviations

CMCC	Colloidal microcrystalline cellulose
CMC	Critical micelle concentration
DLS	Dynamic light scattering
HLB	Hydrophilic Lipophilic Balance
HMW	High molecular weight
HPMC	Hydroxypropyl methylcellulose
HSM	High shear mixer
IEP	Isoelectric point
LMW	Low molecular weight
ME	Membrane emulsification
O/W	Oil-in-water
O/W/O	Oil-in-water-in-oil
PDI	Polydispersity index
RI	Refractive index
RME	Rotating membrane emulsification
SMLS	Static multi-angle light scattering
W/O/W	Water-in-oil-in-water
WPI	Whey protein isolate

Nomenclature

Symbol	Description	Unit
ΔG	Interfacial free energy	J m^{-3}
ΔA	Interfacial area	m^2
ΔF_{ads}	Adsorption free energy	J
ΔP_L	Laplace pressure	Pa
P_v	Power density	W m^{-3}
F_γ	Interfacial tension force	N
F_c	Centripetal force	N
F_D	Viscous drag force	N
F_{BG}	Buoyancy force	N
F_I	Inertial force	N
F_L	Dynamic lift force	N
F_{SP}	Static pressure force	N
$F_{\text{push-off}}$	Push-off force	N
k_B	Boltzmann constant	J K^{-1}
J_d	Dispersed phase flux	$\text{m}^3 \text{m}^{-2} \text{h}^{-1}$
T	Temperature	K
D_{oil}	Diameter of naked oil droplet	m
D_p	Hydrodynamic diameter of particle	m
r_p	Particle radius	m
V_p	Volume of particle	m^3
V_{oil}	Volume of oil droplet	m^3

V_d	Volume of dispersed phase	m^3
V	Volume of emulsion	m^3
N_{oil}	Number of oil droplets	-
N_p	Number of particles in emulsion	-
$N_{p,1}$	Number of particles for complete monolayer of one oil droplet	-
N_p^*	Number of particles for complete monolayer coverage of all oil droplets	-
A	Consistency	$Pa\ s^{2-n}$
n	Power law index	-
K	Constant	-
C	Particle concentration in emulsion	% w/w
C_{cr}	Critical particle concentration in emulsion	% w/w
m_c	Particle concentration in continuous phase	$kg\ m^{-3}$
M_d	Mass of dispersed phase	kg
M_p	Total mass of particles in the continuous phase	kg
M_e	Mass of emulsion	kg
u	Particle velocity close to membrane surface	$m\ s^{-1}$
u_c	Cross-flow velocity of continuous phase	$m\ s^{-1}$
u_t	Tangential velocity of membrane surface	$m\ s^{-1}$
u_d	Average dispersed phase velocity	$m\ s^{-1}$
k_L	Lift coefficient	-
k_w	Wall correction factor	-
f	Friction factor	-

N	Rotational velocity of membrane	rpm
R_1	Membrane outer radius	m
R_2	Inner radius of vessel	m
t_{ads}	Adsorption time	s
t_p	Processing time	s
t_{drop}	Droplet formation time	s
d_p	Average membrane pore diameter	m
L_p	Membrane thickness	m
L_s	Average membrane pore spacing	
Q_d	Average dispersed phase flow rate pore	$m^3 s^{-1}$
P	Power draw	W
N_{pore}	Number of pores on membrane surface	-
N_a	Number of active pores	-
K_m	Membrane permeability	$m^3 m^{-1}$
A_m	effective membrane surface area	m^2
ΔP_L	Laplace pressure	Pa
ΔP	Transmembrane pressure	Pa
Re_c	Reynolds number for continuous phase	-
Ta	Taylor number for continuous phase	-
Z_D	Average intensity weighted mean diameter	m
Greek letters		
α	Membrane active pore fraction	-
α_n	Cross sectional area of the droplet neck	m^2
γ	Interfacial tension	$N m^{-1}$

$\dot{\gamma}$	Shear rate	s^{-1}
Γ_M	Surface excess concentration	$kg\ m^{-2}$
ε_v	Energy density	$J\ m^{-3}$
$\varepsilon_{v\ \text{spont ME}}$	Energy density in the absence of continuous phase flow	$J\ m^{-3}$
η_c	Viscosity of continuous phase	$Pa\ s$
η_d	Viscosity of dispersed phase	$Pa\ s$
θ	Contact angle	rad
ξ	Mean pore tortuosity	-
ρ_c	Density of continuous phase	$kg\ m^{-3}$
ρ_d	Density of dispersed phase	$kg\ m^{-3}$
ρ_p	Particle mass density	$kg\ m^{-3}$
σ	Standard deviation	
τ_w	Wall shear stress	Pa
φ	Membrane porosity	-
φ_{hp}	hexagonal packing density	-
ω	Angular velocity of membrane surface	$rad\ s^{-1}$

Chapter 1

Introduction

1.1. Background and motivation

Emulsions compose a large proportion of everyday products that are available to consumers; e.g. personal care and cosmetic products (shampoo, toothpaste, lotions), foods (spreads, mayonnaise, margarine) and pharmaceuticals (ointments, creams). These are complex structures, but in essence, they all consist of a liquid phase that is dispersed in the form of immiscible droplets within another external liquid phase. For example, mayonnaise is an oil-in-water emulsion (O/W), and butter is water-in-oil (W/O) emulsion, but the internal phase may also comprise more phases thus multiple emulsions exist either O/W/O or W/O/W.

Due to the thermodynamic incompatibility of both liquid phases, destabilisation is inevitable and these will ultimately separate over time. Phase separation results in alterations to the sensory characteristics of the product; e.g. reduced mouthfeel, loss of flavour or unwanted release of functional ingredients that are undesirable for the consumer.

Emulsifiers have been widely used to delay this process of separation by ‘coating’ the droplet surface and inducing a type of barrier between droplets, thus rendering the emulsion kinetically stable. For similar reason, particulate structures have been utilised to substitute classic emulsifiers in the sense of providing extended stability because they are able to attach strongly at the oil-water interface creating a more robust solid barrier than classic emulsifiers that tend to migrate and deform.

Particle-stabilised emulsions or ‘Pickering’ emulsions have been extensively studied for these unique attributes they offer [1, 2]. Although various types and shapes of particulates can be used as Pickering stabilisers, many of the studies focus on particles with specifically designed surface properties such as chemically modified or inorganic particles which consumers may

not find attractive particularly in a food emulsion, because they are associated with possible side effects [3].

Arguably, because of the increasing awareness of the health risks of artificial ingredients the consumers' preference has shifted towards more "clean label" products with natural ingredients. Naturally occurring particulates could be a viable and sustainable alternative as they are abundant in nature and inexpensive; e.g. cellulose and flavonoids. The question then is 'How to make such emulsions?'

Traditionally, high shear mixers, ultrasound and high-pressure homogenisers or microfluidisers are used to dissipate large amounts of energy to repeatedly break down the emulsion through turbulent mixing into small droplets. However, one of the disadvantages of these methods is that a large proportion of the dissipated energy is lost in the form of heat in the bulk emulsion potentially harming sensitive ingredients and altering the viscosity. Another disadvantage is that the high dissipation of energy and highly turbulent environment may result in violent collisions of droplets that could initiate destabilisation mechanisms. Furthermore, the random droplet breakage favours the formation of non-uniform sized droplets that could be a source of destabilisation through Ostwald ripening.

Alternatively, droplets may be formed utilising a bottom-up approach. The new interfacial area is created from zero and one drop forms at a time enabling the production of uniform droplets with controlled size [4, 5]. For the past 30 years, such novel methods, e.g. microchannels and membrane emulsification have been developed for production of a wide variety of emulsion structures. Those methods are promising especially for multiple emulsions that are sensitive in processing and can be used for controlled delivery of actives. In microchannel emulsification droplets are formed by adjusting the flow rates of the phases

that are introduced by two individual channels into a junction. These techniques have been found to utilise up to 4 orders of magnitude less energy than conventional high energy methods [6]. In direct membrane emulsification, the dispersed phase is injected through the pores of a membrane to the external phase. Droplet characteristics such as drop size and uniformity are controlled by the dispersed phase flux, the magnitude of shear forces and the membrane properties [7]. However, the downside is the low production rate firstly because of the inherent resistance of the narrow capillaries, and secondly because low flux is essential to maintain a uniform drop size [8]. In this thesis, a rotating membrane emulsification (RME) set-up is used where the dispersed phase is pushed through a porous membrane into an external phase. This configuration was developed 12 years ago by Schädler and Windhab and is relatively novel [9]. The balance of forces applying on the droplet during rotation will determine whether the droplet will remain attached to the membrane surface or it will detach and this can be manipulated by adjusting the rotational velocity and the transmembrane pressure.

Given the ability of membrane emulsification to control emulsion microstructure as well as the established capacity of a range of colloidal particles (synthetically or naturally derived) to enhance emulsion stability via high-energy methods [10, 11], the potential to produce stable particle-stabilised emulsions via membrane emulsification seemed promising. However, the low diffusivity and minimal capacity of the colloidal particles to reduce interfacial tension are limiting factors in the effort to stabilise such emulsions, particularly via a low-energy process such as membrane emulsification [12, 13]. A feasible strategy to improve emulsion stability is the combination of particles and emulsifiers. Although this has been widely investigated in high-energy emulsification methods [14], it has only been used once in membrane emulsification and stability of subsequent emulsions was not considered [15]. Furthermore,

sustainable sources of colloidal particles and emulsifiers have never been used in a similar set-up.

Should these challenges are addressed, RME could be a viable alternative to traditional emulsification techniques for the production of extra stable edible Pickering emulsions from sustainable sources. Extending the applicability of this process, more complex structures incorporating sensitive materials such as ‘clean label’ multiple emulsions for targeted delivery of actives or flavours could be fabricated in a controlled manner.

1.2. Aims and objectives

The overall aim of this thesis was to improve the performance of RME for the production of stable edible emulsions of narrow droplet size distribution from sustainable sources utilising less energy than conventional emulsification techniques. The individual aims and objectives are outlined:

- Evaluation of the possibility that colloidal particles of demonstrated Pickering functionality can produce stable Pickering O/W emulsions via RME, by studying the effect of formulation (particle type/ concentration) and process (rotational velocity, transmembrane pressure) on the droplet size and uniformity over time.
- Identification of possible co-stabilisation strategies for the particles that failed to effectively stabilise emulsions alone via RME by combining these with different emulsifiers. Evaluation of the optimum particle/emulsifier type and ratio by studying their effect on the droplet size and uniformity over time.
- Improvement of the RME process performance for the production of stable emulsions co-stabilised by particles and emulsifiers by studying the influence of transmembrane

pressure, membrane (SPG vs Stainless Steel) and fouling on the droplet size and uniformity over time.

- Evaluation of the RME process as an alternative to high-energy methods for production of stable Pickering emulsions; RME was compared with high shear mixing (HSM) in terms of process efficiency (throughput, energy consumption) and emulsion microstructure (droplet size and uniformity).

1.3. Thesis layout

The work presented in this thesis follows the alternative format and it is essentially organised into seven chapters. Three experimental chapters (Chapters 3, 4 and 5), are presented in the form of research papers, each comprising an introductory section, materials and methods, results and discussion and finally the conclusions. A synopsis of all chapters is given below:

- Chapter 1 briefly introduces the context, motivation and challenges addressed in this study setting the aims and objectives of the research.
- Chapter 2 provides the theoretical background on Pickering emulsions and emulsification processes with a special focus and updated literature review on the rotating membrane emulsification process.
- Chapter 3 discusses the methods and materials used to carry out experimental work. Fundamentals of microstructure characterisation and relevant equations are described.
- Chapter 4 investigates the potential of a range of commercially available colloidal particles to stabilise Pickering emulsions through RME. The effect of formulation (particle type and concentration) and processing conditions (rotational velocity, transmembrane pressure) on the emulsion microstructure and stability is demonstrated.

- Chapter 5 advances the knowledge built on Chapter 4 deploying a co-stabilisation approach (particle and emulsifier) for production of stable co-stabilised emulsions. Two types of particles and emulsifiers are investigated and the effect of emulsifier concentration on emulsion microstructure is demonstrated.
- Chapter 6 focuses on the influence of processing conditions such as membrane type/material, transmembrane pressure on the microstructure of emulsions co-stabilised by colloidal particles and emulsifiers. The RME process efficiency is evaluated in terms of production rate, energy consumption and compared with a high shear mixer.
- Chapter 7 presents the concluding remarks obtained from the results of this work and discusses possible suggestions and recommendations for future work.

1.4. Dissemination of research

Data and discussions within this thesis have been disseminated as follows:

Publications

- Arkoumanis, P.G. Norton, I.T. and Spyropoulos, F. (2019). Pickering particle and emulsifier co-stabilised emulsions produced via rotating membrane emulsification. *Colloids and Surfaces A: Physicochemical and Engineering Aspects*, 568, pp. 481-492
- Arkoumanis, P.G., Norton, I.T. and Spyropoulos, F. (2019). Surfactant-free Pickering emulsions via rotating membrane emulsification. *RSC Soft Matter*; in review
- Arkoumanis, P.G., Norton, I.T. and Spyropoulos, F. (2019). Process performance of a rotating membrane for production of emulsions co-stabilised by Pickering particles and emulsifiers. *Journal of Membrane Science*; in preparation

Presentations

- Arkoumanis P., Gonzalez-Espinosa Y., Mills T., Norton I., Spyropoulos F. “Membrane emulsification for production of food-grade emulsions”. Oral presentation at *Manufacturing Food Futures Conference*, Loughborough, March 2016
- Arkoumanis P., Norton I., Spyropoulos F. “Food-grade Pickering emulsions via rotating membrane emulsification”. Oral & poster presentation at *Manufacturing Food Futures Conference*, University of Birmingham, March 2017
- Arkoumanis P., Norton I., Spyropoulos F. “Food-grade Pickering emulsions via rotating membrane emulsification”. *1st International Conference on Sustainable Energy and Resource Use in Food Chains*, Windsor, April 2017.
- Arkoumanis P., Norton I., Spyropoulos F., April 2017. “Food-grade Pickering emulsions via rotating membrane emulsification”. *11th European PhD Workshop on Food Engineering and Technology*, Nestle Product Technology Centre, Singen, April 2017.

Chapter 2

Literature Review

2.1. Emulsions and (in)stability

Emulsions are colloidal dispersions that consist of droplets of a liquid phase (dispersed) that are incorporated into another external phase (continuous), with both phases being immiscible, such as oil and water [16]. Many pharmaceutical, cosmetic and food products are emulsions and they are daily consumed by people; for example hand creams, salad dressings, sauces, beverages even milk which is a natural emulsion consisting of fat globules dispersed within a protein-rich (among other nutrients) water phase. Emulsions may be simple such as oil-in-water (O/W) and water-in-oil (W/O), but they can also form more complex structures that consist of droplets comprising one or more phases and these are known as multiple emulsions [17, 18]. These structures are of great interest in the pharmaceutical and food industry as they can be excellent carriers of multiple hydrophilic/lipophilic active ingredients (e.g. flavours, nutrients, drugs) and they can be designed to release them upon modification of the pH or the temperature [19, 20]. Another class of emulsions is water-in-water (W/W) emulsions that comprise two aqueous phases that are immiscible as a result of the segregative phase separation of two or more thermodynamically incompatible hydrophilic molecules in the aqueous mixture [21, 22]. Emulsions can also be classified according to their droplet size and their thermodynamic stability. (Macro)emulsions, such as the ones studied in this thesis, have typically droplet size between 1 – 100 μm whereas nanoemulsions (also referred as miniemulsions) possess smaller droplet size usually 20 – 200 nm [23, 24]. Both types of emulsions are thermodynamically unstable and they require mechanical energy input to form droplets, unlike microemulsions that form spontaneously and they are thermodynamically stable due to the presence of co-surfactants that interpolate with the surfactants thereby affecting droplet curvature. The latter behave as monophasic systems and their droplet size is so small (less than 100 nm) that they appear transparent to the naked eye [25-27].

Because both phases of the emulsion (oil and water) are thermodynamically incompatible the system will strive to reach its thermodynamic equilibrium which is the state with the minimum surface free energy (ΔG):

$$\Delta G = \gamma \Delta A \quad (2.1)$$

According to Eq. (2.1) [28] and depending on the interfacial tension between the two phases (γ), the interfacial free energy is minimised by reducing the interfacial area between the two liquids (ΔA) and this triggers destabilisation phenomena that will eventually lead to phase separation. An overview of the destabilisation mechanisms is depicted in Fig. 2.1. Gravitational separation occurs when the droplets have a lower density than the surrounding liquid and therefore head upward or downward. This is usually the case for O/W emulsions and the mechanism is also called creaming. For instance, creaming occurs if fresh milk is not homogenised. Fat globules have a low density which results in the formation of a thick cream layer that comprises most of the fat content [29]. If the droplets have a higher density than the surrounding liquid sedimentation occurs. This gravitational separation mechanism is very typical for W/O emulsions. Flocculation happens when two or more droplets come together in the form of an aggregate, but where the initial droplets retain their individual integrity. This process is mainly controlled by attractive and repulsive forces acting between the droplets. If the attractive forces between droplets dominate then flocculation occurs [30]. In coalescence, two or more droplets come together and merge to form a single larger droplet. During Ostwald ripening large droplets grow at the expense of smaller ones due to the difference in the Laplace pressure [31]. Lastly, phase inversion occurs when an O/W emulsion transforms to W/O or the other way around. Understanding the destabilisation process could help to identify the factors that initiated destabilisation and design a better strategy to stabilise

emulsions, however this is difficult because different destabilisation mechanisms are involved not only in a consecutive manner but also simultaneously [32, 33].

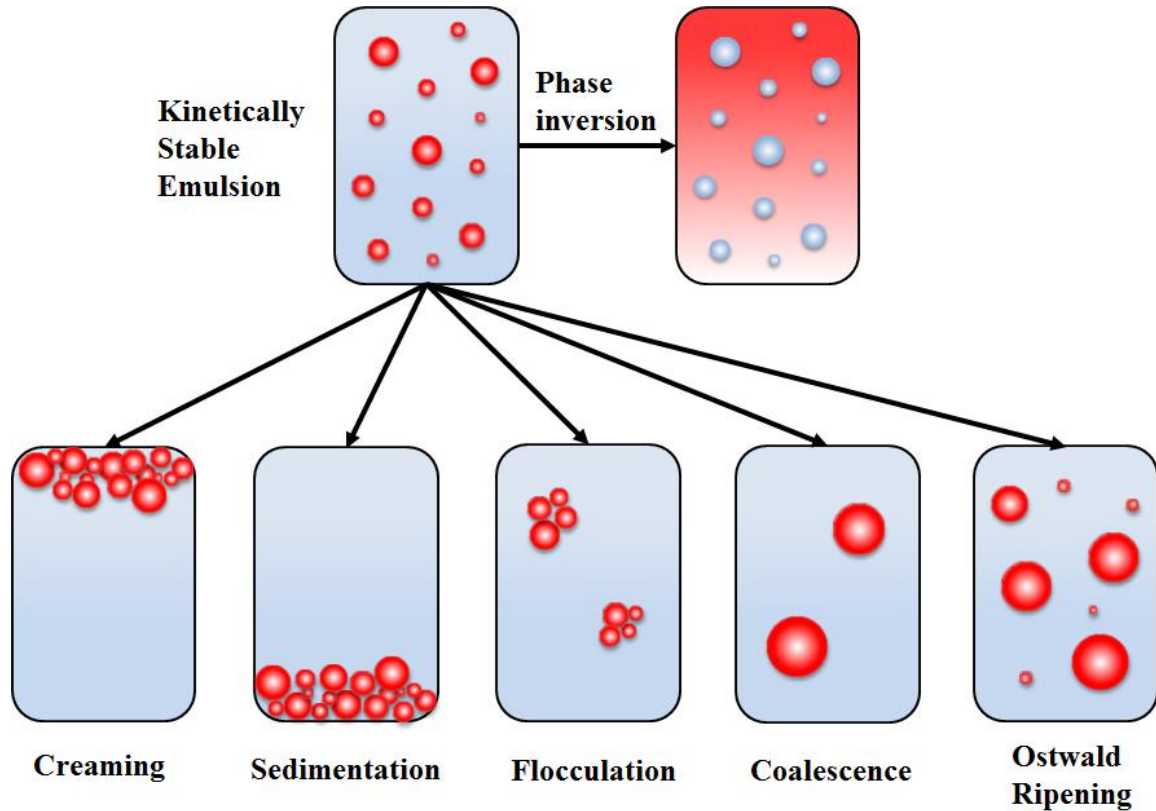


Fig. 2.1: Schematic representation of O/W emulsion destabilisation mechanisms (adapted from [32]).

2.2. Emulsifiers

Despite the thermodynamic incompatibility between the two phases (oil-water), emulsions can be rendered kinetically stable by the adsorption of emulsifiers at the oil-water interface. Emulsifiers are surface active molecules that have a double task, lowering the interfacial tension to facilitate droplet break-up and thus droplet formation and providing a physical barrier for keeping droplets apart to hinder destabilisation phenomena; i.e. coalescence, flocculation. The physical barrier between the droplets may be induced by the repulsive forces

between the charged domains of the emulsifiers adsorbed to droplets or it could be of steric origin (overlapping of electronic clouds of approaching emulsifiers) or both [31, 34].

Emulsifiers are amphiphilic entities that comprise hydrophobic and hydrophilic domains and can be divided in two classes: surfactants and biopolymers. At this point, it should be stressed that colloidal particles are occasionally considered as emulsifiers because of their capacity to adsorb to oil-water interfaces, yet the mechanism of adsorption is different from classic emulsifiers (surfactants and certain biopolymers) as they have not been found to cause a substantial decrease in interfacial tension [2, 35]. Therefore the function of colloidal particles as emulsifiers is discussed in a separate section.

2.2.1. Surfactants

Surfactants are low molecular weight entities consisting of a hydrophilic head and a lipophilic tail and may be derived from nature or composed in the lab. These, according to the existence (or not) of a charge in their hydrophilic domain, can be further distinguished in cationic, anionic, nonionic and zwitterionic [36].

The need to evaluate which surfactants are suitable to stabilise particular types of emulsions was substantiated early by Griffin *et al.* with the HLB value [37]. The HLB value (hydrophilic-lipophilic balance) is a parameter commonly used to classify surfactants and their solubility in a solvent. Surfactants with high HLB value are more hydrophilic and they perform better when placed in the aqueous phase while low HLB indicates a surfactant with affinity to the organic phase. This is an extension of the Bancroft rule that defines the medium in which the surfactant is more soluble as the continuous phase [38]. Therefore by knowing the HLB value of a mixture of surfactants it can be determined at which concentration each should be used to produce an O/W or O/W emulsion.

When the concentration of surfactant in a solution exceeds a specific concentration, surfactant monomers start to form micelles and this value is called critical micelle concentration (CMC). The CMC in aqueous solutions depends on the type of surfactant, temperature and the pH and ionic strength of the system [39]. For instance, CMC of ionic surfactants reaches a minimum at ambient temperature and then follows an increasing trend with increasing temperature whereas for nonionic surfactants the CMC decreases with increasing temperature [40, 41]. As soon as a new surface is created surfactant molecules diffuse from the bulk to the interface to restore equilibrium ($C_{\text{bulk}} = C_{\text{surface}}$). For concentrations above the CMC, surfactant micelles serve as carriers of surfactant monomers diffusing through the interfacial film and they dissociate in surfactant monomers [42, 43]. Upon adsorption, surfactants reorganise and form aggregates (depending on their charge and physicochemical properties) and as a result monolayers or multiple layers form. These cover the surface area of droplets providing steric and electrostatic stabilisation (i.e. ionic surfactants) between droplets.

In traditional emulsification the interfacial area is created abruptly and excess surfactant is required to adsorb fast to the new interface and prevent droplets from recoalescence due to, the high shear conditions. In membrane emulsification however, the interfacial area increases in a slower rate and therefore less surfactant is needed. This means that, at a surfactant concentration close to the CMC, membrane emulsification can be more efficient in the emulsifier usage [44].

2.2.2. Biopolymers

Proteins mainly represent biopolymers as another class of emulsifiers. There are also some polysaccharides that have been reported to possess surface-active domains owing to their small protein content such as gum arabic, sugar beet pectin and citrus pectin [34]. Proteins are

high molecular weight amphiphilic polymers commonly used as emulsifiers in food; especially dairy proteins. These can be classified as globular and flexible random coil [45]. Globular proteins have a spherical shape, they consist mostly of hydrophobic parts located in the core of the protein while the polar groups are located at the external of the molecule thus they are compactly folded and they are not so surface active [46]. An example of globular milk protein is β -lactoglobulin which is the main constituent of WPI. Whey Protein Isolate (WPI) is a concentrated and spray-dried milk powder derived from cheese whey liquid and comprising mainly two globular proteins β -lactoglobulin and α -lactalbumin (over 90 wt. % of dry matter). Random coil proteins have no fixed structure and it varies between molecules and time, e.g. Sodium Caseinate (NaCas) which is a treated casein protein [47]. The most surface active protein in NaCas is β -casein. The proteins that approach to the oil-water interface undergo a degree of unfolding (depending on their structure) and after adsorption they change conformation to occupy as much space as possible, thus creating a viscoelastic film surrounding the droplet [48, 49]. However, random coil proteins incur fast structural rearrangements upon adsorption whereas for globular proteins such as WPI this can be continued even for a long time following adsorption. After adsorption, the hydrophobic groups of the proteins are bound in the organic phase whereas hydrophilic groups direct towards the water phase [50]. Protein-protein interactions on the droplet surface as well as between proteins adsorbed on different droplets will determine the occurrence of destabilisation. The charge of the proteins may result in electrostatic repulsion or attraction between the protein molecules and thus between droplets. At a pH below the isoelectric point (IEP) of the protein, the protein carries a positive charge whereas at pH above the protein molecules are negatively charged [51]. As a consequence, at a pH above or below the IEP

emulsions are electrostatically stabilised while at pH close to the IEP flocculation of droplets and creaming may occur.

2.3. Colloidal particles

Colloidal particles have been seen to stabilise oil-water and air-water interfaces since the reports of Ramsden and S.U. Pickering in the early 20th century [52, 53]. However, emulsions stabilised by colloidal particles (i.e. Pickering emulsions) started to receive significant attention in the past two decades because of their exceptional long-term stability compared to that of the conventional, emulsifier-stabilised ones; a result of the strong adsorption of particles at the oil-water interface that creates a solid mechanical barrier against coalescence [10].

Colloidal particles have been distinguished for their potential to produce multiple Pickering emulsions with higher stability than conventional multiple emulsions stabilised by classic emulsifiers [54]. For example, in W/O/W or O/W/O emulsions the droplets of the internal phase are very unstable, especially in case of high internal phase fraction, and they are subject to coalescence that eventually leads to breakage of the internal structure and formation of simple emulsions. This has been attributed to the diffusion of low molecular weight emulsifiers through the inner and outer interfaces of the double emulsion droplet [35]. On the contrary, colloidal particles are anchored on the specific surfaces providing a mechanical barrier that protects droplets from coalescence and enhances overall stability. There are reports of studies that used mixtures of colloidal particles and emulsifiers to stabilise inner and outer interfaces of droplets of W/O/W emulsions (microcrystalline cellulose and span) and O/W/O (hydrophobic silica, hydrophilic silica particles and surfactant) [55, 56]. However, only one study reports stabilisation of multiple emulsions only by particles. Binks *et al.*

produced stable O/W/O emulsions employing hydrophilic (water soluble) and hydrophobic (oil soluble) silica particles for stabilisation of inner and outer droplets respectively [54].

2.3.1. Pickering stabilisation

The mechanism of Pickering stabilisation comprises three basic steps that are very similar to the classic emulsifier adsorption; however, the last step differentiates this class of emulsions. The particle is first transferred from the bulk phase to the sub-surface via convective transport and then it reaches close to the oil-water interface where particle-particle electrostatic interactions will determine whether the transportation will be either diffusion controlled or barrier controlled [15, 43]. The final step comprises the removal of water between the particle and the oil surfaces and the strength of the adsorption will be determined by the particle size, the wettability of the particle (contact angle) and the interfacial tension between the phases. These factors are all incorporated in the following equation that describes the free energy of adsorption of a particle [57]:

$$\Delta F_{ads} = \pi r_p^2 \gamma (1 - |\cos\theta|)^2 \quad (2.2)$$

where r_p is the particle size, γ the interfacial tension and θ the contact angle formed between the particle and the two immiscible phases, oil and water. As it can be seen from Eq. (2.2) the large particles induce a greater energy barrier for desorption and the adsorption is stronger when both phases equally wet the particle, that is $\theta = 90^\circ$.

As long as the particles are partly wetted by oil and water then it is possible to form a Pickering emulsion [10, 46]. Depending on the contact angle it can be determined which particles are available for a particular type of emulsion. If $\theta < 90^\circ$ the particle is more hydrophilic and the curvature of the interface will encourage formation of O/W emulsion

whereas if $\theta > 90^\circ$ the O/W the particle will be wetted more by the oil phase and these particles are more suitable for W/O emulsions (Fig. 2.2). Chevalier *et al.* discuss that the adsorption energy will always be much larger than the thermal energy $k_B T$, even for a particle as small as 1 nm [57]. However, the wettability of the particle is very influential as well. For example, for a small particle of 10 nm in diameter that is wetted equally by toluene and water ($\theta=90^\circ$, $\gamma=36 \text{ mN m}^{-1}$) the energy of adsorption will be the highest and about 2000 times larger than the thermal energy ($=k_B T$). However, this can change if the particle is too hydrophilic ($0^\circ < \theta < 20^\circ$) or too hydrophobic ($160^\circ < \theta < 180^\circ$) as the energy may drop lower than $k_B T$ and the particle will desorb from the interface resulting in unstable emulsion [1].

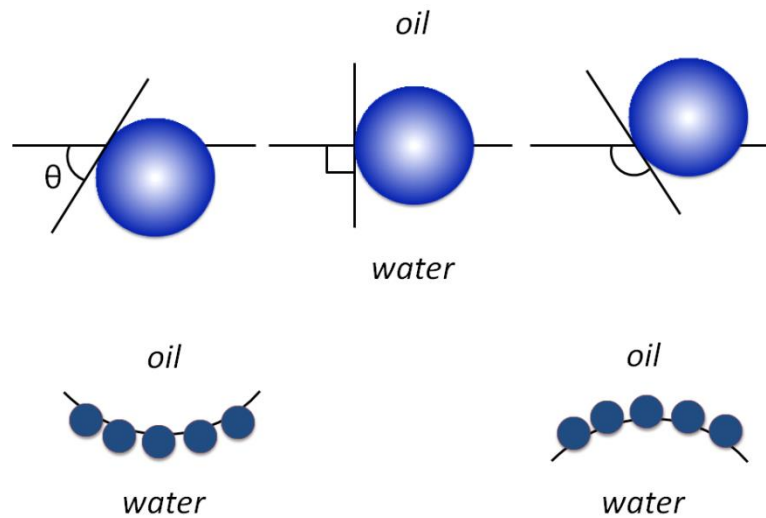


Fig. 2.2: Schematic representation of colloidal particles adsorbed at a planar oil-water interface for different contact angles measured through the water phase (top). Positioning of particles at the curved oil-water interface of O/W ($\theta_w < 90^\circ$) and W/O ($\theta_w > 90^\circ$) emulsions (bottom). Adapted from [1].

2.3.2. Stability conferred by colloidal particles

Despite the limited interfacial tension lowering capacity of particles, particle-stabilised emulsions are stable because they affect ΔG by essentially reducing ΔA (Eq. (2.1)). By adsorbing at the oil-water interface particles reduce the area of contact between the two phases thus also ‘artificially’ reducing ΔA and therefore ΔG . Three methods are distinguished by which stabilisation of droplets is imparted by colloidal particles [10]. The first and idealised method is that the particles form mono- or multiple tightly packed layers around the dispersed droplets. The strength of the steric barrier depends on how difficult it is to remove particles from the interface, thus the greatest the adsorption energy, the stronger the steric barrier. However at the same time, the steric barrier is more effective (and thus the approaching droplets are kept at a longer distance) when the particles are wetted preferentially by the continuous phase. Therefore, according to Dickinson *et al.*, stable Pickering emulsions can be produced as long as the contact angle is close to, but not 0° or 180° as this will allow permanent adsorption and maximum steric effect [10]. The second method is the bridging of particles and this can be conceptualised as particles that are ‘shared’ between two droplets. This is very common in emulsions that do not have a sufficient amount of particles resulting in bridging flocculation of droplets. Steric stabilisation in this case is provided by hindering the adsorbed particles from escaping from the bridging layer. Finally, the last method is the steric hindrance provided to the droplets by a three-dimensional network of weak flocculated particles in the continuous phase. This is common in Pickering emulsions with an excess concentration of particles as the adsorbed particles and the flocculated particles in the continuous phase are held together with interparticle interactions. Extra stability is provided from these networks as their presence in the continuous phase increases the viscosity of the emulsion and prevents coalescence of droplets [57, 58]. It should be noted that, because

particles are not amphiphilic molecules they are not able to lower the interfacial tension thus the emulsion droplet size will be solely influenced by the emulsification technique and the energy it dissipates in the emulsion for droplet break-up. However, because of the high mechanical strength provided by the particles surrounding the droplets, it is possible to produce stable Pickering emulsions with large enough droplet size.

2.3.3. Edible colloidal particles

Understanding of Pickering stabilisation has been linked with the use of inorganic particles such as silica and polystyrene latex. These types of particles are rigid, commercially available and they come at a range of sizes and surface properties, so their Pickering performance can be conveniently predicted. However, because inorganic particles are not biodegradable and they pose potential health risks, their use in foods and pharmaceuticals has been criticised [59]. As such, research interest is gradually focusing on colloidal particles that can be assembled by edible materials and function as Pickering stabilisers in food emulsion based systems. As for all particles, in order to deliver optimum Pickering functionality, these food-grade particles should be wetted by both phases and their size should be significantly smaller (minimum one order of magnitude) than the desired emulsion droplet size [60]. Because of their organic composition that is of protein, carbohydrate or lipid origin, they tend to be soluble in either the oil or water phase [2, 60]. Therefore, a few methods have been developed to impart the desired size (e.g. acid hydrolysis of cellulose crystals to obtain small cellulose particles), wettability and surface properties (e.g. chemical modification through esterification of starch granules or forming complex systems with surfactants through a synergistic effect to tune their wettability) [61].

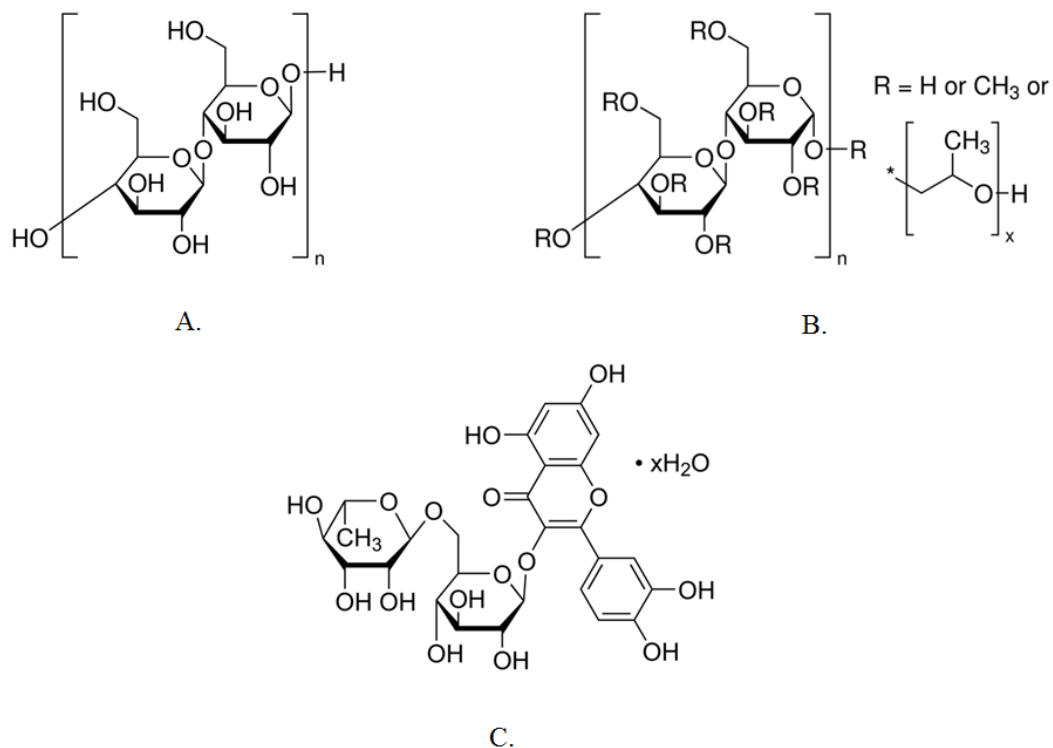


Fig. 2.3: Chemical structures of cellulose (A), hydroxypropyl methyl cellulose (B) and rutin hydrate (C) (adopted by supplier's MSDS documentation).

The inherent organic nature of these polymers that comprise hydrophilic/ hydrophobic groups is causing them to adopt a non-spherical shape when dispersed in a solvent that barely resembles the idealised spherical shape of Pickering particles [1, 62]. For example, very hydrophobic polymers dispersed in water will tend to aggregate due to hydrophobic attraction exposing their hydrophilic domains and they adopt colloidal particle behaviour. Depending on the intramolecular structure and physicochemical properties of the polymer, exposure of hydrophobic/ hydrophilic domains will determine the overall wettability and thus the capacity to stabilise O/W or W/O emulsions. For example, unmodified cellulose is a hydrophilic molecule with a linear backbone consisting of $\beta(1,4)$ -glucose units capable of stabilising O/W emulsions and because of its semi-crystalline structure, it forms rod-shaped particles once dispersed in the water phase [63]. However, as it has been mentioned the performance of a

particle as a Pickering stabiliser is linked to its wettability so if this is too hydrophilic it could result in weak adsorption and loss of stability. Therefore, the surface of cellulose is modified to render the molecule more hydrophobic. An example of modified cellulose that is broadly used in the food and pharmaceutical industry for its viscosity enhancing properties and emulsifying capacity is hydroxypropyl methylcellulose (HPMC) [64]. HPMC is derived by incorporation of methyl (hydrophobic) and hydroxypropyl (hydrophilic) groups to the unhydroglucose backbone imparting a level of hydrophobicity to the molecule thus making it able to adsorb to fluid interfaces [65]. In the same work, it is shown that the methyl: hydroxypropyl ratio suggests an indication of the hydrophobicity of the molecule, e.g. HPMC with high ratio incorporates more methyl than hydroxypropyl groups thus it is more hydrophobic and possesses lower molecular weight.

Rutin is a glucoside that consists of the flavonoid quercetin and rutinose which is a disaccharide comprised of rhamnose and glucose; it is derived from buckwheat, citrus fruits and peels and it is distinguished by its green-yellowish pigment [66]. Apart from the health and nutritious benefits, rutin as most of the flavonoids has antimicrobial and antioxidant properties and the latter is of great importance in emulsions as it can be used to inhibit lipid oxidation [67-69]. The presence of hydroxyl groups imparts the hydrophilic character and the rings impart hydrophobicity to rutin as it can be seen by the chemical structure of the molecule (Fig. 2.3). Therefore, similarly to HPMC, once dispersed in the water rutin forms aggregates that resemble the behaviour of colloidal particles so theoretically they can adsorb and stabilise fluid interface. To date, only a few studies have reported on the emulsifying capacity of rutin and its efficacy to promote stability of emulsions. Murray *et al.* investigated the capacity of a range of flavonoids to stabilise O/W emulsions and he showed that rutin (dispersed in the water phase) is a good stabiliser due to its moderate partition coefficient,

whereas flavonoids that are too hydrophilic or too hydrophobic produced unstable emulsions [70]. The same group also reported on the effect of the pH of the rutin aqueous suspension on the emulsifying capacity of rutin. They found that emulsions with smaller droplet size were produced at the native pH, but this may be related to the low surface charge of the particles that, according to Luo *et al.*, makes them more surface active [71]. Next step was to evaluate the potential of rutin to improve the oxidative stability of O/W emulsions [72]. The authors found that the addition of rutin partially replaced WPI at the oil-water interface and enhanced emulsion stability whilst reducing oxidation upon storage at 50 °C. This study showcased that rutin could be a good alternative to protein for hindering lipid oxidation during thermal processing because proteins denature at high temperature and their antioxidative properties are lost.

Admittedly, utilisation of such particles as Pickering stabilisers offers prolonged stability plus they are sources of nutrients, thus enhancing the nutritional value of emulsions. Another potential for these particulates is the production of responsive 'Pickering-like' emulsions for the controlled release and delivery of two different active ingredients. In recent work, Spyropoulos *et al.* showed that it is possible to encapsulate a hydrophobic active ingredient in oil droplets that are stabilised with electrostatic protein-polysaccharide complexes (Sodium caseinate/chitosan) which contain a secondary hydrophilic ingredient [73]. The latter is released when the complexes collapse upon an increase in pH, triggering also sustained release of the hydrophobic ingredient to the continuous phase. The suggested approach may be adopted for the design and development of Pickering type emulsion structures for the release and delivery of multiple actives.

2.3.4. Combination of colloidal particles and emulsifiers

2.3.4.1. Silica particles as co-stabilisers

As it was mentioned earlier, a level of hydrophobicity of the particles is essential to ensure they partially wet the oil/water phases otherwise the particle may desorb from the interface and diffuse away to the medium where it is preferentially wetted. Various techniques have been used to modify the surface of particles as per their hydrophobicity thereby increasing their performance as Pickering stabilisers. For example, it is reported that the pH of hydrophilic silica aqueous dispersions was adjusted to 2 because at higher pH unstable emulsions were produced, apparently as a result of the tendency of the particles to reside in the aqueous phase [74, 75]. Another option is the chemical grafting of small molecules or polymers on the surface of the particles by covalent bonding that allows particles to be stimuli-responsive (pH, ionic strength) [76]. Lastly, molecular adsorption of low molecular weight ionic emulsifiers on the charged particle surface may result in the formation of modified particles with enhanced wettability; thus achieving contact angles closer to 90° that is associated with higher energy of adsorption and effective stabilisation of emulsions (Eq. (2.2)). Such adsorption could involve electrostatic or hydrophobic interactions. In the first case particles and emulsifiers need to possess opposite surface charges; for example, negatively charged particles interact with anionic sodium dodecyl sulphate (SDS), or positively charged particles with cationic hexadecyltrimethylammonium bromide (CTAB). Nevertheless, emulsifiers may also adsorb to particles via hydrophobic interactions between the lipophilic tail of the emulsifier and the hydrophobic surface of the particle. Alternatively, if the particle surface is hydrophilic, emulsifiers may adsorb via their hydrophilic head group while their lipophilic tails protruding in the continuous phase [77]. Particle: emulsifier ratio will determine the extent of surface modification of the particle. Binks *et al.* discuss that

cationic emulsifiers are able to electrostatically adsorb to hydrophilic silica particles and alter their wettability forming monolayers with their lipophilic tail protruding in the water phase [14]. However, this is subject to change when the emulsifier concentration in the system increases leading to formation of bilayers and even multilayers that will turn the particle surface from hydrophobic to hydrophilic and so on.

Such particle-emulsifier interactions have been found to promote the stability of emulsions stabilised by both species in a synergistic manner. This has been described in the work of Midmore *et al.* who used a combination of weakly flocculated hydrophilic silica particles and nonionic emulsifiers (mixed in the aqueous phase) to stabilise O/W emulsions covering a range of HLB values [56]. When the emulsifier adsorbed to the silica surface and emulsifier was kept at low concentration (where emulsifier alone cannot stabilise emulsion), silica particles governed emulsion stability and stable emulsions were produced. A further increase in the emulsifier concentration above a critical value resulted in reduced emulsion stability. However, when interactions between the species were limited, unstable emulsions were produced.

Indeed, the protocol of mixing particles and emulsifiers was found to be important in the imparted emulsion stability. Hydrophilic silica particles were used in conjunction with oleylamine or lecithin (charged zwitterionic emulsifiers introduced in the oil phase) to stabilise O/W emulsion [78]. This study concluded that the positioning of silica particles together with the emulsifier in the oil phase favoured synergistic long-term stabilisation. When introduced in the water phase, the electrostatic repulsion between the negatively charged silica particles and the negatively charged oil surface and the low attachment energy resulted in the loss of the synergistic effect.

Despite the abundance of literature regarding the synergism between particles-emulsifiers for co-stabilisation of emulsions, the detailed steps of the co-stabilisation mechanism was described later by Pichot *et al.* [79]. The authors discussed the effect of the presence of monoolein in mixtures with hydrophilic silica particles on the coalescence stability of the subsequent emulsions and demonstrated that stabilisation of oil droplets progresses in two stages. First the low molecular weight surfactant (monoolein) adsorbs to the droplet surface providing temporary stability and promoting droplet break-up. Next, silica particles adsorb and induce long-term stability. At this point, the particle: emulsifier ratio will determine the morphology of the oil droplets emulsion stability and this was discussed in an extension of the previous study by the same authors [80]. Low emulsifier concentrations of O/W emulsifiers (Tween 60, NaCas) in aqueous mixtures with silica particles resulted in droplets smaller than emulsions stabilised by each of the individual species alone. At moderate emulsifier concentration, the droplet size increased due to rearrangement of silica particles in the presence of more emulsifier molecules (competition of species to the oil-water interface). Finally, at high emulsifier concentrations the droplet size and morphology matched with the droplets generated solely by emulsifier, confirming the hypothesis that silica particles were displaced from the interface.

Contrary to the common perception that co-stabilisation is imparted by the adsorption of particles and emulsifiers at the oil-water interface, an alternative ‘non Pickering’ mechanism has been proposed recently with non-interfacially adsorbed particles [81]. In this work, bare hydrophilic (non-interfacially active) or surface modified (interfacially active) silica particles were combined with a low concentration of a zwitterionic surfactant in the water phase and the stability of produced emulsions against coalescence was studied. It was found that in both cases the emulsions were synergistically stabilised against coalescence for 1 month, although

in the latter case the hydrophilic particles were not adsorbed at the oil-water interface and they accumulated at the water phase between droplets providing effective steric repulsion.

2.3.4.2. HPMC particles as co-stabilisers

The majority of the literature on the co-stabilisation of interfaces by HPMC and emulsifiers concerns the formation of emulsion-based edible films and coatings. HPMC was shown to combine well with β -Lg in aqueous mixtures for stabilisation of foams showing promising results for applications in emulsions [82]. More specifically, they reported on a competition mechanism between the two polymers to the air-water interface and they quantified this contribution by measuring the surface tension and rheological properties of systems incorporating species alone and mixed in water. It was found that at high concentration of HPMC the contribution of the HPMC in lowering the surface tension was greater than the protein thus it was anticipated that HPMC would dominate the interface prior to adsorption of protein. The presence of HPMC in the protein adsorbed layer also resulted in enhancement of the elastic properties of the interface unlike the effect of surfactant that reduces interfacial elasticity. Of course the behaviour of these systems cannot be easily predicted as electrostatic interactions between polysaccharides (HPMC) and proteins at pH lower than the IEP of the protein might result in complexation and the behaviour of the system with regard to the competitive adsorption may exhibit completely different behaviour [83, 84].

Perez *et al.* examined the behaviour of mixed systems of HPMC of different surface activities and whey protein concentrate (WPC) upon adsorption to the air-water interface by measuring the surface pressure for species alone and mixed in the water phase [85]. When HPMC was more surface active, WPC was displaced from the interface resulting in lower surface pressure whereas when HPMC of low surface activity was used both biopolymers co-existed at the air-

water interface demonstrating a synergistic behaviour, as indicated by the increased surface pressure. In the same study, it is discussed that possible complexation of HPMC and protein could affect the overall adsorption.

The latter hypothesis was tested by Camino *et al.* who investigated the effect of pH on the emulsifying and adsorption capacity of mixtures of HPMC and β -lg at the oil-water interface [86]. At pH 6 no complexation occurred and the competitive adsorption of the species to the oil-water interface favoured the more surface active β -lg to dominate the oil surface that formed a strong elastic film, however emulsions were subject to flocculation and creaming. On the other hand, at pH 3, weak complexation of HPMC and β -lg did not allow for the formation of an elastic film but the produced emulsions were more stable to coalescence, perhaps as a result of the effective steric barrier between oil droplets induced by the complexed particulates.

Finally, one study reports co-stabilisation of O/W emulsions with HPMC particles and hydrophilic/ lipophilic surfactants [87]. The authors demonstrate that in such co-stabilised systems increasing the concentration of the hydrophilic emulsifier results in smaller droplet size, a trend analogous to the reduction of the interfacial tension in emulsions stabilised solely by the emulsifier. On the other hand, utilisation of a lipophilic emulsifier as a co-stabiliser resulted in the opposite trend when increasing its concentration in the system. A synergistic effect occurred by combining HPMC particles and small concentration of emulsifiers regardless of their HLB value. The emulsion droplet size of co-stabilised emulsions was smaller than emulsions stabilised by either of the species alone at the same concentration presenting remarkable stability against coalescence.

2.4. Emulsification

Emulsification, also referred as homogenisation, is the process of forming new oil-water interfacial area using either mechanical means that generate shear, cavitation or turbulence to disrupt (break down) emulsion droplets to smaller ones (top-down approaches), or by spontaneous formation of droplets (bottom-up approaches) [88, 89]. The first class comprises techniques that are high-energy demanding, such as rotor-stator mixers, high-pressure homogenisers, sonicators, whilst there are a number of techniques that utilise lower energy e.g. spontaneous microchannel emulsification, phase inversion temperature or composition [90]. There are also methods such as membrane emulsification which is the process used in the present study for formation of emulsions that is considered a high or low energy method depending on the system utilised and other parameters deployed such as the dispersed phase flux and the targeted dispersed phase volume fraction. When it comes to droplet disruption, it is essential that the magnitude of forces (expressed by the Laplace pressure) applied to the droplet is such as to exceed the interfacial tension forces that resist droplet deformation [91, 92]. This balance is reflected in the following equation:

$$\Delta P_L = \frac{4\gamma}{D} \quad (2.3)$$

where ΔP_L is the Laplace pressure, γ the interfacial tension and D is the average droplet diameter. Apparently as shown from Eq. (2.3) for a formulation that establishes a certain interfacial tension force, a high magnitude of forces and thus, a larger amount of energy is needed in order to obtain a nanosized droplet.

2.4.1. High-energy methods

An overview of the most common conventional emulsification techniques that utilise a large amount of energy is depicted in Fig. 2.4. Emphasis is given on the high-shear mixer as it is the method used to make emulsions in the present study. Rotor-stator (RS) homogenisers consist of a moving element that usually rotates to induce motion and mix the components of a dispersion and a stationary element (stator). An example of RS homogenisers is the high-shear mixer and the colloid mill. It is prevalent in the industry that a coarse emulsion is formed first (primary emulsification) with droplets of an average diameter greater than 2 μm , and then a second emulsification step (secondary emulsification) follows to further reduce the droplet size to produce a fine emulsion. The high-shear mixer is mainly used for primary emulsification whereas the rest of the equipment presented generate extra disruptive forces that are ideal for further reduction of droplets below 1 μm so they are used for secondary emulsification [35, 93]. A high-shear mixer is capable to operate at rotor tip speeds as high as 10 - 50 m s^{-1} producing very high shear rates (20000 - 100000 s^{-1}) and it consists of an overhead stirrer and the rotating shaft at the edge of which a bladed stirrer rotates within a housing (stator). The stator and the rotor blades can be machined such as to provide different geometries that, in turn will generate different levels of disruption forces within the gap created between these two elements [93, 94]. For example, the stator may be a screen with vertical slots, circular or square holes and the rotor may be a toothed disk or rotating blades, providing additional break-up of droplets. The shear rate in the gap between the rotor and the stator elements can be calculated as follows [95]:

$$\dot{\gamma}_{HSM} = \frac{\pi N D_{im}}{\delta} \quad (2.4)$$

where N the rotational velocity of the impeller, D_{im} is the diameter of the impeller and δ the gap between the outer surface of the rotor (impeller) and the inner surface of the stator (the screen).

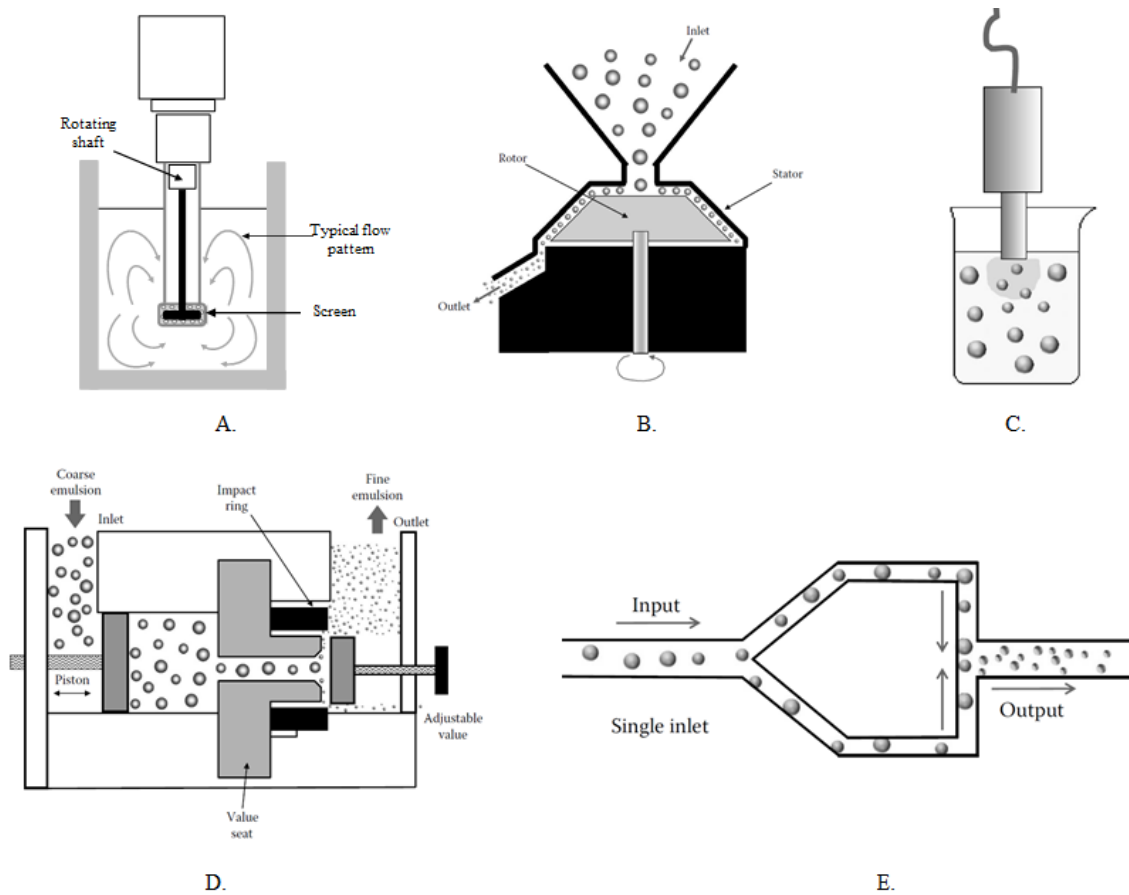


Fig. 2.4: Schematic representation of high-energy emulsification devices and indicated droplet disruption mechanism. (A) high-shear mixer, (B) colloid mill, (C) ultrasonic probe, (D) high-pressure homogeniser, (E) microfluidizer. Adapted from [31].

For batch operations, the rotating shaft with the mixing head are simply submerged in the dispersion within a vessel whereas for continuous operation the dispersion is fed by a peristaltic pump through an opening into the mixing head and following emulsification it exits the mixing chamber. Critical factors influencing the droplet size during high-shear mixing is the viscosity ratio between the two phases, the rotation speed and the dispersed phase volume

fraction and in particular for inline mixers the flow rate that will determine the residence time within the mixing chamber [96, 97]. Colloid mills are set to mainly operate continuously allowing for higher production rates. This type of homogeniser is used for secondary emulsification as the high stress applied into the product is very high and it can produce droplet size below 1 μm whilst it can handle viscous dispersions, unlike high-pressure systems [98]. The dispersion is fed continuously into the device and due to the shear stresses developed between the rotational and the stationary disks droplets are disrupted further to smaller ones. The gap and thus the applied shear can be altered by adjusting the distance between the rotating disk and the stator. Ultrasound probes are also capable of producing macro- or nanoemulsions. Their operation involves the utilisation of the ultrasonic waves that generate acoustic cavitation and microturbulence to disrupt droplets or reduce the size of particles dispersed in the continuous phase. The high-pressure homogenisers are the most common devices for droplet size reduction usually after primary emulsification [99, 100]. A pump pushes the emulsion or dispersion in the homogenising chamber and through the gap that is adjusted by a valve; thus the droplets are broken down by the disruptive forces generated in the narrow passage. In the case of the microfluidizer, the emulsion or dispersion is fed and pulled by a piston pump and after pressurisation it is released in the interaction chamber where two product streams form and collide with each other resulting in droplets with smaller size [101].

The events that coincide during emulsification such as droplet formation, disruption and coalescence, is the result of forces generated within a certain flow pattern established in the continuous phase by the emulsification device [102]. In general, three flow profiles are distinguished. The laminar flow is characterised by a smooth well-defined flow whereas turbulent flow is highly disordered and eddies are formed due to the high flow rates. The

Reynolds number (Re) is used to predict the transition from laminar to turbulent conditions based on the balance of forces applied at a direction perpendicular (inertial forces) and parallel to the droplet surface (viscous forces) [102, 103]. For instance, in cross-flow membrane emulsification where the flow of the continuous phase is parallel to the membrane surface [104], the Reynolds number within the emulsification channel is:

$$Re_c = \frac{u_c D_h \rho_c}{\eta_c} \quad (2.5)$$

where u_c is the cross-flow velocity of the continuous phase, D_h is the hydraulic diameter of the emulsification channel, ρ_c is the continuous phase density and η_c the dynamic viscosity of the of the continuous phase. In this configuration, the direction of the flow is parallel to the membrane surface. As it is shown by Eq. (2.5) when the viscous forces (denominator) dominate Re is small and the flow is characterised as laminar viscous (LV) whereas at increased Re above a critical value the inertial forces are dominant and they cause the formation of turbulent eddies. In general, according to Kolmogorov's work, eddies with a size much larger than the droplet size transfer their energy to smaller eddies that are able to disrupt droplets due to their higher energy content [105]. Therefore two sub-regimes are distinguished for turbulent flow. Turbulent inertial (TI) regime occurs when the size of the eddy is comparable to the droplets thus the inertial forces induce droplet break-up and the requirement is that the Reynolds number of the droplet (Re_d) (for $l=D_{oil}$ where D_{oil} is the droplet diameter) is greater than 1. When the flow is turbulent and the $Re_d < 1$ eddies are larger than the droplets and the regime is turbulent viscous (TV). As it is shown from Eq. (2.5), the viscosity of the continuous phase is expected to have a major effect on the flow regime. Viscous fluids do not facilitate formation of eddies so the flow regime will be more laminar (LV) and Re will be large, whereas at very dilute liquids TI or TV flow is encouraged,

depending on the Re_d . Another parameter that should be considered is the size of the homogeniser as for very small e.g. in laboratory-scale devices the flow will tend to be more laminar.

The time required for adsorption of emulsifier at the oil-water interface has been derived as shown in the work of Walstra *et al.* for high-energy emulsification methods [93, 102]. For laminar viscous (designated with an ‘L’) and turbulent inertial flow (designated with a ‘T’), the adsorption time (t_{ads}) can be estimated respectively by the following equations:

$$t_{ads}^L \sim \frac{6\pi\Gamma_M}{\dot{\gamma}m_cD_{oil}} \quad (2.6)$$

$$t_{ads}^T \sim \frac{\Gamma_M}{m_c} \left(\frac{\rho_c}{D_{oil}\varepsilon_v} \right)^{1/3} \quad (2.7)$$

where $\dot{\gamma}$ is the shear rate, m_c is the bulk particle concentration in the continuous phase, ρ_c the continuous phase density, ε_v the energy density and Γ_M the excess surface concentration (or surface load) of species required for full coverage (monolayer) of oil droplets. For small molecules such as emulsifiers the surface concentration is between 1 – 2 mg m⁻² and for proteins 2 – 3 mg m⁻² [106]. For spherical particles that are closely packed on the oil-water interface with a hexagonal packing fraction ($\varphi_{hp} \sim 0.907$), the surface load is expressed as:

$$\Gamma_M = \frac{4}{3} \rho_p \varphi_{hp} r_p \quad (2.8)$$

where ρ_p is the particle density and r_p is the particle radius. Small particle size results in low surface concentration Γ_M that in turn will yield short adsorption time as it can be observed by Eq. (2.6) & (2.7). This would mean that the oil droplets would be covered fast by particles before coalescence occurs. However, small particle size is also associated with low energy of

adsorption as shown in Eq. (2.2), therefore there is an interplay between these competing events for optimum Pickering stabilisation during high-energy emulsification.

2.4.2. Low-energy methods

In this section, the most common up-to-date low-energy emulsification techniques are discussed, briefly introducing membrane emulsification as it is the technique under investigation in the current study and a thorough mechanistic understanding is provided in section 2.5. Nevertheless, membrane and microchannel emulsification were developed in an effort to spend energy only for the production of oil-water interfacial area. Both techniques share common droplet formation mechanisms and they generate one droplet at a time either spontaneously (in the absence of shear when the magnitude of forces applied overtake Laplace pressure) or as a result of the shear applied by the continuous phase [107]. In microchannel emulsification the dispersed phase is introduced in the continuous phase through parallel grooved microchannels or straight through pores yielding very monodisperse emulsions whose droplet size depends on the microchannel geometry and phase composition [107, 108]. Although membrane emulsification and microchannel emulsification have been reported as very energy efficient methods, they are not yet to be used in the industrial scale. This is because the low dispersed phase flux associated with long processing times makes these methods unfavourable compared to high shear methods, especially when a high dispersed volume fraction is required [109, 110].

Other techniques have been developed based on the formation of droplets by using emulsifiers dissolved in one of the immiscible phases and changing the composition or their environment e.g. dispersed phase fraction and temperature. In spontaneous emulsification an oil phase that contains a hydrophilic emulsifier is added gradually to water whilst stirring (Fig. 2.5D).

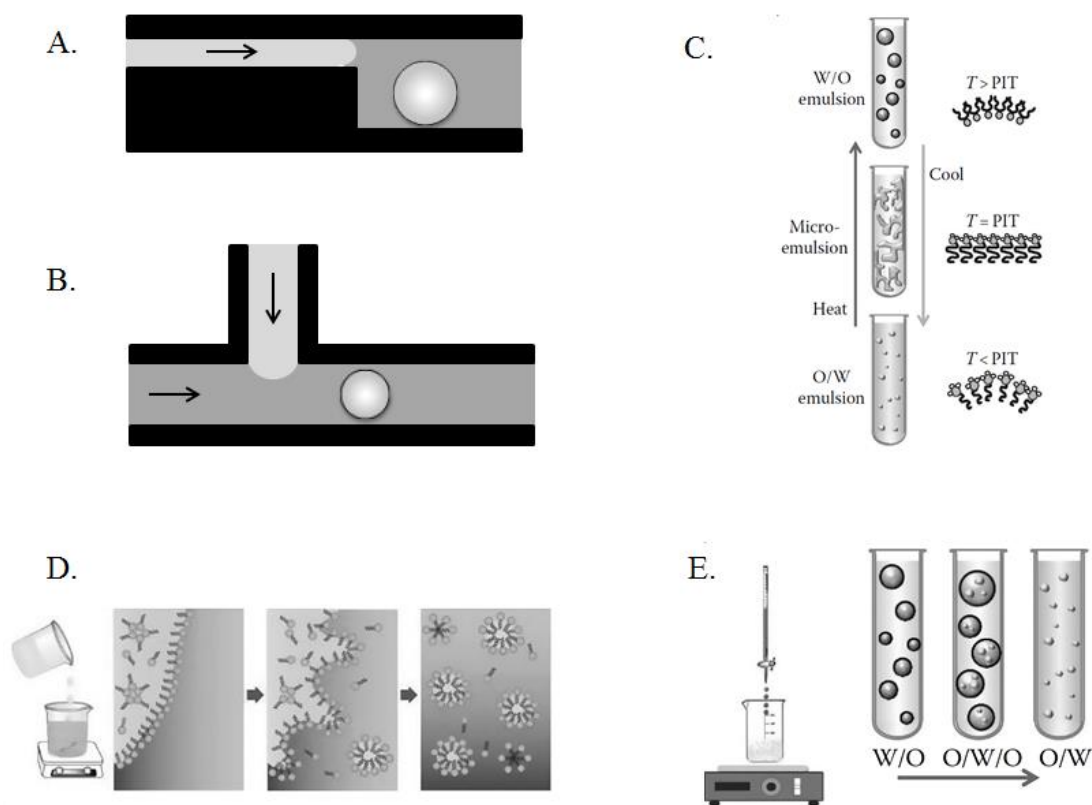


Fig. 2.5: Schematic representation of the main low-energy emulsification methods. (A - B) microfluidic emulsification, (C) phase inversion temperature, (D) spontaneous emulsification, (E) phase inversion composition. Adapted from [31].

Because of the difference of the chemical potential of the emulsifier between the two liquids the hydrophilic emulsifier will head towards the water phase forming small oil droplets. This process is described as ‘fingers’ protruding in the water which due to Rayleigh instability break into small droplets [102]. During phase composition inversion method, water is added in a mixture of oil and hydrophilic emulsifier gradually and a W/O emulsion is initially formed (Fig. 2.5E). As the volume fraction of the water increases, the W/O emulsion turns into an O/W/O double emulsion whose inner oil droplets are formed by spontaneous emulsification. By increasing further the water volume fraction an O/W emulsion is finally produced [31]. The phase inversion temperature method is based on the exploitation of the

sensitivity of nonionic emulsifiers to temperature changing (Fig. 2.5C). For example, when the temperature of an O/W emulsion stabilised by hydrophilic nonionic emulsifier exceeds the phase inversion temperature then the emulsifier becomes more soluble to the oil phase and the formation of a W/O emulsion is favoured.

2.4.3. Emulsification efficiency

During emulsification new oil-water interfacial area is generated, either by breaking down droplets or by creating new ones. In the first case, energy is required to move mechanical elements that will provide shear stress to overcome Laplace pressure and finally break down the droplet, such as in a high shear mixer. The smaller the droplet, the higher the shear stress required to break it so more energy is needed. The consumed energy is much larger due to the random dissipation in the bulk emulsion and the largest proportion that is consumed by the emulsification apparatus is converted into heat that increases the temperature of the emulsion [111]. In the second case, energy is required to push the dispersed phase into the continuous phase and to provide shear stress for droplet detachment, such as in direct membrane emulsification [112]. Nevertheless, a pump or a stirrer will be needed to recirculate the emulsion and provide shear stress through movement of the continuous phase or there will be a moving membrane, so energy is also required for these elements. As understood, the actual energy input that is required to produce an emulsion is higher than the net energy that is required to produce the oil-water interface. This would vary depending on the emulsification apparatus, the amount of material to be emulsified, the phase composition and the required throughput [91]. The concept of energy density has been used by various authors to compare the efficiency of different emulsification processes but most reported examples refer to high-energy methods such as high pressure homogenisation, colloid mill and rotor stator mixing

[91, 98]. The energy density (ε_v) illustrates the amount of mechanical energy input per m^3 of produced emulsion and it can be calculated as follows:

$$\varepsilon_v = \int_0^{t_p} P_v(t) dt \quad (2.9)$$

where P_v is the power density (W m^{-3}) and t_p is the duration of the emulsification process and is valid for all emulsification methods that utilise mechanical energy to produce emulsions. Within literature, the power consumption is used for estimating the energy density in rotor-stator mixers (e.g. by a plug-in power meter connected to the emulsification device) whereas for high-pressure homogenisation and membrane emulsification the applied pressure is used [113, 114]. However, for membrane emulsification only the incorporation of oil into the continuous phase is considered and the power consumed to move the continuous phase or the membrane to provide shear stress should not be neglected. Indeed this has been discussed in the work of Kuzikaki et al. who report the energy input required for droplet formation in membrane emulsification in the presence or absence of continuous flow [115]. In the absence of continuous phase flow, such as in dead-end emulsification where droplet detachment is spontaneous, the energy input per unit volume of emulsion accounts only for the pressure difference between the two phases [116] :

$$\varepsilon_{V,spont ME} = \frac{\Delta P V_d}{V} \quad (2.10)$$

where V_d is the volume of the dispersed phase, ΔP the transmembrane pressure and V the volume of the emulsion.

If continuous phase flow applies, such as in rotating membrane emulsification, the contribution of both should be included into the calculation of the required energy input. Thus, using equations (2.9) and (2.10), the energy density in this case is:

$$\varepsilon_v = \frac{Pt_p}{V} + \frac{\Delta PV_d}{V} \quad (2.11)$$

where V is the volume of the emulsion and P is the power consumed. The first part of the equation can be used to estimate the energy density for a conventional method such as the high shear mixer.

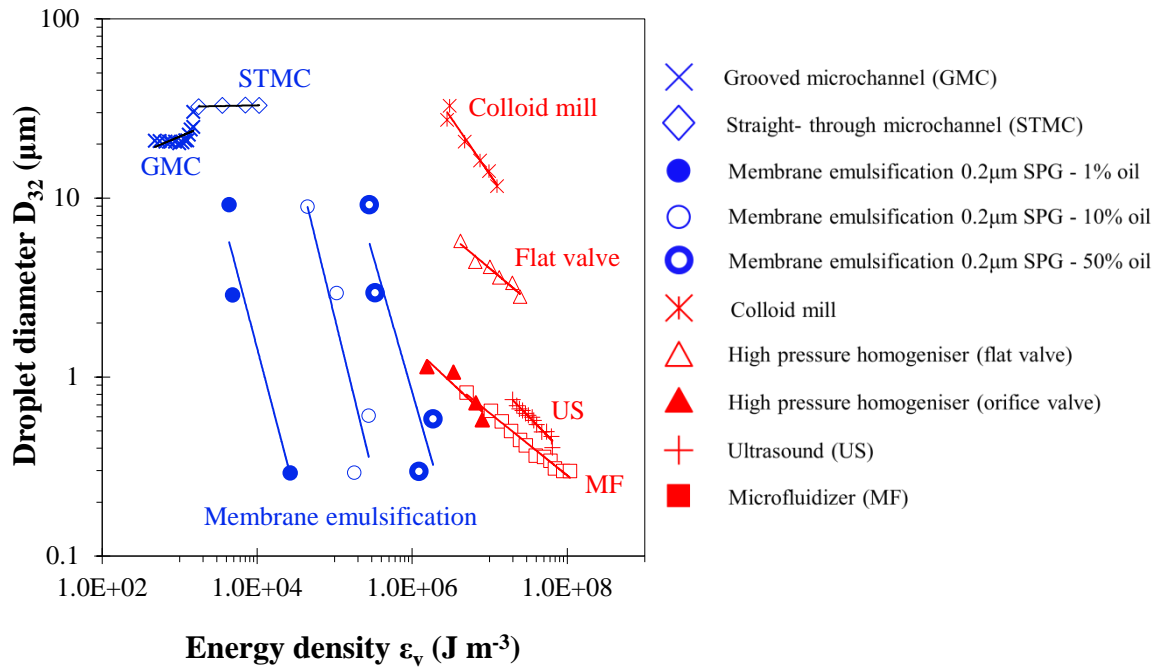


Fig. 2.6: Droplet size as function of energy density for several emulsification devices. Blue: low-energy methods, Red: high-energy methods. Adapted from [6, 91, 117].

An overview of the achieved droplet size as a function of the energy input per volume of the emulsion is illustrated in Fig. 2.6 for various low and high-energy emulsification methods. The rotor-stator homogenisers such as the colloid mill are able to produce mainly emulsions with large droplet sizes whilst with the same energy expenditure microfluidizer and high-pressure homogeniser (orifice valve) are able to produce sub-micron droplet, thus from this aspect, rotor-stator systems are not so efficient. However, this would depend on the application, so these mixers would be ideal to prepare a coarse pre-emulsion (premix) that

would then further processed with the microfluidizer or high-pressure homogeniser. Another benefit against high-pressure methods would be their capacity to breakdown viscous emulsions [31, 102]. Ultrasound emulsification at first glance it appears to be a very efficient technique in breaking down emulsions however the disadvantage comes with the limitation in the volume of emulsion that can be processed. On the other hand, low-energy methods seem to be very efficient in terms of energy usage especially membrane emulsification that can produce macroemulsions as well as nanoemulsions. The main disadvantage here could be the low emulsion production rate; a very common drawback for low-energy methods that is also encountered for microchannel emulsification [102]. However, if the application requires a monodisperse emulsion product where the uniform size of droplets and control over structure is critical for the stability and delivery of certain ingredients, e.g. drug delivery; low-energy methods are advantageous because their intrinsic low shear allows them to handle such sensitive ingredients. The low-energy consumed by these methods is translated in less dissipation of heat into the product that could be ideal, for instance, in dairy emulsion-based products as protein denaturation is hindered.

2.5. Membrane emulsification

Since its conceptualisation almost 30 years ago, membrane emulsification has been the subject of many studies for applications in the food, pharmaceutical and cosmetic sector mainly because of its capacity to produce emulsions with very narrow droplet size distribution, the mild environment of shear in which individual droplets form and the low-energy usage [118, 119]. Common applications include simple and multiple emulsions [104, 120, 121], solid organic and inorganic particles [122, 123], polymer gel beads [124, 125] and Janus (amphiphilic) particles [126].

2.5.1. Membrane technology for emulsion production

Arguably the membrane is the most crucial element in membrane emulsification as its design and properties will determine in a high degree the microstructural characteristics of the produced emulsions. The wettability of the membrane is crucial in making certain types of emulsions. Hydrophilic membranes are ideal for producing O/W emulsions or W/O/W emulsions whereas hydrophobic are used to make W/O or O/W/O emulsions. In any case the continuous phase should ideally wet the membrane material completely; that is in the first case the contact angle (measured through the water phase) formed between the membrane and the two immiscible phases should be smaller than 90 degrees whilst in the second case the contact angle should exceed 90 degrees (Fig. 2.7). For some membranes, their repeated use in emulsification ultimately results in loss of their wettability when the membrane surface stays too long in contact with the dispersed phase encouraging the expansion of the contact angle that could lead to coalescence of neighbouring droplets and thus a polydisperse product [127]. Restoring the properties of the membrane requires surface chemical modification of the membrane however this would mean more waste and costs for agents and water to treat the surface; therefore the selection of the membrane should also consider this. The internal and external pore geometries are also of major importance. The pore size of the membrane influences emulsion droplet size; indicatively the droplet to pore size ratio can range between 2.8 – 10 or more also depending on the processing and formulation parameters [123, 128].

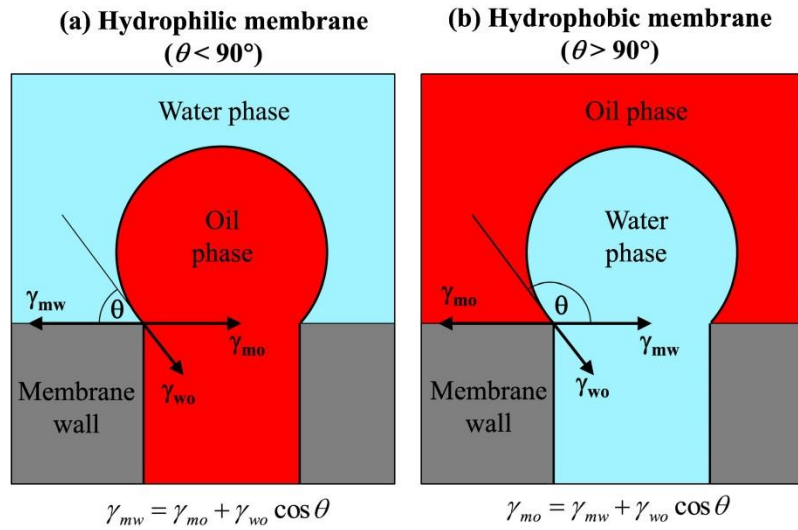


Fig. 2.7: Schematic representation of the type of emulsions produced in membrane emulsification depending on the contact angle (θ) (through the water phase) formed between the membrane and the immiscible phases: (a) for hydrophilic membranes the contact angle favour formation of O/W emulsions and (b) hydrophobic membranes ($\theta > 90^\circ$) are ideal for W/O emulsion. Adapted from [129].

Different pore shape has been seen to influence droplet formation and in particular it was found that non-circular pores (rectangular shape of different aspect ratio) produce more uniform droplets and higher throughputs than circular pores when utilised in a rotating membrane emulsification set-up [130]. The internal structure of the membrane is critical in achieving high throughputs as a membrane with tortuous pore channels and a thicker wall will result in lower production rates. Furthermore, pore spacing should be sufficient so that droplets growing in adjacent pores do not touch each other and this will also help to prevent the ‘push-off-force that causes random pre-mature droplet detachment and thus more polydisperse emulsions to be produced. Other properties a membrane should demonstrate are high resistance to mechanical stresses, broad range of available pore sizes, withstanding high temperatures and low production cost [7].

SPG (Shirasu Porous Glass) is the most common material of membranes used in membrane emulsification. This is a type of glass manufactured by mixing and melting Shirasu (volcanic ash $\text{SiO}_2 - \text{Al}_2\text{O}_3$), B_2O_3 and CaCO_3 and subsequent spinodal decomposition via phase separation of the molten mixture [131]. The result is a highly porous homogeneous material with very narrow pore size distribution and interconnected cylindrical pore channels, as revealed from visualisation of the microstructure through SEM and high-resolution X-ray microtomography [132]. The pore channel tortuosity of SPG membranes has been reported as $\xi=1.3$ where $\xi=1$ corresponds to straight- through channels and the porosity is usually in the range between 50 – 60 %. Because of the high porosity, at a given transmembrane pressure the dispersed phase velocity is distributed across the channels thus resulting in deactivation of pores; it is reported that only 10% of the pores are active [132]. SPG membranes come with a wide range of pore sizes as low as 40 nm and they are available in tubular, circular, square or disc shape from SPG Technology Co. Ltd. , Miyazaki, Japan. The hydrophobicity of SPG membranes may be enhanced by treatment with organosilanes and the porosity and hydrodynamic resistance can be improved through enzymatic reaction involving the enzyme dextransucrase and the to-be catalysed sucrose substrate [133]. The surface of the native SPG membrane is negatively charged at a pH range 2 – 8 because the silanol groups ($-\text{SiOH}$) dissociate to $-\text{SiO}^-$ upon exposure to the aqueous environment. The charge of the membrane may influence droplet formation and emulsifiers should not bind on the membrane to in order to produce more monodisperse emulsions, therefore they should carry the same sign charge [134]. For instance, anionic or nonionic surfactants should be used with negatively charged SPG membrane whereas cationic surfactants with positively charged membranes. The charge of SPG membrane surface can be rendered positive by reaction with trialkosilanes and thus cationic surfactants may be utilised to produce very monodispersed emulsions [135]. Finally,

because SPG is typically a glass material it is susceptible in mechanical stresses and easily breakable so this could make it unsuitable for certain applications or its utilisation in factory scale.

Polymeric membranes typically used in membrane emulsification are fabricated from polycarbonate and polyesters by a track-etch method [136]. These membranes are less prone to fouling than the SPG membranes because they have a membrane thickness that is almost 10 times less than SPG membranes. Despite having straight-through pore channels, their thicker membrane wall increases their hydrodynamic resistance yielding low fluxes. Polymeric membranes are much cheaper than SPG's and they can be rendered more hydrophilic by treating them with plasma.

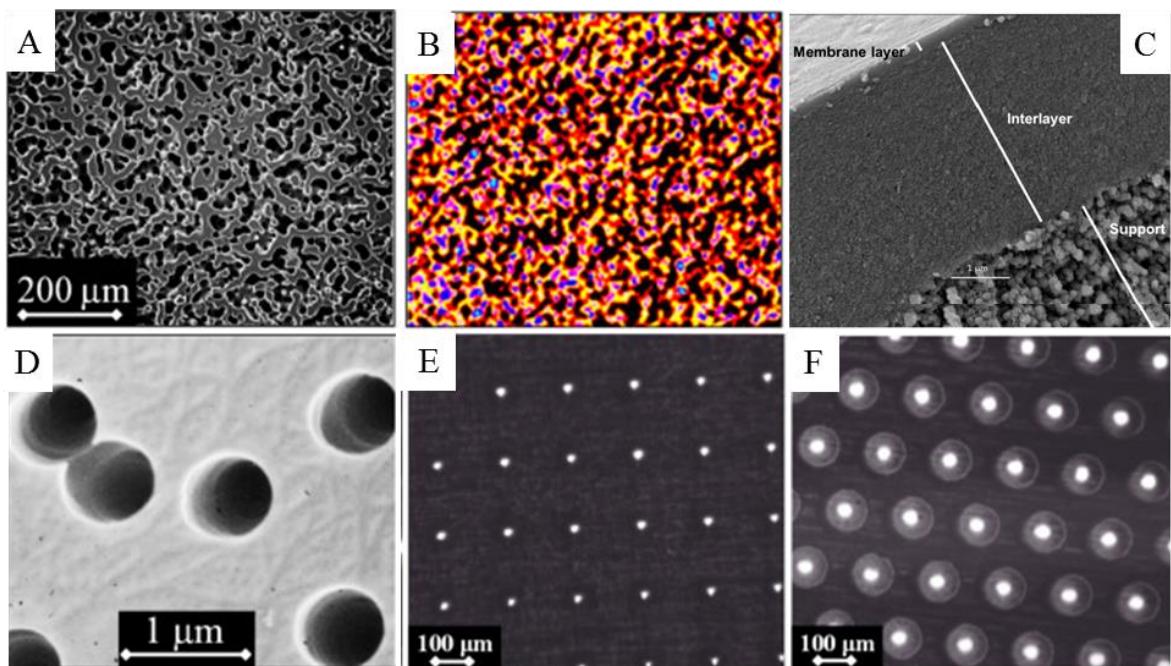


Fig. 2.8: (A-B) SEM and XMT micrographs from surface and cross-section of SPG [132], (C) SEM micrograph of cross-section of ceramic membrane [137], (D) SEM micrograph of polycarbonate membrane [138], (E) optical micrograph of laser-drilled stainless steel membrane [139], (F) optical micrograph of nickel microsieve [139].

Ceramic membranes have also been utilised to produce emulsions via membrane emulsification [140-142]. These are made of α -Al₂O₃ and they may incorporate an additional coating of TiO₂ or ZrO₂ that facilitates pore size reduction and narrower pore size distribution [112]. Ceramic membranes possess a high active pore fraction that is almost 3 – 4 times greater than SPG membranes but their porosity is lower reaching 30 – 40%. The additional coating layers and the support material increase the wall thickness and thus hydrodynamic resistance to flow whilst they can be easily fractured once stress is applied therefore, similar to SPG's, they are not suitable for industrial applications.

Metal membranes are the most promising for their application in various applications including industrial scale. These are microengineered membranes with highly uniform, controlled pore spacing and size distribution and straight-through pore channels, specially designed to maximise dispersed phase flux at high transmembrane pressure as a result of their small thickness. These properties are also making them less prone to fouling and easier to clean. Typical examples are nickel microsieves and stainless steel membranes with laser-drilled pores. Because the first have very low thickness, they are prone to deformation upon application of higher transmembrane pressures and taking into account their high manufacturing costs, their applicability in an industrial scale is still a challenge [110].

2.5.2. Membrane emulsification set-ups

The principle of membrane emulsification process is based on the formation of droplets one-at-a-time by pushing the to be dispersed phase or a coarse pre-emulsion through the pores of a membrane into an external continuous phase; this is shown schematically in Fig. 2.9. A number of membrane emulsification set-ups are available and a first classification can be made depending on whether droplets detach by applying shear from the continuous phase or

they grow at the absence of shear and detach when the capillary force is exceeded (dead-end). An example of the latter set-up also includes systems comprising of a flat disk membrane and a paddle stirrer is used to circulate the produced emulsion droplets in the continuous phase yet applying very low shear that is not sufficient to induce droplet detachment; this is known as stirred cell [143, 144]. The main disadvantage of dead-end membrane emulsification is the increased possibility of coalescence at the membrane surface. This is because, at the absence of a drag force, the droplets growing at neighbouring pores may become very large prior to their detachment. Therefore the system should be operated at low transmembrane pressure to ensure rapid adsorption of emulsifier that will decrease interfacial tension faster. This will

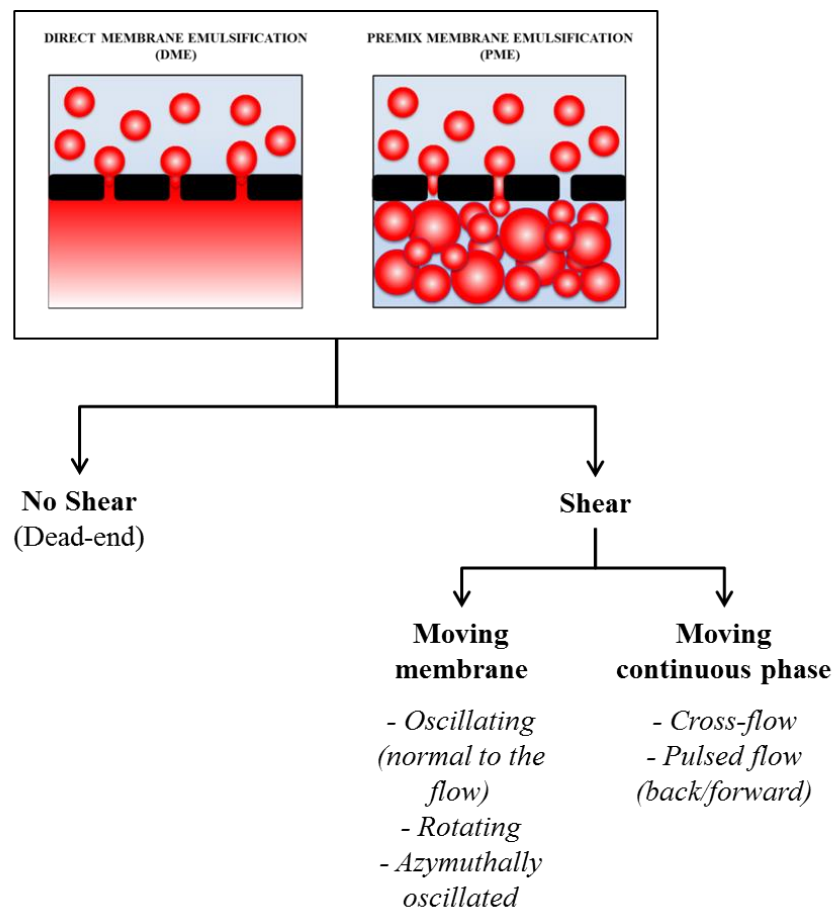


Fig. 2.9: Schematic representation of membrane emulsification configurations.

facilitate earlier droplet detachment but will result in overall lower production rates compared to membrane systems that utilise shear-induced droplet break-up [142]. At shear-based membrane emulsification systems shear is applied at the membrane surface by either moving the membrane or the continuous phase. These configurations allow for adjusting the magnitude of shear forces that the forming droplets experience thereby controlling the time that droplet spends at the membrane surface thus the droplet size can be tuned appropriately depending also on the formulation and the viscosity of both phases. At the same time, the induced continuous phase flow helps to carry away droplets from the membrane proximity and dissipates them throughout the bulk allowing for more homogenous mixing. Either way, the droplets are swept away promptly before they grow too large thus a larger transmembrane pressure can be applied resulting in higher production rates compared to dead-end systems.

2.5.2.1. Moving continuous phase

Cross-flow

Cross-flow membrane emulsification is the most common type of moving continuous phase systems and it has been used both in laboratory and pilot scale to produce various formulations [13, 145]. The configuration of such a system usually consists of a tubular membrane with the continuous phase recirculating in one side of the membrane and flowing parallel to the membrane surface whilst the dispersed phase at the opposite side is pressurised and pushed through the membrane pores into the continuous phase. Two configurations have been reported. The majority of the studies have been performed with the continuous phase positioned at the interior of the tubular membrane while the dispersed phase is introduced from the outer membrane surface. Hancock *et al.* utilised a cross-flow system where the continuous phase is placed at the outer surface as this would prevent collision of droplets

following detachment and shear [141]. A challenge encountered in such systems is the post droplet formation break-up associated with the shear stresses or cavitation that is exerted by the positive displacement or peristaltic pumps used to recirculate the emulsion. In such case, polydisperse emulsions may be produced, however this could be significantly improved when smaller droplets with Laplace pressure higher than the disruption forces are formed by the membrane, therefore production of nanoemulsions through such systems may be advantageous.

Pulsed flow

Recirculation can be avoided utilising pulsed flow to move the continuous phase. This technique has been studied by Holdich *et al.* and it adopts a similar configuration to cross-flow, only in this case the continuous phase is pulsed in both directions parallel to the membrane module with a pulse frequency up to 50 Hz [4]. In this way, emulsions with high dispersed phase fraction (44%) and very uniform were produced. The major disadvantage with this set-up is the excessive shear close to the membrane pores that may lead to through-membrane pore pressure fluctuations leading so finer droplets are formed, however this could be overcome by using a more viscous continuous phase or merely by increasing the dispersed phase injection rate.

2.5.2.2. Moving membrane

Oscillating (vibrating)

This class of membrane systems is represented by membranes whose oscillating or rotating motion within the continuous phase induces shear that in turn encourages droplet detachment. The former configuration involves a membrane that oscillates tangentially clockwise or counter-clockwise in defined periods [146] or parallel to the module's axis with up and down

oscillations [147]. The oscillation frequency ranges between 10 - 90 Hz resulting in emulsions with a dispersed phase fraction as high as 40%.

Rotating

Rotating membrane emulsification (RME) is the process of primary concern that is discussed in this study. A typical set-up consists of a tubular rotating membrane that is submerged in a continuous phase vessel while the dispersed phase is pressurised with compressed air or nitrogen (more details see materials and methods). RME is operated in semi-batch mode whilst most of the studies report for direct rather than premix configurations. The attribute of this method against the other membrane systems is the centrifugal force that is applied to the forming droplets due to the rotation of the membrane. This results in droplets being ‘pulled’ into the continuous phase and detach easier whilst they are carried away from the membrane surface towards the vessel walls reducing the possibility of coalescence at the membrane vicinity. The centrifugal force also results in earlier detachment and thus smaller droplets whilst RME utilises less shear compared to cross-flow systems that make it ideal for very sensitive structures such as multiple emulsions [140].

RME was initially introduced in the work of Schädler *et al.* early in 2005 at the 10th Aachen Membrane Colloquium in Germany where the authors presented their pilot-scale rotating membrane apparatus consisting of a nickel microsieve and varying rotational velocities and gap size whilst dispersed phase throughput was kept constant (Table 2.1). They demonstrated that increasing the gap between the membrane and the continuous phase vessel or increasing the rotational velocity resulted in enhanced formation of Taylor vortices and smaller droplet size, regardless the dispersed phase volume fraction [9]. Following this work, the groups from University of Leeds (R.A. Williams) and Loughborough University (G. Vladisavljevic, formerly in the University of Belgrade) have contributed significantly in this field, focusing

on RME systems for the production of a range of emulsions with uniform droplet size. In their studies, a stainless steel laser-drilled membrane with circular pores of average pore diameter 100 μm is used to evaluate the effect of the rotational velocity and transmembrane pressure for simple O/W emulsions stabilised with hydrophilic or hydrophobic emulsifiers, occasionally using a carbomer to thicken the continuous phase [148, 149]. The droplet size decreased upon increasing the rotational velocity at a fixed transmembrane pressure (3 kPa, close to the critical capillary pressure for the specific pore size and emulsifier) and the increased viscosity of the continuous phase (induced by addition of the carbomer) did not seem to affect emulsion microstructure. The droplet size was found to be affected by the pore geometry as Yuan *et al.* showed that slotted pores may perform better in terms of reducing the droplet size compared to circular pores at lower rotational velocities with a more uniform droplet size (coefficient of variation $\sim 5\%$) [130, 150]. A hydrophobic stainless steel membrane (pore size 100 μm) was used for production of agarose W/O emulsions via RME which after emulsion solidification formed uniform beads with an average diameter of 220 μm and span 0.76 at the optimum process conditions [151].

SPG membrane has also been reported in RME to produce O/W emulsions stabilised by various emulsifiers including WPI protein [152, 153]. A novel approach to form O/W emulsions is reported by placing the hydrophilic nonionic emulsifier in the oil rather than the water phase that resulted in smaller droplets, a technique resembling spontaneous emulsification [154].

Table 2.1: Overview of types of emulsions produced via rotating membrane emulsification.

Material /pore size	Droplet size	Product	Production rate/ flux/ flow rate/ Transmembrane pressure	Rotational velocity/ Shear rate	CV/ Span	Reference
Nickel microsieve 5 μm	6 – 11 μm	Sunflower W/O emulsions stabilised with PGPR	Fixed 12 L h ⁻¹	0 – 8000 rpm	Not specified	[9]
Stainless steel 100 μm	81 – 567 μm	Paraffin wax in water emulsions stabilised with Tween 20, SDS	3 kPa	0 – 1500 rpm	CV 9.8 – 33.6%	[148]
Stainless steel 100 μm	79 – 250 μm	Paraffin wax in water emulsions stabilised with Tween 20	3 kPa	50 – 1500 rpm	CV 4.8 – 20%	[149]
Stainless steel, different pore geometry (48 – 136 μm)	150 – 500 μm	Paraffin wax in water emulsions stabilised with Tween 20	0.075 – 75 mL h ⁻¹	250 – 1000 rpm	CV 5 – 23%	[130, 150]
Stainless steel 100 μm	108 – 385 μm	Agarose beads (W/O emulsion stabilised by hexaglycerinpentaeste r (PO-500))	Not specified	500 – 2000 rpm	Span 0.51 – 1.38	[151]
SPG 1 μm Ceramic 1 μm Stainless steel 15 μm	1 – 32 μm	Sunflower O/W emulsions stabilised by Tween 20, Tween 80, SDS, Lecithin, PGPR	10 – 250 kPa	300 – 2000 rpm	Not specified	[140]

SPG 2.8 μm	8 – 30 μm	Sunflower O/W emulsions stabilised by Tween 20, WPI	25 – 100 kPa	300 – 1500 rpm	Not specified	[152]
SPG 6.1 μm	23 – 216 μm	Sunflower O/W emulsions stabilised by Tween 20	10 – 180 kPa (50 – 12,500 L m ⁻² h ⁻¹)	100 – 2000 rpm	Span 0.72 – 2.21	[153]
SPG 6.1 μm	6 – 138 μm	Sunflower O/W emulsions stabilised by Tween 20, SDS, Brij 97, lecithin (placed in oil or in water phase)	20 – 150 kPa	100 – 2000 rpm	Not specified	[154]
Stainless steel, square 80 x 80 μm	68 - 2,700 μm	Triglycerin O/W emulsions stabilised by silica particles	0.075 – 75 mL h ⁻¹ (0.8 – 800 L m ⁻² h ⁻¹)	500 – 1500 rpm	0.3 – 0.7%	[13]
Stainless steel, square 80 x 80 μm	150 – 2,700 μm	Triglycerin O/W emulsions stabilised by silica particles	0.075 – 75 mL h ⁻¹ (0.8 – 800 L m ⁻² h ⁻¹)	500 – 1500 rpm	Not specified	[12]
Stainless steel, square 80 x 80 μm	130 – 397 μm	Paraffin, ethyl acetate, sunflower O/W emulsions (co-) stabilised by particles (silica, PDMA – PMMA PS latex) and emulsifiers (SDS, HDTMABr, Tween 20)	Fixed 50 kPa	Fixed 1000 rpm	10.2 – 33.7%	[15]

The long-term stability induced by adsorption of colloidal particles at liquid-liquid interfaces also attracted interest for the production of particle-stabilised emulsions via RME. Currently three studies report utilisation of colloidal solid particles (silica, PDMA-PMMA PS latex particles) alone or in combinations with various types of low molecular weight emulsifiers [12, 13, 15]. A critical adsorption time existed for sufficient coverage of droplets by particles and this could be controlled by the oil flux and the rotational speed of the membrane [12, 13]. Additionally, effective co-stabilisation of emulsions depended on the interactions between particles and emulsifiers and their concentrations in the bulk phase [15].

2.5.3. Factors influencing emulsion microstructure in DME

The prediction of the droplet size and distribution of an emulsion prepared with the membrane emulsification process is not an easy task as it involves many parameters that influence the emulsion microstructure simultaneously. Overall, three main groups are distinguished and

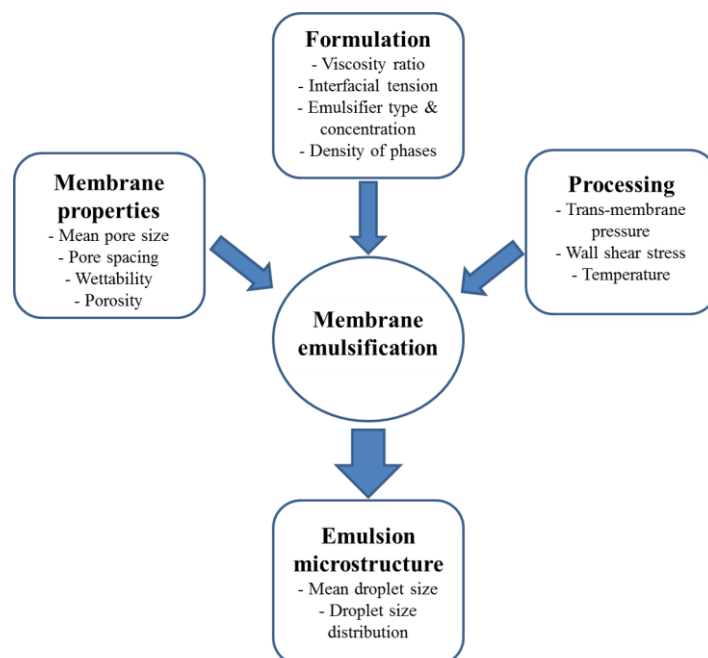


Fig. 2.10: Factors influencing emulsion microstructure as delivered by membrane emulsification.

they are related with the formulation. processing and membrane properties as it can be seen in Fig. 2.10 [112]. In order to discuss these, it is necessary to understand droplet formation mechanisms from droplet growth to detachment from the membrane and the forces that are involved. A force balance model is used to describe single droplet formation and detachment from a membrane pore. According to this model, droplet formation and detachment is a consequence of an imbalance of forces acting on the droplet emerging from the pore. The following forces have been identified [142, 155]:

- *Interfacial tension or capillary force (F_γ):* is the force exerted by the dispersed phase and resists detachment of the droplet.

$$F_\gamma = \gamma \pi d_p \quad (2.12)$$

where γ is the interfacial tension between the two phases and d_p is the average membrane pore diameter.

- *Static pressure force (F_{SP}):* is the force applied to the droplet due to the difference in the pressure between the continuous and the dispersed phase.

$$F_{SP} = \frac{\gamma \pi d_p^2}{D} \quad (2.13)$$

where D is the average droplet diameter.

- *Dynamic lift force (F_L):* is the component of the force applied by the fluid on the surface of a droplet at a perpendicular direction to the flow. The other component is the viscous drag force that is parallel to the flow direction.

$$F_L = \frac{k_L \tau_w^{1.5} D^3 \rho_c^{0.5}}{\eta_c} \quad (2.14)$$

where k_L is the lift coefficient (equal to 0.765 [156]), τ_w the wall shear stress, ρ_c the continuous phase density and η_c the continuous phase viscosity.

- *Buoyancy force* (F_{BG}): is the force generated by the difference in the densities of the two phases.

$$F_{BG} = \frac{\pi D^3 (\rho_c - \rho_d) g}{6} \quad (2.15)$$

- *Inertial force* (F_I): the force caused by the dispersed phase flow through the membrane pore.

$$F_I = \rho_d u_d^2 \alpha_n \quad (2.16)$$

where u_d is the average dispersed phase velocity within the membrane pore and α_n is the cross sectional area of the droplet neck.

- *Viscous drag force* (F_D): exerted by the continuous phase due to the flow that can be in a direction parallel to the membrane (cross-flow) or tangential to the membrane (RME) and is valid for Reynolds numbers smaller than 1000. This expression results from Stokes [157] and in the latter case of RME:

$$F_D = 3k_w \pi \eta_c u_{cm} D \quad (2.17)$$

where k_w is the wall correction factor (equal to 1,7 for RME [158]), u_{cm} is the velocity difference between the continuous phase and the membrane surface and is usually approximated with the tangential velocity of the droplet at the membrane surface, u_t where $u_t = \omega R$, with ω the angular rotational velocity and R the distance between the centre of the membrane and the centre of the droplet and R_l the membrane radius. The angular velocity is $\omega = 2\pi N/60$ where N is the rotational velocity of the membrane in rpm.

- *Push-off force* ($F_{push-off}$): this is the force applied between sterically stabilised droplets as they grow in adjacent pores and contributes to their detachment. This has been derived by Kosvintsev *et al.* [143]:

$$F_{push-off} = \frac{\gamma\pi D^3 L_s \arcsin\left(\frac{(D^6 - L_s^6)^{\frac{1}{2}}}{D^3}\right)(D^6 - 2L_s^6)}{2(D^6 - L_s^6)^{\frac{3}{2}}} + \frac{\gamma\pi d^2 L_s^7}{2(D^6 - L_s^6)\left(\frac{L_s^6}{D^2}\right)^{\frac{1}{2}}} - \frac{2\gamma\pi L_s^2}{3D} \quad (2.18)$$

where L_s is the pore spacing and arcsin is the inverse of the sine function.

A schematic representation of all possible forces acting on a droplet before detachment during RME can be seen in Fig. 2.11.

Two studies report on models that consider the rotational motion of the membrane [151, 158]. In both studies, only the interfacial tension and the viscous tangential drag forces are considered. The buoyant force is neglected because the density difference between the two liquids is minimal and the magnitude of the dynamic lift and inertial forces is much lower than the rest of the forces acting on the droplet [142]. The static pressure force is also neglected when the droplet diameter is equal or greater than the neck diameter (the neck diameter is approximated to the membrane pore diameter [159]). A push-off force should also be considered according to *Egidi et al.*, but this is not expected to be applicable for SPG membranes [143].

Using a torque balance, the droplet size can be predicted as:

$$D = d_p \left(\frac{2\gamma}{3k_w r \eta_c \omega} \right)^{1/2} \quad (2.19)$$

where d_p is the average membrane pore diameter, γ the interfacial tension between oil and water phases, r the distance between the central axis of the membrane and the droplet centre, η_c the viscosity of the continuous phase and ω the angular velocity of the membrane surface. As it can be seen from Eq. (2.19) the droplet size decreases when smaller membrane pore size is used, and also with decreasing interfacial tension. Lower interfacial tension force leaves the

droplet exposed to higher detachment forces (Fig. 2.11) thus the droplet detaches earlier and possesses a smaller volume. This was experimentally confirmed by Van der Graaf *et al.* [160]. Furthermore, the droplet size reduces with increasing continuous phase viscosity and rotational velocity which is also reported by Pawlik *et al.* as a result of the increased viscous drag force [152].

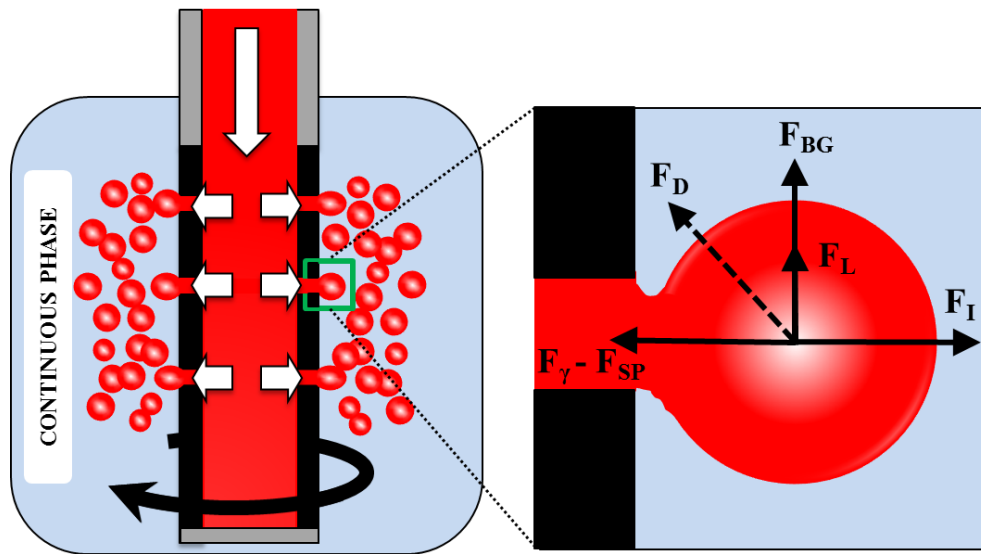


Fig. 2.11: Simplified schematic representation of forces applied on a droplet during RME.

The viscous tangential drag force (F_D) points towards the paper surface.

However, the experimental calculations may present variations due to the model limitations. Firstly, the volumetric contribution through the neck of the droplet during the detachment stage is not considered. This could lead to a significant underestimation of the droplet size because droplets will detach without experiencing ‘necking’ [155]. The rest of the limitations concern the membrane properties such as the pore spacing, pore geometry and wettability. Droplets may be spontaneously deformed from membrane pores that are not perpendicular to the membrane surface or they have a non-circular geometry such as SPG membranes or microsieves. The droplets emerging from such pores are initially deformed due to the asymmetrical forces acting on them, therefore in order to regain a more thermodynamically

favourable status (that is the minimum surface free energy) they detach to adopt a spherical shape instantaneously [161]. The latter mechanism also occurs at low shear and high dispersed phase fluxes due to the ‘push-off’ force and this can affect the accuracy of the model [159]. As the droplets grow from adjacent pores and permeate in the continuous phase, provided they are sufficiently stabilised with emulsifier, a ‘push-off’ force is generated due to steric hindrance that causes droplets to deform and finally they detach as described earlier resulting in smaller droplet size than expected. This mechanism occurs when fast diffusing/adsorbing emulsifiers are used ensuring fast coverage of droplets, whilst membranes with high active pore fraction and small short pore spacing (e.g. laser drilled metal membranes with straight-through pores) are more likely to enhance this event. [143, 159]. Finally, membrane wettability is also not considered. If the dispersed phase wets the membrane (large contact angle between membrane-oil-water) it may result in contact line expansion thus the droplet may occupy two or more pores ultimately leading to detachment and formation of larger droplets [127].

Having seen the types of forces acting on the droplets during DME, two mechanisms may be distinguished depending on which forces prevail [162]. In shear-controlled DME shear stresses dominate droplet formation and larger droplets are produced with increasing dispersed phase flux due to the contribution of the neck during the detachment stage [163]. This mechanism occurs typically in membranes that include circular pores e.g. laser drilled metal and microsieve screens and an example is the ‘push-off force’ droplet formation that was described earlier. Droplet formation can also occur under the interfacial tension (spontaneous detachment)-controlled mechanism involving two regimes that are defined by the dimensionless capillary number of the dispersed phase:

$$Ca_d = \frac{\eta_d u_d}{\gamma} \quad (2.20)$$

where η_d is the viscosity of the dispersed phase and u_d is the average velocity of the dispersed phase inside the pore which can be calculated by the Fanning equation for laminar flow in a cylindrical tube:

$$u_d = \frac{d_p^2}{32\eta_d L_p} \Delta P \quad (2.21)$$

$$L_p = \xi L_m$$

where d_p is the average membrane pore diameter, ΔP is the transmembrane pressure and L_p is the length of the pore channel which is calculated by multiplying the membrane thickness L_m by the mean pore tortuosity ξ (1 for straight-through channels and 1.3 for SPG membrane [132]).

The dispersed phase capillary number then can be used to evaluate the droplet formation regime. When the interfacial tension force (denominator) exceeds the inertial forces (numerator) the droplet forms in the dripping regime and it does not depend on the dispersed phase flux or the shear stress. Dripping occurs at low dispersed phase fluxes where Ca_d is small. At higher fluxes the inertial forces dominate and the droplets form at the continuous outflow regime where they become large prior to their detachment. If the dispersed phase flux is maintained high and high shear is applied, a filament of dispersed phase (jet) will form parallel to the membrane surface and the droplet will detach due to Rayleigh instabilities [164]. A third regime may occur known as a squeezing regime that is likely to occur at low dispersed fluxes and low shear for droplets growing in a narrow downstream channel, however this is unlikely to happen in membrane emulsification as the annular gap between the membrane and the continuous phase vessel wall is much larger than the droplets. Indicatively,

Siugura *et al.* have proposed that transition occurs when the dispersed phase capillary number exceeds roughly 0.056 [162]. Because jetting may cause droplets to break-off randomly very polydisperse emulsions are produced, therefore emulsification in the dripping regime is suggested to ensure high uniformity. Transition from dripping to continuous outflow and jetting does not occur at the same time for all droplets growing at different pores due to different local hydrodynamic conditions at the proximity of each pore.

Finally, the emulsion microstructure is also influenced by the hydrodynamic conditions in the continuous phase and close to the membrane surface so these must also be considered. In RME, operation at high rotational velocities is expected to increase the shear that is applied on the droplets during their formation on the pores thus increasing the magnitude of viscous drag force resulting in smaller emulsion droplets. The shear rate on the membrane surface has been calculated by Vladislavjevic *et al.* based on concentric cylinders geometry (assuming cylindrical continuous phase vessel):

$$\dot{\gamma}_{RME} = \frac{\pi R_1^2 N}{15(R_2^2 - R_1^2)} \quad (2.22)$$

where N is the rotational velocity, R_1 is the outer radius of the membrane and R_2 the inner radius of the emulsion production vessel.

High rotational velocities are possible to give rise to turbulence in the same way it was described for conventional high energy mixing in previous sections and as a consequence Taylor vortices may form in the continuous phase close to the forming droplets. The dimensionless Reynolds is used once more to predict the flow regime in RME however this is adjusted to take into account the concentric cylinder geometry where the inner cylinder rotates. This has been developed by Schadler *et al.* and can be estimated as follows:

$$Re_c = \omega R_1 (R_2 - R_1) \frac{\rho_c}{\eta_c} \quad (2.23)$$

where Re_c is the Reynolds number of the continuous phase, ω the angular velocity of membrane surface, ρ_c the density and η_c the viscosity of the continuous phase. Increasing the gap size and the rotational velocity results in increase in turbulence and the formation of turbulent eddies can be predicted by the Taylor number:

$$Ta = Re_c \sqrt{\frac{2(R_2 - R_1)}{R_1 + R_2}} \quad (2.24)$$

There is a critical Taylor number (~ 41.3) above which small Taylor vortices appear and the flow regime changes from laminar to turbulent inertial. As it can be seen from Eq. (2.23) and (2.24) formation of Taylor vortices is favoured when continuous phases of low viscosity are used.

Chapter 3

Materials and Methods

3.1. Materials

Emulsions were made from distilled water (de-ionised and filtrated in a reverse osmosis unit) and commercial sunflower oil with a viscosity of 0.066 Pa s and density 915 g/l. Particles used as emulsifiers were Ludox SM colloidal silica provided in aqueous suspension 30 wt.%, hydroxypropyl methyl cellulose powder (HPMC, $M_n \approx 10000$), colloidal microcrystalline cellulose (CMCC) and rutin hydrate, all purchased from Sigma - Aldrich, UK. The refractive index (RI) in water was found in the MSDS data sheet from the supplier's database: sunflower oil (1.467), CMCC (1.470), Rutin (1.765), silica (1.450), HPMC (1.470).

Polysorbate 20 (Tween 20) with HLB 16.7 was used as LMW emulsifier and was provided from Sigma - Aldrich, UK as a yellow viscous liquid with a CMC of 0.098 g L^{-1} in the continuous phase (or 0.09 wt.% in a 10 wt.% O/W emulsion).

Whey protein isolate (WPI) was used as high molecular weight (HMW) emulsifier and was provided from Volac UK with a protein content of 91%, fat 0.8%, ash 3%, lactose 3%, bulk density of 0.43 g/ml and 5.5% moisture. Sodium azide was purchased from Sigma - Aldrich UK. Hydrochloric acid (HCl 30 wt.% solution) and sodium hydroxide (NaOH pellets) were also purchased from Sigma - Aldrich UK.

3.2. Methods

3.2.1. Preparation of continuous phase

3.2.1.1. Particle suspensions

Aqueous suspensions of silica particles were prepared by diluting the original 30 wt.% suspension with distilled water to the desired concentration and the pH was adjusted to 2 with

HCl solutions (0.5M and 1M) to decrease the surface charge of particles and enable them to pack closely once they adsorb to oil droplet surface in order to prevent destabilisation.

Suspensions of HPMC, CMCC and rutin particles were made by dissolving the powder in distilled water and were kept at their native pH. All particle suspensions were heated at 45°C for 45-50 mins whilst agitating with a magnetic stirrer. Following this, they were processed in batches of 80 g with an ultrasonic probe (VC750 Ultrasonic Vibra-Cell processor, Sonics & Materials Inc, USA) at 20 kHz for 2 minutes and they were left stirring until cooled down to ambient temperature.

3.2.1.2. Solutions of emulsifiers

Solutions of emulsifiers were made by dissolving the required amount of Tween 20 or WPI in distilled water whilst agitating gently with a magnetic stirrer overnight. The pH was adjusted by addition of HCl or NaOH from stock solutions (0.5M or 1M).

3.2.1.3. Particle-emulsifier mixtures

The aqueous mixtures of particles and Tween 20 were prepared by adding the appropriate amount of Tween 20 in the particle suspension followed by ultrasound treatment as described previously. For the preparation of the mixtures of particles and WPI, the particles were added in the WPI solution, followed by ultrasound. Prior to ultrasound, the pH of the mixtures containing silica particles and HPMC particles was adjusted to 2 and 6.5 respectively. Stock solutions of HCl and NaOH 0.5M and 1M were prepared and where necessary, the pH of the aqueous phase was adjusted.

For all continuous phases containing WPI, sodium azide was used at a concentration of 0.01 wt.% to prevent bacterial growth.

A summary of the continuous phases and their abbreviations used in Chapter 5 can be seen in Table 3.1.

Table 3.1: Composition of continuous phase and their abbreviations used in Chapters 5 & 6. Concentration of all particles was 3 wt.% in all cases. Concentrations were in wt.%: weight of individual species over the weight of the final emulsion.

Aqueous phase	Abbreviation
3% Silica	S
3% HPMC	H
0.05% Tween 20	0.05T
3% Tween 20	3T
0.05% WPI	0.05W
3% WPI	3W
3% Silica / 0.05% Tween 20	S / 0.05T
3% Silica / 3% Tween 20	S / 3T
3% Silica / 0.05% WPI	S / 0.05W
3% Silica / 3% WPI	S / 3W
3% HPMC / 0.05% Tween 20	H / 0.05T
3% HPMC / 3% Tween 20	H / 3T
3% HPMC / 0.05% WPI	H / 0.05W
3% HPMC / 3% WPI	H / 3W

3.2.2. Emulsification

Oil-in-water emulsion batches of 110 g containing 10 wt.% oil in all cases were produced in a 150 ml emulsion production vessel with 55 mm internal diameter. All concentrations are expressed as weight fractions: weight of individual species over the weight of the final emulsion (wt.%). Emulsions were produced via a rotating membrane and a high shear mixer.

3.2.2.1. Rotating Membrane Emulsification (RME)

A rotating membrane emulsification device was used to make 110 g of emulsion that contained 10 wt.% oil at different rotational velocities and transmembrane pressures (Fig. 3.1).

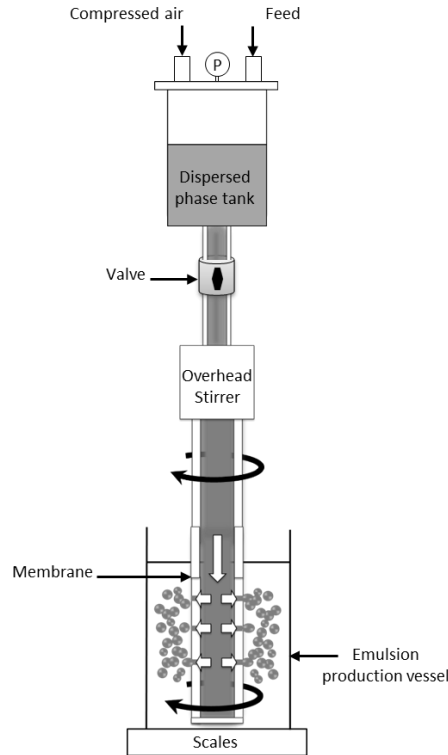


Fig. 3.1: Schematic representation of rotating membrane emulsification set-up.

It consisted of a dispersed phase tank connected with an overhead stirrer under which a metal shaft was placed and a tubular membrane was connected at the bottom of the shaft. Two types of membranes were used, a hydrophilic Shirasu Porous Glass (SPG Technology Co. Ltd, Miyazaki, Japan) and a laser-drilled Stainless Steel membrane (Laser Micromachining Limited, UK); their properties can be seen in Table 3.2. The membrane was allowed to soak in the continuous phase overnight prior to emulsification the next day. Then it was submerged

into a cylindrical plastic vessel with a 55 mm internal diameter which was filled with the continuous phase. A balance was placed under the emulsion production tank to calculate the amount of oil dispersed during the experiment. The sunflower oil was allowed to fill the membrane which also facilitated removal of air from the system and the dispersed phase tank was pressurised with compressed air. The rotational speed was set on the overhead stirrer and the experiment was initiated by opening the dispersed phase valve. Once the desired mass of the dispersed phase was read on the balance, the valve and the overhead stirrer were switched off and the emulsion was taken for analysis within the day. After finishing the experiment the membrane was sonicated in Tween 20 solution until the solution was clear. The same was repeated with pure ethanol for 3 hours and after rinsing with distilled water the membrane was dried in the oven for 12 h at 60 °C followed by sonication in distilled water.

Table 3.2: Specifications of membranes used in this study. The porosity of SPG membrane has been estimated by [132] and of SS is calculated in Appendix C.

Membrane specifications	SPG	SS
Material	Shirasu Porous Glass	Stainless steel
Average pore diameter, d_p (μm)	6.1	50
Porosity (%)	56	0.8
Tortuosity, ζ (-)	1.23	1
Wall thickness, L_m (mm)	1	1
Length (mm)	45	60
Outer radius, R_l (mm)	5	5
Effective surface area, A_m (cm^2)	14.1	15.7

3.2.2.2. High Shear Mixer (HSM)

A Silverson L5M high shear mixer with a stainless steel screen (I.D. 22 mm, wall thickness 0.5 mm), containing circular pores of 1 mm diameter and 21 mm impeller was also used to produce emulsions. The entire amount of oil was directly poured into the vessel which contained the aqueous suspension phase and the rotational speed of the impeller was set at

4000, 7000 and 10000 rpm (max. speed). The process time varied between 1 – 3 minutes and determined the production rate.

An overview of the operating parameters can be seen in Table 3.3. The shear rate is used instead of the shear stress as the latter is changing with varying rotational velocity for shear thickening continuous phases. This has been calculated by Eq. (2.22) and Eq. (2.4) for RME and HSM respectively.

Table 3.3: Operating conditions and shear rate values for all emulsification systems.

Emulsification process		Rotational velocity (rpm)	Shear rate (s⁻¹)
Rotating Membrane (RME)	Transmembrane	100	0.7
	Pressure	1000	7.2
	10 – 150 kPa	2000	14.3
High Shear Mixer (HSM)	Processing time 1 – 3 mins	4000	8800
		7000	15400
		10000	22000

3.2.3. Analytical techniques

3.2.3.1. Particle and emulsion droplet size measurement

The particle size of suspensions and emulsion droplet size were determined by static multi-angle light scattering (SMLS) [165] using a Mastersizer (Malvern Instruments, UK) with a Hydro 2000 SA suspension cell unit. The refractive index of sunflower oil was used to determine the emulsion droplet size, whereas the refractive indices of the particles were used to measure the particle size of the particle suspensions. For mixtures of particles and emulsifiers the refractive index of the particle was used. For suspensions with particle size less than 1 μm a Zetasizer Nano ZS (Malvern Instruments, UK) was used deploying dynamic light scattering (DLS) [166]. Particle size measured with Zetasizer was expressed as the Z-

average or cumulants mean (Z_D), while the polydispersity index (PDI) was used to describe the width distribution. PDI values between 0.1 – 0.4 are considered highly monodisperse values whereas greater than 0.4 are considered more polydisperse [167]. Emulsion droplet size was expressed as D_{43} (volume weighted mean) but another expression is also met D_{32} which is the surface weighted mean diameter. Within this thesis, the emulsion droplet size was reported as D_{43} unless stated otherwise and the value of span represented the width of the distribution. The lower the span value, the more monodisperse an emulsion is, but definite values have not been reported.

$$D_{43} = \frac{\sum n_i D_i^4}{\sum n_i D_i^3} \quad (3.1)$$

$$Span = \frac{D_{90} - D_{10}}{D_{50}} \quad (3.2)$$

$$PDI = \frac{\sigma^2}{Z_D^2} \quad (3.3)$$

Where n_i is the number of droplets, D_i ($i=1 - 100$) indicates the volume diameter of which n% of the volume distribution is below this value, σ is the standard deviation (assuming a Gaussian size distribution), and Z_D is the intensity-weighted mean diameter. Stability of the emulsions was evaluated by measuring emulsion droplet size throughout a 3 week period.

3.2.3.2. Zeta-potential measurements

Zeta potential was measured by electrophoretic light scattering [168] using a Zetasizer Nano ZS (Malvern Instruments. UK). Zeta potential and Z-average size were simultaneously recorded using a MPT-2 Titrator attached to the Zetasizer main unit. Prior to titration, the

samples were prepared at native pH and then the pH was adjusted with 0.1M HCl and NaOH as titrants.

3.2.4. Microstructure visualisation

Images of oil droplets and the membrane surface were captured by a light microscope (Leica DM 2500 LED). A drop of each emulsion sample was placed on a thin glass slide under the microscope and analysed in different magnifications. Membranes were placed directly under the microscope and light was illuminated properly towards the surface to obtain a clear view of the pores. Cryogenic scanning electron microscopy (Cryo-SEM; Philips XL30 FEG ESSEM) was also used to visualise oil droplet surface. One drop of the emulsion was placed on a sample holder and was frozen to -173 °C with liquid nitrogen. Then the sample was transferred to a preparation chamber; the heating was turned on to reach a temperature of -90 °C and the samples were fractured under vacuum in order to remove water components. The heating was turned off, and the samples were dusted with gold particles and scanned whilst maintaining the temperature at -140 °C with the addition of liquid nitrogen.

The surface of oil droplets stabilised by rutin hydrate was visualised through atomic force microscopy (AFM). The droplets were imaged on the imaging-intermittent Contact mode on the atomic force microscope (JPK Instruments, Germany). The measurements were carried out in the diluted emulsion sample with a probe having a spring constant 2.7 N m^{-1} and resonance frequency 80 kHz (Windsor Scientific, UK). The images acquired were analysed with JPKSPM data processing software.

3.2.5. Viscosity measurements

The apparent viscosity of the continuous phase was measured as a function of shear rate with a Kinexus Pro rotational rheometer (Malvern Instruments, UK). A cup and bob geometry was used at 20°C for a range of shear rates between 0.1 and 100 s⁻¹. The viscosity flow curves were fitted to the power law model and the obtained consistency (A) and power law index (n) values were used to evaluate (non-) Newtonian performance of the continuous phase:

$$\eta_c = A\dot{\gamma}^{n-1} \quad (3.4)$$

where η_c is the continuous phase dynamic viscosity, A is the consistency, $\dot{\gamma}$ the shear rate and n is the power law index. For $n \sim 1$ the fluid is Newtonian, $n \gg 1$ shear thickening and $n \ll 1$ shear thinning.

3.2.6. Dispersed phase rate and flux measurements

A lab balance (OHAUS Pioneer Plus Precision PA2202) was placed under the emulsification vessel and was connected with a netbook through a USB communication cable. The mass of oil introduced in the continuous phase was recorded every second and the data were saved in an excel sheet. The oil flux was then estimated:

$$J_d = \frac{M_d}{\rho_d A_m t_p} \quad (3.5)$$

where M_d is the total mass of oil incorporated in the emulsion, ρ_d the density of the oil phase, A_m the effective membrane surface area and t_p the time for processing the emulsion.

3.2.7. Energy consumption measurements

The power consumed during emulsification is subject to change due to the extra work that the overhead stirrer consumes to maintain the rotational velocity of the shaft. This is because in direct ME (thus in RME), the dispersed phase is gradually introduced in the continuous phase increasing the emulsion viscosity that causes greater friction between the rotating shaft and the emulsion. Lloyd *et al.* have described the approach used in this case for batch RME and it involves the average power consumption between two extreme situations that would correspond to the beginning and the end of the emulsification process: pure continuous phase and emulsion containing 10 wt.% oil (or the desired fraction of dispersed phase) [154]. The power consumption was measured by a plug-in power meter (Watts up Pro, Electronic Educational Devices Inc., USA). Thus the average energy density can be estimated for the duration of the emulsification, then Eq. (2.9) becomes:

$$\varepsilon_{v,HSM} = \frac{P t_p \rho_e}{M_e} \quad (3.6)$$

where P is the average power draw measured by the power meter, t_p the duration of the emulsification process, ρ_e the emulsion density and M_e the mass of the produced emulsion. So by decreasing the processing time or the emulsion volume, the process becomes more energy efficient which agrees with the reports of Walstra & Smulders [102].

As discussed in the thesis literature, for RME the compression of the oil should be added so the energy density can be calculated as follows:

$$\varepsilon_{v,RME} = \frac{(P t_p + \Delta P V_d) \rho_e}{M_e} \quad (3.7)$$

where ΔP is the transmembrane pressure and V_d the dispersed phase volume.

Statistical analysis

Analysis of variance (one-way Anova) was performed to evaluate significant differences between the measurements with regards to zeta potential and particle size (obtained from DLS). Data were checked for normal distribution and equality of variance before analysis of variance whilst Tukey's HSD test was deployed for multiple comparisons of means. Significance was chosen as $p < 0.05$. The statistical analysis was performed using SPSS software package (IBM SPSS Statistics, US). All emulsion data plotted in the present work are averaged values of a triplicate of measurements provided as: $\mu \pm 2 s$ (μ : average value, and s : standard deviation). The same approach was taken for the calculation of the error bars shown in all figures. Data is expected to be within this range ($\mu \pm 2 s$) with a confidence of more than 95%.

Chapter 4

Surfactant-free Pickering Emulsions produced via Rotating Membrane Emulsification

Data and discussions contained within this chapter have been submitted for publication within:

Arkoumanis, P.G., Norton, I.T. and Spyropoulos, F. (2019). Surfactant-free Pickering emulsions via rotating membrane emulsification. *RSC Soft Matter*.

Abstract

In this study, O/W emulsions were produced with a range of particles of demonstrated Pickering functionality using a rotating membrane emulsification set-up equipped with a hydrophilic 6.1 μm pore diameter SPG membrane. Emulsion microstructure was investigated with regards to the droplet size and stability under different formulation (particle concentration & type), and processing conditions (transmembrane pressure, rotational velocity). Emulsions prepared with silica nanoparticles presented a stable droplet size between 22 – 36 μm at a rotational velocity of 2000 rpm and up to a transmembrane pressure of 50 kPa (corresponding to production rate of 2.8 kg h^{-1}). Stable emulsions with droplet sizes between 38 – 96 μm were produced by rutin particles at 2000 rpm with production rates up to three times larger than silica ones, whereas emulsions prepared with aqueous suspensions of HPMC and CMCC particles phase separated within hours in all cases. The established hydrodynamic conditions close to the membrane surface were influenced by the rheological behaviour of aqueous particle suspensions upon changing the rotational velocity, resulting in different droplet detachment times. The lower viscosity of silica suspensions for the rotational velocities examined (100 – 2000 rpm), led to enhanced turbulence in the continuous phase that in turn facilitated earlier droplet detachment, resulting in smaller emulsion droplet size than rutin stabilised emulsions by 16 – 29% at the investigated transmembrane pressure of 50 kPa.

4.1. Introduction

Membrane emulsification has been thoroughly studied by numerous researchers as an alternative process to manufacture a wide range of emulsion microstructures for use in food, cosmetic and pharmaceutical products [129]. Benefits of this technique have been attributed to the low energy consumption and controllability of the final product yielding highly monodispersed structures as opposed to the traditional emulsification methods (e.g. rotor-stator machines, colloid mill, high-pressure homogeniser) [91]. Current records include simple and double emulsions stabilised with classic emulsifiers (surfactants and several biopolymers), however the field of Pickering emulsions remains largely unexplored [2]. The challenge stems from the fact that, as a low-energy emulsification method, membrane emulsification cannot deliver antagonistic adsorption rates for particles, as opposed to traditional emulsification methods that operate under continuous mixing and dissipate higher amount of energy in the emulsion.

The importance of adsorption kinetics is discussed in the work of Yuan *et al.*, who studied the effect of certain parameters (processing and formulation) on the microstructure of silica-stabilised emulsions prepared with a rotating membrane reactor [13]. The authors suggested that a critical adsorption time occurs for the sufficient coverage of oil droplets by particles that can be manipulated by process conditions (oil flux, rotating velocity). When the critical adsorption time was longer than the droplet generation time, emulsification failed. This study investigated further the effect of particle concentration on the emulsion, and it was argued that it should be maintained at sufficient levels to increase the possibility of their effective collision with the oil droplets [12].

Another study has focused on the production of monodisperse O/W Pickering emulsions deploying PNIPAM and Kollicoat (pH responsive) particles. For this, they deployed a stirred-cell type SPG membrane kit with different pore size and they showed that it is possible to produce quite monodispersed droplets ($CV \approx 15\%$) up to a droplet size of $50 \mu\text{m}$ [169]. Same membrane set-up but with a metal membrane ($5 \mu\text{m}$ pore diameter) was used by Thompson *et al.*, reporting relatively polydisperse (CV as low as 25%) O/W Pickering emulsions stabilised with polystyrene particles, depending on the stirring rate and oil flux [170].

As understood, despite the huge potential of membrane emulsification to produce monodisperse microstructures, only several studies are available and focus on certain types of Pickering particles with specific functionality, whilst stability of the subsequent Pickering emulsions is not considered. This study investigates the potential of a range of edible particles of demonstrated Pickering functionality to produce controlled stable emulsion microstructures, without the addition of any type of surface active species, via rotating membrane emulsification. Formulation (particle concentration, type) and process parameters (transmembrane pressure, rotating velocity) are used to control emulsion microstructure and the stability of the produced emulsions was tested for a period of 3 weeks.

4.2. Results and discussion

4.2.1. Aqueous particle suspension behaviour

4.2.1.1. Effect of the pH environment

Fig. 4.1 demonstrates the effect of pH on the particle size and zeta potential of a range of particle suspensions at a fixed concentration of $1.5 \text{ wt.}\%$ and ambient temperature. These titrations were carried out to investigate the optimum pH of the suspensions. The investigated

pH range was 2 – 10, covering the native pH values and IEP's of all particles suspended in water. It was observed that at low pH values the zeta potential net value decreased and the particle size appeared to be increased compared to higher pH values (Fig. 4.1A). HPMC had the least variations compared to the rest of the particles throughout the whole pH range. Zeta-potential of HPMC suspensions showed no substantial changes ranging from -8 mV to 2 mV with the IEP appearing at pH 2, demonstrating a rather weak surface charge throughout the pH range. These measurements comply well with the findings of other studies, reporting that HPMC's were found to be of non-ionic nature so they are not expected to be considerably affected by pH [86, 171]. On the other hand, zeta-potential of the rest of the particles was found to vary greatly throughout the pH range. Zeta-potential of rutin particles increased rapidly when pH varied between 6.5 and 10 whilst demonstrating considerable changes at pH values between 2 and 6.5. The IEP was present at pH 5, in line with the IEP observed by Duffus *et al.*, who also studied the zeta-potential of aqueous rutin dispersions at a range of pH values [11]. In the same study, the authors reported a high zeta-potential for aqueous CMCC suspensions due to the oxidation of -OH groups located at the backbone of the molecule. These values are consistent with our findings as the CMCC aqueous suspensions presented the highest net surface charge compared to the rest of the particles at alcalic pH value (~10), and the largest change by approximately 45 mV at pH 2. The zeta-potential of aqueous silica suspensions was approximately -40 mV at its native pH 10, carrying an almost neutral charge (-0.25 mV) at its IEP pH 2.1. These values are in accordance with the work of Hasan *et al.* who investigated the pH dependence on zeta-potential for a range of colloidal silica [172]. The authors found that silica particles carried a strong negative charge (~ -50 mV) at alcalic pH close to 9 that was attributed to the full ionisation of silanol groups at pH >8.

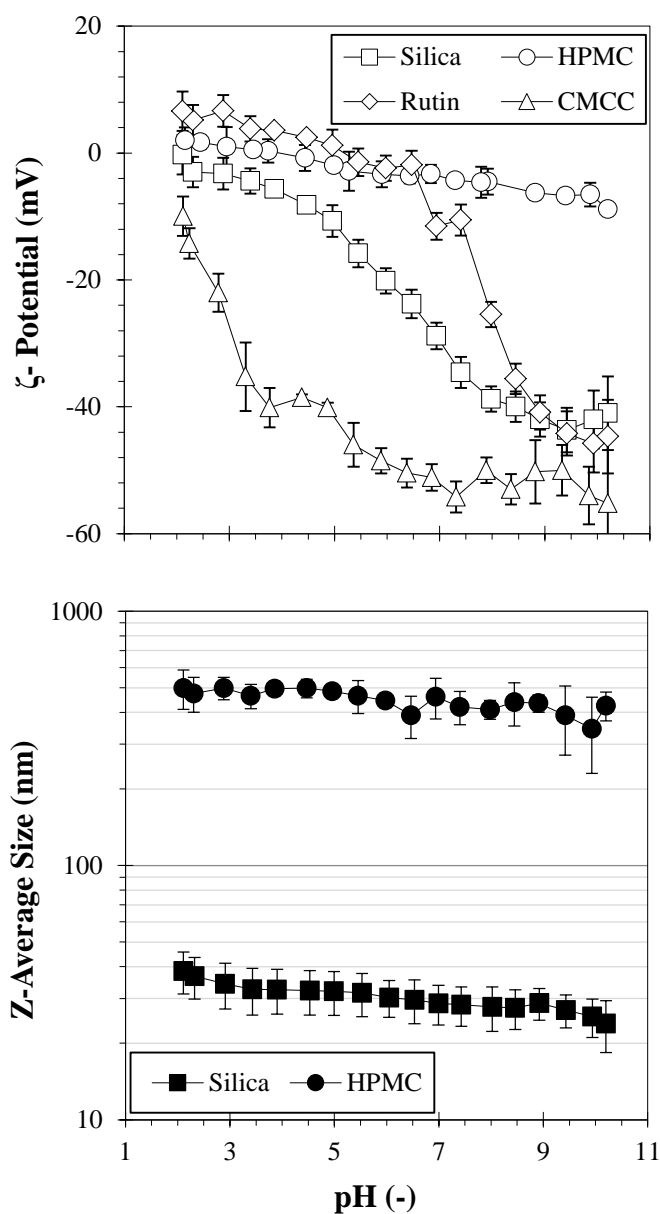


Fig. 4.1: Z-potential and particle size as a function of pH for silica (Native pH: 10), HPMC (Native pH: 6.2), Rutin (Native pH: 5.1) and CMCC (Native pH: 5.9) at a particle concentration of 1.5 wt.%, as measured by DLS. Each data point represents an average of a triplicate of measurements and error bars represent one standard deviation. Where not visible, error bars are smaller than the symbols.

Then by adding HCl the zeta-potential gradually decreased to reach -10 mV at pH 3 close to the IEP; a trend similar to our findings.

Given the decrease in the net surface charge that almost all particle suspensions undergo upon lowering of the pH, with the exception of HPMC that exhibits less significant changes, this effect could reduce the electrostatic repulsion between particles and lead to flocculation. This effect has been discussed before by Wolf *et al.* who reported that lowering the pH resulted in increased particle diameter (as measured through DLS) due to the flocculation of silica particles [74]. Indeed this is confirmed by the changes in the particle size as measured through DLS (Fig. 4.1B). There is no clear trend indicating increase in the particle size of aqueous HPMC suspensions through the entire pH range, however a slight increase for silica suspensions by approximately 15 nm was observed when reducing pH from its native value to its IEP. Particle size of Rutin and CMCC aqueous suspensions was measured through SMLS as their large particle size could decrease accuracy of measurements through DLS, and the results are given in Table 4.1.

Table 4.1: Average particle size D_{32} , and span of 1.5 wt. % particle suspensions at native pH and at the Isoelectric Point (IEP).

Native pH				
Particle type	pH	D_{32} (μm)	Span (-)	PDI (-)
Silica	10	0.02 ± 0.00	-	0.35 ± 0.00
HPMC	6.2	0.42 ± 0.00	-	0.61 ± 0.12
Rutin	5.1	1.59 ± 0.13	26.8 ± 7.04	-
CMCC	5.9	5.20 ± 0.02	1.71 ± 0.09	-
IEP				
Silica	2.1	0.04 ± 0.00	-	0.24 ± 0.00
HPMC	2.2	0.49 ± 0.04	-	0.56 ± 0.13
Rutin	5.2	7.51 ± 0.42	3.02 ± 0.14	-
CMCC	1.9	63.3 ± 0.44	1.91 ± 0.05	-

The results obtained for the rest of the particles through DLS are also included to facilitate comparisons. Again it was observed that decreasing the pH of the suspension led to increased particle diameter of rutin and CMCC that was almost 5 and 12 times larger respectively at the IEP. This suggested that particle flocculation occurred mainly at low pH values, but not at the same extent for all particles and it could be attributed to the approaching of the particles as a result of their reduced surface charge. This could suggest a criterion for choosing the optimum pH of particle suspensions since weak flocculation of particles has been documented to aid the preparation of stable particle-stabilised emulsions [74].

4.2.1.2. Effect of shear on the viscosity of aqueous particle suspensions

In rotating membrane emulsification shear is induced by the rotation of the membrane. By increasing rotational velocity and decreasing the gap between the outer membrane surface and the inner wall of the vessel, the shear on the membrane surface increases [149]. This may cause an increase in the drag force exerted from the continuous phase leading to premature detachment of droplets [144].

Pawlik *et al.* have reported that, during rotating membrane emulsification, emulsion droplets of smaller diameter were able to be produced due to the greater drag force caused by the increased viscosity of the continuous phase [152]. However, the opposite trend was found by Lloyd *et al.* who studied the effect of the viscosity of the continuous phase (by addition of glycerol) on the droplet size of emulsions stabilised with 1 wt.% Tween 20 and produced via a rotating membrane apparatus. They postulate that increased continuous phase viscosity resulted in larger emulsion droplets because detached droplets would not be able to be carried away from the membrane surface, thus giving rise to coalescence events [153]. Therefore, it was necessary to estimate viscosity of different formulations of the continuous phase under a

defined shear rate in order to evaluate the effect of viscosity during emulsification at a constant rotational velocity. Dispersed phase viscosity effects were not considered here, as the same dispersed phase (sunflower oil) was used at all times.

Fig. 4.2 shows the dependency of the apparent viscosity on the shear rate of the aqueous particle suspension for a range of shear rates between 0.1 s^{-1} and 100 s^{-1} . In general it can be seen that throughout the entire range of shear rates, silica and HPMC suspensions demonstrated lower viscosity and a Newtonian behaviour, unlike rutin and CMCC suspensions that followed a shear thinning trend. The Newtonian behaviour of silica particle suspensions agrees with the Einstein equation for dilute particle suspensions, according to the work of Katepalli *et al.* [173]. The authors also reported that the Newtonian behaviour of silica particle suspension persisted in a shear region between 0.1 and 100 s^{-1} , even when inter-particle repulsions were reduced; that could resemble our system of silica particles prepared at pH 2. Furthermore, they discuss that the reason for the Newtonian behaviour was the large inter-particle distances at the particular volume fractions that prevented formation of network. This theory could explain our results as the volume fraction of silica particles in our experiments was also low.

HPMC aqueous suspensions presented constant viscosity against shear that was somewhat surprising as this type of hydrocolloids is commonly characterised by shear thinning [174].

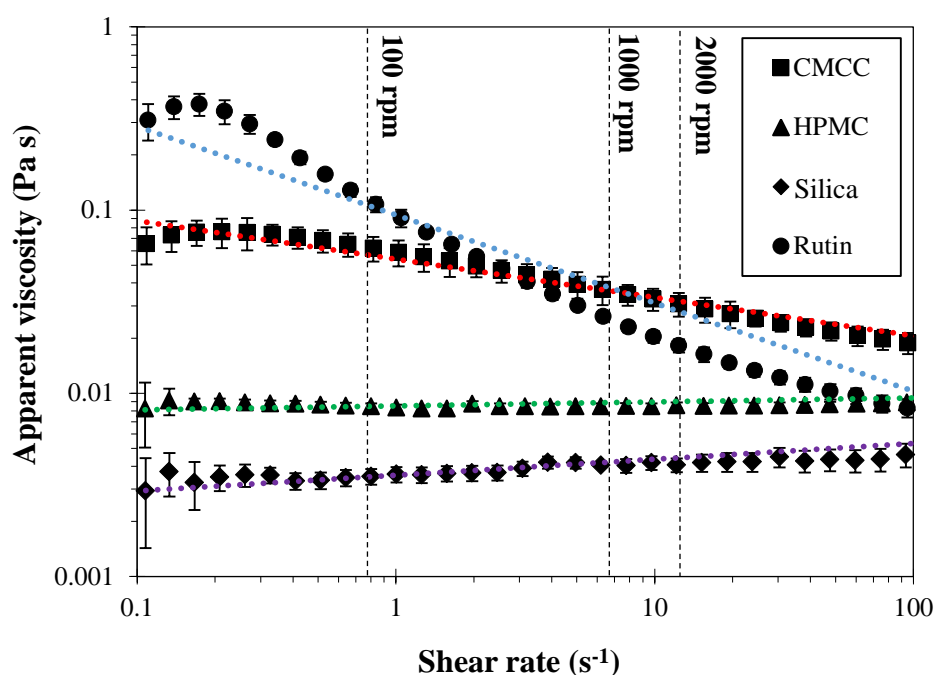


Fig. 4.2: Apparent viscosity of suspensions as function of the shear rate for different types of particles at concentration 1.5 wt. % at 20 °C. Silica was at pH 2 and the rest particle suspensions at their native pH. Each line represents a power law fit with parameters given in Table 4.2. Each data point represents the average of a triplicate of measurements and error bars represent one standard deviation.

The authors also discuss that at low temperature (below gelation temperature) there is a typical low-shear Newtonian region, however, in our experiments HPMC presented Newtonian behaviour throughout the whole shear region, similar to the silica particle suspensions but more robust. This behaviour could be attributed to the small particle size compared to rutin and CMCC, as delivered through DLS measurements. Increased particle size is associated with a decrease in the viscosity because, according to Hill *et al.*, the number of smaller particles (if all other variables remain constant) would be higher resulting in more particle-particle interactions and therefore, greater resistance to flow [175]. Consequently, suspensions incorporating larger particles such as rutin and CMCC demonstrated a shear

thinning behaviour. At low shear rates, rutin suspensions presented the highest viscosity of all suspensions, followed by a steep decrease while CMCC suspensions demonstrated similar behaviour with less dramatic changes in viscosity. At a rotating velocity of 100 rpm the shear rate on the membrane surface was just over 0.7 s^{-1} and rutin had the highest viscosity 160 mPa s followed by CMCC, HPMC and silica particles with a viscosity of 3 mPa s . At 1000 rpm with a shear rate of 7 s^{-1} it was observed that viscosity of rutin suspensions had already decreased to 48 mPa s , very similar to the viscosity of CMCC particles. For the highest rotating velocity of 2000 rpm corresponding to a shear rate of 14 s^{-1} , CMCC presented the highest viscosity value 31 mPa s and rutin viscosity dropped to 18 mPa s , with HPMC and silica showing negligible changes. It could be argued that operation of the rotating membrane at high shear rates could be beneficial for particle suspensions exhibiting shear thinning properties. This is because the viscosity could drop enough to hinder coalescence of droplets caused by the crowding of droplets close to the membrane, an effect demonstrated by Lloyd and co-workers [153]. However, due to the limitation in the rotational velocity of the apparatus (max at 2000 rpm), the shear rate could not exceed 14 s^{-1} suggesting that, although reduced, viscosity still remained a lot higher compared to silica suspensions. The importance of having an adequate number of particles in the aqueous phase during rotating membrane emulsification has been discussed [12, 15]. In these studies high particle concentration was associated with more successful collisions of particles with the droplet surface which in turn resulted in greater surface coverage and improved emulsion stability. As understood, increased particle concentration is imperative in such process, however, this is also expected to increase the viscosity of the particle suspension [176, 177] and consequently to promote coalescence of droplets close to the membrane surface. The effect of particle concentration on the viscosity of aqueous particle suspensions is demonstrated for a range of particles in (Table

4.2), with particular emphasis on the highest achievable shear rate (corresponding to 2000 RPM) of this set-up. Flow curves for all concentrations are included in Table 4.2.

Table 4.2: Effect of concentration on the apparent viscosity of a range of particle suspensions at constant temperature 20°C. The consistency (A) and power law index (n) values are listed for each flow curve fitted to the power law model. Flow curves for all concentrations are presented in Appendix A.1.

Particle type	Concentration (wt. %)	A (Pa s ²⁻ⁿ)	n (-)	$\eta_c, 2000 \text{ rpm}$ (mPa s)
Silica	1.5	0.004	1.086	4.07 ± 0.01
	5	0.003	1.150	4.23 ± 0.00
	10	0.003	1.150	4.54 ± 0.00
HPMC	1.5	0.009	1.022	8.57 ± 0.08
	3	0.022	1.011	21.5 ± 0.04
	5	0.067	1.006	67.5 ± 0.03
Rutin	1.5	0.094	0.519	18.2 ± 0.52
	3	0.306	0.399	50.0 ± 1.08
	5	0.581	0.352	87.7 ± 2.53
CMCC	1.5	0.054	0.791	30.7 ± 0.68
	2	0.173	0.661	70.4 ± 6.84
	2.5	0.589	0.512	163 ± 27.5

The same concentrations were also used to prepare Pickering emulsions. The flow curves for all selected concentrations of all particle suspensions were fitted to the power law model and the obtained consistency (A) and power law index (n) values were used to evaluate (non-) Newtonian performance of aqueous suspensions. From the power law, when $n \sim 1$ the particle suspension is Newtonian, $n \gg 1$ shear thickening and $n \ll 1$ shear thinning as defined by Eq. (3.4).

As shown in Table 4.2, it was confirmed that for all suspensions, increased particle concentration resulted in increased viscosity. Notably, the viscosity of CMCC suspensions

raised dramatically even by increasing concentration at increments of 0.5 wt.% with the 2.5 wt.% reaching 163 mPa s. For silica particles, the effect of concentration on the viscosity was negligible compared to the rest of particles, demonstrating a viscosity of just 4.5 mPa s at a particle concentration of 10 wt.%. It is also worth noting the power law indexes for each type of particle and different concentrations. For silica, the power law index was very close to 1 showing negligible changes upon increasing particle concentration, in accordance with the Newtonian behaviour provided by the power law model. Same observations are made with HPMC suspensions throughout the entire range of concentrations. However, rutin and CMCC presented a shear thinning behaviour as it was mentioned before, and the low power law index of these suspensions ($\ll 1$), also confirmed this. Furthermore, increasing particle concentration in these suspensions resulted in stronger shear thinning behaviour, as evidenced by the further gradual decrease in their power law indices. This is believed to be due to the increased volume fraction of particles that resulted in a higher degree of particle-particle interactions and thus the resistance to flow increased [175].

4.2.2. Pickering emulsions

4.2.2.1. Formulation effects

Effect of particle type

Fig. 4.3 illustrates the effect of particle type on the droplet size and span of fresh emulsions produced via rotating membrane emulsification. Silica suspensions were used at IEP while the rest of the particle suspensions were at their native pH. Emulsion droplet size was found to increase with increasing particle size and the span followed the same trend. Silica and HPMC yielded emulsions with droplet size 29 and 24 μm respectively and narrow distributions as reflected in the low span values averaging lower than, or just above 1. When particle size

increased, for example Rutin and CMCC particles, the emulsion droplet size increased considerably ($38 \pm 0.86 \mu\text{m}$ and $47 \pm 10 \mu\text{m}$ respectively) and the droplet size distribution became wider, with the CMCC presenting the largest span and error bars. One could argue that the particle size would affect collision with the oil droplet surface which in turn could affect droplet formation, however, no such effect was found according to Elimenchem *et al.* [178]. In this work, the collision of polystyrene latex particles (of a range of sizes) with glass beads in porous media was investigated. The authors concluded that the size of particles with the same surface chemistry would not affect collision efficiency. Therefore, the larger emulsion droplet size could be ascribed to the increased viscosity of suspensions incorporating larger particles (the effect has been discussed in section 4.1.1).

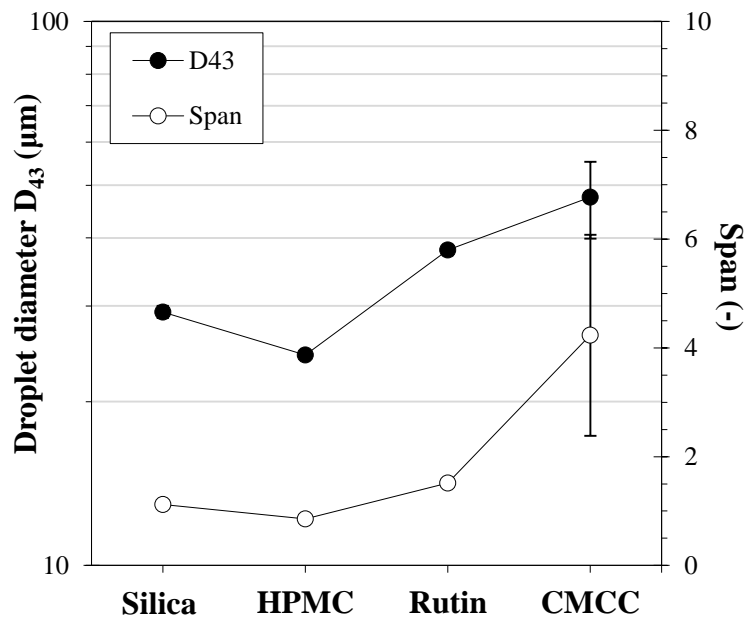


Fig. 4.3: Average droplet size and span values of fresh emulsions stabilised with a range of particles at concentration 1.5 wt. %. An SPG 6.1 μm membrane was used at 10 kPa and 2000 rpm. Symbols represent the average of a triplicate of measurements and error bars represent one standard deviation.

Another factor affecting the emulsion droplet size could be the particle shape. Silica particles used in this study have also been characterised in other studies as per their morphology and they have been found to have a spherical shape [74, 179], whereas HPMC and rutin are regarded to obtain a spherical/ ellipsoidal shape when dispersed in an aqueous medium as a result of hydrophobic interactions [180, 181]. However, the crystalline structure of CMCC upon suspension in the water form rod-shaped particles [182]. A few studies have investigated the effect of particle shape on the stability of Pickering emulsions. Katepali *et al.* report that fumed fractal-shaped silica particles bind easier to the oil-water interface than spherical silica and they also developed a type of network at the interface resulting in more stable emulsions [173]. Furthermore, when attractive forces dominated between fumed silica, their fractal shape enabled them to establish a volume-filling network in the water phase, increasing elasticity and further promoting stability of the emulsions. In another study, the effect of particle shape was also investigated for spindle-shaped hematite and ellipsoidal polystyrene particles on the stability of O/W emulsions [183]. This work showed that there is an optimum aspect ratio of particles that facilitates effective close packing on oil-water interface and this is induced by strong capillary interaction resulting in increased interfacial viscoelasticity.

As demonstrated in previous sections, a decrease in the pH environment of the continuous phase could induce particle flocculation, which in turn could affect continuous phase viscosity. Higher viscosity could contribute to either higher drag force or accumulation of oil droplets close to the membrane surface, thus the droplet size production during rotating membrane emulsification can be affected. Therefore, Pickering emulsions containing continuous phase at native pH and the IEP were prepared for all particles to investigate the effect of pH on the emulsion droplet size and the results are shown in Table 4.3. The droplet size of generated emulsions was recorded after emulsification, the following day, and after 3

weeks to determine optimum pH of the continuous phase. Low transmembrane pressure was applied to provide sufficient time for adsorption of particles whilst high rotation velocity ensured small droplet size [13, 149]. It can be seen that only silica and rutin stabilised emulsions had a stable droplet size after three weeks. Specifically, silica emulsions at IEP presented an oil layer on the top of the emulsion that had a stable thickness throughout the whole period, whereas at the native pH the emulsions phase separated. This could be associated with the fact that at the IEP the silica particles carried a neutral charge, resulting in their weak flocculation due to the absence of particle-particle interactions, which also facilitated their close packing at the oil-water interface. However, it is possible that during emulsification the increasing oil fraction could cause the continuous phase viscosity to increase gradually and thus many droplets to stay at a close distance from the membrane surface. This can be imagined as a cloud of droplets near the membrane surface that would not allow unadsorbed particles to penetrate and reach the fresh forming oil-water interface. This effect could be more enhanced for silica rather than the rest of the particle suspensions at the same concentration due to the high density of the silica. Rotation of the membrane generates a centrifugal force towards the continuous vessel wall and, as in centrifugation, the heaviest molecules (in our case the silica) could accumulate close to the vessel wall, while the less dense oil droplets remain close to the membrane. This effect could prevent access of particles to the fresh interface, particularly at high oil fraction. As a result, oil droplets are stabilised by particles at the beginning of the emulsification process but as the oil fraction increases in the continuous phase the rest of the oil is not emulsified.

Table 4.3: Average droplet diameter (D_{43}) of emulsions stabilised with 1.5 wt. % particle suspensions prepared at native pH and IEP. A 6.1 μm membrane was used at 10 kPa and 2000 rpm. Emulsions that presented phase separation are indicated as ‘PS’.

Droplet diameter D_{43} (μm)			
Native pH			
Particle type	Initial	Day 1	Day 21
Silica	21.1 \pm 0.01	PS	PS
HPMC	24.4 \pm 0.29	PS	PS
Rutin	38.0 \pm 1.73	38.9 \pm 0.96	36.5 \pm 0.14
CMCC	47.5 \pm 7.66	PS	PS
IEP			
Silica	29.2 \pm 0.09	29.3 \pm 0.01	29.1 \pm 0.02
HPMC	40.8 \pm 0.08	PS	PS
Rutin	41.2 \pm 0.33	PS	PS
CMCC	PS	PS	PS

Rutin particles were found to stabilise emulsion droplets at native pH. This could be possibly due to the reduced charge of rutin particles at native pH allowing to establish an interconnected network of particles within the continuous phase as it has also been postulated by other authors for a range of colloidal particles [75, 184]. CMCC and HPMC particles were not able to stabilise emulsion droplets at any of the investigated pH values as the day after preparation these emulsions were completely phase separated with a thick oil layer on the top of the emulsions. The instability of these emulsions could be explained by the rotating membrane emulsification process itself that cannot deliver fast adsorption kinetics to the particles, a feature also postulated in other studies [12, 13]. This is very indicative as the same concentration (1.5 wt.%) of same particle suspensions (CMCC and HPMC) have been used to produce stable oil-in-water emulsions via rotor-stator homogeniser [11]. Another reason could be the particle morphology and wettability of different particle types.

Here, the free energy of adsorption is deployed as a tool to evaluate the capacity of a range of particles to form stable Pickering emulsions. It has been reported that high energy of adsorption is associated with stronger binding of the particle on the oil-water interface, establishing a strong energy barrier against desorption, therefore more stable emulsions are able to be produced [1]. Eq. (2.2) then should be able to describe the outcome of Pickering stabilisation and perhaps to predict the fate of Pickering emulsions by incorporating the effect of particle morphology (particle radius, r_p), particle wettability (contact angle, θ) and oil-water interfacial tension (γ). The kinetic energy (E_K) of the particle prior to adsorption though should not be disregarded as it could provide an indication of the capacity of the particle to induce an energy barrier against desorption. Since with membrane emulsification the applied shear and thus the dissipated energy in the emulsion is far less than high shear mixing processes it would be worth estimating whether this is sufficient for successful adsorption. Consequently, if the kinetic energy of a particle close to the membrane surface was equal or higher than the energy required for adsorption that could result to successful adsorption and would be an indication of successful Pickering stabilisation. Therefore the energy barrier for desorption (or adsorption free energy, ΔF_{ads}) and the kinetic energy for a range of particles were calculated and are shown in Table 4.4. ΔF_{ads} , as shown in Eq. (2.2), depends on several parameters such as the interfacial tension, contact angle and particle size with the latter being the most dominant factor. A number of parameters have been measured experimentally where possible (Appendix A.2) while others were adopted from literature. For all particles the adsorption free energy was found to be greater than the thermal energy ($\sim k_B T$) regardless of the particle size as resulted from Eq. (2.2); moreover the calculated values here were $10^5 - 10^6$ times higher than the thermal energy. The kinetic energy of a particle was calculated by the following formula:

$$E_K = \frac{1}{2} m_p u^2 \quad (4.1)$$

where m_p was the mass of one particle and u the velocity of the particle close to the membrane surface.

Table 4.4: Particle radius, interfacial tension (Appendix A.2), contact angle, adsorption free energy (calculated by Eq. (2.2) and kinetic energy of a range of particles. Contact angle values have been reported for silica [185, 186], HPMC, Rutin and CMCC [11].

	Silica	HPMC	Rutin	CMCC
Particle radius, r_p (μm)	0.02 ± 0.0	0.21 ± 0.0	0.79 ± 0.1	2.60 ± 0.0
Interfacial tension, γ (mN m^{-1})	27.2 ± 0.1	19.7 ± 1.4	15.9 ± 1.4	38.5 ± 1.4
Contact angle, θ (degrees)	90.1 ± 2.5	59.2 ± 0.9	35.2 ± 6.1	38.1 ± 4.3
Adsorption free energy, ΔF_{ads} (k_BT)	7.6×10^3	1.5×10^5	2.5×10^5	8.9×10^6
Kinetic energy, E_K (k_BT)	1.0×10^1	6.2×10^3	5.1×10^5	5.9×10^6

The kinetic energies of the small silica and HPMC particles were the lowest from all particles and at least two orders of magnitude lower than their respective adsorption free energies. This could explain the fact that emulsions with silica presented an oil layer and HPMC was not able to stabilise any oil droplets at all. For the larger particles rutin and CMCC, the values of the kinetic energy agreed well with findings of Salari *et al.* who found that the kinetic energy of PMMA particles with diameters 1.68 - 3 μm for stabilisation of Pickering emulsions was in the order of $\sim 10^5 \text{ k}_B\text{T}$ [187]. Increased kinetic energy was calculated for CMCC due to the large mass of the particle however slightly lower (~ 1.5 times) than the adsorption free energy and this could be the reason these emulsions were also unstable. On the contrary, rutin emulsions were very stable and this can be attributed to the high kinetic energy which was

approximately two times larger than the adsorption energy making it feasible for the particle to adsorb on the oil-water interface. The energy favourable conditions for adsorption of rutin and exceptional stability of these emulsions could also be ascribed to the particle morphology and more specifically to the surface roughness. In a relevant study, San Miguel *et al.* prepared O/W emulsions with silica microparticles whose surface roughness varied [188]. They evaluated the capillary pressure (the maximum pressure that the film between two droplets in contact can withstand and when exceeded coalescence occurs) and they found that there was an optimum surface roughness range of microparticles that is the key for prolonged stabilisation of emulsions. This was valid for homogeneous wetting (e.g. no trapped water ‘pockets’ between particle surface and oil droplet surface). However, microparticles with very high surface roughness were observed to create a ‘re-entrant’ space between particle and oil droplet surface (attributed to the treatment of particles) facilitating heterogeneous mixing that resulted in loss of emulsion stability. Weaker pinning of the rough particle on the oil-water interface (reduced contact angle hysteresis) is associated with lower desorption energy (easier for the particle to desorb back to the water when is already in contact with water). It could be assumed that HPMC and CMCC particles presented very high surface roughness and this could contribute to the destabilisation of HPMC and CMCC emulsions.

Particle availability

The significance of having sufficient amount of particles to cover emulsion droplets has been highlighted in studies on Pickering stabilisation [1, 57]. Within these studies, it is also discussed that, although an excess concentration of particles contributes to sufficient coverage of droplets, the unadsorbed fraction will reside in the continuous phase. This is dependent on the emulsification method. For instance, in high shear processes the continuous breakage of droplets into smaller ones generates new surface that could take up most of the particles until

a finite droplet size is reached. Contrarily, droplets generated by membrane emulsification are less subject to breakage after their initial formation and therefore the adsorption kinetics becomes the limiting factor. High concentration is needed to increase the collision rate of particles with oil surface that would result in lower adsorption time and therefore greater coverage [13]. It could also be advantageous as free particles may attach on adsorbed ones forming multilayers around droplets and increasing the steric barrier. Furthermore, free particles could increase viscosity of continuous phase and through a three dimensional network provide additional stability [1, 57]. However, the disadvantage is that high concentration of particles in general cause viscosity of the continuous phase to increase resulting in congestion of droplets close to the membrane and thus greater possibility of coalescence.

Therefore it was essential to examine whether there was sufficient amount of particles to fully cover the surface of all produced oil droplets and this data could be helpful to explain any instabilities of these emulsions over time. It should be noted that the term full coverage describes the state where the largest proportion of the oil surface is covered by particles, leaving some exposed parts due to the packing of the particles at the interface. This is true particularly for the silica particles that behave as rigid spheres and are not able to deform in the way the rest of the soft particles do (rutin and celluloses) [189]. To do this, some assumptions were made to facilitate calculations: 1. all particles and oil droplets were assumed to have spherical shape, 2. the size of all coated droplets was described by the volume mean diameter D_{43} (provided by SMLS data), 3. homogeneous wetting (no water pockets between particle and oil surface). The diameter of the oil part of the droplet then according to [11] is given by

$$D_{oil} = D_{43} - 2D_p \quad (4.2)$$

where D_p is the particle diameter (obtained from DLS data). Apparently for small particles D_{oil} does not differ substantially from D_{43} , however this can change when larger particles are used and this is considered in calculations. Contribution of D_p becomes even larger when the particle is more hydrophilic so the largest proportion resides in the continuous phase. Another compromise would be the refractive index used for measuring D_{43} through SMLS measurements. In all cases, the refractive index of sunflower oil was used so the actual diameter of droplets covered by particles could be slightly different from our measured values. The number of particles required to coat oil droplets is strongly dependent on the particle size. The smaller the particle size the more particles needed to cover a given oil surface. Consequently, there is a critical concentration of particles C_{cr} above which full coverage is succeeded and it can be calculated as follows:

$$C_{cr} = K \frac{\rho_p D_p}{\varphi_{hp} D_{oil}} \quad (4.3)$$

$$K = \frac{4M_d}{\rho_d M_e}$$

where K is constant and M_d is the total oil mass dispersed in the emulsion, ρ_d is the oil density, M_e the mass of emulsion made, ρ_p is the characteristic density of the particle, φ_{hp} is the hexagonal packing fraction; for rigid spherical particles (silica) it has been calculated to be ~ 0.907 . This is not considered in our calculations for the rest of the particles as they are expected to deform/orientate at the interface thus demonstrating higher packing fraction ($\varphi_{hp} \sim 1$). Full derivation of Eq. (4.3) is given in Appendix A.3. As shown from this equation, for a certain particle type C_{cr} depends on the particle to droplet size ratio. This expression complies with the findings of Ridel *et al.* who extracted a model to predict D_{oil} upon stabilisation of oil

drops by hydrophilic non-aggregated silica particles. [189]. The critical particle concentration is presented in Fig. 4.4 as a function of particle concentration in the emulsion. For $C < C_{cr}$ (above the critical line) the number of particles is not sufficient to cover all oil droplets and below the critical line ($C > C_{cr}$) full coverage may be achieved.

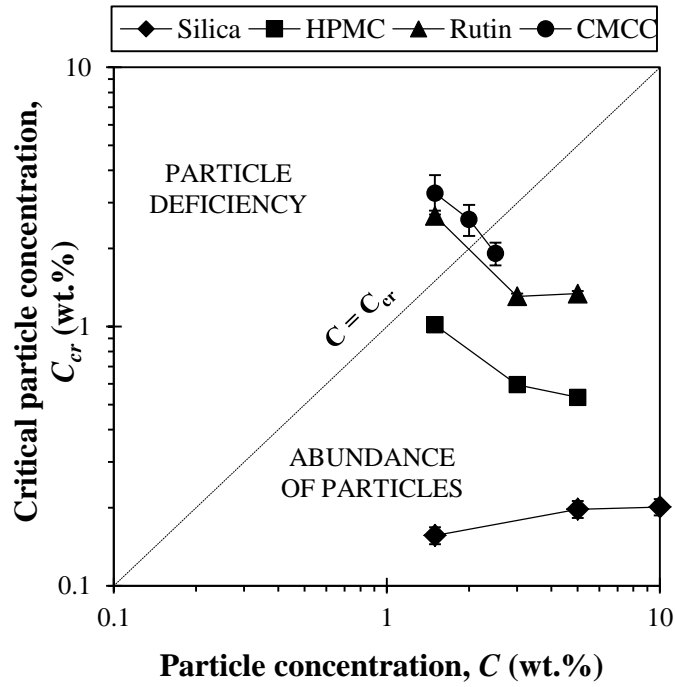


Fig. 4.4: Correlation between critical concentration (C_{cr}) as calculated by Eq. (4.3) and concentration of a range of particles in fresh emulsions. Calculations are shown in Appendix A. All emulsions were 110 g and contained 10 wt. % oil, prepared with a 6.1 μm SPG membrane at 10 kPa and 2000 rpm.

There was a strong dependency on the particle size as it is shown that emulsions with small particles (silica and HPMC) were more probable to consist of droplets fully coated by at least a monolayer of particles whereas some of the emulsions with larger particles (rutin and CMCC) scored above the critical line. Indeed for a given concentration (e.g. 1.5 wt.%) for all particle species the particle size seemed to control the critical concentration. The critical value was not achieved for emulsions prepared with 1.5 and 2 wt. % CMCC and 1.5 wt.% rutin

whereas this was marginally possible for 2.5 wt.% CMCC. A shift towards the ‘fully coated’ part of the graph for all particle species was observed for increased particle concentrations C which was expected as the number of particles increased as well. The critical concentration decreased and reached a plateau for HPMC and Rutin because little changes in the droplet size occurred at increased particle concentrations. A similar plateau was not observed for CMCC due to viscosity limitations associated with high concentrations of CMCC in aqueous suspensions. On the other hand, silica followed a rather upward trend that could be due to the oil droplet diameter which was lower for increased silica concentration. On the whole, emulsions made with silica particles presented the lowest C_{cr} compared to the rest particle species and this is attributed to their lower particle to droplet size ratio (D_p/D_{oil}).

Effect of particle concentration

Having demonstrated whether there is sufficient amount of particles to coat oil droplets the effect of concentration on emulsion droplet size was examined for the different particle species and the evolution of droplet size was recorded for 3 weeks to evaluate stability. As shown in Fig. 4.5 increasing the concentration of HPMC resulted in slightly larger emulsion droplet size. At 3 wt.% concentration the droplet size stood at 28 μm ; that was about 4 μm larger than 1.5 wt.% and further increased at 5% to reach 37 μm . The trend followed was not representative of typical Pickering emulsions as it was expected that the droplet size would decrease with increasing concentration due to the increased collision rate would favour earlier adsorption and thus smaller droplet size [190, 191]. Nonetheless the increase in the droplet size was not necessarily dramatic, however the span increased considerably upon increasing HPMC concentration as it is also shown by the increase in the distribution width in Fig. 4.5. Emulsions stabilised with 1.5% HPMC presented low polydispersity as reflected by the span value of 0.857. Increasing concentration of HPMC resulted in more polydisperse emulsions as

at 3% and 5% the span values were calculated at 1.987 and 1.645 respectively. The following day after emulsification all HPMC stabilised emulsions were phase separated with a clear oil layer appearing for all concentrations. Although there was an abundance of HPMC particles (all concentrations were well above the critical concentration for full coverage of oil droplets) this did not prevent emulsions from coalescing and eventually phase separating the following day (Fig. 4.5A). Similar behaviour was observed for CMCC stabilised emulsions but complete phase separation occurred instantly (Fig. 4.5B) and it was not possible to measure the droplet size the following day. The instant phase separation of the CMCC emulsions could be justified by the critical concentration of CMCC which was not or marginally achieved, in conjunction with the slow adsorption as a result of the large particle size of CMCC.

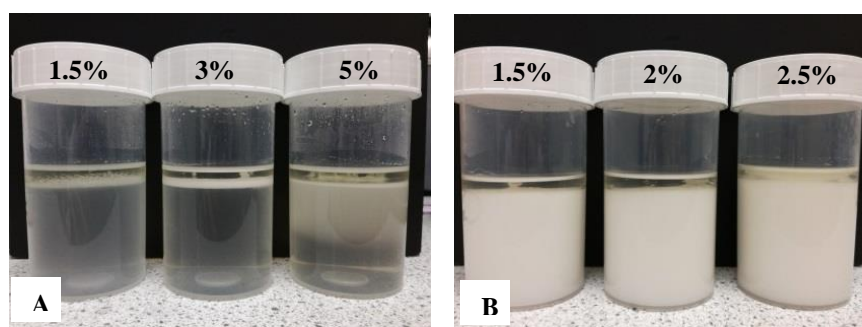
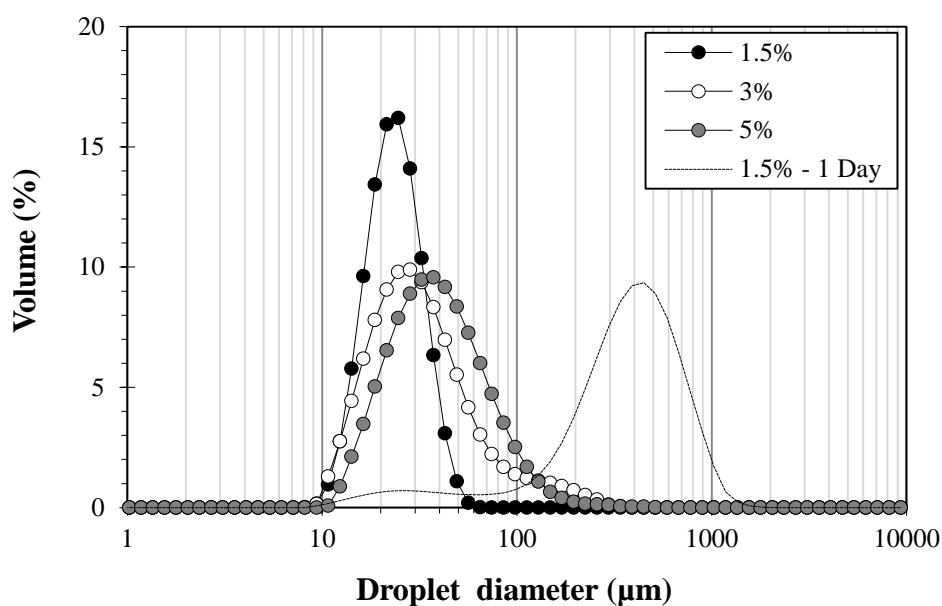


Fig. 4.5: Droplet size distribution of emulsions stabilised with different concentrations of HPMC and pictures of emulsions after standing for 2 hours, prepared with different concentrations of (A) HPMC and (B) CMCC at native pH. All emulsions were 10 wt. % oil made with a 6.1 µm SPG membrane at 10 kPa and 2000 rpm

In addition, the exceptionally high viscosity of CMCC suspensions could result in overcrowding of droplets close to the membrane surface that could increase the possibility of coalescence and phase separation. This effect has been discussed by Lloyd *et al.* who observed that increased continuous phase viscosity resulted in increased droplet size because fresh generated droplets would remain close to the membrane giving rise to coalescence events [153].

Three concentrations of silica suspensions at pH 2 were prepared and adjusted at pH=2 and the subsequent emulsions were produced by rotating membrane emulsification. The droplet size and the span of the emulsions for a period of 3 weeks are presented in Fig. 4.6. After a short period following emulsification all silica stabilised emulsions at all concentrations creamed and a thin oil layer appeared at the top of the cream layer. This effect was discussed earlier and it was attributed to the accumulation of oil droplets close to the membrane, not allowing silica particles to penetrate and reach the new oil-water interface. It was also observed that the thickness of the oil layer remained stable, whereas changes in the thickness of the cream layer were negligible after 3 weeks for all concentrations. It should be noted here though that the unemulsified oil was not regarded in our SMLS measurements. Similar observations have been reported in the work of Yuan *et al.* who utilised a 7 μm pore ceramic rotating membrane to stabilise sunflower oil droplets with silica nanoparticles [15]. The authors discuss that a thick layer of sunflower oil appeared at the top of fresh emulsions. The emulsion droplets produced at the same study were large approximately 400 μm and the emulsion separated completely after a couple of hours, presumably due to the slow adsorption kinetics provided by the process conditions used (50 kPa transmembrane pressure, 1000 rpm rotational velocity).

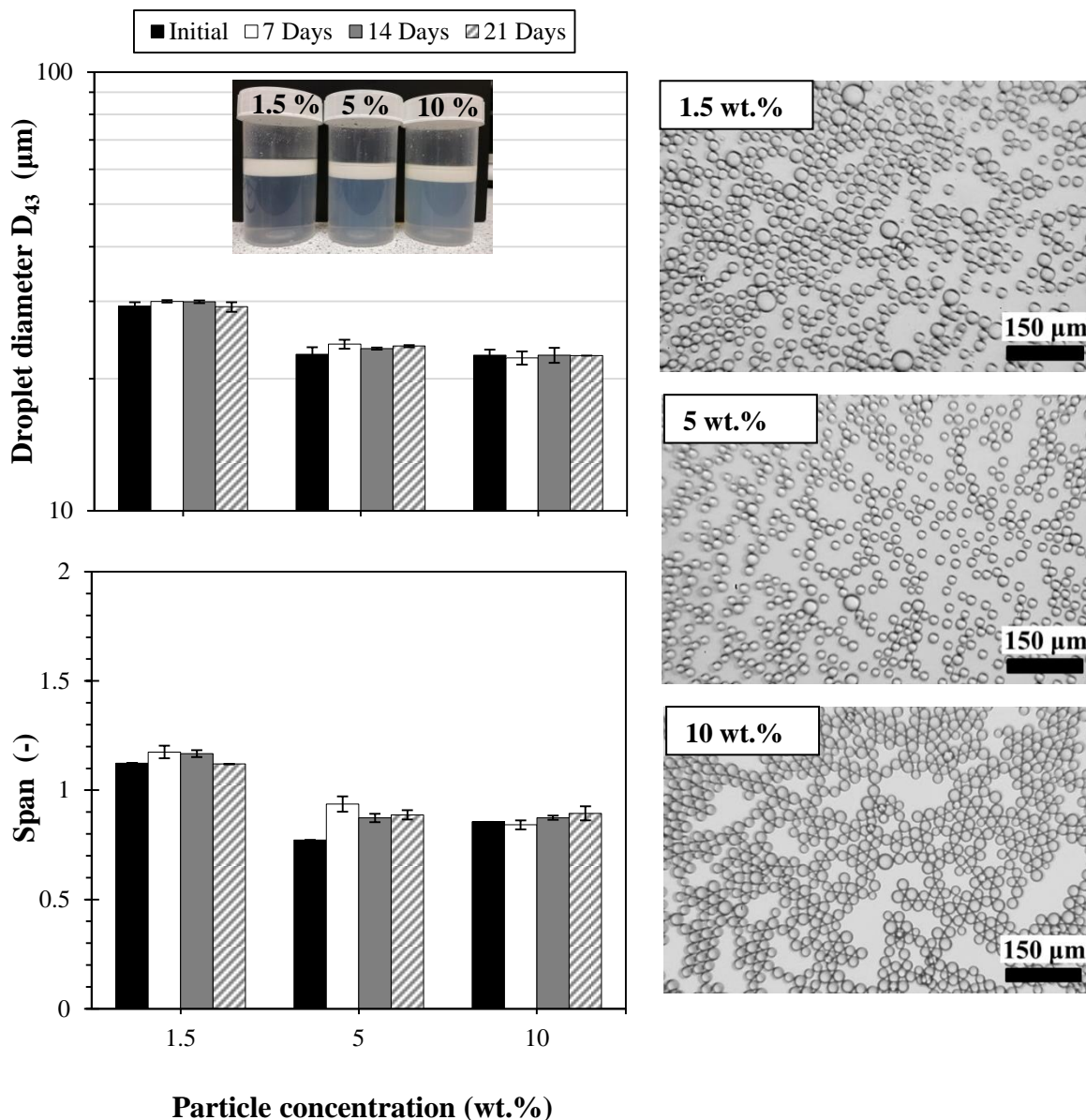


Fig. 4.6: Average droplet size and span values of emulsion droplets stabilised with silica particles as function of concentration, and subsequent stability over 21 days. A 6.1 µm SPG membrane was used at 10 kPa transmembrane pressure and a rotational velocity of 2000 rpm. Photos and micrographs were captured within 24h following emulsification.

As shown in Fig. 4.6, for fresh emulsions, increasing the silica concentration from 1.5 to 5 wt. % resulted in a slight decrease in the droplet size from 29.2 µm to 22.7 µm however there was

no significant change in the droplet size when the concentration increased further to 5 wt.%. This trend agrees with the findings of other studies for hydrophilic silica stabilised emulsions produced by rotor-stator mixer [191, 192]. According to their findings, it was not possible to form stable emulsions (20% oil) with silica concentrations below 1%. Moreover, the plateau was found to appear at concentrations higher than 6%, indicating that the high shear environment promoted more adsorption of particles. For all concentrations, the droplet size was stable for 3 weeks with no substantial differences throughout this period. The span followed a similar trend with droplet size reduction upon increasing the concentration. For emulsions stabilised with 1.5 wt.% silica the span value was 1.12 and was not seen to differ after 3 weeks. At increased concentrations 5 and 10 wt.% more monodisperse emulsions were produced as shown from the values of the span that dropped to less than 1.

The effect of particle concentration on the droplet size of rutin stabilised emulsions and the respective span values throughout 3 weeks are illustrated in Fig. 4.7. Regarding the droplet size, the trend followed was similar to HPMC stabilised emulsions with droplets doubling in size to reach almost 98 μm when the concentration increased from 1.5 to 3 wt.%, and maintained their size with a further increase of the concentration to 5 wt.%. This observation could be explained by the hydrodynamic conditions close to the membrane surface. Increased concentration of rutin could be possible to result in much higher continuous phase viscosity that would not allow the formation of Taylor vortices. Therefore, the forming droplets would have to protrude further to the continuous phase before they are swept away by the drag force, resulting in larger droplets. Lloyd *et al.* report that at low rotational velocity and small annular gap between the membrane and the vessel wall, Taylor vortices were not formed and Reynolds was very low [153]. The result was the formation of larger droplets.

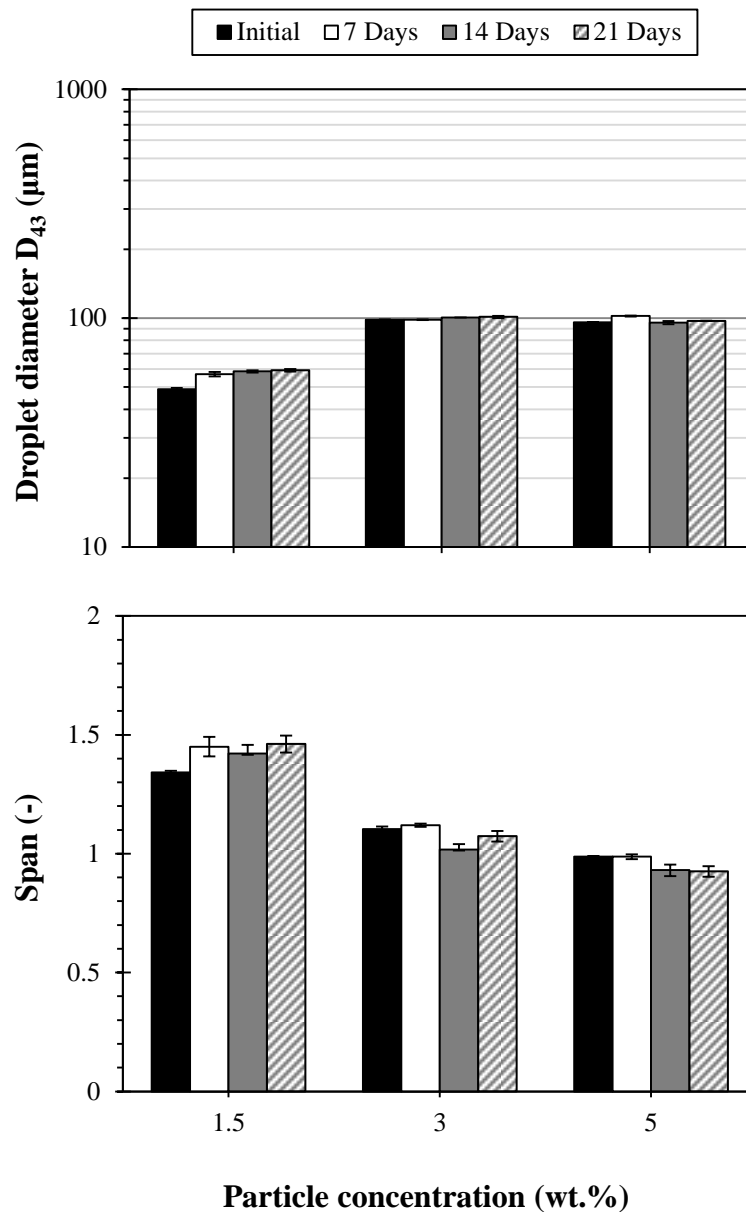


Fig. 4.7: Average droplet size and span values of emulsions stabilised with rutin as function of concentration, and subsequent stability over 21 days. A 6.1 μm SPG membrane was used at 50 kPa transmembrane pressure and a rotational velocity of 2000 rpm.

However, in our experiments a large constant annular gap was used at the maximum rotational velocity, yet it appears that the increased viscosity of the rutin aqueous suspensions also resulted in low Reynolds number and thus no appearance of Taylor vortices.

It was also observed that emulsions stabilised with low rutin concentration 1.5 wt.% creamed, whereas at higher particle concentration sedimentation of oil droplets occurred (Fig. 4.8A). This is probably associated with the large oil droplet size and the formation of large rutin aggregates at high rutin concentration. Fig. 4.8B shows a close-up of an oil droplet surface stabilised by rutin particles and it can also be seen that the size of the largest of these rutin entities falls within the range of sizes measured by SMLS. Moreover, despite the fact that the majority of the rutin particles formed large aggregates in the micron range, it is speculated that the fine fraction was adsorbed to the oil droplets whereas the free particles formed a type of network imparting secondary steric hindrance between oil droplets. This is not an unknown stipulation since it has also been reported by [70] who investigated the emulsifying capacity of flavonoids on oil-water interfaces and it is also discussed in the work of [193] for stabilisation of oil-in-water emulsions by cocoa particles. In either case, no oil layer appeared indicating that all rutin stabilised emulsions were exceptionally stable. Not surprisingly little to no variations in the droplet size was detected after 21 days (Fig. 4.7).

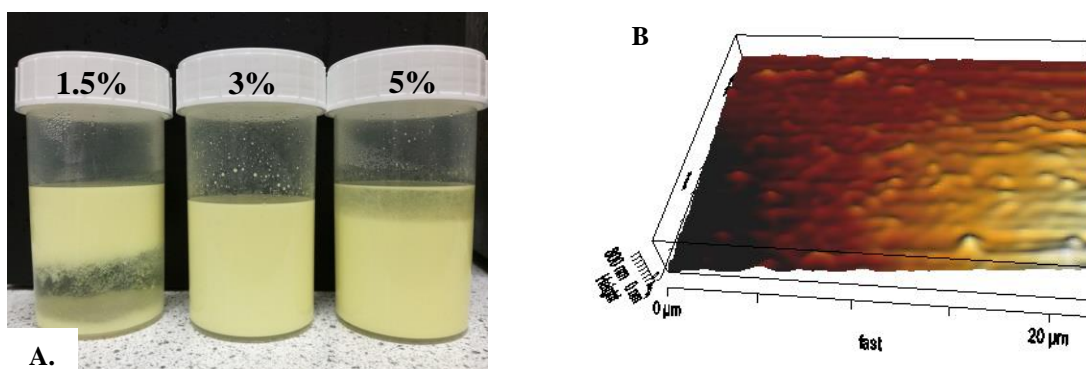


Fig. 4.8: A. *Rutin stabilised emulsions after standing for 2 hours at room temperature and B. 3D AFM captured image of oil droplet surface in emulsion stabilised with 1.5% Rutin particles. All emulsions were 10 wt. % oil made with a 6.1 μm SPG membrane at 50 kPa and 2000 rpm.*

Furthermore, the span was found to decline with increasing concentration of rutin. Again this could be explained by the fact that at high concentrations of rutin more particles were present in the continuous phase and they were able to keep adjacent oil droplets apart upon growth and detachment from the membrane.

4.2.2.2. Processing effects

Adsorption and droplet formation time

Previous studies in rotating membrane emulsification have emphasised the influence of adsorption kinetics on the fate of Pickering emulsions [12, 13]. In high shear processes adsorption kinetics may not influence emulsification. This is because the repeated rupture of droplets reveals new interfacial area able to eventually accommodate more particles and also the higher energy provided may enhance collision between particles and droplets. However, adsorption kinetics becomes the limiting factor in drop-to-drop generation techniques, such as membrane emulsification, as after detachment from the membrane droplets will not break further because of the low shear. Wang *et al.* calculated the adsorption depth for mass transfer (diffusion/convection controlled) of surfactants from the bulk to the oil-water interface for different configurations of microfluidic channels [194]. The authors discuss that the adsorption depth calculated by their model would be very small for macromolecules and some polymers as mass transfer would occur fast and adsorption would be governed by the kinetics. The model suggested by Yuan *et al.* to calculate adsorption time uses a Langmuir adsorption isotherm that considers droplet coverage by particles and the adsorption rate constant can be found experimentally assuming a barrier-controlled adsorption mechanism (diffusion/convection of particles is very fast). For convenience, the adsorption time in the present study was calculated by equations used mainly for conventional emulsification

machines that disrupt droplets (i.e. colloid mill, high-pressure homogeniser) [102] as it was not possible to calculate the kinetic adsorption rate constant of particles and no literature is available to our knowledge for such interfaces. Indeed the adsorption times calculated by the model provided by Wang *et al.* corresponding to a very small adsorption depth, were very close to the ones obtained by Eq. (4.6) - (4.7) for laminar viscous (t_{ads}^L) and turbulent inertial regime (t_{ads}^T) respectively. To determine the flow regime at the surface of a rotating cylinder (membrane) within a cylindrical stationary vessel (emulsion production tank) the Taylor number of the continuous phase was calculated according to Schadler *et al.* [9]:

$$Ta = Re_c \sqrt{\frac{2(R_2 - R_1)}{R_1 + R_2}} \quad (4.4)$$

$$Re_c = \omega R_1 (R_2 - R_1) \frac{\rho_c}{\eta_c} \quad (4.5)$$

where Re_c is the Reynolds number of the continuous phase, ω the angular velocity of membrane surface, ρ_c the density and η_c the viscosity of the continuous phase. There is a critical Taylor number (~ 41.3) above which small vortices appear and the flow regime changes from laminar to turbulent inertial. Depending on the flow regime the respective adsorption time can be estimated [102]:

$$t_{ads}^L \sim \frac{6\pi\Gamma_M}{\dot{\gamma}m_c D_{oil}} \quad (4.6)$$

$$t_{ads}^T \sim \frac{\Gamma_M}{m_c} \left(\frac{\rho_c}{D_{oil}\epsilon_v} \right)^{1/3} \quad (4.7)$$

where ε_v is the power density and Γ_M the surface excess concentration. As discussed by Wang *et al.*, for small adsorption depth, the oil-water interface will quickly become occupied by particles and the surface concentration Γ approaches the maximum value (Γ_M) that corresponds to maximum coverage, and it can be calculated by Eq. (4.8) [189]:

$$\Gamma_M = \frac{4}{3} \rho_p \varphi_{hp} r_p \quad (4.8)$$

where r_p is the particle radius as measured by DLS.

It is possible that the low shear and low energy dissipated in the emulsion through the membrane emulsification process may result in long adsorption times, as it is also shown in Eq. (4.6) - (4.7). Therefore it is important to ensure that droplets spend as much time as possible at the membrane before detachment so that sufficient coverage by particles is promoted. Assuming that one droplet detaches per pore simultaneously, the droplet formation time (t_{drop}) can be roughly estimated:

$$t_{drop} = \frac{2\eta_d L_m D_{oil}^3}{3d_p^4 \varphi^{0.5} \Delta P} \quad (4.9)$$

where η_d is the dispersed phase viscosity, L_m the membrane thickness, d_p the membrane pore size, φ the membrane porosity which is 0.56 [132] and ΔP the applied transmembrane pressure. Derivation of Eq. (4.9) is given in Appendix A. As shown from this equation, the droplet formation time is expected to be dependent on the $D_{oil}^3 / \Delta P$ ratio.

The advantage of rotating membrane emulsification is the ability to manipulate adsorption time (t_{ads}) and droplet formation time (t_{drop}) by adjusting the shear/ energy dissipated in the emulsion and the flux through the membrane respectively. In the first case, increased

rotational velocity will generate higher shear at the membrane surface and the droplet will detach earlier from the membrane surface resulting in shorter formation time. At the same time however, by operating membrane at maximum rotational velocity, higher shear and more energy is dissipated in the emulsion that will produce shorter adsorption times (Eq.(4.6) - (4.7)). In the second case, it is possible to manipulate droplet formation time by changing transmembrane pressure. Decreasing transmembrane pressure will result in decreased oil flux and as a consequence formation time will be longer (Eq. (4.9)).

Adsorption times for both silica and rutin particles were very low in the μs range as it is shown in Table 4.5. For rutin particles the adsorption time was 25 – 30 times higher than silica, given the large size of this particle as well as its higher viscosity of aqueous suspensions that could hinder transportation of particles to the oil-water interface. It should be noted again that the calculated adsorption times are a rough estimate as the equations apply for high-shear homogenisation; however the trends illustrate the influence of processing. Changes in the adsorption time of silica particles were negligible with increasing transmembrane pressure emulsions followed the typical trend also reported in other studies for both conventional emulsifiers stabilised from 10 to 150 kPa, whereas a slight decrease by 28% (corresponding to 13.5 μs) is noticed for rutin particles; this is due to the greater changes in D_{oil} for rutin-stabilised emulsions. The effect of rotational velocity was stronger than transmembrane pressure for both particles. The flow regime was turbulent in all cases except for 100 rpm where it was laminar for rutin particles ($Re_c=1.72$, $Ta=2.02$) due to the high viscosity of the rutin suspensions hindering formation of Taylor vortices. This was reflected in the adsorption time that was dramatically higher by two orders of magnitude at 100 rpm. Increasing further the rotational velocity to 1000 rpm resulted in occurrence of turbulence and the adsorption time fell from 25.1 to 0.5 ms.

Table 4.5: Adsorption and droplet formation time of 1.5 wt.% particles in emulsions made with a SPG 6.1 μm membrane at varied transmembrane pressure and rotational velocity of the membrane.

Transmembrane pressure (kPa)	Rotational velocity (RPM)	t_{ads} (ms)		t_{drop} (ms)	
		Silica	Rutin	Silica	Rutin
10	2000	0.018	0.491	105.3	179.4
50	2000	0.016	0.448	40.22	81.72
70	2000	0.017	0.451	23.93	55.24
100	2000	0.015	0.441	48.26	46.49
150	2000	0.013	0.356	115.9	213.7
50	100	0.024	25.15	430.9	1100.9
50	1000	0.019	0.544	89.86	126.8

The droplet formation time was also greater for rutin particles due to the higher $D_{\text{oil}}^3 / \Delta P$ ratio. For both particles, the droplet formation time reduces with increasing transmembrane pressure as the droplets expand faster towards the continuous phase and as a consequence they detach faster from the drag force. This is in accordance with the correlation between the droplet surface expansion rate and the droplet generation time during membrane emulsification reported by Van der Graaf *et al.* [160]. The authors also report similar timescales for droplet formation varying between 10 – 40 ms depending on the emulsifier concentration and processing conditions.

Effect of transmembrane pressure

Fig. 4.9 shows the effect of transmembrane pressure on the droplet size and the span of Pickering emulsions for a period of 3 weeks. As a first observation it can be seen that silica stabilised fresh emulsions had approximately 18 – 20% smaller droplet size than rutin emulsions and they also presented lower span values throughout the transmembrane pressure range. This difference has been discussed in previous section (3.3.2.1) and could be attributed to a set of formulation parameters such as the particle morphology (size, shape, wettability) as well as increased viscosity of the rutin suspensions. The droplet size of silica and rutin stabilised emulsions increased with increasing transmembrane pressure. The same trend was noticed for conventional emulsifier stabilised emulsions [44, 140, 153] as well as emulsions stabilised with silica nanoparticles, all produced by rotating membrane emulsification [13]. This can be explained by the activation of more pores with increasing transmembrane pressure that resulted in coalescence of droplets growing in neighbouring pores. Furthermore, the droplet formation was considerably higher for the rutin particles (Table 4.5) at all pressures except for 150 kPa, suggesting that these droplets spent more time at the membrane surface before their detachment and as a consequence they were larger than the silica stabilised ones. The faster adsorption of silica particles at a certain transmembrane pressure also resulted in faster coverage of droplets during their growth on the membrane that hindered coalescence of neighbouring droplets to some extent, as indicated by the lower span values compared to the respective rutin ones. Silica stabilised emulsions (cream layer) remained stable at low transmembrane pressure (10 – 50 kPa) after standing for 3 weeks. Yuan *et al.* report a critical oil flux of $0.1 \text{ m}^3 \text{ m}^{-2} \text{ h}^{-1}$ below which, stable silica stabilised emulsions were produced at a rotational velocity of 0.39 m s^{-1} [13].

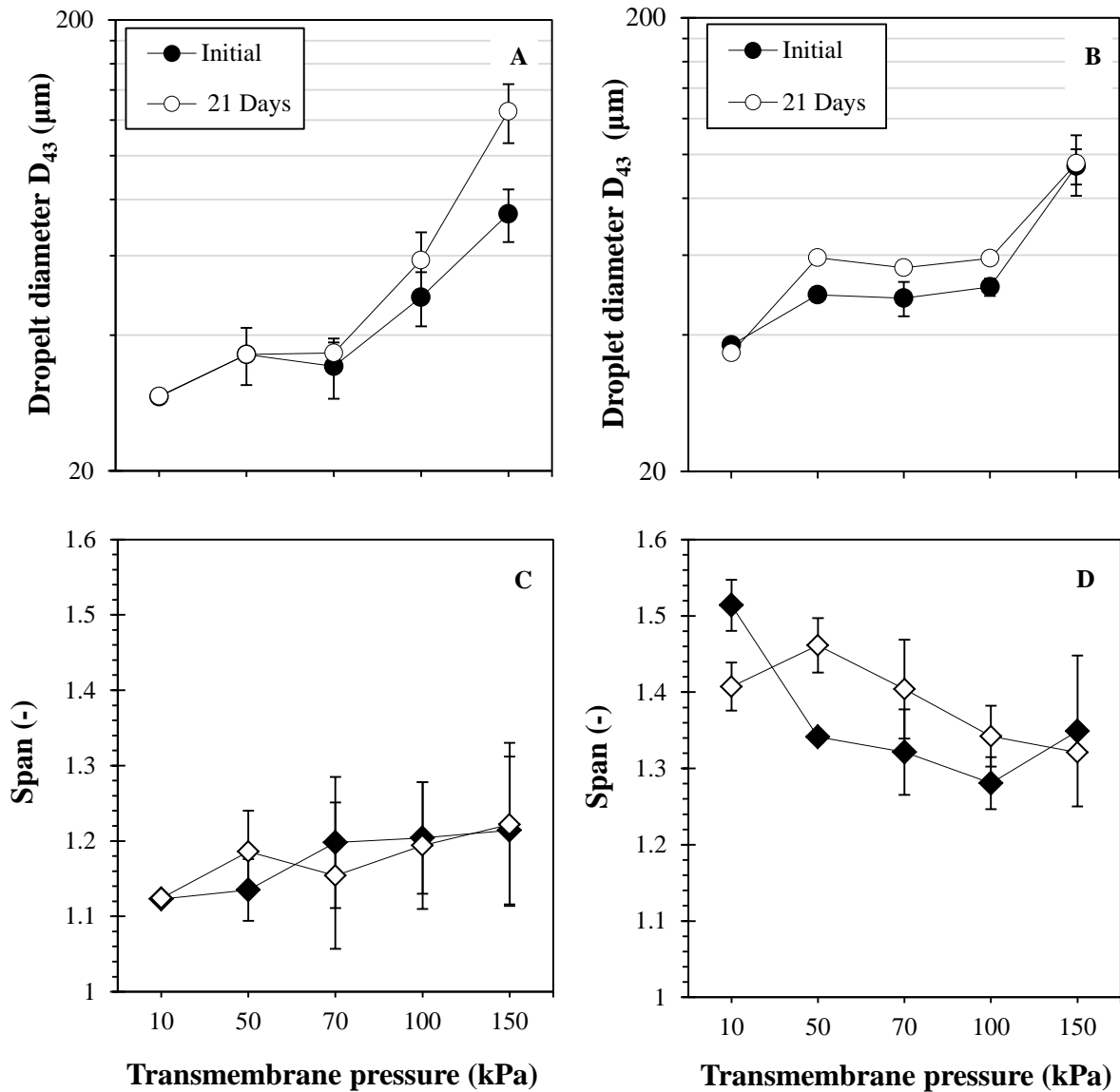


Fig. 4.9: Average droplet size and span values of emulsions as function of the transmembrane pressure stabilised with 1.5 wt.% Silica (A & C) and 1.5 wt.% rutin (B & D). An SPG 6.1 μm membrane was used at 2000 rpm.

Our results correlate well with the findings of Yuan *et al.* as the flux at 50 kPa was approximately $0.18 \text{ m}^3 \text{ m}^{-2} \text{ h}^{-1}$ for silica stabilised emulsions. That is a little higher than the reported critical value, however it is possible that the higher rotational velocity ($\sim 1.05 \text{ m s}^{-1}$ corresponding to 2000 rpm) resulted in higher collision frequency of particles and droplets

delivering stable emulsions, since the adsorption time remained very short. Rutin stabilised emulsions had stable droplet size for 3 weeks at low transmembrane pressure 10 kPa and no oil layer appeared up to a transmembrane pressure of 100 kPa corresponding to an oil flux of $0.65 \text{ m}^3 \text{ m}^{-2} \text{ h}^{-1}$. The stability at such high transmembrane pressure could be related with the morphology of rutin particles allowing them to build an interconnected volume-filling network in the continuous phase hindering coalescence of droplets [173, 193].

Effect of rotational velocity

The effect of the rotational velocity was investigated to obtain a better insight on how the droplet size is affected by the hydrodynamic conditions in the continuous phase vessel. It was expected that at a constant oil flux, high rotational velocity would generate more shear at the membrane surface and hence droplets would detach earlier from the membrane resulting in smaller droplet size; however that would also reduce droplet formation time, so the time available for adsorption of particles should be reduced as well. In addition, high shear is associated with higher energy dissipation and shorter adsorption time (Eq. (4.6) - (4.7)). Nevertheless, from these equations it is apparent that the rotational velocity influences both adsorption and droplet formation times but has a stronger effect on the latter one.

Fig. 4.10 shows the effect of rotational velocity on the droplet size of emulsions stabilised with silica and rutin particles on the day of production and after standing for 3 weeks. The droplet size reduced with increasing rotational velocity for both silica and rutin stabilised emulsions as a consequence of the increase in the shear close to the membrane surface, causing the droplets to detach earlier. Notably, a steep decline was observed in the droplet size of rutin emulsions between 100 – 1000 rpm by almost 50% of the initial size followed by a further slight reduction reaching 49 μm . Droplet size of silica emulsions followed a

smoother gradual reduction starting from almost 80 μm ending at above 36 μm at the highest rotational velocity. Using the model of Aryanti *et al.* (Eq. (2.19)), it can be seen that the droplet size is underestimated. This could be related to the wall correction factor, which in this case was 1.7, that corresponded to a sunflower oil droplet moving within a Tween 20 solution. However, the continuous phase viscosity is much larger for silica and rutin particles and thus the η_d/η_c ratio would be expected to be much smaller than for Tween 20. Furthermore, the ratio of the droplet radius to the distance of the droplet from the membrane wall is so small that is expected to give a wall correction factor that is lower than 0.1 as it is reported by Chen *et al.* [157].

The effect of rotational velocity on the droplet size was also discussed by Yuan *et al.* for silica stabilised emulsions through rotating membrane emulsification at a constant oil flux $0.08 \text{ m}^3 \text{ m}^{-2} \text{ h}^{-1}$. The authors reported a decrease in the droplet size until the rotational velocity approached 0.36 m s^{-1} , however at higher rotational velocities they noticed an increase in the droplet size that they attributed to the small droplet formation time that did not allow sufficient coverage by the particles leading to coalescence of droplets at the membrane surface. On the contrary, in our experiments at a similar constant oil flux and rotational velocities between $0.05 - 1.05 \text{ m s}^{-1}$, the droplet size followed a monotonic decrease and all emulsions prepared at the maximum rotational velocity were stable for 3 weeks. For the silica stabilised emulsions, perhaps this difference could be due to the absence of surface charge of the silica particles in our experiments that facilitated their close packing to the interface. At low rotational velocity (100 rpm) the shear was not sufficient to drive detachment of droplets therefore they continued to grow on the membrane giving large droplet size and span for both particles and presenting large error bars and these emulsions were not stable. The large difference in the droplet size between silica and rutin stabilised emulsions, especially at low

rotational velocity (100 rpm), is also related to the hydrodynamic conditions close to the membrane surface.

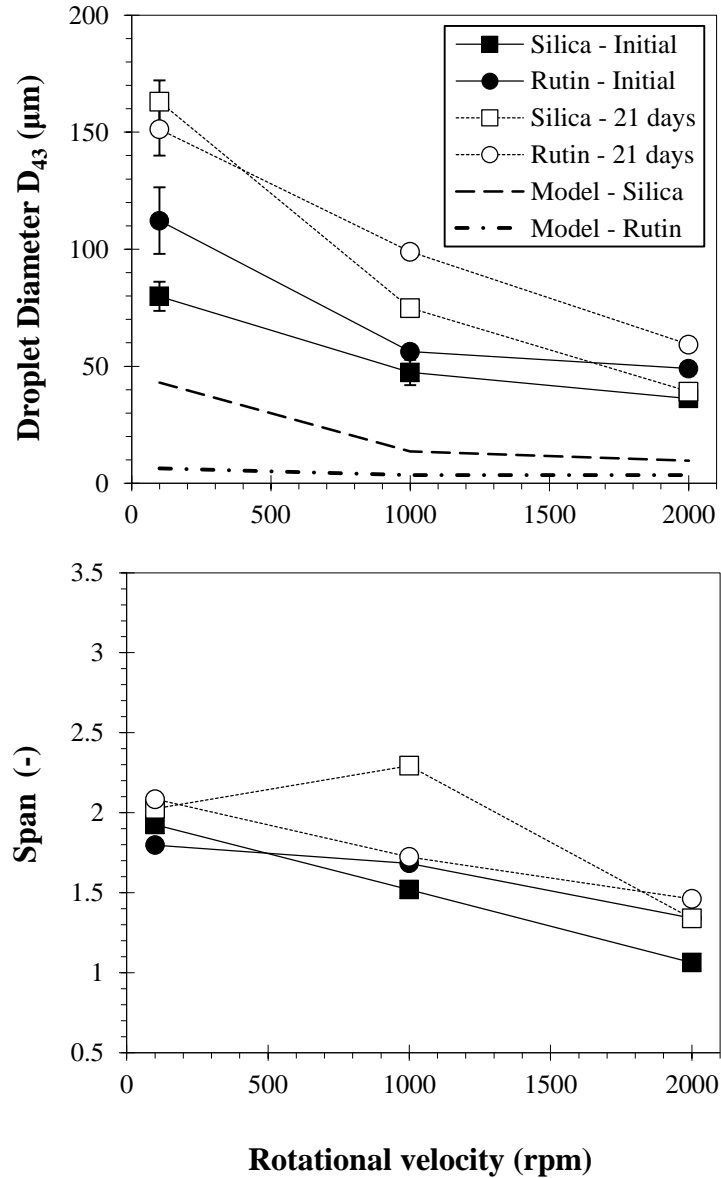


Fig. 4.10: Average droplet size (top) and span (bottom) of emulsions as function of rotational velocity stabilised with 1.5 wt.% particles. An SPG 6.1 μm membrane was used at 50 kPa transmembrane pressure.

Table 4.6: Rotational velocity, shear rate, viscosity, shear stress and Taylor number (Ta) of silica and rutin suspensions at particle concentration 1.5 wt.%. Viscosity data obtained from Table 4.2.

rpm	Shear rate (s^{-1})	Silica			Rutin		
		Viscosity (mPa s)	Shear stress (Pa)	Ta (-)	Viscosity (mPa s)	Shear stress (Pa)	Ta (-)
100	0.72	4.1	0.003	57	110	0.079	2
1000	7.16	4.1	0.029	470	37	0.265	61
2000	14.3	4.1	0.059	886	18	0.257	170

As it can be seen in Table 4.6, the higher viscosity of rutin suspensions at low rotational velocity (so low shear rate) did not allow formation of Taylor vortices. The Taylor number calculated by Eq. (4.4) - (4.5) was found to be very small < 41 which is the critical Taylor number for vortices to occur. On the other hand, silica stabilised droplets formed in the transitional regime with the presence of small eddies in the continuous phase, whose diameter was smaller than droplets, promoting earlier detachment. At higher rotational velocity (1000 rpm) the viscosity of rutin suspension had decreased dramatically giving rise to formation of Taylor vortices as indicated by the higher Taylor number, yet in a lesser extent than silica suspensions. Consequently, the droplets for both particle stabilised emulsions became smaller in size as they now grow under the presence of small eddies that facilitated earlier droplet detachment from the membrane surface. However, even at the highest rotational velocity (2000 rpm) the viscosity of the rutin suspensions, although substantially decreased, it was still a lot higher than the silica counterpart that will even pass to fully developed turbulent flow

($Ta > 400$). Therefore the droplet size of these emulsions was generally smaller than the rutin stabilised ones.

Fig. 4.11 shows the influence of rotational velocity at the oil injection rate for silica and rutin stabilised emulsions. For both particle stabilised emulsions at 100 and 1000 rpm, the mass of oil added in the continuous phase increased in a steady rate until reaching 10 wt.% oil in the emulsion as it can be seen by the straight lines. This is in line with the findings of Lloyd *et al.* who also reported that for direct rotating membrane emulsification and surfactant positioned 100% in the continuous phase, the oil injection rate followed a linear trend at transmembrane pressure 50 kPa and a rotational velocity of 1000 rpm (shear rate 6 s^{-1}). However, a small ‘bump’ was noticed at the initial stages of the process in our experiments for the highest rotational velocity of 2000 rpm that contributed in the measurement of oil added to our system of particles and water.

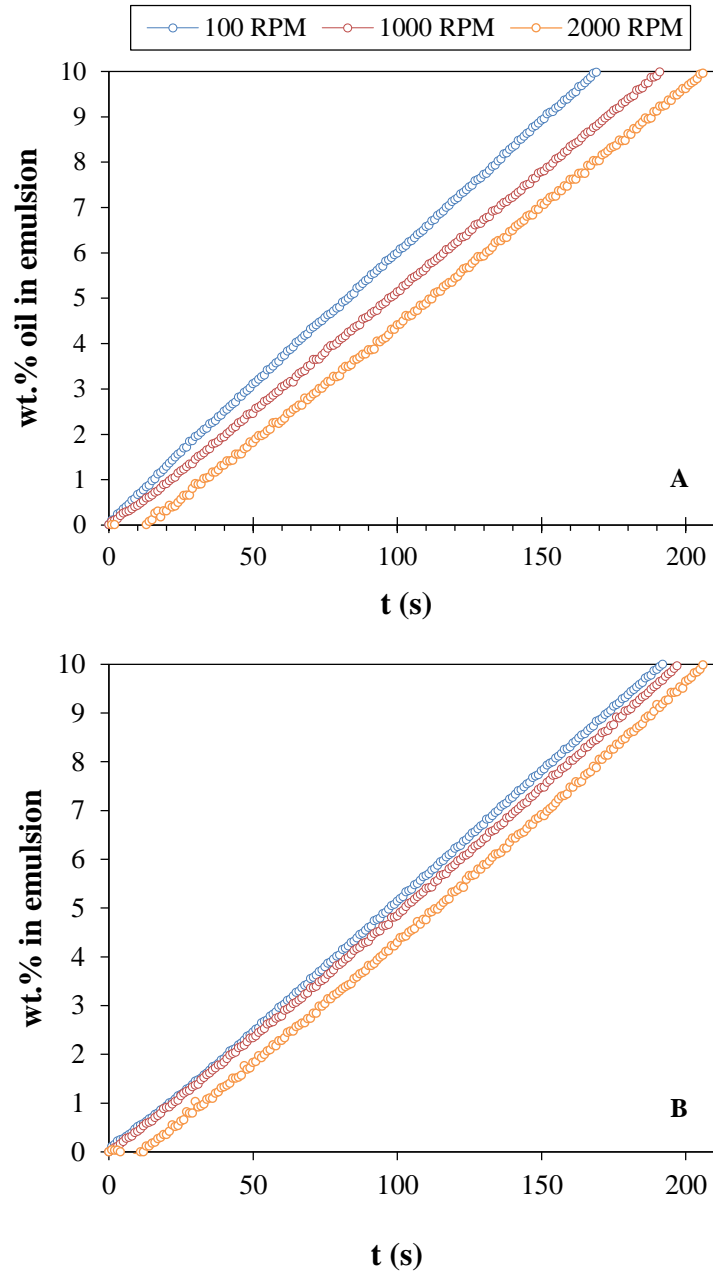


Fig. 4.11: Rate of oil added in the continuous phase during production of emulsions stabilised with (A) 1.5 wt.% silica and (B) 1.5 wt.% rutin particles using an SPG 6.1 μm membrane at different rotating velocities at constant transmembrane pressure 50 kPa.

This is believed to be caused by small vibrations of the membrane at high rotational velocity, particularly at the initial stages of the process until the pressure builds up in the tortuous internal structure of the pore channel. Lower emulsion production rates were also observed by

increasing rotational velocity. This effect was stronger for silica stabilised emulsions as it can be seen by the greater shift of the line at 2000 rpm towards longer processing times. This could be ascribed to the density difference between the continuous and the dispersed phase. The increased centrifugal force generated by the high rotational velocity pushes the denser continuous phase towards the vessel wall whereas the oil droplets would stay closer or, even float on the membrane surface, an effect also discussed by Lloyd *et al.* [153]. In the same study it was also discussed that slower oil flux (so longer process time) could be experienced at high rotational velocity. This could be caused by the frictional losses generated by the high centrifugal force as the dispersed phase is forced at one side of the pore channel.

4.3. Conclusions

A range of edible particles was used to prepare Pickering emulsions via rotating membrane emulsification. This study provides a better insight on the potential to manufacture surfactant-free Pickering emulsions with a low-energy method and identifies the key formulation and processing parameters for long-term stability.

The utilisation of celluloses (HPMC, CMCC) as Pickering particles resulted in complete phase separation in all cases. However, stable silica and rutin stabilised emulsions were produced at a constant rotational velocity of 2000 rpm and transmembrane pressures up to 50 kPa and 100 kPa respectively whereas at pressures higher than 100 kPa phase separation occurred for both types of emulsions. The demonstrated ability of rutin to stabilise emulsions at transmembrane pressures up to 100 kPa (as opposed to 50 kPa for silica) is suggested to occur due to the morphology of the rutin particles, being able to establish a more robust interconnected network within the continuous phase that prevented coalescence of droplets. Stable rutin stabilised emulsions with large droplet size of approximately 98 μm were also

produced for rutin concentration equal and greater than 3 wt.% at 50 kPa and 2000 rpm. The maximum rotational velocity of 2000 rpm was found to be the optimum velocity to achieve the smallest possible droplet size at a specified transmembrane pressure, as the turbulent hydrodynamic conditions favoured earlier droplet detachment. Particularly for Pickering emulsions formed in a shear-thinning continuous phase (e.g. rutin stabilised emulsions), operation of RME at the maximum rotational velocity may be favourable as the subsequent reduction in the continuous phase viscosity may result to easier formation of Taylor vortices and thus smaller emulsion droplet size. A compromise is made regarding the droplet size uniformity, especially at pressures higher than 10 kPa where the highest span values for both silica and rutin stabilised emulsions were observed. However, this could be improved by using a membrane with a lower porosity and narrower pore size distribution than the SPG membrane used in this study, such as a metal laser drilled membrane.

Addressing these milestones, rotating membrane emulsification could be deployed for a wider range of food and pharmaceutical applications that low shear is required to handle sensitive ingredients and sustainable manufacturing of highly controlled structures with enhanced nutritional/ health benefits.

Chapter 5

Pickering particle and Emulsifier Co-stabilised Emulsions produced via Rotating Membrane Emulsification

Data and discussions contained within this chapter have been published within:

Arkoumanis, P.G., Norton, I.T. and Spyropoulos, F., (2019). Pickering particle and emulsifier co-stabilised emulsions produced via rotating membrane emulsification. *Colloids and Surfaces A: Physicochemical and Engineering Aspects*, 568, pp.481-492.

Abstract

Producing stable particle-stabilised emulsions of small droplet sizes and high monodispersity via membrane emulsification approaches is hindered by the poor mixing environment during processing and the low diffusivity and minimal interfacial tension lowering capacity of colloidal particles. The present study investigates the co-stabilisation (particles and emulsifiers) of O/W emulsions formed by rotating membrane emulsification. Formulation aspects of the employed co-stabilisation strategy (type/concentration of emulsifiers and type/size of particles) were assessed at a fixed transmembrane pressure (10 kPa) and rotational velocity (2000 rpm). Emulsion microstructure was shown to be affected by the occurrence of emulsifier/particle interactions. In formulations where these interactions are synergistic and emulsifier content is low, interfacial stabilisation is carried out by both species and resulting emulsions possess smaller droplet sizes, higher monodispersity indices and enhanced stability against coalescence, compared to systems stabilised by either of the two components alone. This work concludes that a carefully controlled co-stabilisation strategy can overcome the current challenges associated with the production of particle-stabilised emulsions via membrane emulsification methods.

5.1. Introduction

The incorporation of one phase into another immiscible phase is the basis of the microstructure of many emulsion-based products. A variety of emulsification processes have been developed to deliver this microstructure which usually requires high energy dissipation to effectively breakup droplets to a finite size thereby improving stability and overall quality of the finished product [195]. However, the high mechanical stresses generated by these processes may be unfavourable in the case of sensitive ingredients (e.g. bioactives) incorporated in the system thus making them less functional. Additionally, the repeated random breakup of droplets can increase re-coalescence rates and hence emulsion polydispersity [28]. What is more, emulsification techniques based on comminution are typically associated with high energy inputs and significantly low energy efficiencies [196].

Membrane emulsification (ME) is a promising technique that requires a much lower energy input compared to traditional emulsification methods, whilst at the same time produces emulsions with low polydispersity [110, 197]. Droplets are formed one-at-the-time by introducing the to-be-dispersed phase through a porous membrane into the external continuous and in response to a number of forces acting on the developing droplet [110]. Droplet size can be tuned depending on process conditions (e.g. transmembrane pressure, rotational velocity), formulation characteristics (surfactant/stabiliser type and concentration, dispersed phase fraction) and membrane properties (pore size, porosity, hydrophilicity/hydrophobicity) [149]. Several configurations of membrane emulsification have been identified including cross-flow, stirred vessel, vibrating and pulsed membrane set-ups [198]. The advantage of rotating membrane emulsification (RME) against other process configurations primarily stems from the additional centrifugal force exerted on the emerging

phase, which not only promotes earlier detachment but also assists in moving formed droplets away from the membrane surface [199].

Because of the crucial role of emulsifiers in aiding droplet detachment, current membrane emulsification literature is primarily focused on emulsions produced in the presence of such surface active species and studies investigating alternative emulsion stabilisation approaches, such as Pickering stabilisation, are limited. Pickering emulsions have received great attention in literature predominantly due to their superior stability and the Pickering functionality of a range of colloidal particles (including species formed from edible sources) has been extensively studied [2, 11, 200, 201]. However, the vast majority of Pickering emulsion literature focuses on the utilisation of conventional high energy input emulsification methods. The reason for this is that ME operation is not well placed to facilitate particle adsorption at the oil/water interface and thus emulsion stability is either compromised or is achieved at the expense of large emulsion droplet sizes.

Conversely to classic emulsifiers that spontaneously adsorb at an interface through diffusion, colloidal particles need to possess adequate kinetic energy to initially be transferred via convection to the droplet subsurface and from there to finally overcome the energy barrier associated with their adsorption at the oil/water surface [46, 187]. Particle wettability (contact angle) and size will then determine whether adsorption will be irreversible [58]. Due to its low-energy input and poor mixing environment, the RME (and ME in general) operation does not encourage particle transfer towards the droplet subsurface and thus Pickering stabilisation is significantly delayed and often ineffective. In recent studies, the stability and droplet size of emulsions prepared with silica and latex nanoparticles and processed with a rotating membrane device was investigated [12, 13]. The authors reported large droplet sizes and

enhanced coalescence phenomena, which were attributed to the fact that the critical time for adsorption of particles at the interface was higher than the droplet formation time.

A feasible strategy to enhance the Pickering stabilisation of emulsions produced by high shear methods has been to combine colloidal particles with emulsifiers [202, 203]. For example, in both silica particles/Tween 20 [80] and hydroxypropyl methyl cellulose particles/Tween 60 [87] co-stabilisation approaches, advances in Pickering stabilisation under high shear mixing were indeed reported but only at a low emulsifier content. Despite its relative prevalence in emulsions formed by high shear techniques, the utilisation of a co-stabilisation strategy in ME has only been reported once. Co-stabilised O/W Pickering emulsions were produced by RME using a laser-drilled stainless membrane and silica and latex particles in combination with a variety of low molecular weight (LMW) emulsifiers [15]. The authors reported co-stabilisation by either competitive (no interaction between the two species) or synergistic adsorption (electrostatic and/or hydrophobic attraction between species) onto oil droplets.

The present study aims to extend the currently limited scientific understanding on the effectiveness of co-stabilisation approaches in O/W emulsions produced by RME. The strategy employed here is devised to assess for the first time the effectiveness of a protein (whey protein isolate) as the emulsifier species within the co-stabilisation formulation and compare it to the behaviour of a small molecular weight emulsifier (Tween 20). Emulsions are formed using a RME device in the presence of either emulsifier (Tween 20 or WPI) together with two types of colloidal particles (silica or hydroxypropyl methyl cellulose particles) of demonstrated Pickering functionality [14, 80, 87]. The effectiveness of the co-stabilisation approach was assessed at a fixed transmembrane pressure of 10 kPa and a constant rotational velocity of 2000 rpm. Formulation aspects of the co-stabilisation strategy were related to the droplet size, droplet size distribution and coalescence stability over time (up to three weeks)

of the produced emulsions. Only considering Pickering emulsions produced under the same RME processing conditions, co-stabilised systems with only a 0.05 wt.% emulsifier content are shown to produce emulsions of much lower droplet sizes (20 μm rather than 40 μm), higher monodispersity (span value of 0.7 as opposed to 2) and enhanced long term stability.

5.2. Results and discussion

5.2.1. Particle and mixed particle-emulsifier aqueous suspensions

The coexistence of particles and classic emulsifiers in the aqueous phase could trigger electrostatic and/or hydrophobic interactions between the species owing to the surface chemistry of each entity and this could affect emulsification and emulsion stability [2, 10]. An increase of the particle size and/ or the increase of the zeta potential of particles towards a net value upon addition of emulsifiers could be a valid indication that interactions occur between the species. For example in the work of Binks *et al.* the adsorption of a cationic surfactant (CTAB) to silica nanoparticles was accompanied by an increase in the magnitude of the zeta potential from negative to positive value [14]. However, it is rather difficult to identify precisely the type and strength of underlying interactions in such systems; therefore, a combined approach was used to describe the events based on the available characterisation data. The particle size and the zeta potential of species alone and mixed in water was measured (Table 5.1). In general, it can be seen that for aqueous suspensions of silica particles the addition of emulsifier caused a statistically significant ($p < 0.05$) rise in the particle size whereas the effect on HPMC suspensions was negligible. The zeta potential did not change considerably when Tween 20 was present in mixtures with silica particles however this was different when HPMC was utilised as a Pickering particle. Furthermore, the zeta potential of

both particle suspensions in the presence of WPI increased towards more positive values as it was confirmed by statistical analysis ($p < 0.05$).

5.2.1.1. Effect of Tween 20

Addition of Tween 20 molecules in the native silica suspension (hydrophilic particles carrying a strong negative charge) and subsequent reduction of pH to 2 resulted in extensive sedimentation. Even the presence of a small amount of Tween above CMC resulted in depletion interaction causing the uncharged silica particles to approach and cluster. As a result, large flocs of silica particles formed and sank to the bottom of the vial. A similar mechanism is reported as effective inter-particle attraction between silica nanoparticles due to depletion interaction caused by the addition of non-ionic nonethylene glycol dodecyl ether ($C_{12}E_9$) [204]. Consequently, two distinct layers appeared after a short time, a Tween 20 rich phase (clear transparent) formed at the top and a silica-rich phase (turbid sediment) at the bottom (Fig. 5.1). The higher the Tween 20 concentration, the stronger the depletion interaction between silica particles became. At high concentration of Tween 20 (3 wt.%) silica particles grouped in larger heavier flocs thus the thickness of the sediment layer appears smaller and denser. The large size of the particle flocs did not allow for measurement through DLS, so the size distribution data are presented in Fig. 5.2 as delivered through SMLS. Suspensions of silica particles containing a high concentration of Tween 20 presented large particle aggregates with an average diameter of 18.7 μm , almost double the size measured when a low concentration of Tween was used. Smaller particle size was identified for both mixtures as well at 4 μm approximately. Mixtures of silica containing 0.05 wt.% Tween 20 generated narrower distribution corresponding to a span value of 0.943 as opposed to mixtures of silica and 3 wt.% Tween 20 with a span of 1.178. The zeta potential values of the mixed silica-Tween 20 suspensions at pH 2 (Table 5.1) were almost equal to the silica alone

(no significant difference found by statistical analysis) suggesting that no significant adsorption of Tween 20 molecules on silica particle took place.

Table 5.1: Z- average size, zeta potential and the corresponding span or polydispersity index (PDI) of aqueous particle suspensions and their mixtures with emulsifiers. Particle concentration was 3 wt.% in all cases. Samples annotated with a star presented more than one peaks and their particle size distribution is presented in Appendix B.

Aqueous phase	pH	Z-average size (nm)	PDI (-)	Zeta potential (mV)
Species alone				
3T	2	8.3 ± 2.4	0.19 ± 0.02	-0.21 ± 1.3
3T	6.5	8.5 ± 2.1	0.23 ± 0.02	-0.06 ± 0.9
3W*	2	206 ± 11	0.30 ± 0.03	17.9 ± 0.6
3W	6.5	18.3 ± 6.3	0.44 ± 0.09	-7.14 ± 0.3
S*	2	38.1 ± 0.5	0.25 ± 0.4	-0.02 ± 0.1
H	6.5	389 ± 12	0.45 ± 0.05	-4.5 ± 0.6
Mixed species				
S / 0.05T	2	Out of range		-0.46 ± 0.3
S / 3T	2	Out of range		0.82 ± 0.2
S / 0.05W	2	182 ± 12.1	0.55 ± 0.04	18.9 ± 0.8
S / 3W*	2	208 ± 9.8	0.34 ± 0.02	20.4 ± 0.1
H / 0.05T	6.5	404 ± 11	0.42 ± 0.18	-2.1 ± 0.4
H / 3T	6.5	409 ± 7	0.51 ± 0.05	-1.9 ± 0.3
H / 0.05W	6.5	394 ± 5	0.43 ± 0.12	-2.6 ± 0.1
H / 3W	6.5	401 ± 12	0.46 ± 0.09	-2.1 ± 0.4

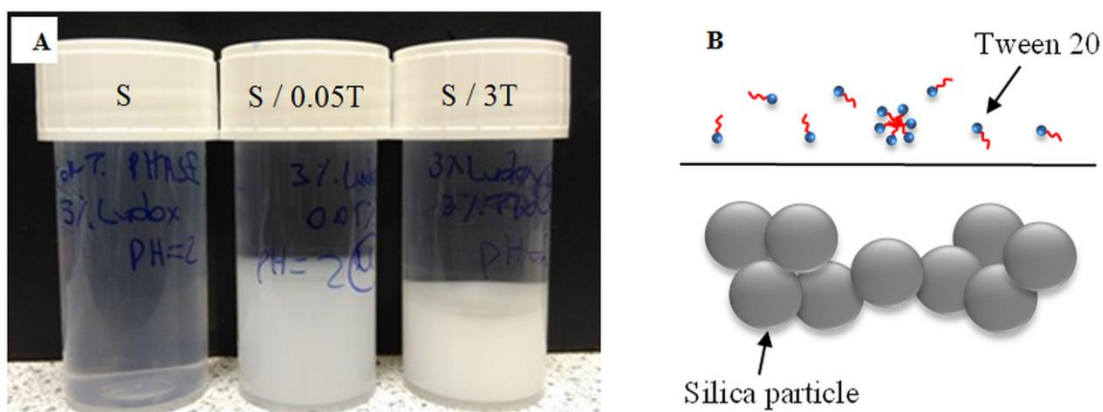


Fig. 5.1: (A) Aqueous suspensions of 3 wt.% silica particles alone, mixed with 0.05 wt.% and 3 wt.% Tween 20, 1 day after preparation, all at pH 2. (B) Schematic of the top and bottom layers of the aqueous mixtures.

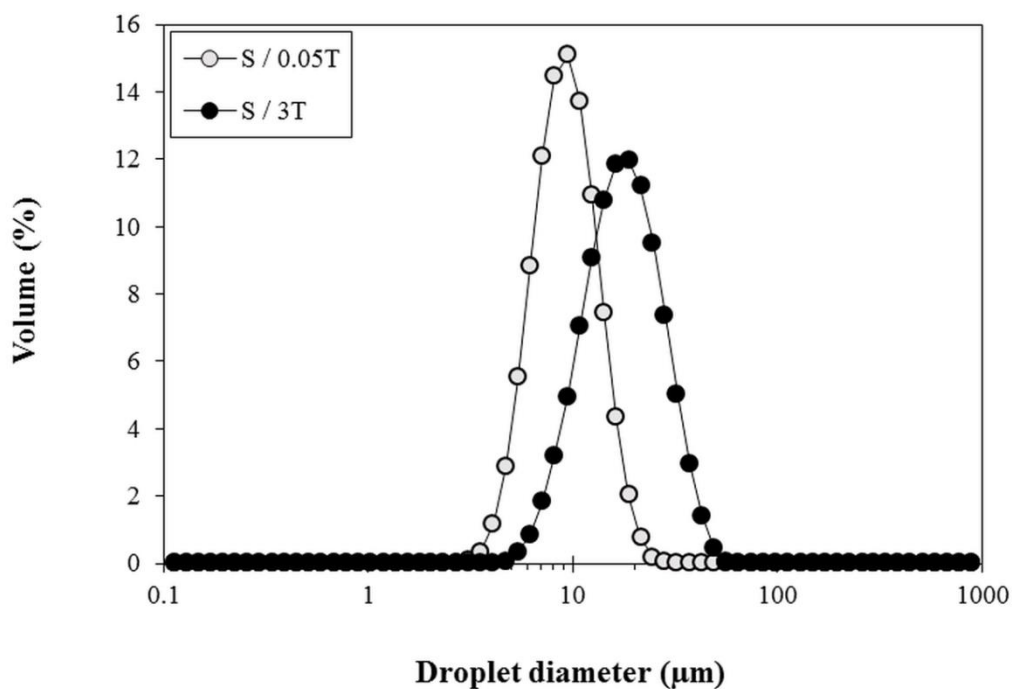


Fig. 5.2: Particle size of aqueous suspensions of 3 wt.% silica particles mixed with Tween 20 at pH 2.

HPMC exhibits a certain degree of hydrophobicity therefore in an aqueous environment the molecule folds and exposes its hydrophilic domains resembling the structure of a soft colloidal particle [65]. Addition of Tween to aqueous HPMC suspensions had a different effect than when silica particles were used. HPMC particles alone carried a weak negative charge at their native pH which slightly moved towards a neutral charge upon addition of Tween (Table 5.1). This change in the zeta potential of the HPMC particles was found statistically significant ($p < 0.05$) and it could imply adsorption of Tween on the HPMC surface, however this is debatable given the minor change in the size. Indeed several studies have focused on interactions occurring in mixtures of cellulose and LMW emulsifiers though this is mainly limited to ionic surfactants [205, 206]. Admittedly, interactions between surfactant and cellulose surfaces is reported and increased surfactant concentration is associated with increased coverage of cellulose particles by surfactant molecules [171, 207]. Furthermore, it was found that the surfactant hydrophilic head group interacts with the hydrophilic cellulose surface as evidenced by atomic force microscopy [208]. A schematic representation of the possible arrangements of species in the HPMC - Tween 20 aqueous mixtures is given in Fig. 5.3.

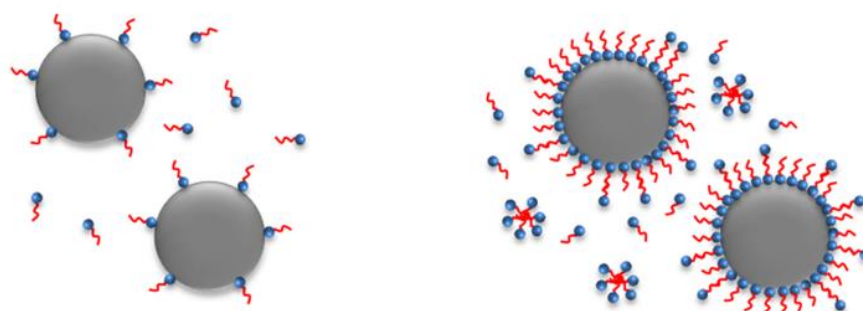


Fig. 5.3: Schematic representation of aqueous suspensions of 3 wt.% HPMC particles mixed with 0.05 wt.% (left) and 3 wt.% Tween 20 (right), at pH=6.5.

At low concentration of Tween 20 close to the CMC, the emulsifier molecules are sparsely distributed along the surface of HPMC particles with the hydrophobic tail protruding in the aqueous phase forming a monolayer of Tween molecules. At a high concentration of Tween (well above the CMC) the abundance of Tween molecules allows for full coating of the HPMC particles. The Tween molecules are densely packed on the particle surface and a double layer of Tween molecules may be formed due to the hydrophobic attraction between the tails of the surfactants, so this can explain the minor change in the size and the slight decrease of the net charge towards the neutral value. As a result, particle wettability could switch from hydrophilic to hydrophobic and back to hydrophilic. This scenario has been reported for mixtures of negatively charged silica particles and cationic surfactants [14], although in the case of HPMC particles and Tween 20 both species are nonpolar so electrostatic interactions are unlikely to occur.

5.2.1.2. Effect of WPI

WPI is an amphiphilic globular molecule and can adsorb both to hydrophobic and hydrophilic interfaces giving rise to steric interactions [31]. Unlike non-ionic Tween 20, WPI is carrying a strong charge away from its isoelectric point (IEP), that being approximately at pH values between 4.5 and 5.5. At pH values below IEP WPI carries a positive charge whereas at pH above IEP it is negatively charged [51]. This is confirmed by the zeta potential measurements (Table 5.1). As a result, electrostatic interactions may occur either between neighbouring proteins and/ or protein - particle surface. Stability of aqueous mixtures of particles and WPI can be affected by both steric and electrostatic interactions and the surface character of the particle should also be considered.

In Table 5.1 it is shown that the size of the silica particles when WPI was present at pH 2 was larger by approximately 150 – 170 nm compared to silica alone. Furthermore, the zeta potential of the silica particles moved from almost zero to higher positive values, demonstrating a significant change ($p < 0.05$) which suggested adsorption of WPI molecules on the silica surface. During preparation of the mixed silica - WPI suspension at its native pH 10 it is possible that some WPI molecules adsorbed to silica particles despite both carrying a net negative charge. Reducing the pH closer to the IEP of the protein caused nanoparticle aggregation and the aqueous mixture became turbid. Finally, when pH reached 2 below the IEP of the protein, the WPI obtained a net positive charge and repulsive forces between the coated silica particles dominated thus the aqueous mixture became clear again (Fig. 5.4A). Similar observations could explain these findings for aqueous mixtures of silica particles and β -lactoglobulin in other studies, and since β -lactoglobulin is the main constituent of the WPI molecule (48 wt.% on dry basis) [209], these are reported here. In one of the studies the authors argue that despite the net negative charge of the protein at high pH, protein may reveal positive charges that appear due to the patchy distribution of the charges on the protein surface [210]. Exposure of the positive charges of WPI at high pH may appear due to the unfolding of the molecule whereas at pH lower than the IEP WPI folds [211]. As such, at high pH the protein could be electrostatically attracted to the surface of negatively charged silica particles, yet maintaining an overall net negative charge that would keep coated silica particles apart from each other and this could explain the clarity of the suspension at high pH. In another study it was shown that the aqueous mixtures of silica particles and β -lactoglobulin were stable at pH values far from the IEP while close to the IEP nanoparticle aggregation was induced due to the absence of electrostatic interactions [212] so this explains the turbidity of

the suspension close to the IEP of the protein and the fact that the suspension became clear again upon further reducing pH to 2.

The presence of WPI in HPMC aqueous suspensions is expected to affect the behaviour of the mixture as it has been documented that mixtures of proteins and polysaccharides under certain conditions may form electrostatic complexes [213]. Moreover upon reduction of the pH to values lower than the IEP of the protein electrostatic attraction between the two biopolymers - positively charged protein and anionic polysaccharide- may occur resulting in their association forming very stable conjugates that remain soluble in the aqueous phase.

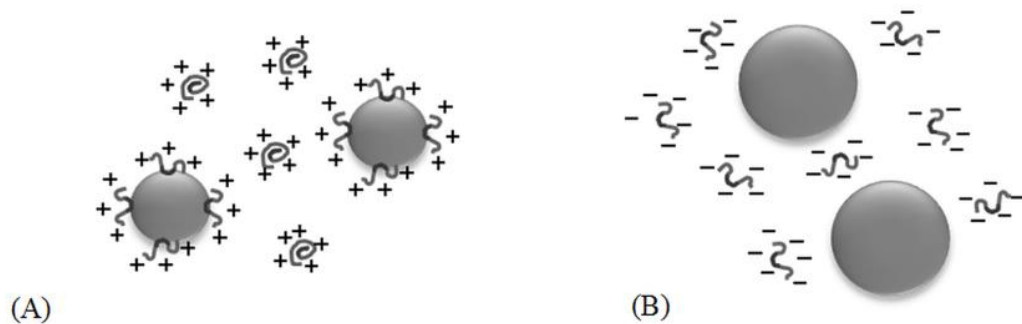


Fig. 5.4: Schematic representation of aqueous suspensions of WPI mixed with (A) silica at pH=2 and (B) HPMC particles at pH=6.5.

However, the pH of the studied HPMC - WPI aqueous mixtures were maintained at 6.5 above the IEP of the WPI so the formation of the complexes should be ruled out. This theory agrees with the experimental data as it is shown in Table 5.1 the size of the HPMC particles did not change substantially ($p > 0.05$). Similar observations were highlighted for mixtures of HPMC and β -lactoglobulin as it is reported that complexation was not possible due to the negligible increase of the particle size or modification of the zeta potential [86]. Consequently, it is possible that HPMC particles and WPI molecules co-existed as separate entities in the

aqueous phase with the latter interfering between HPMC particles and preventing flocculation as it is shown schematically in Fig. 5.4B.

5.2.2. Co-stabilised Pickering emulsions

5.2.2.1. Effect of Tween 20

Fig. 5.5 shows the effect of Tween 20 concentration on the droplet size and span of emulsions prepared with a fixed concentration of silica particles and varying concentrations of Tween 20 as a co-stabiliser. Emulsions stabilised with each species alone were also produced and their stability was tested throughout 3 weeks. It can be seen that silica particles alone yielded emulsions whose droplet size did not change dramatically after 21 days however an oil layer of stable thickness was present from the day of production. Despite the abundance of silica particles to coat all formed droplets, the kinetic energy of the particles was not sufficient to adsorb to the oil droplets due to the poor energy dissipation in the emulsion via the RME process (data not shown here). Another possible explanation for this could be the gradual accumulation of oil droplets within short proximity from the membrane. If this was the occasion, as emulsification continued it would be difficult for the silica particles located to the outer bulk to travel through the dense “cloud” of droplets and this could explain the oil layer that appeared by the end of emulsification.

Compared to 3 wt.% Tween alone, emulsions stabilised with a low concentration of Tween (0.05 wt.%) presented a gradual increase in their droplet size and span that was more evident after 7 days as also indicated by the growing thickness of the oil layer that appeared following emulsification. This could be due to the rapid depletion of emulsifier at low concentration of emulsifier that caused the rate of adsorption to decrease close to the membrane surface and thus coalescence of adjacent droplets resulted in larger droplet size and width distribution. It

was argued that at low concentrations of emulsifier formulation is the limiting factor and not the processing conditions [141]. Indeed a substantial increase in the droplet size and span of Tween 20 stabilised emulsions (1% oil content) through RME was found for concentrations lower than 0.2 wt. % [140].

The addition of small amount of Tween (0.05 wt.%) in the silica suspension did not have tremendous influence at the resultant droplet size of co-stabilised emulsions showing a slight increase by 2 μm compared to silica alone, however, there was a moderate increase in the span. This could be due to the presence of the two non-interacting species in the aqueous phase: flocculated silica particles and Tween 20 free molecules (see Table 5.1) that could trigger competitive adsorption. Competition between silica particles and non-ionic emulsifiers for adsorption to the surface of oil droplets has been discussed before suggesting that the small surfactants adsorb initially providing short-term stabilisation facilitating larger silica particles to follow [185, 202]. Because of the increased viscosity of the mixture, adsorption of Tween molecules was delayed resulting in larger droplet size compared to 0.05 wt.% Tween alone. However, the subsequent attachment of silica particles improved steric repulsion between droplets as confirmed by the extremely stable span and droplet size values after 21 days. Increasing the concentration of Tween in the mixture generated emulsions with droplet size smaller than silica alone, yet closer to the droplet size of emulsions stabilised solely by 3 wt.% Tween 20. Unsurprisingly, the behaviour of these emulsions resembled that of surfactant stabilised emulsions because adsorption of the LMW emulsifiers dominated the droplet surface, excluding the adsorption of silica particles [185]. As a result of this competition, the span was kept at an intermediate level of 0.848 as opposed to 1.026 and 0.725 for silica and Tween stabilised emulsions respectively; a considerably low value to consider these emulsions fairly monodisperse.

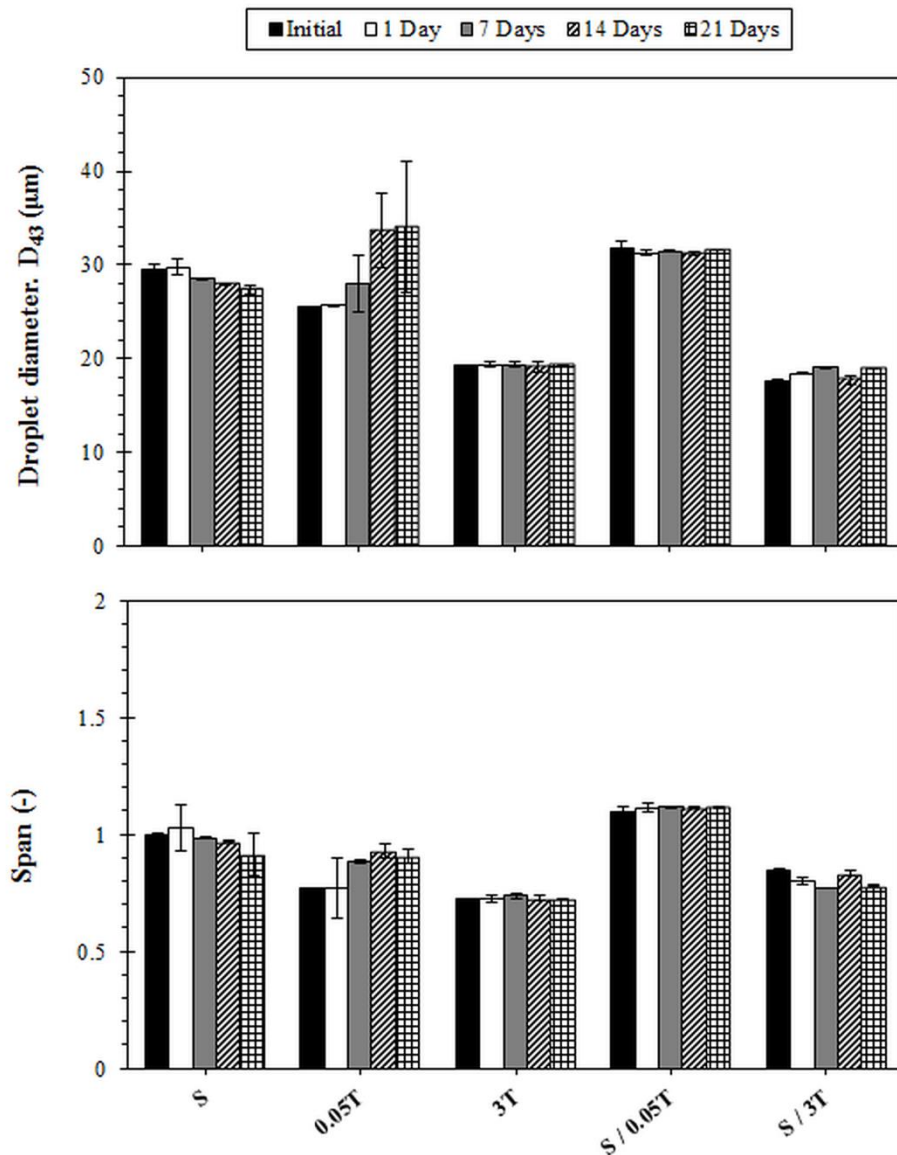


Fig. 5.5: Average droplet diameter and span values of emulsions stabilised with a fixed concentration of 3 wt.% silica and its mixtures with Tween 20 at pH 2. For co-stabilised emulsions, the average values account for droplets from all layers (see Fig. 6). An SPG 6.1 μm membrane was used at 10 kPa and 2000 rpm.

When comparing the two co-stabilised emulsions, it can also be seen that the droplet size of silica - 3 wt.% Tween emulsions was almost half the size of silica - 0.05 wt.% Tween emulsions and the span was much lower. This is attributed to the availability of the surfactant

close to the membrane surface and the higher viscosity of the silica - 3 wt.% Tween mixtures contributing to higher drag forces and thus smaller droplets [15]. It is worth noting that all co-stabilised emulsions were exceptionally stable after 21 days. In particular, emulsions co-stabilised with silica and 0.05 wt.% Tween 20 were stable with no signs of coalescence and no oil layer on the top, unlike emulsions stabilised by each species alone.

It should be noted that the resultant droplet size and span values of the co-stabilised emulsions is the contribution of two populations of droplets as a consequence of the co-stabilisation mechanism the droplets undergo. After emulsification the emulsions stabilised by silica - Tween mixtures formed gradually three layers: a cream layer on the top of the emulsions, a clear serum and a sediment at the bottom of the sample pot. This agrees with studies showing that sedimentation occurred for emulsions stabilised by mixtures of silica particles and non-ionic emulsifier due to flocculation of silica particles upon addition of surfactant [202]. Excluding the cream layer, the appearance of these emulsions was similar to the silica - Tween aqueous suspensions because of the large size of the silica flocs (Table 5.1 & Fig. 5.2). However, in this case both the cream and sediment contained droplets as it is shown in the micrographs (Fig. 5.6). The cream layer was denser containing more droplets that were strongly flocculated as opposed to droplets residing at the bottom and this is reported elsewhere [15]. Therefore it was suggested that the creamy layer consisted primarily of droplets stabilised by Tween whereas flocs of silica particles dominated on the surface of oil droplets at the bottom layer. As it is shown by the droplet size distribution, droplets of similar size existed at both layers however smaller sizes were picked up by DLS measurements from the bottom layer due to the presence of free silica aggregates and that also explains the larger span value.

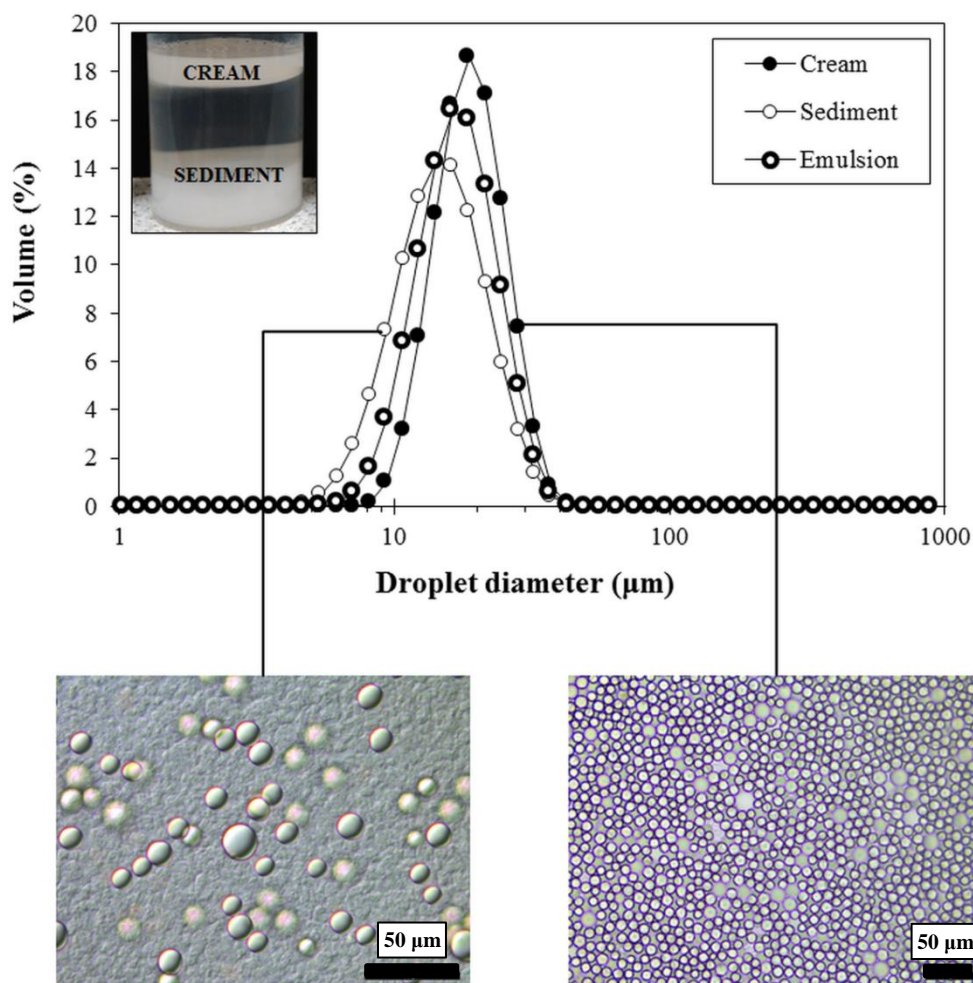


Fig. 5.6: Droplet size distribution of emulsion co-stabilised with 3 wt.% silica and 3 wt.% Tween 20 at pH 2 after 1 day. Micrographs were taken from the cream and the sediment layer of the emulsion. The scale is 50 µm in all cases.

To confirm this, oil droplets stabilised by mixtures of silica-Tween were visualised through Cryo-SEM and their surface morphology was compared with those stabilised by either of the species alone. Fig. 5.7A-B shows an oil droplet stabilised solely by silica particles whose surface is clearly occupied by flocs of small silica particles in very close packing with size comparable to our findings (Table 5.1). The surface of this droplet shows some irregularities when compared to the solely Tween stabilised droplet which has a smoother surface (Fig. 5.7C). These ‘wrinkles’ have been previously suggested to indicate the presence of particles at

the oil-water interfaces [214]. In order to clearly visualise oil droplets through Cryo-SEM most of the water was removed by freeze fracturing of emulsion samples and this was followed by dusting the samples with gold particles under vacuum. It is this process that generated large pressure gradients and caused the particle-stabilised droplets to appear a corrugated surface [215].

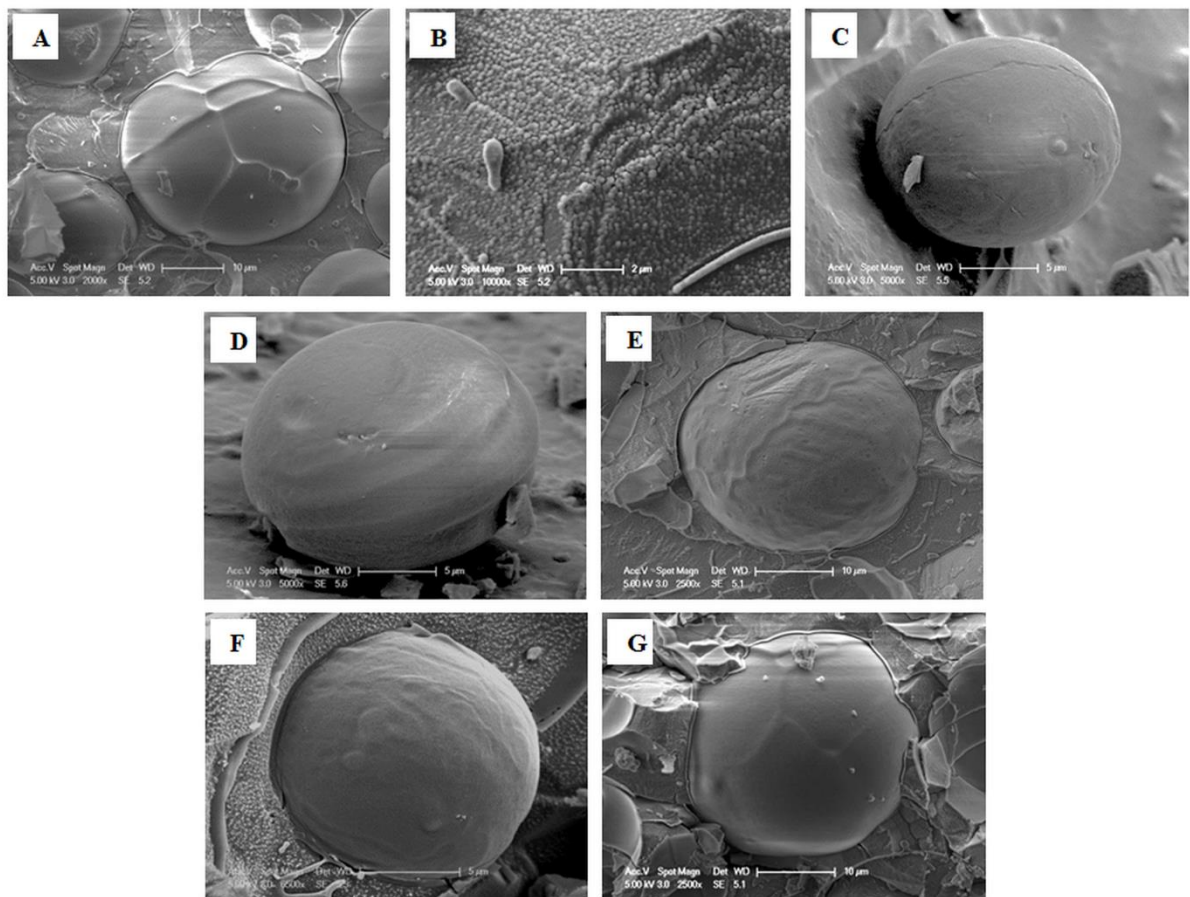


Fig. 5.7: Cryo-SEM micrographs of emulsion droplets stabilised by 3 wt.% silica alone with a close-up of the droplet surface (A-B), 3 wt.% Tween 20 alone (C), 3 wt.% silica mixed with 0.05 wt. % Tween 20 top and bottom layer (D-E), 3 wt.% silica mixed with 3 wt.% Tween 20 top and bottom layer (F-G). All emulsions were produced by an SPG 6.1 μm at 10 kPa and 2000 rpm. All pictures were taken 3 days following emulsification.

Collapsing of a monolayer of particles adsorbed on the oil-water interface, also reported as 'buckling', took place when surface pressure equalised with the interfacial tension of oil/water [216]. Presumably, a small amount of oil can escape making the total surface area of droplets smaller so the strongly adsorbed particles compress in order to cover a smaller area. This is clearly seen in Fig. 5.7E & G where droplets from the bottom layer of co-stabilised emulsions presented wrinkles alongside their surface. On the contrary droplets from the creamy layer had a different morphology and their surface appeared smoother (Fig. 5.7D & F). Hence the top layer consisted of drops stabilised mainly by Tween while the sediment contained mainly drops stabilised by silica particles.

The effect of the concentration of Tween20 on the droplet size and span of emulsions co-stabilised with mixtures of HPMC and Tween and adjusted at pH 6.5 is shown in Fig. 5.8 for a period of 21 days. Emulsions prepared using HPMC alone phase separated completely within a short time after production and therefore no further stability data are presented. These results correlate with data showing that emulsions produced by cellulose nanocrystals were unstable in the absence of surfactant [217]. Furthermore, it was shown that due to the low energy dissipation via RME the kinetic energy of this particle close to the membrane surface was not sufficient to induce an energy barrier for adsorption (data not shown here).

For freshly produced emulsions containing 0.05 wt.% Tween 20 at pH 6.5, the droplet size and the span were found larger compared to the same emulsions prepared at pH 2. Although in general non-ionic emulsifiers are considered to be pH insensitive, it is reported that the hydration rate of Tween molecules (initial concentration 0.02%) dissolved in aqueous medium at pH 2 was almost four times higher than pH 6.5 [218]. Furthermore in another study it was shown that increasing the pH of non-ionic Tween 40 would cause less hydration per unit mass of surfactant and the critical micelle concentration is decreased considerably

which means more surfactant micelles in the aqueous solution [219]. Consequently, it is possible that the availability of Tween molecules for adsorption at low pH was increased causing faster reduction of the interfacial tension and thus smaller drops. This effect was not pronounced at higher concentrations of surfactant therefore droplet size and span of Tween only stabilised emulsions were similar at both pH values. As expected, low concentration of emulsifier led to droplet coalescence after production as reflected by the slight increase in the drop size and the significant increase in the span from 0.914 to 1.159 after 21 days whereas high concentration of emulsifier resulted in stable emulsions with 12 μm smaller droplet size and very narrow distribution.

The presence of low concentration of Tween 20 in mixtures with HPMC allowed for the formation of co-stabilised emulsions with a remarkably smaller droplet size and span than emulsions stabilised by single species. Specifically, the droplet size of co-stabilised emulsion appeared 50% and 40% smaller than emulsions stabilised by HPMC alone and 0.05% Tween alone respectively. This behaviour is a typical example of the synergistic effect exhibited by the co-existence of two emulsifying agents in emulsions and has been reported for mixtures of small molecular surfactants with inorganic (silica) as well as other edible Pickering particulate structures (e.g. cellulose nanocrystals) [79, 217]. HPMC particles benefit from their interaction with the LMW emulsifiers (Table 5.1) rendering them partially hydrophobic, thereby enhancing their affinity to the oil surface. The co-stabilised emulsions were very monodisperse demonstrating a span of approximately 0.71 which is indicative of their robust stabilisation by HPMC particles. A similar system encompassing HPMC and Tween 80 has been found to operate in the same fashion [87]. The authors describe a surfactant-limiting co-stabilisation mechanism, clearly underlying the effect of surfactant concentration on the resultant droplet size and ultimate stability.

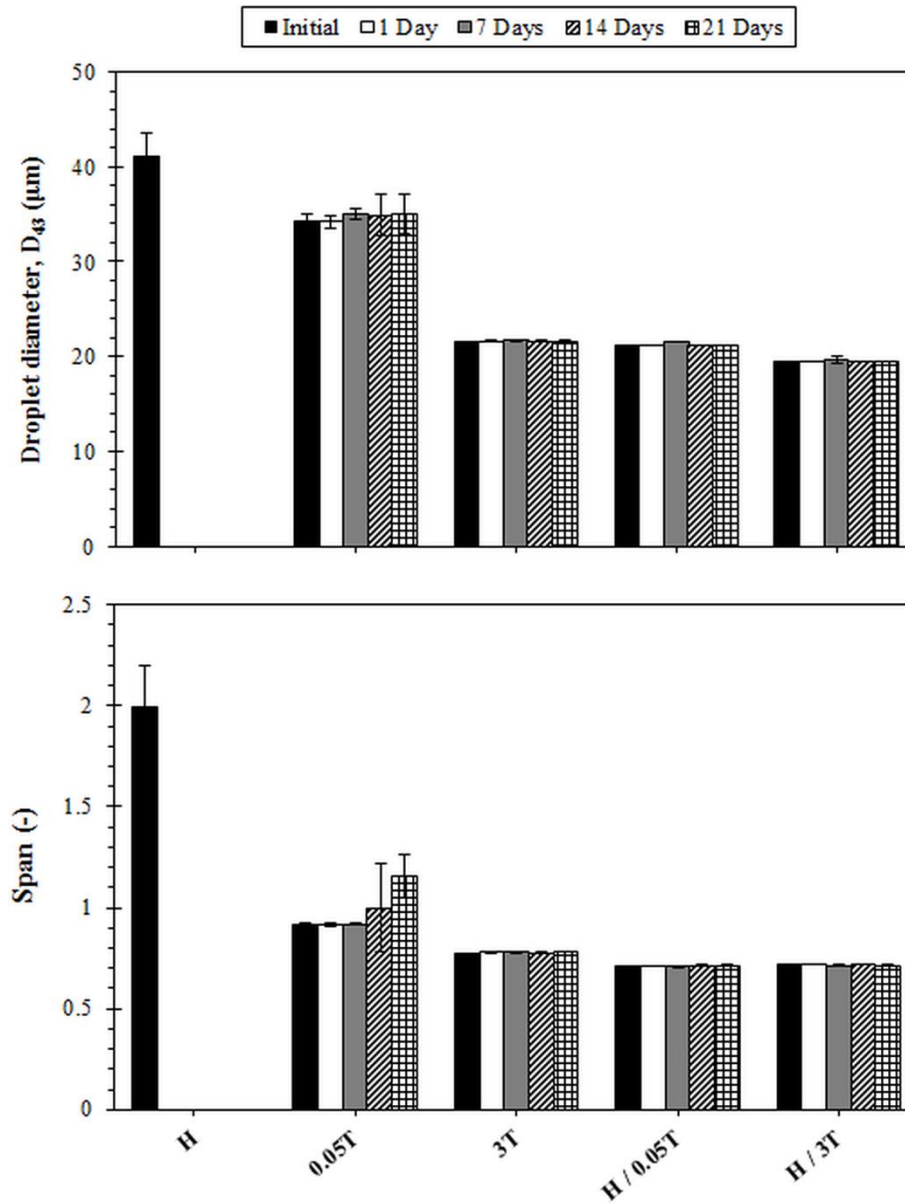


Fig. 5.8: Average droplet diameter and span values of emulsions stabilised with 3 wt.% HPMC and its mixtures with Tween 20 at pH 6.5. An SPG 6.1 μm membrane was used at 10 kPa and 2000 rpm.

They found that by increasing surfactant concentration considerably smaller droplets were produced as a consequence of the dominance of Tween molecules at the interface and their ability to induce droplet breakup. This is in contrast with our findings as it was observed that even at a higher emulsifier concentration (3 wt.%) the droplet size and span of co-stabilised

emulsions remained practically the same. This could be ascribed to the different structuring of the aqueous phase upon increasing Tween concentration as it can be seen in Fig. 5.9. At low emulsifier concentration, small particle aggregates were visible in the aqueous phase and on the droplet surface (Fig. 5.9A-B). This is in accordance with findings reporting that aggregates of cellulose nanocrystals and surfactant were sighted on the surface of PMMA particles [220]. Upon increasing of Tween concentration a gel network formed in the aqueous phase as shown in Fig. 5.9C. Formation of gel network has been reported for mixtures of non-ionic polymers and surfactants as interactions become significant when surfactant concentration reaches the critical aggregation concentration value [171]. More specifically, it is possible that the presence of more emulsifiers could cause HPMC particles to turn back to hydrophilic as new Tween20 molecules deposited on the existed emulsifier layer with the head groups exposed in the aqueous phase (see Fig. 5.3B) thereby decreasing their affinity for the oil droplet surface critical aggregation concentration value [171]. More specifically, it is possible that the presence of more emulsifiers could cause HPMC particles to turn back to hydrophilic as new Tween20 molecules deposited on the existed emulsifier layer with the head groups exposed in the aqueous phase (see Fig. 5.3B) thereby decreasing their affinity for the oil droplet surface. Consequently, the oil droplets were occupied by the free Tween20 whereas the association of the excluded HPMC particles coupled with less amount of water in the aqueous phase led to the formation of a gel network as it is seen in Fig. 5.9D. The increased viscosity of the gel network prevented collision of droplets and enhanced stability of emulsions, confirmed by the low span (0.717) that was very similar to HPMC – 0.05% Tween emulsions. Despite exhibiting different stabilisation mechanisms, very monodisperse small sized co-stabilised emulsions were produced by both concentrations of Tween 20 as a result of the use of the rotating membrane.

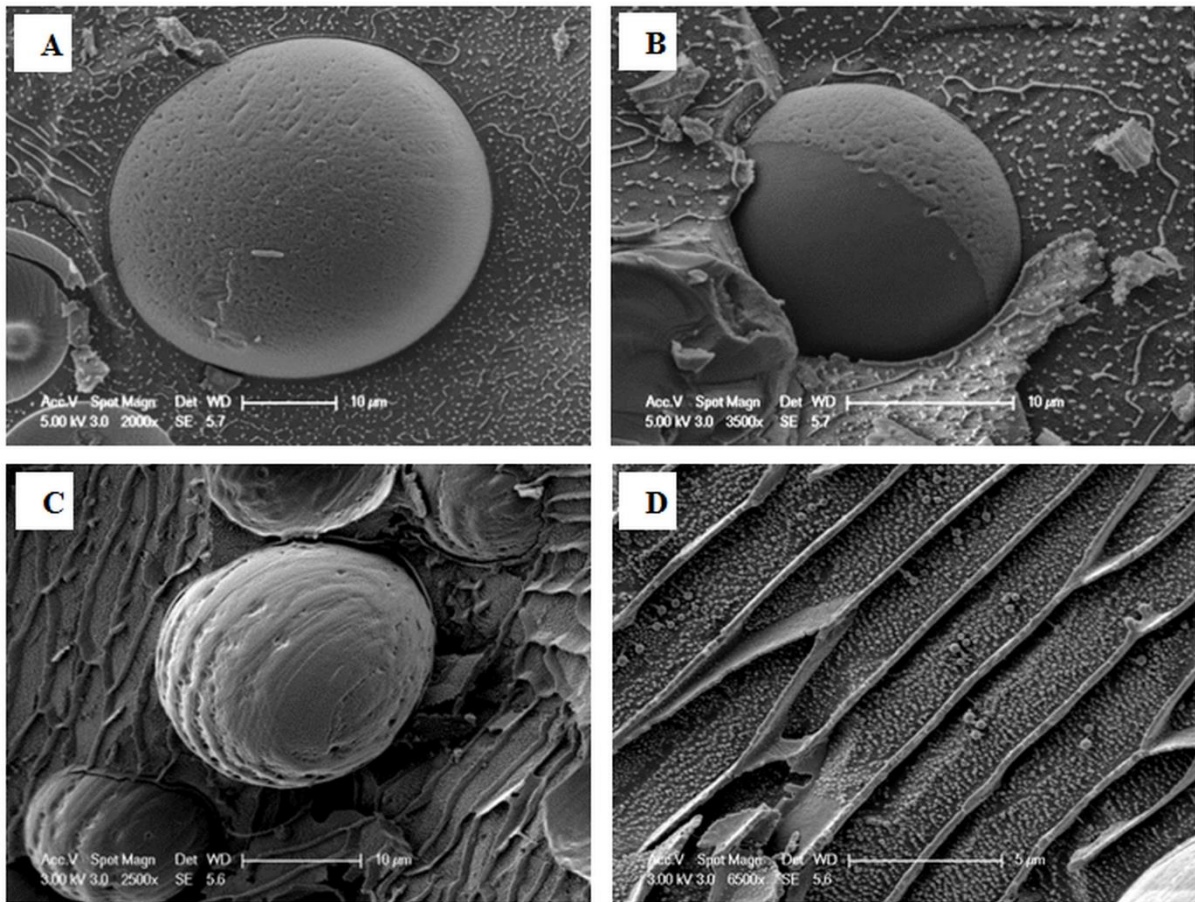


Fig. 5.9: Cryo-SEM micrographs of emulsion droplets stabilised by 3 wt.% HPMC mixed with (A-B) 0.05 wt.% Tween 20, (C-D) 3 wt.% Tween with a close-up of the aqueous phase gel network. All emulsions were produced by an SPG 6.1 µm at 10 kPa and 2000 rpm.

5.2.2.2. Effect of WPI

Fig. 5.10 illustrates the droplet size and span values of emulsions co-stabilised by silica particles and two concentrations of WPI and their stability after 21 days. For convenience, emulsions stabilised solely by silica are plotted again in order to facilitate comparisons and trends between the samples. Focusing on the systems with single WPI a similar trend can be distinguished with the Tween only stabilised emulsion; that is the reduction of the droplet size and span with increasing concentration of emulsifier. High concentration of emulsifier (3

wt.%) resulted in higher availability of emulsifiers close to the membrane surface causing a faster decrease in the interfacial tension and as a consequence smaller droplet size and span values after 21 days. To our knowledge there are not available literature findings for WPI stabilised emulsions prepared by membrane emulsification therefore sodium caseinate is mentioned here as a reference as it is a milk protein, yet it has a random coil structure so it is likely that it would behave differently during adsorption to oil-water interface compared to the globular WPI. It was reported that for SPG membrane at constant transmembrane pressure and rotational velocity, the droplet size of emulsions stabilised by sodium caseinate reduced upon increasing concentration of the protein from 0.1% to 3% whereas the droplet size distribution became narrower [127]. Because WPI is an HMW emulsifier transfer of the molecule to the oil-water interface was considerably slower than smaller Tween 20 and as a result the interfacial tension decreased at a slower rate. Hence low concentration of WPI (0.05 wt.%) in the aqueous phase generated larger droplets than the same concentration of Tween 20. In contrast at high concentration of emulsifier this effect was counteracted by the larger availability of emulsifier, and as a consequence, the droplet size and span values were very similar for both species. Therefore in this case droplet size appears to be governed by processing conditions rather than formulation-specific circumstances. As mentioned previously emulsions prepared with silica particles alone presented coalescence at a certain degree which was also the case for the emulsions made with 0.05 wt. % only. However, the presence of low concentration of WPI in the aqueous suspension of silica particles at pH 2 resulted in emulsions with droplet size that was 24% than silica alone and a span as low as 0.725. Certainly, both values were far smaller than systems whose aqueous phase included only 0.05 wt.% WPI. The emulsions showed remarkable stability throughout the entire period of 21 days as indicated by the minor changes in their droplet size and span values. This

behaviour could be related to the adsorption of WPI monomers on the silica surface rendering them more hydrophobic whilst surrounded by a positive charge (Fig. 5.4A).

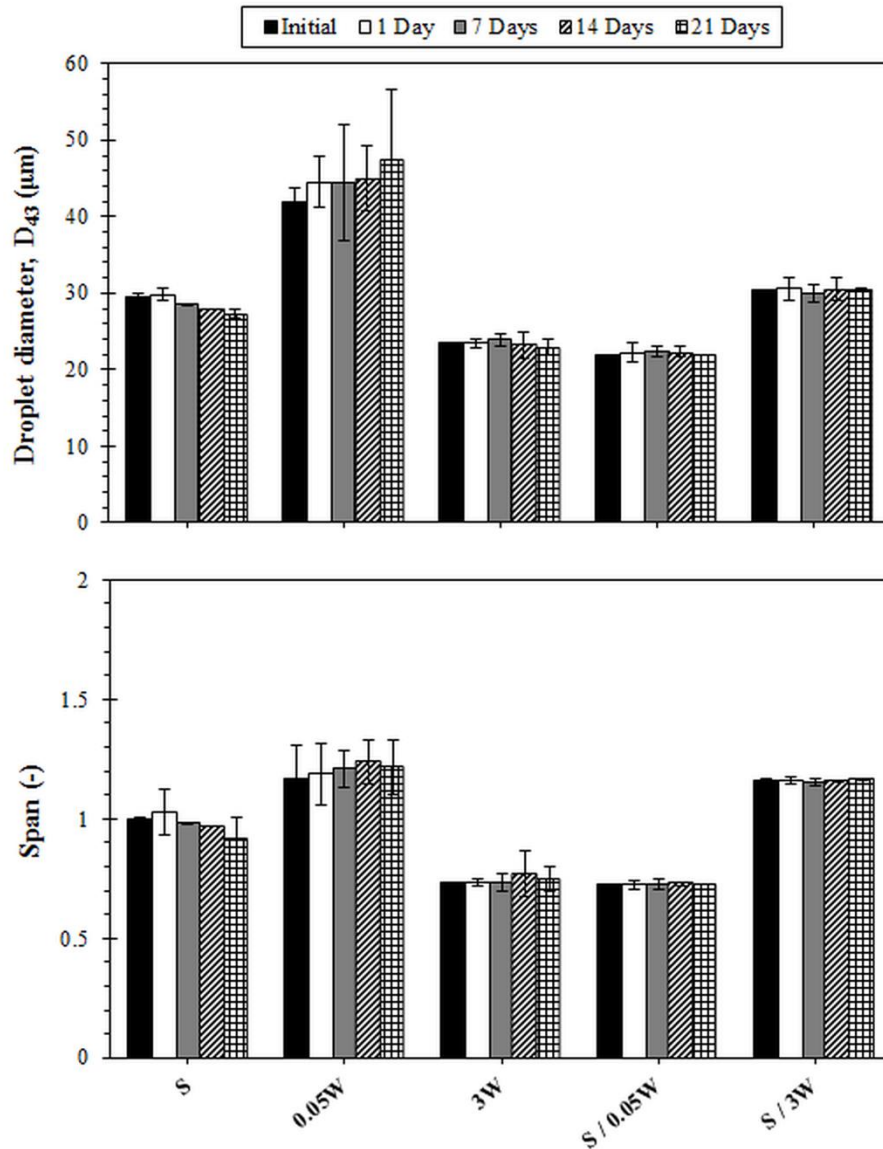


Fig. 5.10: Average droplet diameter and span values of emulsions stabilised with 3 wt.% silica and its mixtures with WPI at pH 2. An SPG 6.1 μm membrane was used at 10 kPa and 2000 rpm.

It is suggested that the modified silica particles were able to effectively decrease interfacial tension thus forming smaller droplets than silica particles alone whilst providing effective

stabilisation through steric and electrostatic repulsion between neighbouring droplets. The synergy between silica particles and β -lactoglobulin has been confirmed in the case of long-term stabilisation of foams [221]. In this study, it was found that the extent of Ostwald ripening was considerably delayed compared to the pure protein systems owing to an increase in the interfacial elasticity as delivered by the adsorbed protein so the same mechanism could also apply in our system and could be responsible for the remarkable stability of the investigated emulsions. Furthermore, it is possible that silica particles could be entrapped in the viscoelastic thin film created by the adsorbed proteins thereof constituting an additional layer that provides additional repulsive forces between droplets [222]. In a separate study, instead of β -lactoglobulin another milk protein sodium caseinate was used in mixtures with silica to show that significant reduction in the interfacial tension between oil-water took place when both species were present in the aqueous phase [185]. Surprisingly, high concentration of WPI in mixtures with silica particles yielded polydisperse emulsions with droplet size larger than when species were used alone. This could be associated with the increased viscosity of the aqueous mixture when high concentrations of WPI are present as the transfer of the emulsifier towards the oil-water interface is substantially lowered. At the same time due to higher viscosity, the newly generated droplets cannot move away from the membrane surface therefore the probability of coalescence was increased [153].

Emulsions prepared with HPMC-WPI mixtures exhibited very similar behaviour to the silica-Tween systems owing to the weak interactions between particles and co-stabilisers in the bulk that could signify competitive adsorption between the individual species. However unmodified HPMC particles are too hydrophilic to adsorb to the oil-water interface, and this was confirmed by complete phase separation of emulsions stabilised with HPMC alone shortly after emulsification. Therefore it was expected that WPI would dictate adsorption. As

it is seen in Fig. 5.11 the presence of low concentration of WPI in the aqueous mixture resulted in emulsions with similar droplet size to emulsions prepared with 0.05 wt.% WPI alone and their stability was also poor as it is shown by the dramatic increase in both the droplet size and the span particularly that was apparent from day 1.

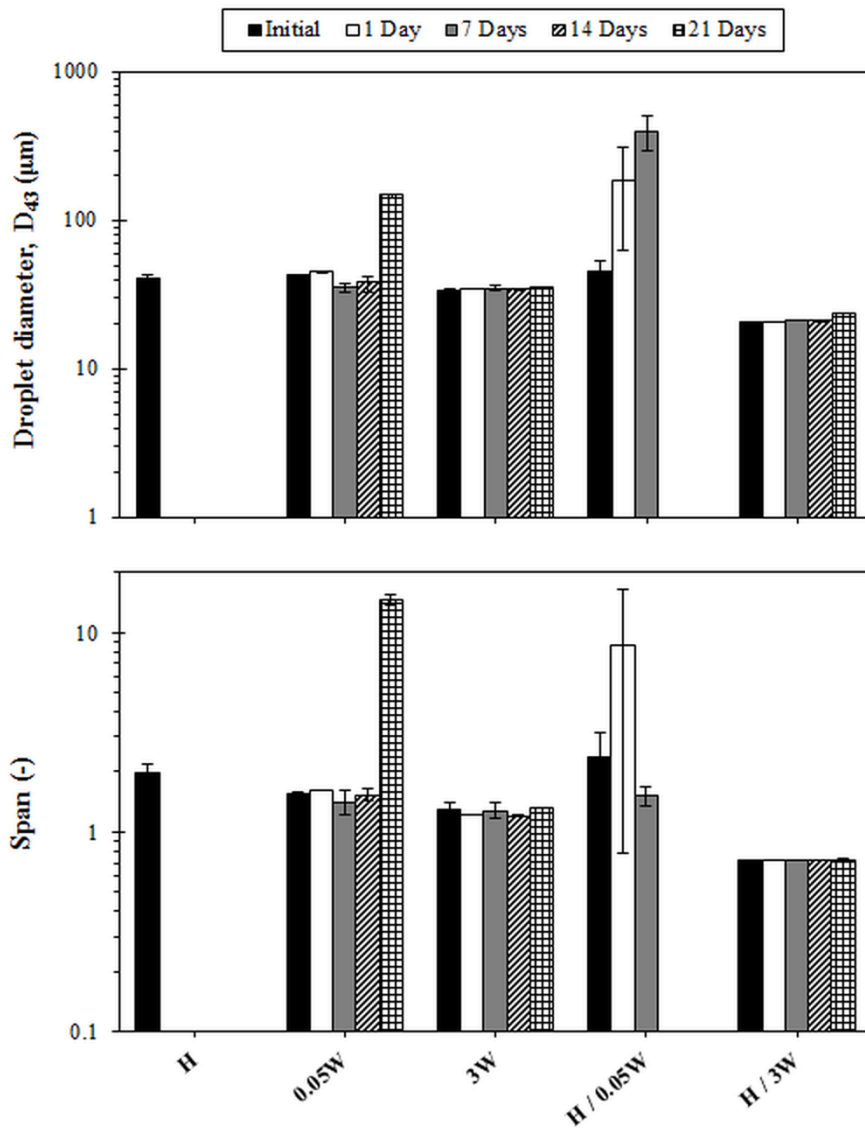


Fig. 5.11: Average droplet diameter and span values of emulsions stabilised with 3 wt.% HPMC and its mixtures with WPI at pH 6.5. An SPG 6.1 μm membrane was used at 10 kPa and 2000 rpm.

Previous studies in mixtures of HPMC and β -lactoglobulin confirm this hypothesis [86]. In this work, although a more hydrophobic type of HPMC has been used in conjunction with β -lactoglobulin it was documented that the protein dominates the oil-water interface as evidenced by the surface pressure measurements. The HPMC exclusion as it is mentioned occurred at pH 6 and the emulsions were characterised by a thin viscoelastic film which was indicative of WPI adsorption. This was also observed in our results as with the presence of high concentration of WPI in the mixture, emulsions appeared to have 51% smaller droplet size and approximately 50% smaller span than emulsions stabilised by these species alone. Although no significant interactions took place between HPMC particles and WPI molecules, the possibility of formation of a weak gel network as a result of induced particle flocculation in the aqueous phase should not be ruled out, especially in the presence of high concentration of WPI; that could explain the narrow droplet size distribution of emulsions stabilised by HPMC and 3 wt.% WPI via rotating membrane emulsification.

5.3. Conclusions

The effect of colloidal particle type and size, as well as the concentration and type of emulsifier has been demonstrated for the production of co-stabilised O/W Pickering emulsions with enhanced stability to coalescence, via rotating membrane emulsification. The bulk and interfacial behaviour of the aqueous particle-emulsifier mixtures was related to the resultant emulsion microstructure. Due to the low energy profile of the process, adsorption of colloidal particles to the oil-water interface was not encouraged, thereby yielding unstable emulsions. The synergism occurred when a low concentration of emulsifier adsorbed on particles, resulted in co-stabilised Pickering emulsions that were stable to coalescence with smaller droplets and lower polydispersity than emulsions prepared with either of the two

species alone at the same concentration. When adsorption of emulsifier on particles did not occur, species behaved as individual entities and competed to the surface of droplets. Hence, at low emulsifier concentration, silica-Tween 20 emulsions presented larger droplet size than those prepared by each species alone whereas emulsification failed for mixtures of HPMC and WPI. Upon increase of emulsifier concentration the oil droplet surface was dominated by the emulsifier and the increased viscosity of the aqueous particle-emulsifier mixture contributed to even smaller droplet size than emulsions stabilised solely with emulsifier. Notably, the exclusion of HPMC particles from the oil-water interface resulted in extra-stable monodisperse emulsions via the establishment of a weak gel network due to the depletion flocculation in the presence of high emulsifier concentrations. Depending on the surface chemistry of a particle, WPI could be a good alternative to Tween 20 to make stable Pickering emulsions via rotating membrane emulsification, as it can be used in low concentrations to achieve comparable results. The positioning of all species in the continuous phase rather than the internal oil phase suggests a feasible strategy for minimisation of internal fouling of the membrane that could improve production rates. In this context, rotating membrane emulsification offers a viable alternative to traditional techniques for the development of well-controlled edible microstructures that could be incorporated in foods as well as pharmaceuticals for example for controlled release of flavours or nutrients or targeted drug delivery purposes.

Chapter 6

Processing performance of rotating membrane emulsification for production of emulsions co-stabilised by Pickering particles and emulsifiers

Abstract

Despite the superior stability of Pickering emulsions compared to conventional surfactant-stabilised ones, their production through low-energy emulsification techniques such as membrane emulsification is restricted by the low diffusivity and minimal interfacial tension lowering ability of the colloidal particles. In this study, two types of colloidal particles of demonstrated Pickering functionality (silica and HPMC) were used in mixtures with small concentration (0.05 wt.%) of Tween 20 or WPI in water to produce O/W co-stabilised emulsions via rotating membrane emulsification (RME). The effect of the transmembrane pressure ranging between 10 – 150 kPa and two different types of membranes, with different pore size and porosity, on the emulsion microstructure was investigated at a fixed rotational velocity of 2000 rpm. Despite the larger droplet size produced by the stainless steel (SS) membrane with a mean pore size of 50 μm compared to the SPG of 6.1 μm mean pore size, the emulsions presented lower polydispersity indices with span values as low as 0.6 for the SS membrane. There was evidence that the interactions between the stabilising species and the SPG membrane could potentially influence the emulsification performance as it was realised by the reduction in the oil throughput when increasing the concentration of the emulsifier (WPI) in the co-stabilisation formulation, however this would be expected to contribute only at the initial stages. On the contrary, this was not observed for the SS membrane. RME produced stable emulsions at a transmembrane pressure of 50 kPa using 3 wt.% HPMC and 0.05 wt.% Tween 20 as co-stabilising species, with similar droplet size to HSM utilising less energy (44 as opposed to 104 MJ m^{-3}). RME was also capable of achieving narrower distribution than HSM compromising though the production rate.

6.1. Introduction

Pickering particles are of great interest as they have been used to enhance stability of emulsions (i.e. Pickering emulsions). Due to their capacity to bind strongly to the emulsion droplet surface, a large amount of energy is required to displace them, thus they provide superior stability against conventional surface active species [1, 10, 46, 57]. Several studies have highlighted the advantage of the synergism of Pickering particles and surface active species in interfacial stabilisation that results in emulsions with prolonged stability. The co-existence of both silica particles and small concentration of Tween 60 or NaCas in water resulted in emulsions that had smaller droplet size and were more stable than emulsions prepared with either of the individual species alone at the same concentration [80]. The authors reported that the species competed for the surface of the droplets at small concentration of emulsifier and the emulsifier lowered the interfacial tension that facilitated droplet break-up whilst providing short term stabilisation until adsorption of particles. Increasing the concentration of emulsifier beyond a critical value resulted in droplets with interfaces resembling those stabilised solely by the emulsifier. Another advantage of co-stabilised emulsions is the increased stability conferred by the weak flocculation of particles upon addition of emulsifier resulting in the formation of bridges between stabilised droplets and increase of the emulsion viscosity [223].

Despite the benefits associated with the co-stabilisation mechanism, the majority of the co-stabilised Pickering emulsions have been produced by energy intensive techniques such as high shear mixing, high pressure homogenisation, microfluidizer or ultrasound [11, 87, 217]. However, these processes utilise a large amount of energy to repeatedly break down droplets to smaller ones and the largest proportion of this energy is released as heat in the bulk emulsion [28]. Furthermore, because of the random breakup of the droplets the final emulsion

structure is very polydisperse whilst the resulting high temperature realised during processing is not desirable for sensitive ingredients [196]. Membrane emulsification (ME) is an ideal process for the production of monodisperse emulsions as the emulsion microstructure can be controlled by adjusting a set of formulation (interfacial tension, concentration and type of emulsifying species, dispersed phase fraction) and process (transmembrane pressure, rotational velocity) parameters [112]. Additionally, the low-energy profile of ME is recommended for structures sensitive to high temperatures and shear [7, 9]. Because of the inherent low-shear mixing environment of the ME, transportation of the emulsifying species to the O/W interface is mainly diffusion controlled [156]. Therefore most of the studies have focused on emulsions stabilised by fast diffusing surface active species such as classic surfactants whereas literature on Pickering stabilisation of emulsions via ME is limited. This is because particles do require a large amount of energy to be transferred to the interface and their transportation is usually driven by convection rather than diffusion; this is best provided under the mixing environment produced by the high shear techniques described earlier. Lately it has been proposed that the key for effective stabilisation of droplets by particles through ME is to ensure that sufficient time is provided for their adsorption and a critical coverage is achieved before the droplet detaches from the pore [13]. The authors used a Langmuir isotherm model to derive the critical adsorption time of silica particles on oil droplets (via a cross-flow ME rig equipped with ceramic membranes) and argued that if this is lower than the droplet formation time, monodisperse emulsions are produced; however in the opposite case emulsions are not stable. In another study by the same group, a stainless steel rotating membrane (square pores 80 x 80 μm) was used to produce O/W emulsions stabilised with silica colloids (800 nm size) [12]. The rotating membrane emulsification (RME) arrangement allowed the adjustment of droplet formation time by tuning the oil flux

(transmembrane pressure) and the drag force for detachment of the droplets (rotational velocity); it was demonstrated that an optimum rotational velocity exists for successful stabilisation of the produced emulsions. In an extension of these studies, a co-stabilisation approach was used for the production of stable emulsions (Cross-flow and RME) with silica particles and different types of surfactants (cationic, anionic and non-ionic) [15]. This approach was suggested as an alternative scenario for production of stable particle-stabilised emulsions when the critical adsorption time criterion for the particles was not met. However, no stability data are available in either of these studies and the effect of processing conditions on the microstructure of co-stabilised emulsions produced via RME was not well understood.

This study aims to provide a better insight on how the processing conditions during rotating membrane emulsification (RME) affect the microstructure and stability of O/W emulsions co-stabilised by particles and emulsifiers. The RME rig used in the present study was equipped with two types of membranes; a Shirasu Porous Glass and a laser drilled stainless steel (SS) with circular pores. The effects of the transmembrane pressure (10 – 150 kPa) at a fixed rotational velocity of 2000 rpm (corresponding to a shear rate of 14 s^{-1}) and the type of the membrane on the emulsion microstructure were investigated. Two types of particles (silica, HPMC) and two different surface active species (Tween 20, WPI) were examined. The concept of the energy density was used to evaluate the efficiency of the RME process against a conventional high shear mixer (HSM) according to Schubert *et al.* [224]. Despite the larger droplet size produced with the SS membrane compared to the SPG, the co-stabilised emulsions presented improved monodispersity with span values as low as 0.6 and the oil mass throughput was considerably larger than SPG, potentially due to the minimisation of fouling effects. The energy consumed during RME when utilising an SPG membrane was significantly higher than expected due to operation at the maximum rotational velocity and the

longer processing time caused by SPG fouling. Regardless, the RME managed to produce stable emulsions at a transmembrane pressure of 50 kPa using 3 wt.% HPMC and 0.05 wt.% Tween 20 as co-stabilising species, with similar droplet size and utilising less energy than HSM (44 as opposed to 104 MJ m⁻³). The RME was also capable of achieving narrower distribution than HSM (span values 0.9 as opposed to 1.3) compromising though at the production rate, achieving to produce 2.2 kg of emulsion per hour, almost 6 times less than the HSM.

6.2. Results and discussion

6.2.1. Formulation effects on membrane fouling and performance

Similar to membrane separation/ filtration technologies, it is possible to encounter membrane fouling during rotating membrane emulsification and depending on the processing time this could result in significant flux decrease, thus reduced production rate. Reduced flux caused by fouling could also influence droplet size especially under shear-driven droplet formation mechanism. In this case, droplets will spend more time attached to the pore increasing their volume before they protrude enough into the continuous phase and eventually detach by the drag forces; therefore larger droplets are formed [129].

Fouling may occur due to deposition or accumulation of inorganic or organic (oil, proteins) material over time within the pores (internal fouling) or at the membrane surface (external fouling) [225]. Internal fouling of the membrane is more prominent in premix membrane emulsification as the emulsifying agents used to stabilise pre-emulsified droplets, in many cases are proteinaceous material that can internally adsorb on the surface of the membrane pores resulting in clogging of the pores and dramatic flux decrease, especially after a number of emulsification cycles [226]. The experimental set-up used in the current study utilises

direct membrane emulsification (pure oil is injected in the continuous phase through the membrane pores at a constant transmembrane pressure), therefore the occurrence of internal fouling should be normally ruled out. However, upon initial immersion of the membrane in the aqueous suspension/solution it is possible that self-diffusion of some molecules could allow their entry in the membrane pores and cause internal fouling prior to the onset of the emulsification process itself, resulting in lower oil flux. The membrane mean pore size has also been reported to affect fouling. Caric *et al.* studied the effect of two different pore sizes of membranes on the permeate flux during cross-flow filtration of WPI solution and they concluded that the adsorption-related pore plugging was more important for the larger pore size membrane (200 nm) than for the smaller pore size (50 nm) [227]. Therefore with the membrane used in this study (mean pore size 6.1 μm) it is likely that both external and internal fouling would occur.

Fig. 6.1 shows the influence of formulation on the oil flux at a constant transmembrane pressure and rotational velocity. Two different pH values were used for the suspensions that represented the optimum pH for Pickering performance of the investigated particles: silica (pH 2) and HPMC (pH 6.5). It is interesting to note that, despite the standard cleaning treatment of the membrane between experimental runs, the oil flux was dependant on the formulation used at a constant transmembrane pressure. In general, the produced oil fluxes were lower than the ones found by Lloyd *et al.* for 1 wt.% Tween 20 produced by the same membrane at 10 kPa (dashed line, Fig. 6.1) [153].

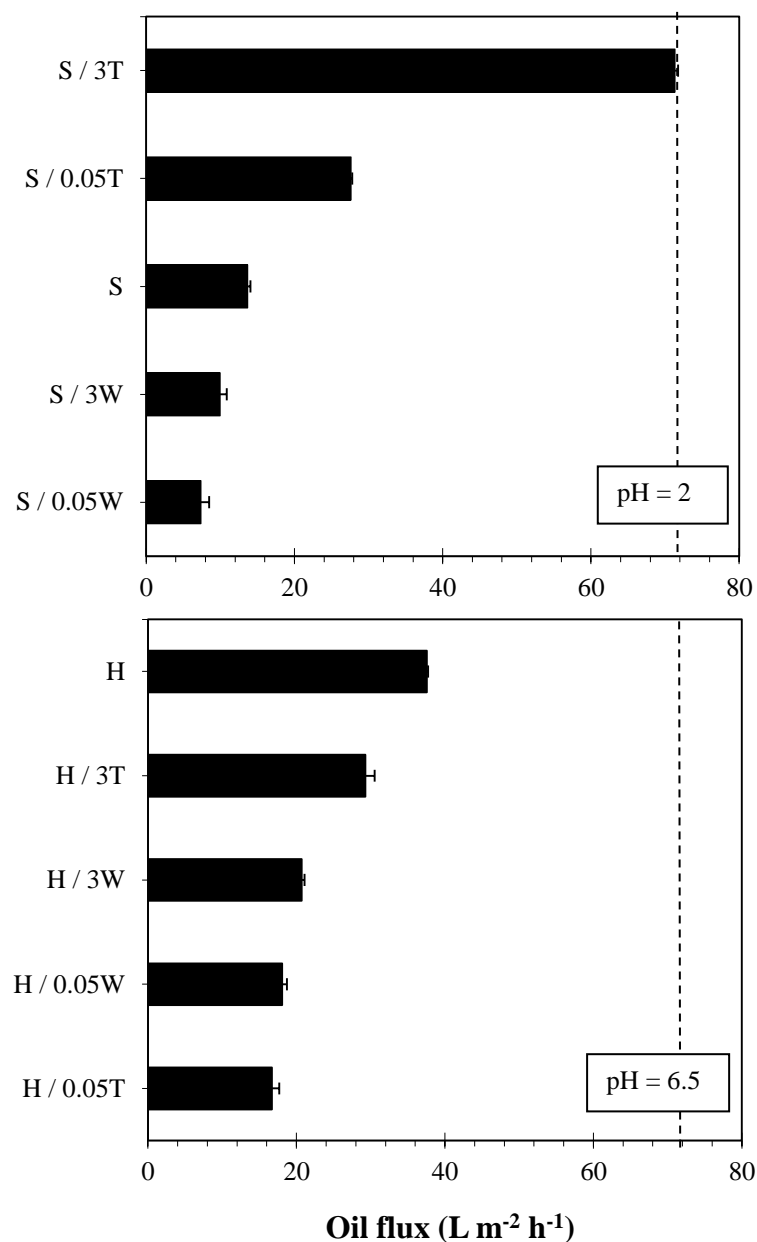


Fig. 6.1: Average oil flux of emulsions prepared with an SPG 6.1 μm membrane at constant transmembrane pressure 10 kPa and constant rotational velocity 2000 rpm. The dashed line represents the oil flux achieved at the same set-up for 1 wt.% Tween 20.

The lowest flux was found for emulsions prepared at pH 2, particularly the ones that contained WPI. WPI molecules have a positive charge below their IEP (4.5 – 5.5) and a negative charge above IEP [51], whereas the hydrophilic SPG membrane has a negative

charge at a pH range between 2 – 8 with an IEP at a pH ~ 1.5 [132, 228]. Nakamura *et al.* reported irreversible adsorption of bovine serum albumin (BSA) molecules on the surface of pores of a hydrophilic SPG membrane during microfiltration [229]. Furthermore, they argue that the maximum adsorption was observed at the IEP of the protein as the electrostatic interactions between the proteins that are closely packed at the adsorbed layer were minimised. The absence of charges close to the IEP of the protein could also facilitate the deposition of more protein molecules forming multilayers, as it has been seen in another study by the same authors [230]. Therefore it is likely that the electrostatic attraction of WPI molecules to the membrane surface at pH 2 resulted in accumulation of WPI and caused oil flux to decrease. This may explain the much lower fluxes for formulations containing WPI at pH =2 (S/0.05W, S/3W) compared to pH 6.5 (H/0.05W, H/3W) where both the membrane surface and WPI are negatively charged.

Particles alone have been seen to cause internal and external fouling as well [231]. Boussu *et al.* tested a number of hydrophobic and hydrophilic membranes of different surface roughness for their ability to filter aqueous suspensions of various types of silica particles. The authors concluded that the electrostatic interactions between membrane surface and colloidal particles again govern the fouling process and the higher the surface roughness, the greater the tendency of particles to transport to areas of the membrane with the least resistance (valleys). It is possible that the cleaning treatment of the membrane with HCl solution in between runs to remove foulants resulted in rougher membrane surface and slight enlargement of the pore size [225, 232]. In this way, foulants have greater access to the membrane surface and the pore surface. This perhaps could explain the lower flux for all particle- stabilised emulsions when compared to Lloyd *et al.* (dashed line). Furthermore, the oil flux of HPMC stabilised emulsions (pH 6.5) was 3 times higher than the silica stabilised ones (pH 2). This could be

due to the slight negative charge of the HPMC particles causing weak electrostatic repulsion between HPMC and the membrane surface that potentially could also reduce the occurrence of fouling.

Finally, the access of the species to the membrane is considered. A large particle size would hinder access of particles to the membrane pores and potentially transportation towards the membrane surface resulting in less fouling (internal and external). S/0.05T and S/3T suspensions had the largest particle aggregates so that could explain the higher oil flux of their respective emulsions compared to the pure silica-stabilised ones. With regard to the viscosity of the suspensions, it should be expected that high viscous forces would oppose the inertial force exerted by the oil phase leading to flux decrease. However, the opposite was found as the higher the viscosity of the suspension the higher the oil flux became. This can be attributed to the difficulty in transferring the species through a viscous phase towards the membrane surface again resulting in less fouling, thus higher oil flux (Fig. 6.1B).

Although in theory fouling could be taking place here, this was not confirmed by any other direct methods (e.g. microscopy). However fouling could indeed take place and therefore affect to some extent RME emulsification performance. This section is designed to raise fouling as a potential factor in shaping RME performance as presented hereafter rather than to claim it is a governing influence.

6.2.2. Effect of transmembrane pressure

A common drawback in ME is the small pore size of the membrane that results in considerably low oil fluxes and thus reduced emulsion production rates compared to high shear techniques [233, 234]. SPG membranes have an average porosity of 50 - 60%, however only a small fraction of the total pores are active, typically 1 - 10%, which is proportional to

the applied transmembrane pressure [235, 236]. Considering also the possibility of fouling caused by the formulation as previously described, the oil flux could be further reduced. Therefore, it is important to know how the SPG membrane performs in terms of oil flux, under different transmembrane pressures. This is presented in Fig. 6.2 for emulsions co-stabilised by colloidal particles and small concentration of emulsifiers.

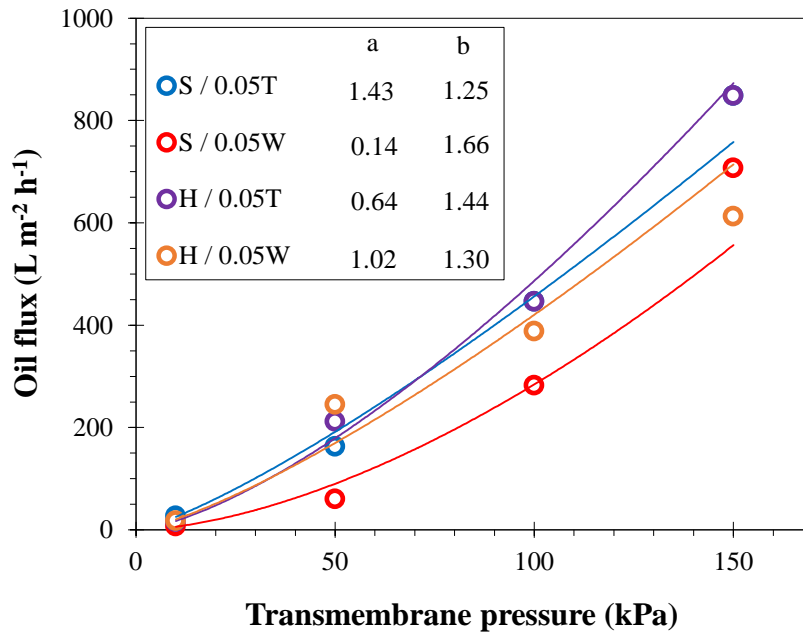


Fig. 6.2: Influence of transmembrane pressure on the oil flux through a 6.1 μm SPG membrane used at a constant rotational velocity of 2000 rpm to produce co-stabilised emulsions. Each line represents a power law fit ($y = a x^b$) with parameters given next to the legend.

Complying with Darcy's law [110], the oil flux increased with increasing transmembrane pressure for all investigated formulations reaching a maximum of 850 $\text{L m}^{-2} \text{h}^{-1}$ at 150 kPa. This value was almost 3 times lower than the oil flux achieved in the work of Lloyd *et al.* who used 1 wt.% Tween 20 in water as an emulsifier [153]. This could be attributed to the membrane fouling caused by the colloidal particles and/ or WPI in the water phase resulting

in considerably lower oil fluxes. It is worth noting that the oil flux for emulsions co-stabilised by silica and WPI at pH 2 (red line) was lower at all transmembrane pressures; the only exception being the oil flux measured at the highest transmembrane pressure of 150 kPa. A possible explanation could be that the higher inertial forces generated high mechanical stresses at the pore channel wall causing the foulants to diffuse away from the membrane pore/ surface. Despite the lower oil flux compared to the literature, fitting of the experimental data to the power law model gave the power values between 1.25 – 1.66 which is very close to the values reported by Lloyd *et al.* [153].

Although a high transmembrane pressure is desirable to achieve a high production rate, it is possible that the high surface expansion rate of the droplets would not allow their sufficient coverage by particles or emulsifiers, increasing the possibility of coalescence at the membrane surface and as a result the production of unstable emulsions [160]. Furthermore, it has been pointed out that high transmembrane pressure could cause the oil droplet to form in the ‘jetting’ regime that could potentially lead to coalescence of drops forming at adjacent pores, especially in the presence of low emulsifier concentration, where steric hindrance between droplets has not been established [237, 238].

According to Sugiura *et al.* transition from dripping to jetting is estimated to occur when the capillary number of the dispersed phase (Ca_d) approaches or exceeds 0.056 [162]. This value should be considered as a rough estimation as in our setup there was always shear applied on droplets whereas in Sugiura’s system droplets grow and detach in the absence of shear. As it can be seen from Eq. (2.21), for an SPG membrane with pore size 6.1 μm and 1 mm membrane thickness, Ca_d increases proportionally with the transmembrane pressure and decreases with increasing interfacial tension. To operate at the jetting regime, Ca_d should exceed 0.056, and selecting the highest transmembrane pressure of 150 kPa used in this study,

the respective interfacial tension should be lower than approx. 3.11 mN m^{-1} . The equilibrium interfacial tension between sunflower oil and water phase that contains high concentration of Tween 20 (up to 2 wt.%) has been found to be as low as 4.9 mN m^{-1} [152, 153]. Also, considering that the time scales for droplet formation in membrane emulsification are in the order of ms (indicatively between 1 – 300 ms [239, 240]), the interfacial tension at the moment of breakup would be expected to be a lot higher. This implies that the capillary number would be smaller than 0.056 at the investigated transmembrane pressure range and thus droplet formation is possible to take place in the dripping regime. Fouling effects could also contribute towards further decrease of Ca_d as the effective pore size would be smaller as well.

Fig. 6.3 shows the influence of transmembrane pressure on the droplet size and span of emulsions co-stabilised by silica and low concentration of Tween 20 and also of emulsions stabilised by each of the two species alone. Focusing on the emulsions stabilised solely by Tween 20 it can be seen that the droplet size increases rapidly with increasing transmembrane pressure reaching a plateau. This is a typical trend occurred in shear-driven direct membrane emulsification where lowering of the interfacial tension is not sufficient to induce droplet break-up, so droplets continue to grow in volume with increasing transmembrane pressure until they are detached by the drag forces [163]. The plateau region is attributed to the generation of an additional push-off force between sterically stabilised droplets growing in adjacent pores that become active by the application of higher transmembrane pressure [159]. This seems to be the case for a low concentration of emulsifier e.g. 0.05 wt.% Tween 20 that is well below the CMC of Tween 20 (0.98wt.% [144]), as well as for colloidal particles that have low diffusivity and interfacial tension lowering capacity, and hence mixtures of particles and low concentrations of emulsifiers.

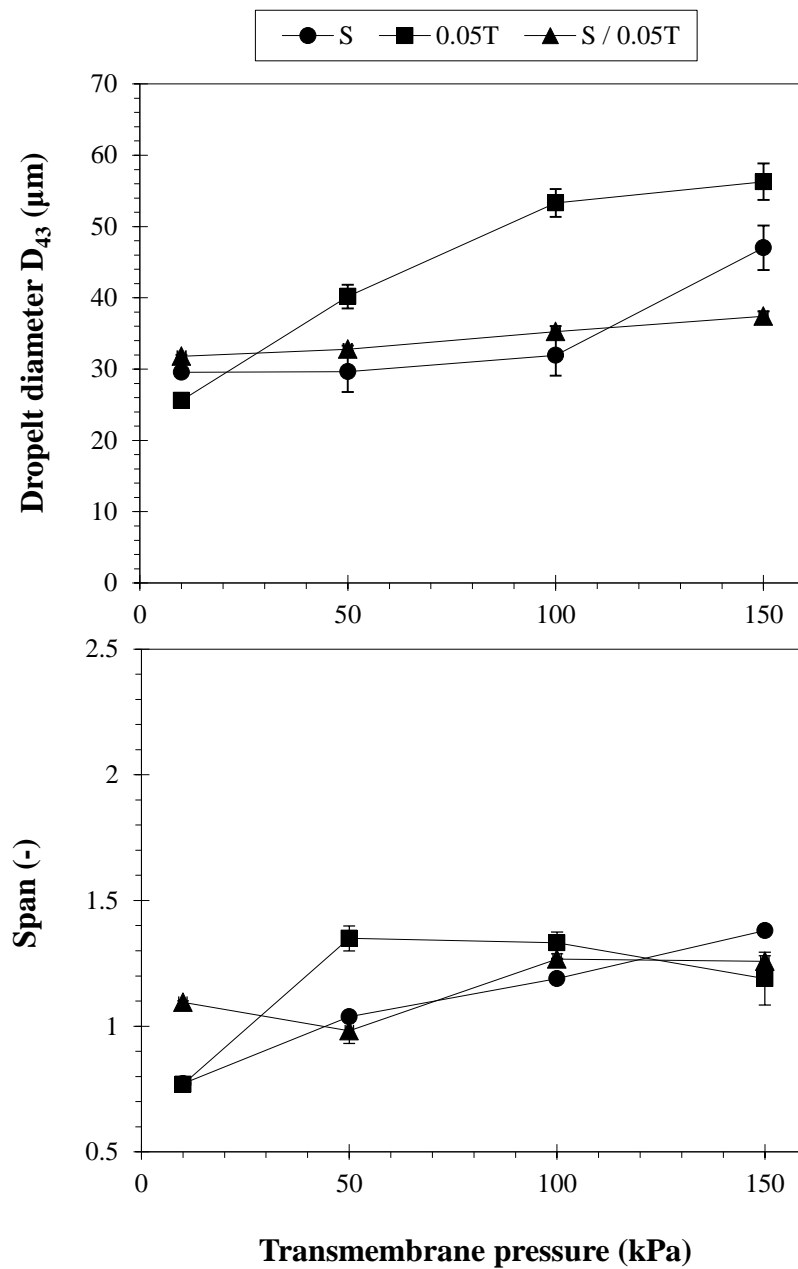


Fig. 6.3: Effect of transmembrane pressure on average droplet diameter and span values of emulsions stabilised with 3 wt. % silica, 0.05 wt.% Tween 20 and both species at pH 2. An SPG 6.1 μm membrane was used at 2000 rpm.

This behaviour is different than the findings of Lloyd *et al* who used a 6.1 μm SPG rotating membrane to produce emulsions stabilised by 1 wt.% Tween 20 (above CMC) at high rotational velocity 2000 rpm. They reported a rather constant droplet size at transmembrane

pressures between 10 – 150 kPa, followed by a subsequent increase in the droplet size, resembling a typical interfacial tension driven droplet formation [153]. Surprisingly, the latter trend was observed for silica and mixed silica - Tween stabilised emulsions that presented constant droplet size between 10 – 100 kPa, that could be related to the increased viscosity of the suspensions and the generation of higher drag forces that aid droplet detachment [104]. Increasing transmembrane pressure further to 150 kPa resulted in a substantial increase in the droplet size of silica stabilised emulsions from 32 μm to 47 μm whereas the droplet size remained almost constant for the mixed silica-Tween stabilised emulsions. The latter observation could be related to the enhanced steric stabilisation and overall stability of oil droplets, during their formation and after their detachment from the membrane that is provided by the interconnected network of large silica aggregates in the presence of Tween 20 molecules (see Chapter 4).

In general, low transmembrane pressure favoured the formation of considerably monodisperse emulsions whereas increasing transmembrane pressure resulted in more polydisperse emulsions. At the lowest transmembrane pressure (10 kPa) emulsion droplets stabilised solely by silica or Tween 20 were considerably monodisperse as it is indicated by the low span value that was approximately 0.76 for both systems, whereas when both species were present the span of the emulsions was raised at 1.09. At transmembrane pressures exceeding 50 kPa all emulsions also presented span values close to or greater than 1 that indicated high polydispersity.

The effect of transmembrane pressure on the droplet size and span of emulsions was also investigated employing HPMC as a Pickering particle instead of silica, this time at pH 6.5 (optimum Pickering functionality, see Chapter 3) and the results are shown in Fig. 6.4. All emulsions prepared with HPMC alone at 10 kPa phase separated within 24 h and the same

emulsions made at transmembrane pressures > 10 kPa phase separated instantly. It can be seen that, unlike S/0.05T co-stabilised emulsions, the droplet size of emulsions co-stabilised by HPMC and Tween 20 followed an upward trend with increasing transmembrane pressure complying with the predicted shear-driven droplet formation mechanism. It is also worth noting that the graph can be divided into two regions. At low to intermediate transmembrane pressures (10 – 50 kPa) the droplet size and span values of H/0.05T emulsions is much smaller than emulsions stabilised solely by Tween 20. At higher transmembrane pressures the two values become very close. That could be an indication that as droplet generation is increased (short droplet formation time) the droplet size appears to be increasingly controlled by the emulsifier content in the co-stabilised system. As this was not observed in the case of S/0.05T, one could argue that such behaviour relates to the size of the colloidal species in the co-stabilisation formulation that in turn could influence their diffusivity towards the oil-water interface and thus the competition on interfacial adsorption by the two species. The higher viscosity of H/0.05T suspensions could also result in even lower diffusivity according to Einstein – Stokes equation [241].

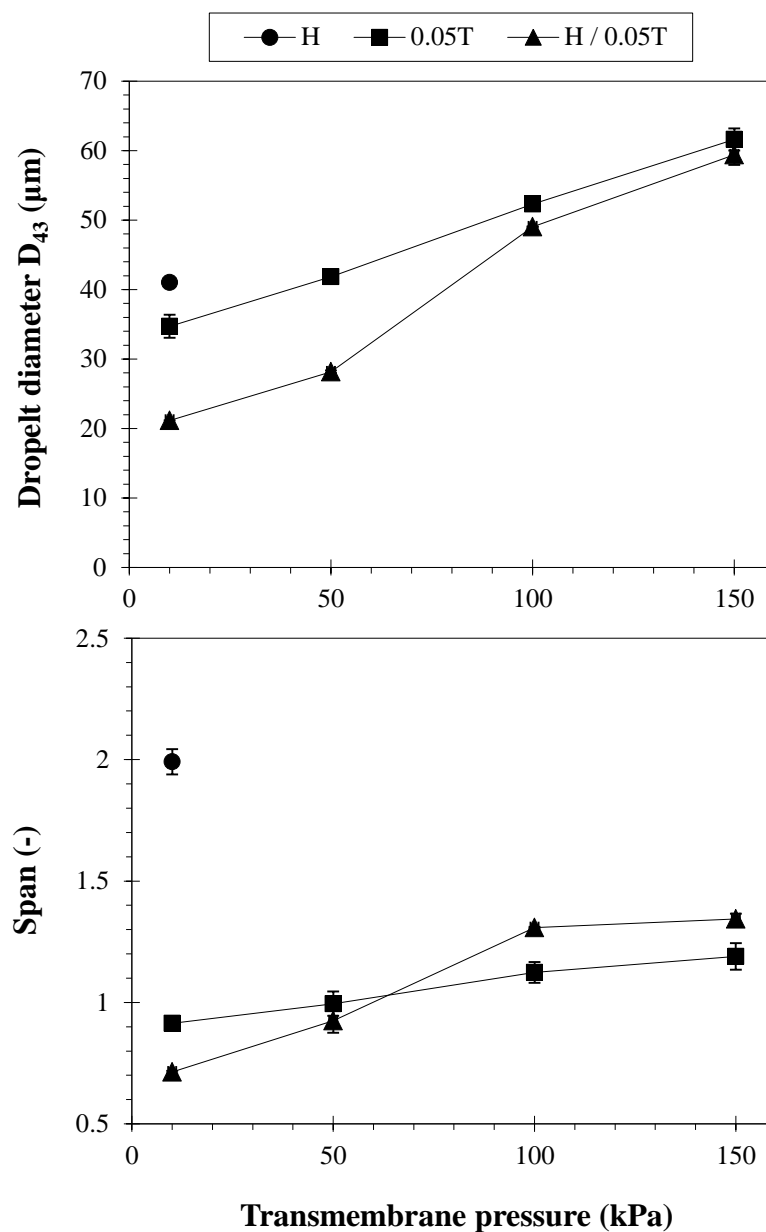


Fig. 6.4: *Effect of transmembrane pressure on average droplet diameter and span values of emulsions stabilised with 3 wt.% HPMC, 0.05 wt.% Tween 20 and both species at pH 6.5. An SPG 6.1 μm membrane was used at 2000 rpm.*

Furthermore, it has been discussed that the increased viscosity of the continuous phase would cause detached droplets to concentrate close to the membrane surface resulting in greater

probability for coalescence and thus larger droplet sizes and span values [153]. Table 6.1 summarises the droplet size evolution of all emulsions 21 days after production.

Table 6.1: % change in the average droplet size (D_{43}) of emulsions for a range of transmembrane pressures after storing at room temperature for 3 weeks. The (+) symbol indicates an increase and (-) a reduction in the droplet size. Values annotated with a star (*) refer to emulsions that showed evidence of phase separation and a cross mark (†) indicates the existence of an oil layer without phase separation. PS indicates phase separation of the samples within less than 24 h.

TMP (kPa)	pH=2			pH=6.5		
	S	0.05T	S / 0.05T	H	0.05T	H / 0.05T
10	- 7.52 [†]	+ 10.2 [*]	- 0.68	PS	+ 10.9 [*]	+ 0.10
50	+ 2.06 [†]	+ 12.7 [*]	- 7.80	PS	+ 15.7 [*]	- 0.27
100	+ 38.2 [*]	+ 12.3 [*]	+ 2.95 [*]	PS	+ 31.8 [*]	+ 22.2 [*]
150	+ 70.6 [*]	+ 63.2 [*]	+ 59.9 [*]	PS	+ 45.9 [*]	+ 61.8 [*]

All emulsions prepared with HPMC as the sole emulsifier phase separated in less than 24 h at all transmembrane pressures, so it was not possible to measure the droplet size. It can be seen that all emulsions produced at high transmembrane pressure (100 – 150 kPa) were unstable showing evidence of phase separation with a layer of oil on the top of the emulsions that gradually increased in thickness in the course of 21 days. This should be related to the poor coverage of oil droplets by the stabilising species at short droplet formation times. For those emulsions that were prepared at low to intermediate pressures (10 – 50 KPa), different observations were made. Silica stabilised emulsions presented an oil layer of stable thickness throughout the period of 3 weeks and the droplet size measured from the cream layer

remained constant. The volume of the oil layer was calculated to be approximately 0.0785 mL at both pressures, indicating that at both pressures 0.78 wt.% of the oil contained in the emulsion was not emulsified. It was also observed that the oil layer was not present at the beginning of the emulsification but it appeared later and during the process. This has been attributed to the gradual formation of a cloud of droplets close to the membrane that creates a barrier for particles located closer to the vessel wall to approach the newly emerging droplets. This effect could also be enhanced by the density difference of the two phases (very high density of silica particles) that ‘pushes’ silica particles towards the vessel wall whilst the less dense oil droplets remain at close proximity, as a result of the large centrifugal force generated at high rotational velocity. All Tween stabilised emulsions prepared at pH 2 and pH 6.5 were unstable at both pressures again with a gradually growing oil layer. Finally, co-stabilised emulsions prepared with either silica or HPMC particles were stable, without any indication of oil layer, as it is shown by the negligible change in their droplet size that is mainly attributed to the co-stabilisation mechanism.

6.2.3. Effect of membrane

The type of membrane used has also been reported to influence the performance of membrane emulsification. Charcosset *et al.* list a number of parameters that may determine the performance of a membrane e.g. porosity, mean pore size, material [242]. There is a variety of membrane materials used in membrane emulsification, however the most common types are ceramic, laser drilled and Shirasu Porous Glass (SPG) membranes; each of these combines certain benefits and disadvantages depending on the application [141]. In this section two membranes are compared. A standard SPG tubular hydrophilic membrane this (mean pore size of 6.1 μm) and a stainless steel (SS) membrane with a mean pore size of 50 μm in a cubic array. Although the theoretical minimum capillary pressure for the formation of a droplet via

the SS membrane was very small (~2.6 kPa) because of the larger pores compared to the SPG, a much higher transmembrane pressure of 50 kPa was used to achieve a satisfactory oil flux. For transmembrane pressure lower than 50 kPa it was observed that the generated oil droplets float along the membrane surface, and are not carried away despite the large drag force (2000 rpm) and subsequent large centrifugal force. This could be linked with the wettability of the SS membrane and its ability to produce certain type of emulsion. Li *et al.* used RME to produce agarose beads via a laser-drilled SS membrane and they reported that the membrane was hydrophobic and was more suitable to make W/O rather than O/W emulsions [151]. For this reason, the rotational velocity in the present study was kept at the maximum to ensure optimum mixing conditions with the highest possible drag/centrifugal force that in turn would give the smallest possible droplet size. Same processing conditions were applied for the SPG membrane and the two membranes were compared for their capacity to produce emulsions co-stabilised with silica particles and WPI. This formulation was chosen as in previous chapter it was shown to provide stable emulsions through the synergism between the silica particle and the WPI molecules.

Fig. 6.5 shows the droplet size distribution and the obtained span values of co-stabilised emulsions produced by the two types of membranes at the same processing conditions. Monomodal distributions were obtained in all cases that are representative of drop-by-drop generation. This is because the shear is not high to disrupt droplets once they have been formed and therefore does not skew the obtained monomodal distribution, even at the highest rotational velocity that can be achieved with this rig (2000 rpm corresponding to a shear rate of 14 s^{-1}).

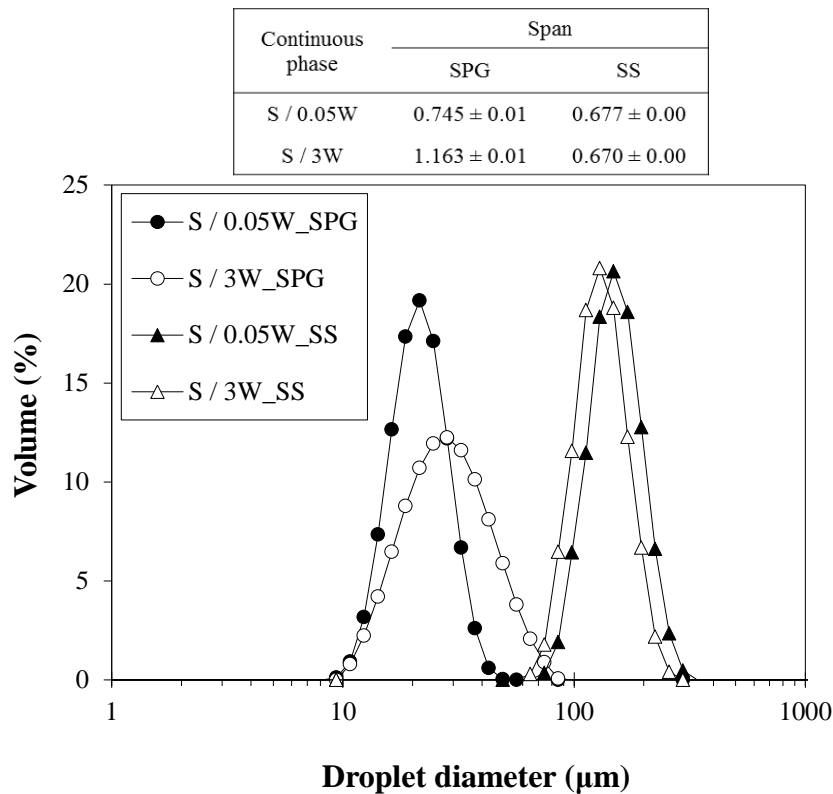


Fig. 6.5: Particle size distribution and average span values of fresh emulsions co-stabilised by 3 wt.% silica and WPI at pH 2, produced with an SPG 6 μm and a Stainless Steel (SS) 50 μm membrane at constant transmembrane pressure of 50 kPa and constant rotational velocity of 2000 rpm.

Furthermore, emulsions with larger droplet size were produced by the SS membrane for both formulations as a result of the larger mean pore size and also the droplet to pore size ratio was smaller compared to the SPG (2.5 – 2.9 as opposed to 3.5 – 4.5 respectively). This has been reported by Hancock *et al.* who investigated the effect of the membrane morphology on emulsions produced via RME and stabilised with Tween 20 [140]. In that study, the authors utilised an SPG, a ceramic and a SS laser-drilled membrane and they found that the SS membrane had the lowest droplet to pore size ratio. This was associated with the morphology

of the pores that were perpendicular to the tube surface and the smoother surface of the SS membrane enabled the development of a fully established shear field close to the pore, resulting in droplets with a size similar to the pore diameter and sometimes even smaller. This could also explain the larger span of emulsions produced with the SPG membrane in our experiments compared to the ones made with the SS for both formulations. The lower porosity of the SS membrane (< 1%) could be another explanation according to the same study. The higher the porosity of the membrane, the closer the proximity between active adjacent pores generating droplet thus increased possibility of droplet coalescence at the membrane and/or its vicinity.

Another observation is the stable span of co-stabilised emulsions prepared with the SS membrane for both formulations. Monodisperse emulsions with similar distribution width were able to be produced with the SS membrane, regardless of the formulation, corresponding to span values of approximately 0.67. These observations also agree with the findings of Vladislavljevic *et al.* who found a rather constant coefficient of variation (CV) for emulsions produced via a SS membrane at rotational velocities up to 2000 rpm, corresponding to 31 s^{-1} that is almost double the shear used in our experiments [149]. Furthermore, the described trend was also confirmed in the work of Aryanti *et al.* who used the same membrane and found a constant CV, approximately 10%, that was independent of the rotational velocity and the oil flux [158].

Increased amount of WPI did not have a significant effect on the droplet size for co-stabilised emulsions prepared with the SS membrane, whereas for the SPG membrane an increase in the average droplet diameter was identified. In the latter case, the larger droplet size and span values produced at high concentration of WPI could be related to the interactions between the SPG membrane and the charged protein species within the continuous phase.

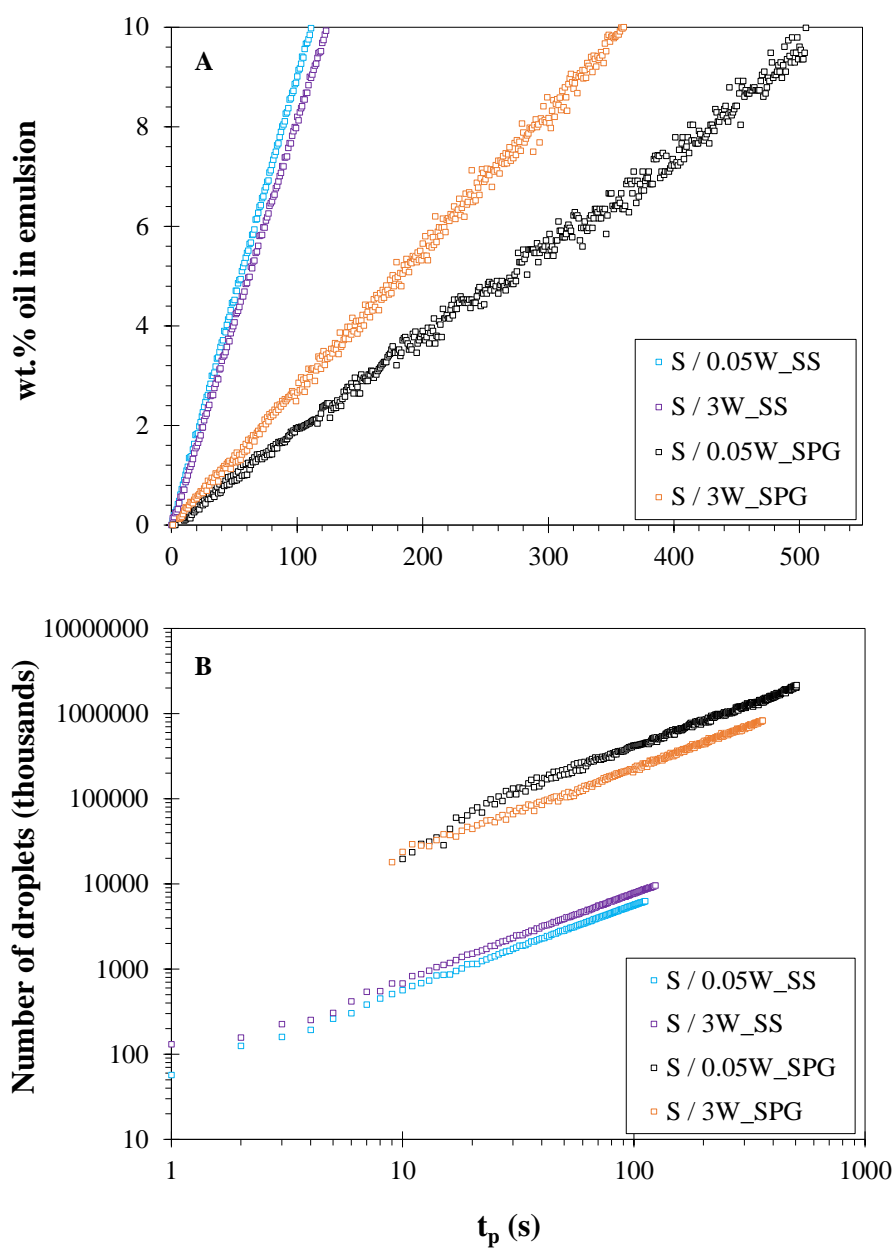


Fig. 6.6: (A) Rate of oil added in the continuous phase at pH 2 and (B) number of droplets generated during production of co-stabilised emulsions (10 wt.% oil) by a Shirasu Porous Glass (SPG) and a Stainless Steel (SS) membrane at a constant transmembrane pressure of 50 kPa and constant rotational velocity of 2000 rpm.

It is also possible that the slightly increased viscosity of the S/3W (compared to S/0.05W) continuous phases could have resulted in a reduction of the diffusion rate of the species

towards the membrane surface thus less material transported to the forming droplets to stabilise them leading to larger droplets. Less material transportation could also imply less internal and external fouling; consequently the oil flux would be slightly larger resulting in larger droplets. Hence, the larger span value observed for S/3W co-stabilised emulsions could be explained by the insufficient coverage of oil droplets by the emulsifying species in combination with the higher oil flux resulting in coalescence at the membrane surface. Indeed the difference in the oil flux is confirmed by measurements of the rate of oil introduced to the continuous phase through the membrane (Fig. 6.6A). It can be seen that there was a constant linear increase in the rate of oil added in the emulsion that has also been reported in the work of Lloyd *et al.* [154]. The SS membrane achieved a higher oil flux as it is indicated by the steep slope for both formulations; this is because of the straight pore channels of minimal resistance. On the other hand, the SPG membrane presented lower fluxes as a result of the increased wall thickness, interconnected pore channels and the polydisperse in size pores. The tortuosity of the pore channels of the SPG membrane could also significantly contribute to local fluctuations of pressure within the pores that affected the amount of oil entering the continuous phase at a specific amount of time. It is worth noting that when the SPG membrane was used the rate of oil added in the emulsion was higher for S/3W co-stabilised emulsions than the respective S/0.05W. This could be attributed to the higher viscosity of S/3W suspensions as diffusion of the species towards the membrane surface could be considerably delayed resulting in less fouling and thus larger permeation of oil through the pores. The same graph is plotted in terms of number of droplets generated each second of emulsification to consider the differences in the droplet size. Assuming spherical droplets the number of droplets was calculated by:

$$N_{oil} = \frac{V_d}{V_{oil}} = \frac{6M_d}{\pi\rho_d D_{oil}^3} \quad (6.1)$$

where V_d is the oil volume added in the emulsion, M_d is the oil mass corresponding to the volume of oil added, ρ_d the oil density, V_{oil} the volume of a spherical oil droplet with a diameter D_{oil} . Silica particle size is very small compared to the measured droplet size so the measured D_{43} by DLS is used as D_{oil} . Fig. 6.6B shows that droplets were generated at a constant rate for both formulations for the SS membrane as they both are parallel straight lines with very similar slope. In the case of the SPG membrane it can be seen that at the first 20 – 30 s equal number of droplets was generated at the same rate for both formulations from which point onwards the number of droplets increased for S/0.05W; the droplet generation rate however remained the same for both formulations. This could perhaps imply that at the onset of RME with an SPG membrane gradual accumulation of foulants at the membrane occurred when using S/0.05W as co-stabilising formulation, however it affects droplet generation only at the initial stages. This effect is less evident for S/3W co-stabilised emulsions potentially due to the slightly higher viscosity that does not facilitate diffusion of the species and their deposition on the membrane. Consequently, the performance of the SPG membrane is possible to be influenced by the formulation and the interactions of the species with the membrane which was not the case for the SS membrane.

6.2.4. Process efficiency

In this section, the process efficiency of RME is compared with that of a conventional emulsification device (HSM). The focus is on the production of co-stabilised emulsions which are assessed in terms of droplet size, polydispersity, while the two devices are scrutinised in terms of their operation by examining their throughputs and energy consumption.

Table 6.2: List of species mixed in water to form 10 wt.% O/W emulsions and measured emulsion densities. Concentrations are in wt.%, weight of individual species over the weight of the final emulsion

Continuous phase	Emulsion density ρ_e (kg m ⁻³)		
	$\rho_{0\%}$	$\rho_{10\%}$	Average
S	1010	968	989
H	1004	955	980
S / 0.05T	1010	968	989
S / 3T	1013	969	991
S / 0.05W	1009	968	988
S / 3W	967	949	958
H / 0.05T	1004	955	980
H / 3T	1007	956	982
H / 0.05W	1003	955	979
H / 3W	961	936	949

The densities of the emulsions were measured (Table 6.2) and the energy density was estimated for both processes according to Eq. (3.6) and (3.7). The power consumption was recorded for both processes. For HSM the optimum shear rate was chosen and the process time varied between 1 – 3 min whereas for RME the operated transmembrane pressure determined the process time.

Having examined the optimum performance of the RME for the production of co-stabilised emulsions, with regards to processing parameters (rotational velocity, transmembrane pressure, membrane), a similar approach was carried out for the HSM. In this case, the process parameters for this batch operation were the mixing time and the application of shear which is controlled by the rotational velocity of the impeller. It should be noted here that the calculated shear values for the HSM correspond to the space where the highest energy dissipation is experienced; that is the gap between the screen and the impeller.

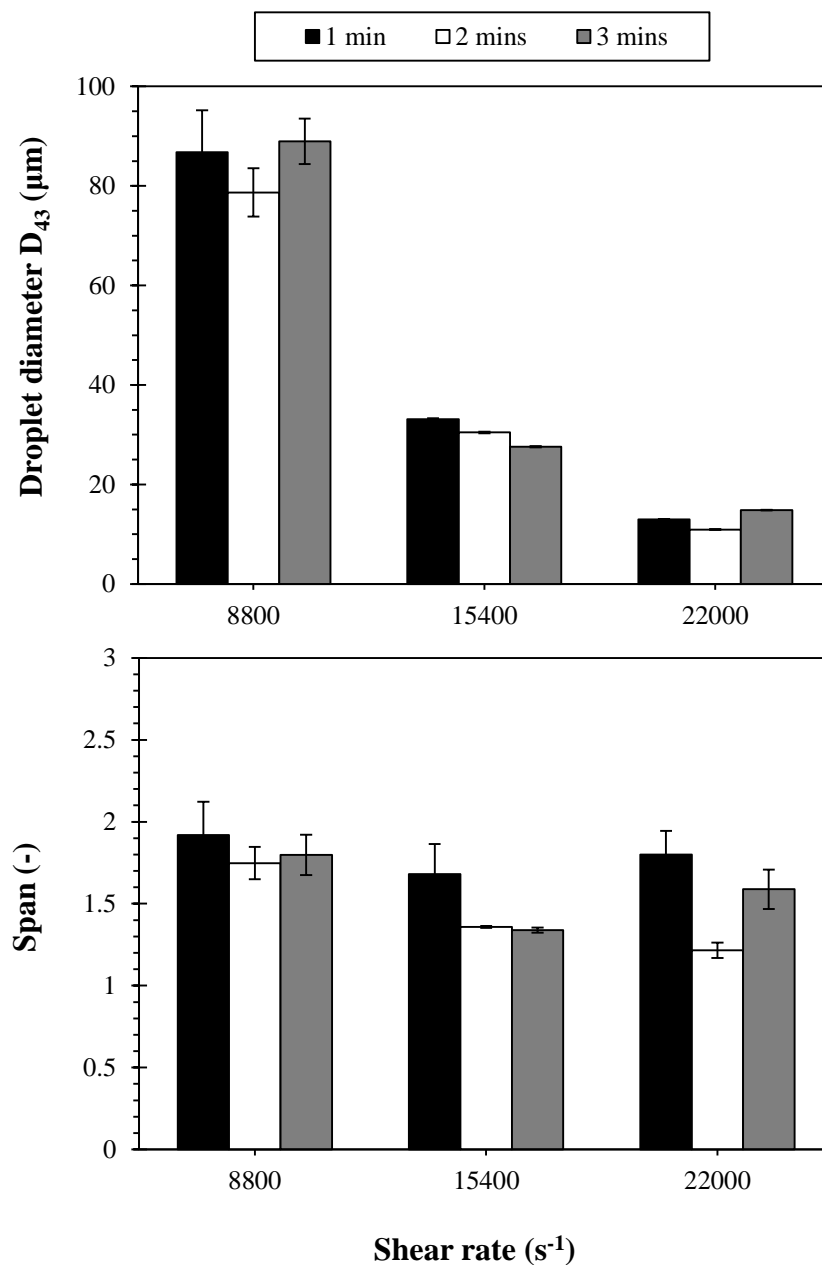


Fig. 6.7: Effect of shear rate on the average droplet diameter of emulsions co-stabilised with 3 wt.% silica mixed and 0.05 wt.% Tween 20 at pH 2, prepared with HSM at different processing times.

Emulsions co-stabilised with 3 wt.% silica particles and 0.05 wt.% Tween 20 were produced with the HSM at three different shear rates and processed for 1, 2 or 3 min; the resulting droplet size and span values are shown in Fig. 6.7. As expected, the increased shear rate

resulted in emulsions with smaller droplet size at all processing times, due to the higher dissipated energy in the emulsion that allowed for further disruption of droplets [31, 243]. At a constant shear rate of $15,400 \text{ s}^{-1}$, processing time had some influence on the droplet size as for each minute of processing the droplet size dropped by approximately 10%. However, this change was not observed when operating the HSM at $22,000 \text{ s}^{-1}$. Apparently, under the current conditions (geometry of emulsification vessel, volume of emulsion) at the highest achievable shear, a finite size for the droplet size was reached and the processing time would not have a significant effect [244]. The average produced droplet size at this shear agrees with the droplet size produced in the work of Pawlik et al ($\sim 13.6 \pm 0.6 \mu\text{m}$) and is also comparable to the droplet size reported by Yuan *et al.* who produced emulsions stabilised solely by silica particles with a rotor-stator homogeniser at a similar operating shear rate [13, 104]. The span of the co-stabilised emulsions was well above 1.2 in all cases indicating a highly polydisperse emulsion microstructure that is representative of droplet disruptive emulsification techniques [245]. All produced co-stabilised emulsions were stable except the ones generated at the lowest shear that phase separated following emulsification. This is due to the insufficient shear provided for droplet disruption and the poor mixing resulting in large droplets and unemulsified oil respectively that gradually promoted further coalescence and finally phase separation. This explains the much larger droplet size and standard deviations of these emulsions.

To ensure production of small-sized co-stabilised emulsions with the lowest energy consumption possible and without overheating the sample, the optimum shear rate for the HSM was selected at $15,400 \text{ s}^{-1}$ (rotational velocity 7000 rpm) while the production rate varied by adjusting the processing time between 1 – 3 min. For the RME the maximum shear rate was selected (14 s^{-1} at a rotational velocity of 2000 rpm), to ensure maximum drag and

centrifugal forces for the production of small droplets and homogenous mixing respectively, while the production rate varied by adjusting the transmembrane pressure between 10 – 50 kPa.

In general, the more energy is dissipated to the emulsion, the smaller the droplet size becomes [154]. This is confirmed by the decreasing trend of the droplet size for increasing energy density for both processes (Fig. 6.8). RME can achieve comparable droplet size with equal or less energy for both formulations containing either Tween 20 or WPI in small amounts. However, the emulsions produced at higher TMP (100 – 150 kPa) corresponding to the lowest energy densities, were not stable due to the short droplet formation time that resulted in their insufficient coverage by the stabilising species. The large energy densities at low transmembrane pressure (so low production rate) are associated with longer processing time. This translates into one order of magnitude more energy than HSM to produce droplets with approximate size 25 μm . Lloyd *et al.* reported energy densities between 4.6 – 30 MJ m^{-3} for production of emulsions containing 10 wt.% stabilised with 1 wt.% Tween 20 in water, utilising the same rotating membrane [154]. The amount of energy required to produce co-stabilised emulsions with RME was at least 32.8 MJ m^{-3} reaching up to 1.2 10^3 MJ m^{-3} when a transmembrane pressure of 10 kPa was applied. However, co-stabilised emulsions presented droplet sizes that were 25 – 72% smaller than Lloyd *et al.* as a result of the co-stabilisation strategy. The span values for all co-stabilised emulsions and for both processes increased with increasing production rate, however emulsions produced via RME approach gave consistently lower span values than those delivered by HSM.

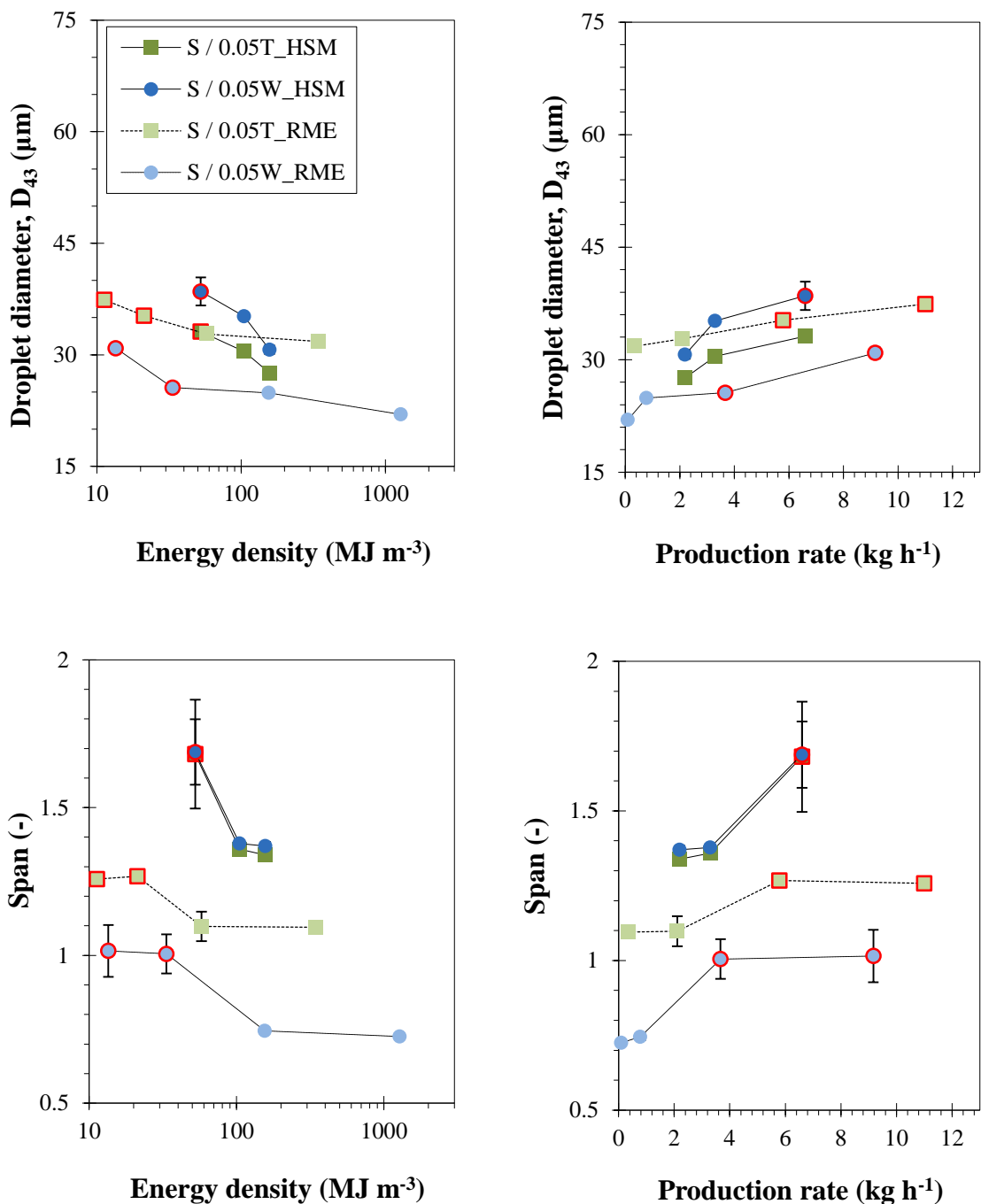


Fig. 6.8: Droplet size (top) and span (bottom) as a function of energy density and production rate, for emulsions co-stabilised by 3 wt.% silica particles produced by RME equipped with an SPG 6.1 μm membrane at 2000 rpm, and HSM at 7000 rpm. All emulsions contained 10 wt.% oil at production rates between 0.1 and 11 kg h^{-1} . Symbols with red border indicate an unstable emulsion.

Stable emulsions co-stabilised with silica particles and Tween 20 were produced with the RME at the same production rate with HSM, that were more monodisperse than their HSM counterparts as it is indicated by the low span values accounting for 1.09 as opposed to 1.37. Furthermore, with the RME process it was possible to produce such stable emulsions (S/0.5T) with span value as low as 0.72 with the expense of dramatically low production rate though that was approximately 0.1 kg h^{-1} . Stable emulsions co-stabilised with silica and WPI were prepared via RME at slightly higher production rate 2 kg h^{-1} , compared to the respective S/0.05T emulsions that were prepared at the same transmembrane pressure, however they were significantly more polydisperse with a span value of 1.09 as opposed to 0.74.

The trends followed for the droplet size and the span of emulsions co-stabilised with HPMC and Tween 20/ WPI were similar to silica stabilised the ones (Fig. 6.9). However in this case the co-stabilised emulsions with HPMC and small amount of WPI made via RME had considerably larger droplet size and span values than all the rest of the emulsions prepared by any of the two processes at all production rates. This is attributed to the absence of significant interactions between HPMC and WPI (see Chapter 4). More specifically, the WPI dictated adsorption upon exclusion of HPMC from the oil surface, however the small concentration of WPI resulted in higher interfacial tension and thus larger droplets. As a consequence, these emulsions were not stable. On the contrary, the same emulsions that were prepared with HSM were stable under the current process conditions owing to the better mixing environment of this process. The co-stabilised emulsions incorporating 0.05 wt.% Tween 20 and prepared with the HSM presented a droplet size that ranged between $28 - 37 \mu\text{m}$. That was almost 7 times higher than the droplet size reported by Zafeiri *et al.* for emulsions co-stabilised by HPMC and Tween 80 and processed with a HSM for 2 mins at 10000 rpm (corresponding to a shear rate of 22000 s^{-1}) [87].

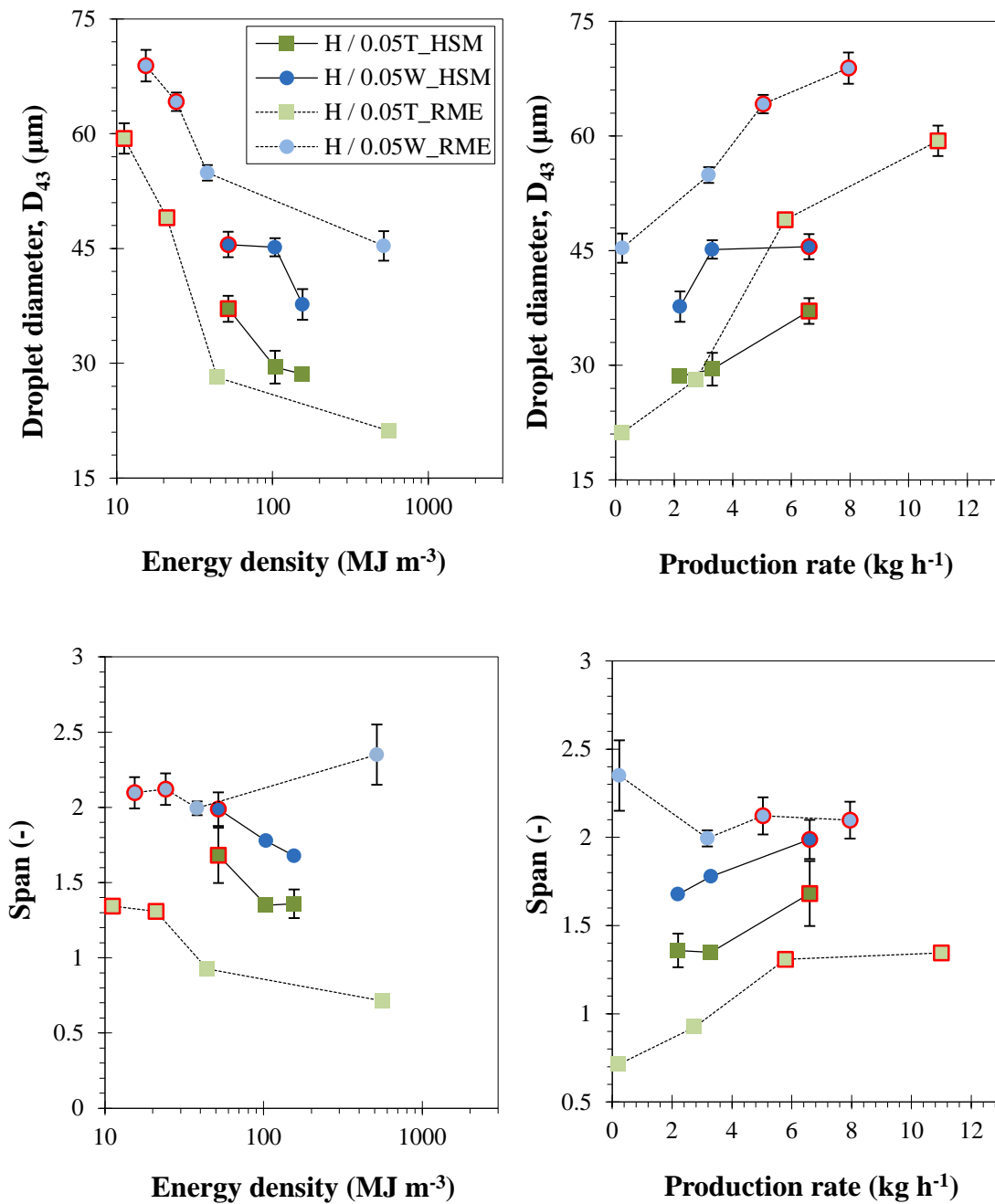


Fig. 6.9: Droplet size (top) and span (bottom) as a function of energy density and production rate, for co-stabilised emulsions produced by RME equipped with an SPG 6.1 μm membrane at 2000 rpm, and HSM at 7000 rpm. All emulsions contained 10 wt.% oil at production rates between 0.1 and 11 kg h^{-1} .

The lowest droplet size was achieved for emulsions co-stabilised with H/0.05T and processed via RME, reaching as low as 21.2 μm , with large consumption of energy that accounted for 561 MJ m^{-3} due to the long processing time at low transmembrane pressure (10 kPa). Furthermore, stable H/0.05T co-stabilised emulsions processed with RME had a similar size to those prepared with HSM but were formed utilising 57% less energy. These emulsions also had more uniform droplets when prepared with RME rather than HSM as it is indicated by the span values (0.92 as opposed to 1.34).

6.3. Conclusions

The effect of process conditions on the microstructure of co-stabilised emulsions produced through rotating membrane emulsification (RME) has been investigated and the efficiency of the process has been evaluated as per the utilised energy and the production rates achieved in comparison to a high shear mixer (HSM). A transmembrane pressure lower than or equal to 50 kPa was a prerequisite for the production of stable co-stabilised emulsions via RME operating at 2000 rpm. The morphology of the membrane may influence its performance terms of oil throughput when formulations incorporating charged polymers (WPI) and particles (silica, HPMC) are considered. These species can potentially electrostatically adsorb to the external or the pore surface of the rougher negatively charged SPG membrane causing internal and/or external fouling that could significantly decrease oil flux; unlike a stainless steel membrane that maintains a high constant oil throughput regardless the formulation. Overall, co-stabilised emulsions with small droplet sizes were produced by RME at production rates of up to 11 kg h^{-1} , however only those produced at production rates up to 0.9 kg h^{-1} were stable and utilised 44 - 1200 MJ m^{-3} of energy. The RME process can compete with the efficiency of HSM to produce emulsions co-stabilised with HPMC and a small

amount of Tween 20, as under certain process conditions (50 kPa, 2000 rpm) it offers stable emulsion microstructures of similar droplet sizes that are more monodisperse and are formed utilising less energy. In this context, a different membrane, ideally free of surface charges with a smoother surface such as the stainless steel could be utilised for minimising fouling and improve production rate and monodispersity. As such, by carefully selecting the formulation process conditions, RME is capable of producing a wide range of co-stabilised emulsion microstructures and offers a viable alternative to traditional high-energy consuming emulsification techniques.

Chapter 7

Conclusions and recommendations for future
work

7.1. Overall Conclusions

The work presented in this thesis aims to investigate the key formulation and processing conditions for manufacturing stable particle-stabilised emulsions with improved droplet size uniformity via a mild emulsification process; rotating membrane emulsification. The current traditional emulsification routes are based on the excessive application of energy to form emulsion microstructures, creating a product that lacks uniformity that could be susceptible to destabilisation. Although low-energy methods such as RME imagine as great alternatives to conventional emulsification devices, their performance in manufacturing particle-stabilised emulsions is limited by the kinetics of the particles and their minimal propensity to lower interfacial tension. These obstacles were encountered initially by screening the capacity of a range of colloidal particles of demonstrated Pickering functionality to produce stable surfactant-free Pickering emulsions whilst manipulating the processing conditions in the RME device and at a second stage by ‘assisting’ particles that were unsuccessful combining them with different types/ concentration of surface-active species. The main conclusions derived from this work are summarised in the next sections.

Surfactant-free Pickering emulsions produced via RME

- Cellulose particles (HPMC, CMCC) are not effective Pickering stabilisers for production of Pickering O/W emulsions via RME.

HPMC and CMCC particles were unsuccessful in stabilising emulsions produced via RME at all investigated formulation (particle concentration 1.5 – 5 wt.%) and processing conditions (transmembrane pressure 10 – 150 kPa, rotational velocity 100 – 2000 rpm) although these have been seen to perform well in high- energy emulsification methods [11]. This is believed to be due to a combination of their surface physicochemical properties and their size that

affects their performance within the poor mixing environment realised in RME. HPMC particles were smaller than rutin but larger than silica particles; however it is possible that their diffusivity towards the oil-water interface was hindered by the poor mixing conditions of the RME process, as indicated by their low kinetic energy close to the membrane surface. Therefore, it is likely that these particles were not able to reach the oil-water interface in time to induce an energy barrier against desorption, resulting in coalescence of droplets during or post droplet formation close to the membrane surface that ultimately led to phase separation. This is also confirmed by the CMCC particles which, despite their large size and thus their theoretically higher energy of adsorption compared to the rest of the particles, they were also unsuccessful in stabilising O/W emulsions, possibly because of the poor mixing conditions in the continuous phase during RME but also their minimal diffusivity associated with their large size.

- Silica and rutin particles can successfully stabilise Pickering O/W emulsions produced via RME.

O/W Pickering emulsions were successfully stabilised by silica and rutin particles and they were stable for three weeks in ambient temperature. The optimum rotational velocity for both types of Pickering emulsions was the maximum one at 2000 rpm as the droplet size distribution became wider at lower velocities; an indication of coalescence that could be due to lower transportation rate of particles to the oil-water interface. Silica stabilised emulsions were stable at pressures between 10 – 100 kPa whereas rutin stabilised emulsions at pressures between 10 – 150 kPa.

Using silica at concentrations greater than 1.5 wt.% resulted in emulsions with slightly smaller droplet size and less polydisperse due to the increased availability of the silica particles. However, only a certain volume of oil is possible to be emulsified and this occurs

during the initial stages of emulsification regardless of the concentration of particles, whilst the rest of the oil remains unemulsified and it can be seen as an oil layer of stable thickness on the top of the emulsions. This is possible because of the increased particle density of the silica particles causing them to move towards the emulsification vessel wall as a result of the high centrifugal force generated by the high rotational velocity of the membrane. The less dense oil droplets populate close to the membrane surface thus after a certain point the silica particles cannot access the forming oil droplets through the 'cloud' of droplets surrounding the membrane. The density of the colloidal particles should therefore be considered when producing Pickering emulsions through direct RME.

For the rutin-stabilised emulsions, the effect of concentration had the opposite effect with the droplet size increasing for rutin concentrations greater than 1.5 wt.%. Similar to silica, rutin stabilised emulsions became less polydisperse however still with a much wider droplet size distribution than the respective silica stabilised emulsions.

The presence of unadsorbed particle aggregates within the continuous phase was essential for the stabilisation of oil droplets. These aggregates may occupy the space between the particle-stabilised droplets preventing their approaching and subsequent coalescence. This is in line with the literature reporting that weak particle flocculation can dramatically increase emulsion stability forming a type of physical barrier between droplets and it is even possible to keep large droplets stable even for 3 months [246, 247]. This is possible to occur for rutin stabilised emulsions which at certain processing conditions (transmembrane pressure of 100 kPa, rotational velocity of 2000 rpm) maintained their large droplet size (98 μm) for 3 weeks. It is possible that when such an interconnected network of particles exists between droplets, complete coverage of droplet surface by particles is not a prerequisite to impart enhanced stabilisation.

- Colloidal particles demonstrating shear-thinning behaviour can produce Pickering emulsions with small droplet size via RME.

Operation of the membrane at the highest possible rotational velocity can promote earlier detachment of droplets from the membrane surface. This is enhanced even more when a substance with shear thinning rheological behaviour is used as the continuous phase, in this case, rutin dispersions. The reduction of the continuous phase viscosity upon increasing of the rotational velocity in the system facilitates the formation of Taylor vortices, as shown from the increased Taylor numbers that cause the droplets to detach faster. Therefore, if the goal is to produce Pickering emulsions with small droplet size, particles that present a shear-thinning behaviour are highly recommended.

Co-stabilised emulsions produced via RME: formulation effects

- Particles with poor Pickering performance in RME may be combined with emulsifiers to dramatically enhance emulsion stability.

Silica particles were not able to emulsify the whole volume of oil and an oil layer of stable thickness appeared at the top of the emulsions. Emulsions were phase separated when HPMC particles were used as Pickering stabilisers. Combination of silica particles and small concentration of Tween 20/WPI resulted in emulsions that were stable for 3 weeks and no oil appeared at the top of the emulsion. Furthermore, emulsions produced by small concentrations of Tween 20 or WPI alone were unstable and phase separated. It is therefore possible that the presence of small concentration of emulsifier aided short-term stabilisation until the adsorption of silica particles that is in alignment with the available literature [79]. Same observation was also made with HPMC and small concentration of Tween 20 but not with an equal concentration of WPI that could be attributed to the lower surface activity of the protein molecules compared to Tween 20.

- Particle-emulsifier interactions and the type/ concentration of emulsifier determine the final emulsion microstructure as delivered by RME

The occurrence of interactions between small concentration of emulsifier and particles resulted in co-stabilised emulsions with droplet size smaller than when either of the species was used alone. This synergistic effect has also been reported in other studies that utilised high energy emulsification methods (high-shear mixing) [248] and it was successfully applied in this thesis for production of stable co-stabilised emulsions via RME. This applied for mixtures of silica and WPI at pH 2 and mixtures of HPMC and Tween 20 at pH 6.5, that were found to interact with each other. When particles and emulsifiers did not interact with each other, competitive adsorption of the two species to the surface of the droplets occurred. As a result, at low concentration of emulsifier silica – Tween 20 co-stabilised emulsions presented a larger droplet size than either of the two species alone whereas HPMC – WPI emulsions were very unstable leading to phase separation. At higher emulsifier concentration the emulsifier dominated the oil-water interface resembling the surface of an emulsion stabilised solely by the emulsifier.

Co-stabilised emulsions produced via RME: processing effects

- Stable co-stabilised emulsions can be produced at transmembrane pressures up to 50 kPa at the maximum rotational velocity of 2000 rpm.

The effect of the transmembrane pressure at a range between 10 – 150 kPa was investigated on the effect on the droplet size and span of emulsions co-stabilised by particles (silica / HPMC) and a small concentration of emulsifier (0.05 wt.%). The optimal transmembrane pressure for stable co-stabilised emulsions was less or equal to 50 kPa, as beyond this value the droplet formation time became very small for any of the species to adsorb prior to detachment resulting in droplet coalescence and therefore wider droplet size distribution as

realised by the larger span values of the emulsions. Stability was confirmed not only by the stable droplet size after 3 weeks but also visually as no oil layer on the top of these emulsions detected. For emulsions prepared with silica – Tween 20 at transmembrane pressures greater than 50 kPa the droplet size remained practically the same, however an oil layer of growing thickness was observed. Therefore, these emulsions were unstable and the negligible change in their droplet size is possibly due to the increased viscosity of the continuous phase caused by the interconnected network of silica aggregates in the presence of Tween 20 molecules. At pressures lower than 50 kPa the droplet size and span values of emulsions prepared with HPMC – Tween 20 are much smaller than emulsions made solely with Tween 20. However, at higher transmembrane pressures both types of emulsions have almost equal droplet size. This could happen because at short droplet formation time (higher transmembrane pressure), the droplet size is governed by the emulsifier content. Emulsions prepared with silica – Tween 20 did not present such behaviour, therefore it is suggested that the size of the colloidal particles affected their diffusivity towards the oil-water interface.

- RME performance can be affected by the interactions of the membrane used with molecular/colloidal species in the formulation being processed.

For an SPG membrane that has a rough surface and it is negatively charged, two types of interactions can occur between the species dispersed in the continuous phase and the membrane surface; electrostatic and spontaneous deposition. In the first case, species with the opposite charge to the SPG membrane surface will lead to electrostatic adsorption and fouling of the membrane as it is observed by the decreased oil flux for formulations containing WPI below their isoelectric point (where proteins are positively charged). Spontaneous diffusion and deposition of species can also be experienced and this applies for particles as well as emulsifiers. If the size of the species is smaller than the pores, deposition of foulants on the

pore channel surface (internal fouling) results in reduction of the oil flux. Increased viscosity of the continuous phase may delay if not prevent the transportation of species towards the membrane. Therefore the oil flux can be influenced by a combination of all those factors; thus in any case, internal and/or external fouling can significantly affect droplet formation mechanism and the final emulsion microstructure. When compared to an uncharged SS membrane that has a smooth surface and straight through channels, the SPG membrane presents lower oil flux for co-stabilised emulsions. However, the droplet generation rate appears to be very similar for all co-stabilised systems examined, therefore it is possible that fouling only affects the performance of the SPG membrane only at the initial stages of emulsification.

- RME can be competitive against high-energy emulsification methods (High shear mixer) in terms of process efficiency (energy consumption, droplet size, polydispersity)

RME can produce co-stabilised emulsions with small droplet sizes via RME at production rates of up to 11 kg h^{-1} (150 kPa) however only those produced at production rates up to 0.9 kg h^{-1} (50 kPa) were stable and utilised $44 - 1200 \text{ MJ m}^{-3}$ of energy. RME can be competitive against HSM to produce emulsions co-stabilised by HPMC and a small amount of Tween 20, as under certain processing parameters (50 kPa, 2000 rpm) stable emulsion microstructures of similar droplet sizes can be produced that are more monodisperse, utilising less energy.

7.2. Future Outlook

The overall goal of this thesis was to identify the key formulation and processing parameters to improve the performance of rotating membrane emulsification towards the production of stable particle-stabilised emulsions. The hypotheses and objectives set were addressed and the respective conclusions were drawn. However, a few research areas, that haven't been investigated here, have also been identified and are proposed. Further research study along what is suggested here would complement this work as well as assist in overcoming possible future challenges associated with membrane emulsification.

Creaming stability

In this work, no effort was made to prevent creaming, instead the stability against coalescence was assessed by evaluating the droplet size and polydispersity and also by reporting the appearance of an oil layer via visual observation of the emulsions in the course of 3 weeks (21 days). Stability tests against creaming would be recommended as this would actually determine the overall stability of the emulsion; this could be done by estimating the creaming index (CI %). It would also be worth to explore ways to further prevent creaming e.g. by using appropriate ingredients to increase the emulsion bulk viscosity (e.g. thickeners, gelling agents) as this would expect to create an additional barrier for the emulsion droplets to approach each other and thus to delay creaming.

Effect of particle size

In this research the potential of a range of particles to function as Pickering stabilisers was studied, however the particle size was not considered. The particle size is expected to affect emulsification as small particles are able to diffuse faster and thus in theory they could arrive faster to the oil-water interface in order to attach. However, large particles attach stronger at

the oil-water interface providing a more effective steric barrier [191]. The former would be an advantage because in the low-energy RME the kinetics becomes extremely important in stabilising effectively droplets. Silica particles are available in a range of sizes and the specific ones used in this study were already dispersed in an aqueous medium and they were also very uniform in size. However, the investigated ‘natural’ particles came in a powder form, thus their dispersion and size reduction with the available high-shear technology was a challenge due to the random breakage occasionally resulting in wide particle size distribution. Should this issue is addressed, it would worth to identify if there is an optimum size for ‘natural’ particles to effectively stabilise emulsions via RME.

Further exploitation of ‘natural’ particles

Although a range of commercially available ‘natural’ particles was examined in this thesis, it is also worth to investigate the potential of other candidates for Pickering stabilisation via RME that may be derived by carbohydrates, proteins or lipids. Many of these have been seen to perform well in high-energy methods and have also been used both as Pickering particles as well as encapsulants of active ingredients simultaneously, e.g. electrostatic complexes of proteins-polysaccharides [73]. An example is an O/W emulsion that consists of oil droplets containing a lipophilic active which are stabilised by electrostatic complexes that contain a hydrophilic active. Such functional emulsions could be produced in the RME set-up with narrower droplet size distribution that would enable uniform release rate of the actives.

Co-stabilisation through spontaneous emulsification

Spontaneous emulsification has been previously used in RME to make O/W emulsions [154]. By adding high HLB emulsifiers that are also soluble in the oil phase, smaller droplets were produced than placing the same emulsifiers in the continuous water phase. This is because the

difference in the chemical potential of the emulsifier between the two phases causes the emulsifier to head towards the water phase creating small droplets. Since particles do not possess the same level of interfacial activity as emulsifiers, it would not make sense to place them in the dispersed phase as there would be no driving force to transfer them to the interfacial layer. However, it might be worth to explore this approach for emulsions co-stabilised by Pickering particles and emulsifiers by adding the latter in the dispersed instead of the continuous phase. Short-term stabilisation of oil droplets then would be provided by the fast diffusing emulsifiers towards the water phase reducing the interfacial tension, followed by adsorption of the slower particles that would provide long-term stabilisation. If this hypothesis is valid, exceptionally stable co-stabilised emulsions could be produced with even smaller droplet size and narrow droplet size distribution as delivered by RME.

Pickering-stabilised multiple emulsions

Multiple emulsions are very sensitive to breakage when they are subject to high shear stresses, therefore gentle techniques such as membrane emulsification are ideal for this type of emulsions [249]. One disadvantage of conventional multiple emulsions stabilised by classic emulsifiers is that occasionally emulsifiers tend to migrate from the outer to the inner interface causing this delicate structure to collapse. An interesting study by Binks *et al.* showed that double O/W/O emulsions stabilised entirely by hydrophobic silica particles at the outer interface and hydrophilic silica particles at the inner interface presented remarkable stability [54]. This approach could be used to make extra stable multiple emulsions with narrow droplet size distribution for controlled delivery of encapsulated ingredients. As an extension of this study, ‘natural’ particles with appropriate wettability could be used instead of silica particles to make an entirely sustainable multiple Pickering emulsion with controlled droplet size and distribution via RME.

Pre-mix RME for production of Pickering emulsions

An alternative to direct RME for making Pickering emulsions is by pushing a pre-mix Pickering emulsion that has been previously homogenised by high-energy methods, through a membrane. This method has been used for classic emulsions in several configurations of membrane emulsification but never for Pickering emulsions in a RME set-up. This method allows for control over the droplet size and a narrow droplet size distribution can be achieved by repeating passes. Theoretically, pre-mix RME could reduce the fouling as the dispersed phase would not come into contact with the membrane surface which is usually wetted by the continuous phase. However, there is still a risk that large particles or particles with affinity to the continuous phase could adsorb to the membrane causing fouling, therefore the choice of the membrane should take into account those factors.

Emulsion gels

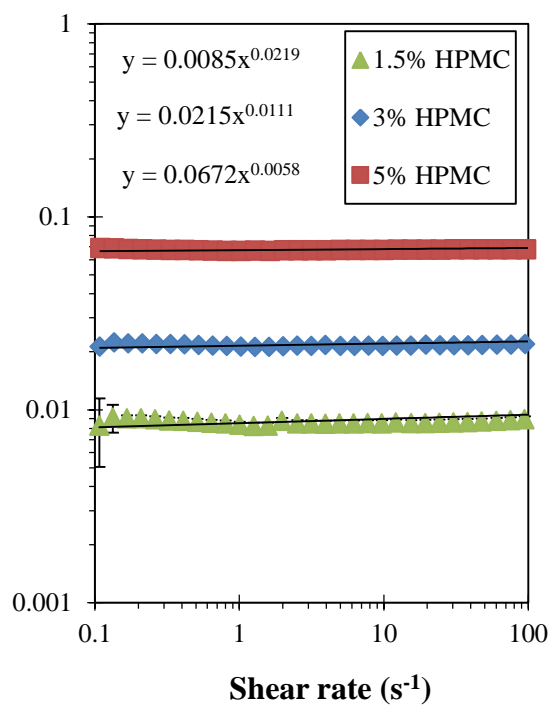
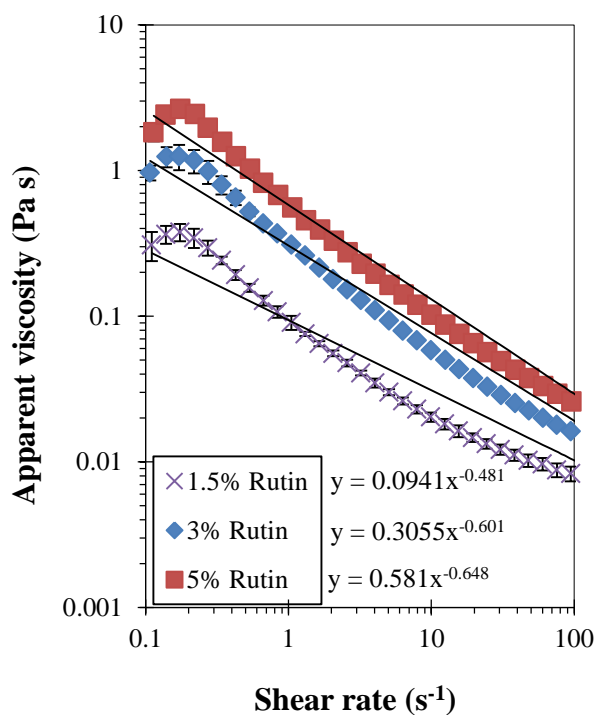
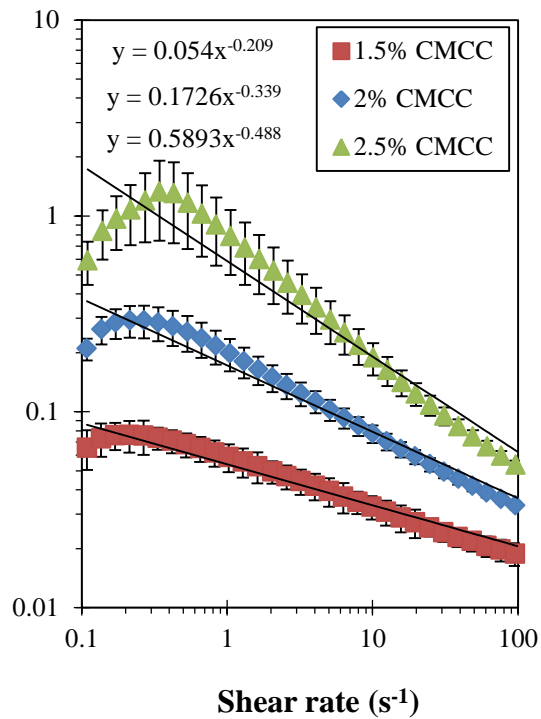
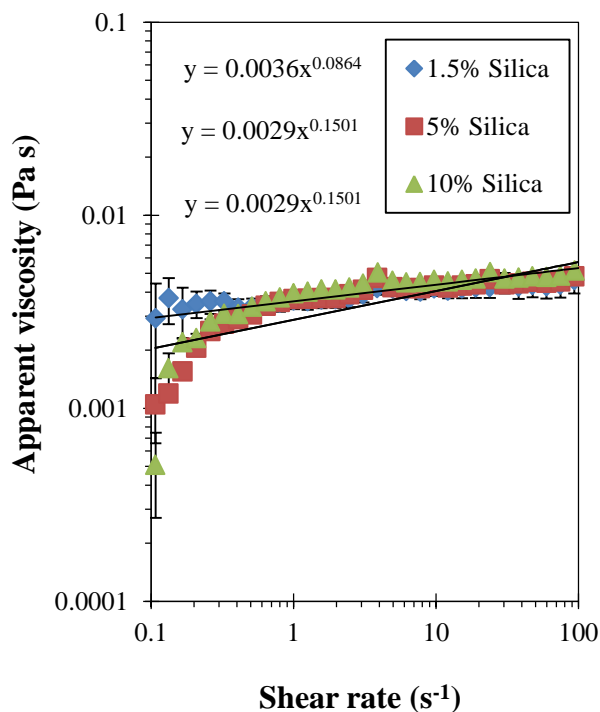
Under certain conditions of pH and temperature, inter-particle interactions within the continuous phase may result in the formation of a gel network. This mechanism could be further exploited for the production of emulsion gels. These are in essence emulsions that consist of droplets embedded in a gelled continuous phase. In this case, particles serve two missions: to adsorb on the droplets creating a barrier against coalescence whilst the free particles in the continuous phase form a gel network under quiescent conditions that minimises droplet mobility and thus the possibility to approach each other [250]. The latter is expected to equip the emulsion gel with the highest level of stability as the emulsion structure is literally trapped within the gel network. Gelation could be manipulated by adjusting the temperature in the continuous phase. The key in this design is to keep the droplets as stable as possible during emulsification until the desired dispersed phase fraction is achieved and then

cooling should take place as soon as possible to convert into an emulsion gel. The main benefit of these structures is that no stabilisers or thickeners (E-numbers) would be necessary since the gel network itself would be enough to keep droplets apart. Furthermore, a ‘clean label’ stable emulsion gel could be formed by combining “natural” particles and proteins as these have been utilised to create emulsion gels. Such structures could have applications in food or cosmetic products e.g. lipsticks, hand creams, spreads and pastes.

Appendix A

Supplementary data to Chapter 4

A.1. Apparent viscosity of particle suspensions as a function of shear rate at different particle concentrations.



A.2. Calculation of free energy of adsorption and kinetic energy

The mass of the particle was calculated assuming a spherical shape:

$$m_p = \rho_p V_p = \frac{4}{3} \pi \rho_p r_p^3$$

Assuming that particle velocity u would be approximately equal to the average of cross-flow velocity u_c and the tangential membrane surface velocity u_t :

$$u = \frac{1}{2} (u_c + u_t)$$

with $u_c = \left(\frac{\dot{\gamma} \eta_c}{0.5 f \rho_c} \right)^{0.5}$ [104] and $u_t = 0.105 R_1 N$

where $\dot{\gamma} = 14.31 \text{ s}^{-1}$ corresponding to $N=2000$ rpm from: $\dot{\gamma} = \frac{\pi R_1^2 N}{15(R_2^2 - R_1^2)}$

The friction factor f from Fanning equation is calculated as:

$$f = 16/Re_c \quad \text{Laminar flow}$$

$$f = 0.0791/Re_c^{0.25} \quad \text{Turbulent flow}$$

$Re_c = \omega R_1 (R_2 - R_1) \frac{\rho_c}{\eta_c}$ with $\omega = \frac{N}{60}$, for $N=2000$ rpm.

The adsorption free energy can be calculated by:

$$\Delta F_{ads} = \pi r_p^2 \gamma (1 - |\cos\theta|)^2$$

Using nonlinear regression to fit the equation $y = -a \ln(x)+b$ where y is the interfacial tension and x is the time, from the data obtained by IFT measurements the dynamic interfacial tension γ_{ow} at early stages of droplet formation ($t= 0.5$ ms) was estimated.

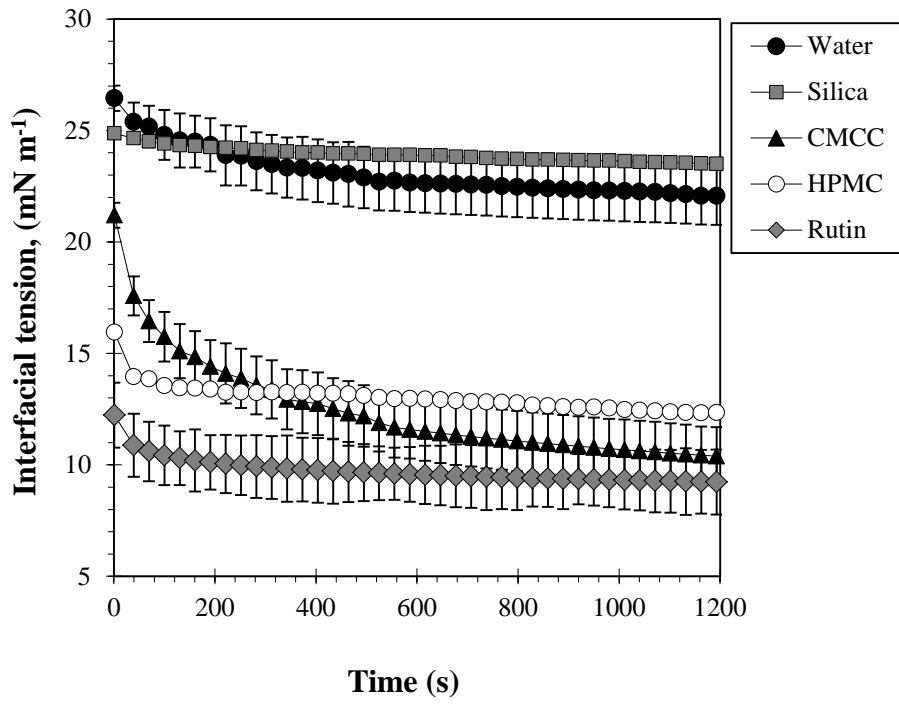


Fig. A.1. Interfacial tension between sunflower oil and different particles suspensions at particle concentration 1.5 wt.% and 20°C. Silica (pH 2), CMCC (pH 6), HPMC (pH 6), Rutin (pH 5)

Consequently, the the kinetic energy of the particle would be (Eq. (4.1))

$$E_K = \frac{1}{2} m_p u^2$$

A.3. Calculation of critical concentration

The diameter of an oil droplet is given by **Eq. (4.2)**:

$$D_{oil} = D_{43} - 2D_p$$

The volume of one oil droplet can be calculated by:

$$V_{oil} = \frac{4}{3} \pi \left(\frac{D_{oil}}{2} \right)^3$$

If V_t is the total volume of oil in the emulsion and ρ_d is the dispersed phase density and M_d the dispersed phase mass, the number of oil droplets in the emulsion would be:

$$N_{oil} = \frac{V_d}{V_{oil}} = \frac{M_d / \rho_d}{V_{oil}} = \frac{6M_d}{\pi \rho_d D_{oil}^3}$$

The number of particles required to form complete monolayer on one oil droplet is:

$$N_{p,1} = \frac{A_{oil}}{A_p} = \frac{4D_{oil}^2}{D_p^2}$$

where A_{oil} is the surface of one oil droplet and A_p is the surface occupied by a spherical particle (equal to the surface of a circle of diameter D_p).

Consequently the number of particles required to coat all oil droplets is:

$$N_p^* = N_{oil} \cdot N_{p,1} = \frac{24M_d}{\pi \varphi_{hp} \rho_d D_{oil} D_p^2}$$

The number of particles available for adsorption in the continuous phase can be calculated:

$$N_p = \frac{M_p}{\rho_p V_p} = \frac{6M_p}{\pi \rho_p D_p^3} = \frac{6M_e C}{\pi \rho_p D_p^3}$$

where M_p is the mass of particles in the continuous phase, ρ_p is the particle density, V_p is the volume of one particle, M_e the mass of emulsion produced, and C the concentration (% w/w) of particles in the emulsion.

The critical concentration can be estimated:

$$\frac{6M_e C_{cr}}{\pi \rho_p D_p^3} = \frac{24M_d}{\pi \rho_d \varphi_{hp} D_{oil} D_p^2}$$

And by rearranging **Eq. (4.3)** is derived:

$$C_{cr} = K \frac{\rho_p D_p}{\varphi_{hp} D_{oil}}$$

with $K = 4M_d / \rho_d M_e$

Eq. (4.3) is used to calculate C_{cr} .

$C_{cr,m}$ is the average value between two extreme conditions: D_p is considered and D_p is very small ($D_p \approx 0$).

Constant: $M_d = 11$ g, $M_e = 110$ g, $\rho_d = 0.915$ g ml⁻¹

Particle type	ρ_p (g/cm ³)	D_p (μ m)	C (wt. %)	D_{43} (μ m)	C_{cr} (wt. %)	$C_{cr(D_p \approx 0)}$ (wt. %)	$C_{cr,m}$ (wt. %)
Silica	2.6	0.038	1.5	29.0	0.15	0.15	0.15
			5	23.0	0.19	0.19	0.19
			10	22.6	0.19	0.19	0.19
HPMC	1.39	0.400	1.5	24.4	1.03	1.00	1.01±0.02
			3	41.0	0.61	0.59	0.60
			5	46.2	0.54	0.53	0.53±0.01
Rutin	1.82	1.590	1.5	49.0	2.76	2.59	2.67±0.13
			3	98.5	1.33	1.28	1.31±0.03
			5	96.0	1.36	1.32	1.34±0.03
CMCC	0.6	5.200	1.5	47.5	3.67	2.87	3.27±0.57
			2	58.4	2.84	2.34	2.59±0.36
			2.5	76.8	2.05	1.78	1.91±0.19

A.4. Calculation of droplet formation time

The number of pores on the membrane surface is given by Vladislavljevic *et al.* [132] :

$$N_{pore} = \frac{4A_m\phi}{\pi d_p^2 \xi}$$

where A_m is the effective membrane surface area, ϕ is the porosity of the membrane (=0.56 for SPG) and ξ is the mean pore tortuosity (=1.28 for SPG), d_p is the mean pore size of the membrane.

At a certain transmembrane pressure the number of active pores will be:

$$N_a = \alpha N_{pore}$$

where $\alpha = K_m/d_p^2\phi^{1.5}$ (O'Brien *et al.*) is the active pore fraction and the membrane permeability can be calculated as follows [153]:

$$K_m = \frac{\eta_d L_m \xi M_d}{\rho_d A_m t_p \Delta P}$$

where η_d is the dispersed phase viscosity, L_m the membrane thickness, t_p the process time, ΔP the transmembrane pressure.

Assuming that one droplet detaches per active pore simultaneously, the dispersed phase flow rate of the pore would be:

$$Q_d = \frac{M_d}{\rho_d t_p N_a}$$

So for a droplet with volume V_{oil} the droplet formation time is:

$$t_{drop} = \frac{V_{oil}}{Q_d} = \frac{2\eta_d L_m D_{oil}^3}{3d_p^4 \phi^{0.5} \Delta P}$$

Appendix B

Supplementary data to Chapter 5

B.1. Viscosities of aqueous phases

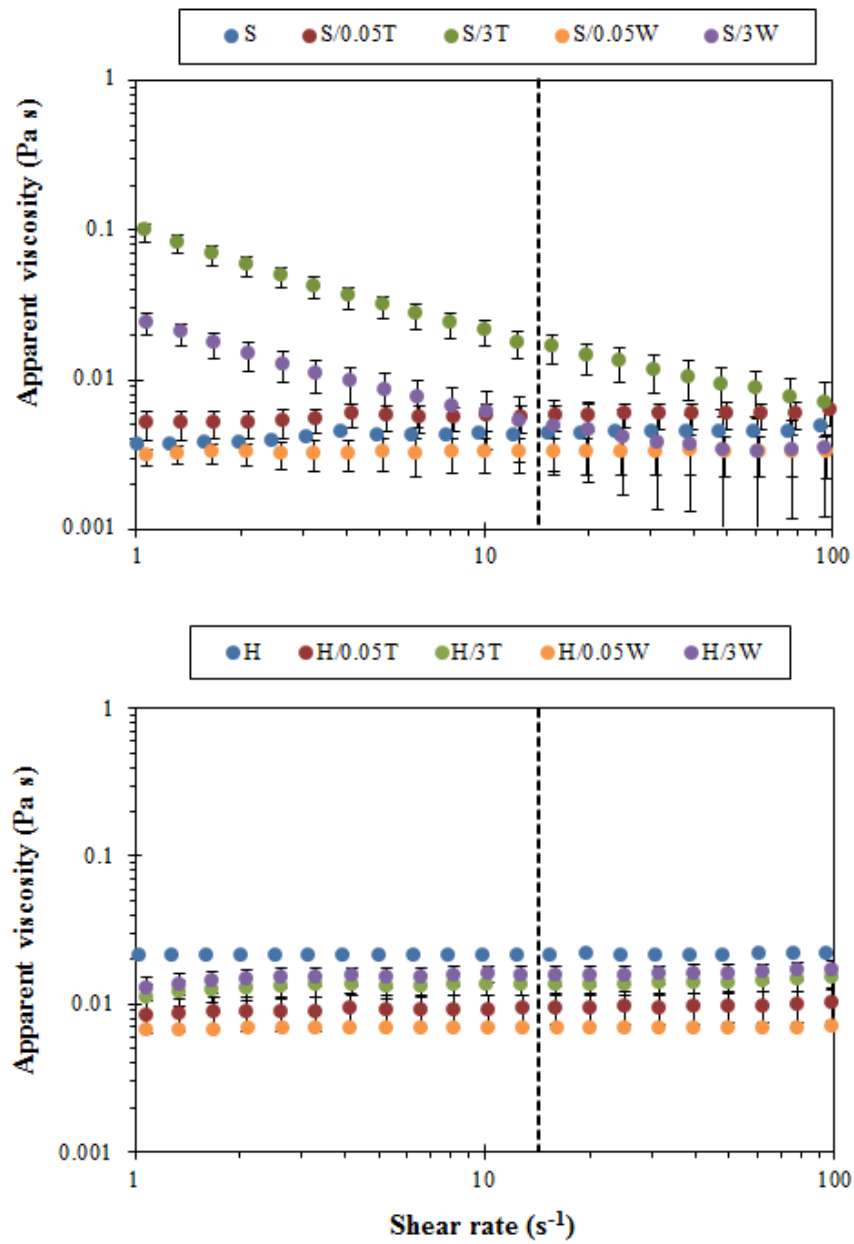


Fig. B.1: Viscosity as a function of shear rate for aqueous suspensions of particles and their mixtures with emulsifier (top: silica suspensions at pH 2 and bottom: HPMC suspensions at pH 6.5). The dotted line represents the fixed shear rate at the membrane surface used in this study (14 s⁻¹).

B.2. Particle size distributions

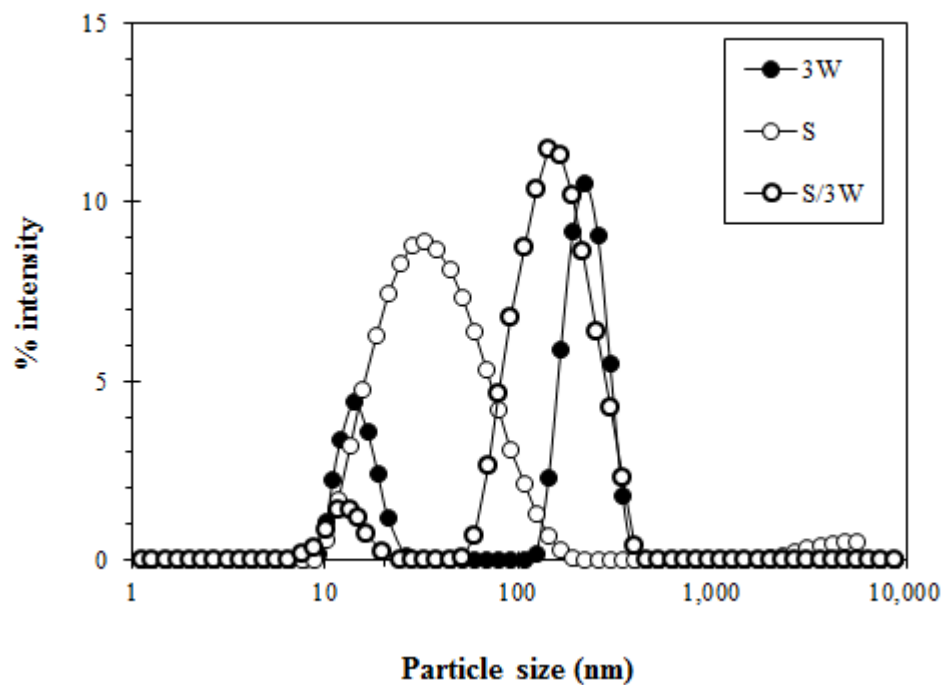


Fig. B.2: Particle size distribution of aqueous phases as obtained from DLS, all prepared at pH=2. Each curve represents the average of three subsequent measurements.

Appendix C

Supplementary data to Chapter 6

C.1. Calculation of porosity of Stainless Steel (SS) membrane

Assuming a small square surface (A_m) within the membrane surface area with dimensions 0.5 x 0.5 mm, pore spacing 0.5 mm in a cubic array, average membrane pore size 50 μm (D_p) and A_p the surface occupied by the pores, then the porosity can be calculated as follows:

$$\text{Porosity} = \frac{A_p}{A_m} = \frac{\pi D_p^2}{4} \approx 0.8 \%$$

List of References

- [1] B. P. Binks, "Particles as surfactants—similarities and differences," *Current opinion in colloid & interface science*, vol. 7, pp. 21-41, 2002.
- [2] C. C. Berton-Carabin and K. Schroën, "Pickering emulsions for food applications: background, trends, and challenges," *Annual review of food science and technology*, vol. 6, pp. 263-297, 2015.
- [3] I. Capron and B. Cathala, "Surfactant-free high internal phase emulsions stabilized by cellulose nanocrystals," *Biomacromolecules*, vol. 14, pp. 291-296, 2013.
- [4] R. G. Holdich, M. M. Dragosavac, G. T. Vladisavljević, and E. Piacentini, "Continuous membrane emulsification with pulsed (oscillatory) flow," *Industrial & Engineering Chemistry Research*, vol. 52, pp. 507-515, 2012.
- [5] Y. Wang and Y. Xia, "Bottom-up and top-down approaches to the synthesis of monodispersed spherical colloids of low melting-point metals," *Nano letters*, vol. 4, pp. 2047-2050, 2004.
- [6] A. A. Maan, K. Schroën, and R. Boom, "Spontaneous droplet formation techniques for monodisperse emulsions preparation—Perspectives for food applications," *Journal of food engineering*, vol. 107, pp. 334-346, 2011.
- [7] G. T. Vladisavljević, I. Kobayashi, and M. Nakajima, "Membrane Emulsification Principles," *Encyclopedia of Membranes*, pp. 1228-1231, 2016.
- [8] G. T. Vladisavljević and H. Schubert, "Influence of process parameters on droplet size distribution in SPG membrane emulsification and stability of prepared emulsion droplets," *Journal of membrane science*, vol. 225, pp. 15-23, 2003.
- [9] V. Schadler and E. Windhab, "Continuous membrane emulsification by using a membrane system with controlled pore distance," *Desalination*, vol. 189, pp. 130-135, 2006.
- [10] E. Dickinson, "Food emulsions and foams: Stabilization by particles," *Current Opinion in Colloid & Interface Science*, vol. 15, pp. 40-49, 4// 2010.
- [11] L. J. Duffus, J. E. Norton, P. Smith, I. T. Norton, and F. Spyropoulos, "A comparative study on the capacity of a range of food-grade particles to form stable O/W and W/O Pickering emulsions," *Journal of colloid and interface science*, vol. 473, pp. 9-21, 2016.
- [12] M. S. Manga, O. J. Cayre, R. A. Williams, S. Biggs, and D. W. York, "Production of solid-stabilised emulsions through rotational membrane emulsification: influence of particle adsorption kinetics," *Soft Matter*, vol. 8, pp. 1532-1538, 2012.
- [13] Q. Yuan, O. J. Cayre, M. Manga, R. A. Williams, and S. Biggs, "Preparation of particle-stabilized emulsions using membrane emulsification," *Soft Matter*, vol. 6, pp. 1580-1588, 2010.
- [14] B. P. Binks, J. A. Rodrigues, and W. J. Frith, "Synergistic interaction in emulsions stabilized by a mixture of silica nanoparticles and cationic surfactant," *Langmuir*, vol. 23, pp. 3626-3636, 2007.
- [15] Q. Yuan and R. A. Williams, "CO-stabilisation mechanisms of nanoparticles and surfactants in Pickering Emulsions produced by membrane emulsification," *Journal of Membrane Science*, vol. 497, pp. 221-228, 2016.
- [16] T. Förster and W. von Rybinski, "Applications of emulsions," *Modern aspects of emulsion science*, pp. 395-426, 1998.

- [17] H.-J. Kim, E. A. Decker, and D. J. McClements, "Preparation of multiple emulsions based on thermodynamic incompatibility of heat-denatured whey protein and pectin solutions," *Food Hydrocolloids*, vol. 20, pp. 586-595, 2006.
- [18] N. Garti and C. Bisperink, "Double emulsions: progress and applications," *Current opinion in colloid & interface science*, vol. 3, pp. 657-667, 1998.
- [19] G. Muschiolik, "Multiple emulsions for food use," *Current Opinion in Colloid & Interface Science*, vol. 12, pp. 213-220, 2007.
- [20] J. Embleton and B. Tighe, "Regulation of polyester microcapsule morphology," *Drug Targetting and delivery (microencapsulation of drugs)*, pp. 45-54, 1992.
- [21] F. Spyropoulos, A. Portschi, and I. Norton, "Effect of sucrose on the phase and flow behaviour of polysaccharide/protein aqueous two-phase systems," *Food Hydrocolloids*, vol. 24, pp. 217-226, 2010.
- [22] J. Esquena, "Water-in-water (W/W) emulsions," *Current Opinion in Colloid & Interface Science*, vol. 25, pp. 109-119, 2016.
- [23] N. Anton, J.-P. Benoit, and P. Saulnier, "Design and production of nanoparticles formulated from nano-emulsion templates—a review," *Journal of Controlled Release*, vol. 128, pp. 185-199, 2008.
- [24] C. Solans, P. Izquierdo, J. Nolla, N. Azemar, and M. J. Garcia-Celma, "Nano-emulsions," *Current Opinion in Colloid & Interface Science*, vol. 10, pp. 102-110, 2005/10/01/ 2005.
- [25] N. Anton and T. F. Vandamme, "Nano-emulsions and micro-emulsions: clarifications of the critical differences," *Pharmaceutical research*, vol. 28, pp. 978-985, 2011.
- [26] E. Ruckenstein, "Microemulsions, macroemulsions, and the Bancroft rule," *Langmuir*, vol. 12, pp. 6351-6353, 1996.
- [27] D. J. McClements, "Nanoemulsions versus microemulsions: terminology, differences, and similarities," *Soft Matter*, vol. 8, pp. 1719-1729, 2012.
- [28] S. Friberg, K. Larsson, and J. Sjoblom, *Food emulsions*: CRC Press, 2003.
- [29] P. Walstra, P. Walstra, J. T. Wouters, and T. J. Geurts, *Dairy science and technology*: CRC press, 2014.
- [30] D. J. McClements, "Lipid-based emulsions and emulsifiers," in *Food lipids*, ed: CRC Press, 2002, pp. 82-121.
- [31] D. J. McClements, *Food emulsions: principles, practices, and techniques*: CRC press, 2015.
- [32] D. J. McClements, "Critical review of techniques and methodologies for characterization of emulsion stability," *Critical Reviews in Food Science and Nutrition*, vol. 47, pp. 611-649, 2007.
- [33] T. F. Tadros, *Applied surfactants: principles and applications*: John Wiley & Sons, 2006.
- [34] D. J. McClements and C. E. Gumus, "Natural emulsifiers — Biosurfactants, phospholipids, biopolymers, and colloidal particles: Molecular and physicochemical basis of functional performance," *Advances in Colloid and Interface Science*, vol. 234, pp. 3-26, 2016/08/01/ 2016.
- [35] D. J. McClements and S. M. Jafari, "Improving emulsion formation, stability and performance using mixed emulsifiers: A review," *Advances in colloid and interface science*, vol. 251, pp. 55-79, 2018.
- [36] R. Nagarajan, "One hundred years of micelles: evolution of the theory of micellization," in *Surfactant Science and Technology*, ed: CRC Press, 2014, pp. 30-79.

- [37] W. C. Griffin, "Classification of surface-active agents by" HLB", *J. Soc. Cosmet. Chem.*, vol. 1, pp. 311-326, 1949.
- [38] W. D. Bancroft, "The theory of emulsification, V," *The Journal of Physical Chemistry*, vol. 17, pp. 501-519, 1913.
- [39] L. S. Romsted, *Surfactant science and technology: retrospects and prospects*: CRC Press, 2014.
- [40] M. J. Rosen and J. T. Kunjappu, *Surfactants and interfacial phenomena*: John Wiley & Sons, 2012.
- [41] L.-J. Chen, S.-Y. Lin, C.-C. Huang, and E.-M. Chen, "Temperature dependence of critical micelle concentration of polyoxyethylenated non-ionic surfactants," *Colloids and Surfaces A: Physicochemical and Engineering Aspects*, vol. 135, pp. 175-181, 1998.
- [42] G. Geeraerts and P. Joos, "Dynamic surface tensions of micellar Triton X-100 solutions," *Colloids and Surfaces A: Physicochemical and Engineering Aspects*, vol. 90, pp. 149-154, 1994.
- [43] K. D. Danov, P. A. Kralchevsky, and I. B. Ivanov, "Equilibrium and dynamics of surfactant adsorption monolayers and thin liquid films," *Handbook of Detergents, Part A: Properties*, vol. 9, pp. 303-418, 2008.
- [44] F. Spyropoulos, R. D. Hancock, and I. T. Norton, "Food-grade emulsions prepared by membrane emulsification techniques," *Procedia Food Science*, vol. 1, pp. 920-926, 2011.
- [45] W. Norde, *Colloids and interfaces in life sciences and bionanotechnology*: CRC Press, 2011.
- [46] S. Tcholakova, N. Denkov, and A. Lips, "Comparison of solid particles, globular proteins and surfactants as emulsifiers," *Physical Chemistry Chemical Physics*, vol. 10, pp. 1608-1627, 2008.
- [47] P. Walstra, T. J. Geurts, P. Walstra, and J. T. Wouters, *Dairy science and technology*: CRC press, 2005.
- [48] D. Graham and M. Phillips, "Proteins at liquid interfaces: I. Kinetics of adsorption and surface denaturation," *Journal of Colloid and Interface Science*, vol. 70, pp. 403-414, 1979.
- [49] S. Nakai and E. Li-Chan, "Recent advances in structure and function of food proteins: QSAR approach," *Critical Reviews in Food Science & Nutrition*, vol. 33, pp. 477-499, 1993.
- [50] P. Wilde, A. Mackie, F. Husband, P. Gunning, and V. Morris, "Proteins and emulsifiers at liquid interfaces," *Advances in Colloid and Interface Science*, vol. 108, pp. 63-71, 2004.
- [51] D. Pelegrine and C. Gasparetto, "Whey proteins solubility as function of temperature and pH," *LWT-Food Science and Technology*, vol. 38, pp. 77-80, 2005.
- [52] W. Ramsden and F. Gotch, "Separation of solids in the surface-layers of solutions and 'suspensions' (observations on surface-membranes, bubbles, emulsions, and mechanical coagulation).—Preliminary account 72 Proceedings of the Royal Society of London <http://doi.org/10.1098/rspl.1903.0034>," 1903.
- [53] S. U. Pickering, "Cxcvi.—emulsions," *Journal of the Chemical Society, Transactions*, vol. 91, pp. 2001-2021, 1907.
- [54] H. Barthel, B. P. Binks, A. Dyab, and P. Fletcher, "Multiple emulsions," ed: Google Patents, 2010.

- [55] K. P. Oza and S. G. Frank, "Multiple emulsions stabilized by colloidal microcrystalline cellulose," *JOURNAL OF DISPERSION SCIENCE AND TECHNOLOGY*, vol. 10, pp. 163-185, 1989.
- [56] B. Midmore and T. Herrington, "Silica-stabilised multiple emulsions," in *Trends in colloid and interface science xiii*, ed: Springer, 1999, pp. 115-120.
- [57] Y. Chevalier and M.-A. Bolzinger, "Emulsions stabilized with solid nanoparticles: Pickering emulsions," *Colloids and Surfaces A: Physicochemical and Engineering Aspects*, vol. 439, pp. 23-34, 2013.
- [58] F. Leal-Calderon and V. Schmitt, "Solid-stabilized emulsions," *Current Opinion in Colloid & Interface Science*, vol. 13, pp. 217-227, 8// 2008.
- [59] R. Peters, E. Kramer, A. G. Oomen, Z. E. Herrera Rivera, G. Oegema, P. C. Tromp, *et al.*, "Presence of nano-sized silica during in vitro digestion of foods containing silica as a food additive," *ACS nano*, vol. 6, pp. 2441-2451, 2012.
- [60] I. Tavernier, W. Wijaya, P. Van der Meeren, K. Dewettinck, and A. R. Patel, "Food-grade particles for emulsion stabilization," *Trends in Food Science & Technology*, vol. 50, pp. 159-174, 2016.
- [61] J. Xiao, Y. Li, and Q. Huang, "Recent advances on food-grade particles stabilized Pickering emulsions: Fabrication, characterization and research trends," *Trends in Food Science & Technology*, vol. 55, pp. 48-60, 2016.
- [62] F. Gautier, M. Destribats, R. Perrier-Cornet, J.-F. Dechézelles, J. Giermanska, V. Héroguez, *et al.*, "Pickering emulsions with stimuable particles: from highly-to weakly-covered interfaces," *Physical Chemistry Chemical Physics*, vol. 9, pp. 6455-6462, 2007.
- [63] I. Kalashnikova, H. Bizot, P. Bertoncini, B. Cathala, and I. Capron, "Cellulosic nanorods of various aspect ratios for oil in water Pickering emulsions," *Soft Matter*, vol. 9, pp. 952-959, 2013.
- [64] D. G. Coffey, D. A. Bell, and A. Henderson, "Cellulose and cellulose derivatives," *Food polysaccharides and their applications*, pp. 147-180, 2006.
- [65] N. A. Camino, C. C. Sánchez, J. M. R. Patino, and A. M. Pílosof, "Hydroxypropylmethylcellulose at the oil–water interface. Part I. Bulk behaviour and dynamic adsorption as affected by pH," *Food Hydrocolloids*, vol. 25, pp. 1-11, 2011.
- [66] C.-H. Yang, Y.-C. Huang, and C.-Y. Chen, "Degradation of rutin by *Thermoactinomyces vulgaris* and other thermophilic compost isolates," *Journal of agricultural and food chemistry*, vol. 57, pp. 5095-5099, 2009.
- [67] E. van der Watt and J. C. Pretorius, "Purification and identification of active antibacterial components in *Carpobrotus edulis* L.," *Journal of Ethnopharmacology*, vol. 76, pp. 87-91, 2001.
- [68] S. G. Parkar, D. E. Stevenson, and M. A. Skinner, "The potential influence of fruit polyphenols on colonic microflora and human gut health," *International journal of food microbiology*, vol. 124, pp. 295-298, 2008.
- [69] A. S. Macedo, S. Quelhas, A. M. Silva, and E. B. Souto, "Nanoemulsions for delivery of flavonoids: formulation and in vitro release of rutin as model drug," *Pharmaceutical development and technology*, vol. 19, pp. 677-680, 2014.
- [70] Z. Luo, B. S. Murray, A. Yusoff, M. R. Morgan, M. J. Povey, and A. J. Day, "Particle-stabilizing effects of flavonoids at the oil– water interface," *Journal of agricultural and food chemistry*, vol. 59, pp. 2636-2645, 2011.

- [71] Z. Luo, B. S. Murray, A.-L. Ross, M. J. Povey, M. R. Morgan, and A. J. Day, "Effects of pH on the ability of flavonoids to act as Pickering emulsion stabilizers," *Colloids and Surfaces B: Biointerfaces*, vol. 92, pp. 84-90, 2012.
- [72] L. Atarés, L. J. Marshall, M. Akhtar, and B. S. Murray, "Structure and oxidative stability of oil in water emulsions as affected by rutin and homogenization procedure," *Food chemistry*, vol. 134, pp. 1418-1424, 2012.
- [73] F. Spyropoulos, D. Kurukji, P. Taylor, and I. T. Norton, "Fabrication and Utilization of Bifunctional Protein/Polysaccharide Coprecipitates for the Independent Codelivery of Two Model Actives from Simple Oil-in-Water Emulsions," *Langmuir*, vol. 34, pp. 3934-3948, 2018.
- [74] B. Wolf, S. Lam, M. Kirkland, and W. J. Frith, "Shear thickening of an emulsion stabilized with hydrophilic silica particles," *Journal of Rheology*, vol. 51, pp. 465-478, 2007.
- [75] B. P. Binks and C. P. Whitby, "Nanoparticle silica-stabilised oil-in-water emulsions: improving emulsion stability," *Colloids and Surfaces A: Physicochemical and Engineering Aspects*, vol. 253, pp. 105-115, 2005.
- [76] J. Tang, P. J. Quinlan, and K. C. Tam, "Stimuli-responsive Pickering emulsions: recent advances and potential applications," *Soft Matter*, vol. 11, pp. 3512-3529, 2015.
- [77] Z. Wang and Y. Wang, "Tuning amphiphilicity of particles for controllable pickering emulsion," *Materials*, vol. 9, p. 903, 2016.
- [78] N. G. Eskandar, S. Simovic, and C. A. Prestidge, "Synergistic effect of silica nanoparticles and charged surfactants in the formation and stability of submicron oil-in-water emulsions," *Physical Chemistry Chemical Physics*, vol. 9, pp. 6426-6434, 2007.
- [79] R. Pichot, F. Spyropoulos, and I. T. Norton, "Mixed-emulsifier stabilised emulsions: Investigation of the effect of monoolein and hydrophilic silica particle mixtures on the stability against coalescence," *Journal of Colloid and Interface Science*, vol. 329, pp. 284-291, 1/15/ 2009.
- [80] R. Pichot, F. Spyropoulos, and I. T. Norton, "O/W emulsions stabilised by both low molecular weight surfactants and colloidal particles: The effect of surfactant type and concentration," *Journal of Colloid and Interface Science*, vol. 352, pp. 128-135, 12/1/ 2010.
- [81] B. K. Pilapil, H. Jahandideh, S. L. Bryant, and M. Trifkovic, "Stabilization of Oil-in-Water Emulsions with Noninterfacially Adsorbed Particles," *Langmuir*, vol. 32, pp. 7109-7116, 2016.
- [82] J.-C. Arboleya and P. J. Wilde, "Competitive adsorption of proteins with methylcellulose and hydroxypropyl methylcellulose," *Food Hydrocolloids*, vol. 19, pp. 485-491, 2005.
- [83] J. M. R. Patino and A. M. Pilosof, "Protein-polysaccharide interactions at fluid interfaces," *Food Hydrocolloids*, vol. 25, pp. 1925-1937, 2011.
- [84] E. Dickinson, "Interfacial structure and stability of food emulsions as affected by protein-polysaccharide interactions," *Soft Matter*, vol. 4, pp. 932-942, 2008.
- [85] O. E. Pérez, C. Carrera-Sánchez, J. M. Rodríguez-Patino, and A. M. Pilosof, "Adsorption dynamics and surface activity at equilibrium of whey proteins and hydroxypropyl-methyl-cellulose mixtures at the air-water interface," *Food hydrocolloids*, vol. 21, pp. 794-803, 2007.
- [86] N. A. Camino, C. C. Sanchez, J. M. R. Patino, and A. M. Pilosof, "Hydroxypropylmethylcellulose- β -lactoglobulin mixtures at the oil-water interface.

- Bulk, interfacial and emulsification behavior as affected by pH," *Food Hydrocolloids*, vol. 27, pp. 464-474, 2012.
- [87] I. Zafeiri, C. Horridge, E. Tripodi, and F. Spyropoulos, "Emulsions Co-Stabilised by Edible Pickering Particles and Surfactants: The Effect of HLB Value," *Colloid and Interface Science Communications*, pp. 5-9, 2017.
- [88] S. Brösel and H. Schubert, "Investigations on the role of surfactants in mechanical emulsification using a high-pressure homogenizer with an orifice valve," *Chemical Engineering and Processing: Process Intensification*, vol. 38, pp. 533-540, 1999.
- [89] Y. H. Roos and Y. D. Livney, *Engineering foods for bioactives stability and delivery*: Springer, 2017.
- [90] D. J. McClements, "Edible nanoemulsions: fabrication, properties, and functional performance," *Soft Matter*, vol. 7, pp. 2297-2316, 2011.
- [91] H. Karbstein and H. Schubert, "Developments in the continuous mechanical production of oil-in-water macro-emulsions," *Chemical Engineering and Processing: Process Intensification*, vol. 34, pp. 205-211, 1995.
- [92] P. Walstra, *Physical chemistry of foods*: CRC Press, 2002.
- [93] P. Walstra, "Principles of emulsion formation," *Chemical Engineering Science*, vol. 48, pp. 333-349, 1993.
- [94] K. Urban, G. Wagner, D. Schaffner, D. Röglin, and J. Ulrich, "Rotor-stator and disc systems for emulsification processes," *Chemical Engineering & Technology: Industrial Chemistry-Plant Equipment-Process Engineering-Biotechnology*, vol. 29, pp. 24-31, 2006.
- [95] A. T. Utomo, M. Baker, and A. W. Pacek, "Flow pattern, periodicity and energy dissipation in a batch rotor–stator mixer," *Chemical engineering research and design*, vol. 86, pp. 1397-1409, 2008.
- [96] S. Hall, M. Cooke, A. El-Hamouz, and A. Kowalski, "Droplet break-up by in-line Silverson rotor–stator mixer," *Chemical Engineering Science*, vol. 66, pp. 2068-2079, 2011.
- [97] J. Zhang, S. Xu, and W. Li, "High shear mixers: A review of typical applications and studies on power draw, flow pattern, energy dissipation and transfer properties," *Chemical Engineering and Processing: Process Intensification*, vol. 57, pp. 25-41, 2012.
- [98] J. Perrier-Cornet, P. Marie, and P. Gervais, "Comparison of emulsification efficiency of protein-stabilized oil-in-water emulsions using jet, high pressure and colloid mill homogenization," *Journal of Food Engineering*, vol. 66, pp. 211-217, 2005.
- [99] A. Håkansson, C. Trägårdh, and B. Bergenståhl, "Studying the effects of adsorption, recoalescence and fragmentation in a high pressure homogenizer using a dynamic simulation model," *Food Hydrocolloids*, vol. 23, pp. 1177-1183, 2009.
- [100] S. Schultz, G. Wagner, K. Urban, and J. Ulrich, "High-pressure homogenization as a process for emulsion formation," *Chemical Engineering & Technology*, vol. 27, pp. 361-368, 2004.
- [101] L. Lee and I. T. Norton, "Comparing droplet breakup for a high-pressure valve homogeniser and a Microfluidizer for the potential production of food-grade nanoemulsions," *Journal of food engineering*, vol. 114, pp. 158-163, 2013.
- [102] P. Walstra and P. E. Smulders, "Emulsion formation," *Modern aspects of emulsion science*, pp. 56-99, 1998.
- [103] A. Sommerfeld, *Ein beitrag zur hydrodynamischen erklärung der turbulenten fluessigkeitsbewegungen*, 1909.

- [104] A. K. Pawlik and I. T. Norton, "Encapsulation stability of duplex emulsions prepared with SPG cross-flow membrane, SPG rotating membrane and rotor-stator techniques—A comparison," *Journal of Membrane Science*, vol. 415, pp. 459-468, 2012.
- [105] V. G. e. Levich, "Physicochemical hydrodynamics," 1962.
- [106] M. A. Bos and T. van Vliet, "Interfacial rheological properties of adsorbed protein layers and surfactants: a review," *Advances in colloid and interface science*, vol. 91, pp. 437-471, 2001.
- [107] G. Vladislavljević, I. Kobayashi, and M. Nakajima, "Production of uniform droplets using membrane, microchannel and microfluidic emulsification devices," *Microfluidics and nanofluidics*, vol. 13, pp. 151-178, 2012.
- [108] I. Kobayashi, M. Nakajima, K. Chun, Y. Kikuchi, and H. Fujita, "Silicon array of elongated through-holes for monodisperse emulsion droplets," *AIChE Journal*, vol. 48, pp. 1639-1644, 2002.
- [109] I. Kobayashi, Y. Wada, K. Uemura, and M. Nakajima, "Microchannel emulsification for mass production of uniform fine droplets: integration of microchannel arrays on a chip," *Microfluidics and Nanofluidics*, vol. 8, pp. 255-262, 2010.
- [110] F. Spyropoulos, D. M. Lloyd, R. D. Hancocks, and A. K. Pawlik, "Advances in membrane emulsification. Part B: recent developments in modelling and scale-up approaches," *Journal of the science of food and agriculture*, vol. 94, pp. 628-638, 2014.
- [111] M. Rayner and P. Dejmek, *Engineering aspects of food emulsification and homogenization*: CRC Press, 2015.
- [112] S. M. Joscelyne and G. Trägårdh, "Membrane emulsification — a literature review," *Journal of Membrane Science*, vol. 169, pp. 107-117, 4/30/ 2000.
- [113] M. Stang, H. Schuchmann, and H. Schubert, "Emulsification in high-pressure homogenizers," *Engineering in Life Sciences*, vol. 1, pp. 151-157, 2001.
- [114] Y. MIYAGAWA, M. SHIMA, R. MATSUNO, and S. ADACHI, "Energy efficiency of different emulsification methods: a comparative evaluation," *Japan Journal of Food Engineering*, vol. 16, pp. 71-74, 2015.
- [115] M. Kukizaki and M. Goto, "A comparative study of SPG membrane emulsification in the presence and absence of continuous-phase flow," *Journal of chemical engineering of Japan*, vol. 42, pp. 520-530, 2009.
- [116] W. Jing, J. Wu, W. Jin, W. Xing, and N. Xu, "Monodispersed W/O emulsion prepared by hydrophilic ceramic membrane emulsification," *Desalination*, vol. 191, pp. 219-222, 2006.
- [117] U. Lambrich and H. Schubert, "Emulsification using microporous systems," *Journal of membrane science*, vol. 257, pp. 76-84, 2005.
- [118] T. Nakashima, M. Shimizu, and M. Kawano, "Articles of porous glass and process for preparing the same," ed: Google Patents, 1987.
- [119] C. Charcosset, I. Limayem, and H. Fessi, "The membrane emulsification process—a review," *Journal of chemical technology and biotechnology*, vol. 79, pp. 209-218, 2004.
- [120] R. Liu, G.-H. Ma, Y.-H. Wan, and Z.-G. Su, "Influence of process parameters on the size distribution of PLA microcapsules prepared by combining membrane emulsification technique and double emulsion-solvent evaporation method," *Colloids and Surfaces B: Biointerfaces*, vol. 45, pp. 144-153, 2005.

- [121] J. Yang, D.-X. Hao, C.-X. Bi, Z.-G. Su, L.-Y. Wang, and G.-H. Ma, "Rapid synthesis of uniform magnetic microspheres by combing premix membrane emulsification and in situ formation techniques," *Industrial & Engineering Chemistry Research*, vol. 49, pp. 6047-6053, 2010.
- [122] K. Kandori, K. Kishi, and T. Ishikawa, "Preparation of uniform silica hydrogel particles by SPG filter emulsification method," *Colloids and surfaces*, vol. 62, pp. 259-262, 1992.
- [123] M. Kukizaki and M. Goto, "Preparation and evaluation of uniformly sized solid lipid microcapsules using membrane emulsification," *Colloids and Surfaces A: Physicochemical and Engineering Aspects*, vol. 293, pp. 87-94, 2007.
- [124] L.-Y. Wang, G.-H. Ma, and Z.-G. Su, "Preparation of uniform sized chitosan microspheres by membrane emulsification technique and application as a carrier of protein drug," *Journal of Controlled Release*, vol. 106, pp. 62-75, 2005.
- [125] X. Liu, D. Bao, W. Xue, Y. Xiong, W. Yu, X. Yu, *et al.*, "Preparation of uniform calcium alginate gel beads by membrane emulsification coupled with internal gelation," *Journal of Applied Polymer Science*, vol. 87, pp. 848-852, 2003.
- [126] T. Tanaka, M. Okayama, Y. Kitayama, Y. Kagawa, and M. Okubo, "Preparation of "mushroom-like" Janus particles by site-selective surface-initiated atom transfer radical polymerization in aqueous dispersed systems," *Langmuir*, vol. 26, pp. 7843-7847, 2010.
- [127] N. C. Christov, D. N. Ganchev, N. D. Vassileva, N. D. Denkov, K. D. Danov, and P. A. Kralchevsky, "Capillary mechanisms in membrane emulsification: oil-in-water emulsions stabilized by Tween 20 and milk proteins," *Colloids and Surfaces A: Physicochemical and Engineering Aspects*, vol. 209, pp. 83-104, 9/4/ 2002.
- [128] I. Kobayashi, M. Nakajima, and S. Mukataka, "Preparation characteristics of oil-in-water emulsions using differently charged surfactants in straight-through microchannel emulsification," *Colloids and Surfaces A: Physicochemical and Engineering Aspects*, vol. 229, pp. 33-41, 2003.
- [129] G. T. Vladislavljević, "Structured microparticles with tailored properties produced by membrane emulsification," *Advances in Colloid and Interface Science*, vol. 225, pp. 53-87, 11// 2015.
- [130] Q. Yuan, N. Aryanti, G. Gutiérrez, and R. A. Williams, "Enhancing the throughput of membrane emulsification techniques to manufacture functional particles," *Industrial & Engineering Chemistry Research*, vol. 48, pp. 8872-8880, 2009.
- [131] M. Kukizaki and T. Nakashima, "Acid leaching process in the preparation of porous glass membranes from phase-separated glass in the Na₂O-CaO-MgO-Al₂O₃-B₂O₃-SiO₂ system," *Membrane*, vol. 29, pp. 301-308, 2004.
- [132] G. T. Vladislavljević, I. Kobayashi, M. Nakajima, R. A. Williams, M. Shimizu, and T. Nakashima, "Shirasu Porous Glass membrane emulsification: Characterisation of membrane structure by high-resolution X-ray microtomography and microscopic observation of droplet formation in real time," *Journal of Membrane Science*, vol. 302, pp. 243-253, 2007.
- [133] H. Kawakita, K. Hamamoto, H. Seto, K. Ohto, H. Harada, and K. Inoue, "Porosity estimation of a membrane filled with dextran produced by immobilized dextranase," *AIChE journal*, vol. 55, pp. 275-278, 2009.
- [134] T. Nakashima, "Effect of surfactant on production of monodispersed O/W emulsion in membrane emulsification," *Kagaku Kogaku Ronbunshu*, vol. 19, pp. 991-997, 1993.

- [135] T. Kai, Y. Suma, S. Ono, T. Yamaguchi, and S. i. Nakao, "Effect of the pore surface modification of an inorganic substrate on the plasma-grafting behavior of pore-filling-type organic/inorganic composite membranes," *Journal of Polymer Science Part A: Polymer Chemistry*, vol. 44, pp. 846-856, 2006.
- [136] P. Apel, "Track etching technique in membrane technology," *Radiation Measurements*, vol. 34, pp. 559-566, 2001.
- [137] A. Kayvani Fard, G. McKay, A. Buekenhoudt, H. Al Sulaiti, F. Motmans, M. Khraisheh, *et al.*, "Inorganic membranes: Preparation and application for water treatment and desalination," *Materials*, vol. 11, p. 74, 2018.
- [138] Y. Chen, Z. Zhao, J. Dai, Y. Liu, H. Ma, and R. Nie, "Etching characteristic for tracks of multicharged ions in polymer," *Radiation Measurements*, vol. 43, pp. S111-S115, 2008.
- [139] R. Othman, G. T. Vladisavljević, H. Shahmohamadi, Z. K. Nagy, and R. Holdich, "Formation of size-tuneable biodegradable polymeric nanoparticles by solvent displacement method using micro-engineered membranes fabricated by laser drilling and electroforming," *Chemical Engineering Journal*, vol. 304, pp. 703-713, 2016.
- [140] R. Hancocks, F. Spyropoulos, and I. Norton, "The effects of membrane composition and morphology on the rotating membrane emulsification technique for food grade emulsions," *Journal of Membrane Science*, vol. 497, pp. 29-35, 2016.
- [141] R. D. Hancocks, F. Spyropoulos, and I. T. Norton, "Comparisons between membranes for use in cross flow membrane emulsification," *Journal of Food Engineering*, vol. 116, pp. 382-389, 5// 2013.
- [142] V. Schröder, O. Behrend, and H. Schubert, "Effect of dynamic interfacial tension on the emulsification process using microporous, ceramic membranes," *Journal of Colloid and Interface Science*, vol. 202, pp. 334-340, 1998.
- [143] S. R. Kosvintsev, G. Gasparini, and R. G. Holdich, "Membrane emulsification: droplet size and uniformity in the absence of surface shear," *Journal of Membrane Science*, vol. 313, pp. 182-189, 2008.
- [144] M. M. Dragosavac, M. N. Sovilj, S. R. Kosvintsev, R. G. Holdich, and G. T. Vladisavljević, "Controlled production of oil-in-water emulsions containing unrefined pumpkin seed oil using stirred cell membrane emulsification," *Journal of Membrane Science*, vol. 322, pp. 178-188, 2008.
- [145] A. J. Gijbetsen-Abrahamse, A. Van der Padt, and R. M. Boom, "Status of cross-flow membrane emulsification and outlook for industrial application," *Journal of Membrane Science*, vol. 230, pp. 149-159, 2004.
- [146] P. S. Silva, M. M. Dragosavac, G. T. Vladisavljević, H. C. Bandulasena, R. G. Holdich, M. Stillwell, *et al.*, "Azimuthally oscillating membrane emulsification for controlled droplet production," *AIChE Journal*, vol. 61, pp. 3607-3615, 2015.
- [147] R. G. Holdich, M. M. Dragosavac, G. T. Vladisavljevic, and S. R. Kosvintsev, "Membrane emulsification with oscillating and stationary membranes," *Industrial & Engineering Chemistry Research*, vol. 49, pp. 3810-3817, 2010.
- [148] A. Nita, W. A. Richard, R. Hou, and G. T. Vladisavljevic, "Performance of rotating membrane emulsification for o/w production," *Desalination*, vol. 200, pp. 572-574, 2006.
- [149] G. T. Vladisavljević and R. A. Williams, "Manufacture of large uniform droplets using rotating membrane emulsification," *Journal of colloid and interface science*, vol. 299, pp. 396-402, 2006.

- [150] Q. Yuan, N. Aryanti, R. Hou, and R. A. Williams, "Performance of slotted pores in particle manufacture using rotating membrane emulsification," *Particuology*, vol. 7, pp. 114-120, 2009.
- [151] X.-Q. Li, Q. Li, F.-L. Gong, J.-D. Lei, X. Zhao, G.-H. Ma, *et al.*, "Preparation of large-sized highly uniform agarose beads by novel rotating membrane emulsification," *Journal of Membrane Science*, vol. 476, pp. 30-39, 2015.
- [152] A. K. Pawlik and I. T. Norton, "SPG rotating membrane technique for production of food grade emulsions," *Journal of Food Engineering*, vol. 114, pp. 530-537, 2013.
- [153] D. M. Lloyd, I. T. Norton, and F. Spyropoulos, "Processing effects during rotating membrane emulsification," *Journal of Membrane Science*, vol. 466, pp. 8-17, 9/15/2014.
- [154] D. M. Lloyd, I. T. Norton, and F. Spyropoulos, "Process optimisation of rotating membrane emulsification through the study of surfactant dispersions," *Journal of Food Engineering*, vol. 166, pp. 316-324, 2015.
- [155] S. Peng and R. A. Williams, "Controlled production of emulsions using a crossflow membrane: Part I: Droplet formation from a single pore," *Chemical Engineering Research and Design*, vol. 76, pp. 894-901, 1998.
- [156] D. M. Lloyd, "Mechanistic understanding of the rotating membrane emulsification process towards the development of design and scale-up theory," University of Birmingham, 2016.
- [157] H. J. Keh and P. Y. Chen, "Slow motion of a droplet between two parallel plane walls," *Chemical Engineering Science*, vol. 56, pp. 6863-6871, 2001.
- [158] N. Aryanti, R. Hou, and R. A. Williams, "Performance of a rotating membrane emulsifier for production of coarse droplets," *Journal of Membrane Science*, vol. 326, pp. 9-18, 2009.
- [159] E. Egidi, G. Gasparini, R. G. Holdich, G. T. Vladisavljević, and S. R. Kosvintsev, "Membrane emulsification using membranes of regular pore spacing: Droplet size and uniformity in the presence of surface shear," *Journal of Membrane Science*, vol. 323, pp. 414-420, 2008.
- [160] S. Van der Graaf, C. Schroën, R. Van der Sman, and R. Boom, "Influence of dynamic interfacial tension on droplet formation during membrane emulsification," *Journal of colloid and interface science*, vol. 277, pp. 456-463, 2004.
- [161] M. Rayner, G. Trägårdh, C. Trägårdh, and P. Dejmek, "Using the surface evolver to model droplet formation processes in membrane emulsification," *Journal of colloid and interface science*, vol. 279, pp. 175-185, 2004.
- [162] S. Sugiura, M. Nakajima, N. Kumazawa, S. Iwamoto, and M. Seki, "Characterization of spontaneous transformation-based droplet formation during microchannel emulsification," *The Journal of Physical Chemistry B*, vol. 106, pp. 9405-9409, 2002.
- [163] S. Van der Graaf, T. Nisisako, C. Schroen, R. Van Der Sman, and R. Boom, "Lattice Boltzmann simulations of droplet formation in a T-shaped microchannel," *Langmuir*, vol. 22, pp. 4144-4152, 2006.
- [164] S. Van der Graaf, M. Steegmans, R. Van Der Sman, C. Schroën, and R. Boom, "Droplet formation in a T-shaped microchannel junction: a model system for membrane emulsification," *Colloids and Surfaces A: Physicochemical and Engineering Aspects*, vol. 266, pp. 106-116, 2005.
- [165] R. Xu, "Light scattering: A review of particle characterization applications," *Particuology*, vol. 18, pp. 11-21, 2015.

- [166] W. Brown, *Dynamic light scattering: the method and some applications* vol. 313: Clarendon press Oxford, 1993.
- [167] S. Bhattacharjee, "DLS and zeta potential—what they are and what they are not?," *Journal of Controlled Release*, vol. 235, pp. 337-351, 2016.
- [168] R. Pecora, *Dynamic light scattering: applications of photon correlation spectroscopy*: Springer Science & Business Media, 2013.
- [169] G. Sun, F. Qi, J. Wu, G. Ma, and T. Ngai, "Preparation of uniform particle-stabilized emulsions using SPG membrane emulsification," *Langmuir*, vol. 30, pp. 7052-7056, 2014.
- [170] K. Thompson, S. Armes, and D. York, "Preparation of pickering emulsions and colloidosomes with relatively narrow size distributions by stirred cell membrane emulsification," *Langmuir*, vol. 27, pp. 2357-2363, 2011.
- [171] S. C. Joshi, "Sol-gel behavior of hydroxypropyl methylcellulose (HPMC) in ionic media including drug release," *Materials*, vol. 4, pp. 1861-1905, 2011.
- [172] F. B. Hasan and D. D. Huang, "Characterization of colloidal silica and its adsorption phenomenon with silicon-base surfactants with relation to film strength," *Journal of colloid and interface science*, vol. 190, pp. 161-170, 1997.
- [173] H. Katepalli, V. T. John, A. Tripathi, and A. Bose, "Microstructure and rheology of particle stabilized emulsions: Effects of particle shape and inter-particle interactions," *Journal of Colloid and Interface Science*, vol. 485, pp. 11-17, 2017.
- [174] S. M. C. Silva, F. V. Pinto, F. E. Antunes, M. G. Miguel, J. J. S. Sousa, and A. A. C. C. Pais, "Aggregation and gelation in hydroxypropylmethyl cellulose aqueous solutions," *Journal of Colloid and Interface Science*, vol. 327, pp. 333-340, 2008/11/15/ 2008.
- [175] A. Hill and S. Carrington, "Understanding the links between rheology and particle parameters," *American Laboratory*, vol. 38, p. 22, 2006.
- [176] A. Einstein, *Investigations on the Theory of the Brownian Movement*: Courier Corporation, 1956.
- [177] H. Brinkman, "The viscosity of concentrated suspensions and solutions," *The Journal of Chemical Physics*, vol. 20, pp. 571-571, 1952.
- [178] M. Elimelech and C. R. O'Melia, "Effect of particle size on collision efficiency in the deposition of Brownian particles with electrostatic energy barriers," *Langmuir*, vol. 6, pp. 1153-1163, 1990.
- [179] E. Rampazzo, E. Brasola, S. Marcuz, F. Mancin, P. Tecilla, and U. Tonellato, "Surface modification of silica nanoparticles: a new strategy for the realization of self-organized fluorescence chemosensors," *Journal of Materials Chemistry*, vol. 15, pp. 2687-2696, 2005.
- [180] M. Ioelovich, "Optimal conditions for isolation of nanocrystalline cellulose particles," *Nanoscience and Nanotechnology*, vol. 2, pp. 9-13, 2012.
- [181] M. H. Asfour and A. M. Mohsen, "Formulation and evaluation of pH-sensitive rutin nanospheres against colon carcinoma using HCT-116 cell line," *Journal of Advanced Research*, 2017.
- [182] S. Pérez and D. Samain, "Structure and engineering of celluloses," *Advances in carbohydrate chemistry and biochemistry*, vol. 64, pp. 25-116, 2010.
- [183] R. Van Hooghten, L. Imperiali, V. Boeckx, R. Sharma, and J. Vermant, "Rough nanoparticles at the oil–water interfaces: their structure, rheology and applications," *Soft Matter*, vol. 9, pp. 10791-10798, 2013.

- [184] S. Abend and G. Lagaly, "Bentonite and double hydroxides as emulsifying agents," *Clay minerals*, vol. 36, pp. 557-570, 2001.
- [185] R. Pichot, F. Spyropoulos, and I. T. Norton, "Competitive adsorption of surfactants and hydrophilic silica particles at the oil–water interface: Interfacial tension and contact angle studies," *Journal of Colloid and Interface Science*, vol. 377, pp. 396-405, 7/1/ 2012.
- [186] S. S. Adkins, D. Gohil, J. L. Dickson, S. E. Webber, and K. P. Johnston, "Water-in-carbon dioxide emulsions stabilized with hydrophobic silica particles," *Physical Chemistry Chemical Physics*, vol. 9, pp. 6333-6343, 2007.
- [187] J. W. Salari, G. Mutsaers, J. Meuldijk, and B. Klumperman, "Deformation of the water/oil interface during the adsorption of sterically stabilized particles," *Langmuir*, vol. 30, pp. 7327-7333, 2014.
- [188] A. San-Miguel and S. H. Behrens, "Influence of nanoscale particle roughness on the stability of Pickering emulsions," *Langmuir*, vol. 28, pp. 12038-12043, 2012.
- [189] L. Ridel, M.-A. Bolzinger, N. Gilon-Delepine, P.-Y. Dugas, and Y. Chevalier, "Pickering emulsions stabilized by charged nanoparticles," *Soft Matter*, vol. 12, pp. 7564-7576, 2016.
- [190] M. Kargar, K. Fayazmanesh, M. Alavi, F. Spyropoulos, and I. T. Norton, "Investigation into the potential ability of Pickering emulsions (food-grade particles) to enhance the oxidative stability of oil-in-water emulsions," *Journal of colloid and interface science*, vol. 366, pp. 209-215, 2012.
- [191] J. Frelichowska, M.-A. Bolzinger, and Y. Chevalier, "Effects of solid particle content on properties of o/w Pickering emulsions," *Journal of colloid and interface science*, vol. 351, pp. 348-356, 2010.
- [192] S. Arditty, C. Whitby, B. Binks, V. Schmitt, and F. Leal-Calderon, "Some general features of limited coalescence in solid-stabilized emulsions," *The European Physical Journal E: Soft Matter and Biological Physics*, vol. 11, pp. 273-281, 2003.
- [193] J. Gould, J. Vieira, and B. Wolf, "Cocoa particles for food emulsion stabilisation," *Food & function*, vol. 4, pp. 1369-1375, 2013.
- [194] K. Wang, L. Zhang, W. Zhang, and G. Luo, "Mass-transfer-controlled dynamic interfacial tension in microfluidic emulsification processes," *Langmuir*, vol. 32, pp. 3174-3185, 2016.
- [195] D. J. McClements, *Food emulsions: principles, practices, and techniques*: CRC press, 2004.
- [196] H. Schubert and H. Karbstein, "Mechanical emulsification," in *Developments in Food Engineering*, ed: Springer, 1994, pp. 9-14.
- [197] T. Nakashima, "Membrane emulsification by microporous glass," *Key Eng. Mater.*, vol. 61, pp. 513-516, 1991.
- [198] E. Piacentini, E. Drioli, and L. Giorno, "Membrane emulsification technology: Twenty-five years of inventions and research through patent survey," *Journal of Membrane Science*, vol. 468, pp. 410-422, 2014.
- [199] F. Spyropoulos, D. M. Lloyd, R. D. Hancocks, and A. K. Pawlik, "Advances in membrane emulsification. Part A: recent developments in processing aspects and microstructural design approaches," *Journal of the science of food and agriculture*, vol. 94, pp. 613-627, 2014.
- [200] I. Zafeiri, J. E. Norton, P. Smith, I. T. Norton, and F. Spyropoulos, "The role of surface active species in the fabrication and functionality of edible solid lipid particles," *Journal of colloid and interface science*, vol. 500, pp. 228-240, 2017.

- [201] M. Rayner, M. Sjöö, A. Timgren, and P. Dejmek, "Quinoa starch granules as stabilizing particles for production of Pickering emulsions," *Faraday discussions*, vol. 158, pp. 139-155, 2012.
- [202] S. Zou, Y. Yang, H. Liu, and C. Wang, "Synergistic stabilization and tunable structures of Pickering high internal phase emulsions by nanoparticles and surfactants," *Colloids and Surfaces A: Physicochemical and Engineering Aspects*, vol. 436, pp. 1-9, 2013.
- [203] E. Santini, E. Guzmán, M. Ferrari, and L. Liggieri, "Emulsions stabilized by the interaction of silica nanoparticles and palmitic acid at the water-hexane interface," *Colloids and Surfaces A: Physicochemical and Engineering Aspects*, vol. 460, pp. 333-341, 2014.
- [204] K. P. Sharma, V. K. Aswal, and G. Kumaraswamy, "Adsorption of nonionic surfactant on silica nanoparticles: structure and resultant interparticle interactions," *The Journal of Physical Chemistry B*, vol. 114, pp. 10986-10994, 2010.
- [205] J. Penfold, I. Tucker, J. Petkov, and R. Thomas, "Surfactant adsorption onto cellulose surfaces," *Langmuir*, vol. 23, pp. 8357-8364, 2007.
- [206] A. Avranas and V. Tasopoulos, "Aqueous solutions of sodium deoxycholate and hydroxypropylmethylcellulose: dynamic surface tension measurements," *Journal of colloid and interface science*, vol. 221, pp. 223-229, 2000.
- [207] M. Manousakis and A. Avranas, "Dynamic surface tension studies of mixtures of hydroxypropylmethylcellulose with the double chain cationic surfactants didodecyldimethylammonium bromide and ditetradecyldimethylammonium bromide," *Journal of colloid and interface science*, vol. 402, pp. 237-245, 2013.
- [208] S. K. Singh and S. M. Notley, "Adsorption of Nonionic Surfactants (C_nE_m) at the Silica-Water and Cellulose-Water Interface," *The Journal of Physical Chemistry B*, vol. 114, pp. 14977-14982, 2010.
- [209] A. Kilara and M. Vaghela, "Whey proteins," in *Proteins in food processing*, ed: Woodhead Publishing, Cambridge, England, 2004, pp. 72-99.
- [210] J. Meissner, A. Prause, B. Bharti, and G. H. Findenegg, "Characterization of protein adsorption onto silica nanoparticles: influence of pH and ionic strength," *Colloid and polymer science*, vol. 293, pp. 3381-3391, 2015.
- [211] F. J. Monahan, J. B. German, and J. E. Kinsella, "Effect of pH and temperature on protein unfolding and thiol/disulfide interchange reactions during heat-induced gelation of whey proteins," *Journal of Agricultural and Food Chemistry*, vol. 43, pp. 46-52, 1995.
- [212] X. Wu and G. Narsimhan, "Characterization of secondary and tertiary conformational changes of β -lactoglobulin adsorbed on silica nanoparticle surfaces," *Langmuir*, vol. 24, pp. 4989-4998, 2008.
- [213] A. Benichou, A. Aserin, R. Lutz, and N. Garti, "Formation and characterization of amphiphilic conjugates of whey protein isolate (WPI)/xanthan to improve surface activity," *Food Hydrocolloids*, vol. 21, pp. 379-391, 2007.
- [214] T. Ngai and S. A. Bon, *Particle-stabilized emulsions and colloids: formation and applications*: Royal Society of Chemistry, 2014.
- [215] J. R. Jones, D. Prime, M. C. Leaper, D. J. Richardson, C. D. Rielly, and A. G. Stapley, "Effect of processing variables and bulk composition on the surface composition of spray dried powders of a model food system," *Journal of Food Engineering*, vol. 118, pp. 19-30, 2013.

- [216] R. Aveyard, J. H. Clint, D. Nees, and N. Quirke, "Structure and collapse of particle monolayers under lateral pressure at the octane/aqueous surfactant solution interface," *Langmuir*, vol. 16, pp. 8820-8828, 2000.
- [217] Z. Hu, S. Ballinger, R. Pelton, and E. D. Cranston, "Surfactant-enhanced cellulose nanocrystal Pickering emulsions," *Journal of colloid and interface science*, vol. 439, pp. 139-148, 2015.
- [218] T. R. BATES, C. H. NIGHTINGALE, and E. DIXON, "Kinetics of hydrolysis of polyoxyethylene (20) sorbitan fatty acid ester surfactants," *Journal of Pharmacy and Pharmacology*, vol. 25, pp. 470-477, 1973.
- [219] J. Bloor, J. Morrison, and C. Rhodes, "Effect of pH on the micellar properties of a nonionic surfactant," *Journal of pharmaceutical sciences*, vol. 59, pp. 387-391, 1970.
- [220] S. A. Kedzior, H. S. Marway, and E. D. Cranston, "Tailoring cellulose nanocrystal and surfactant behavior in miniemulsion polymerization," *Macromolecules*, vol. 50, pp. 2645-2655, 2017.
- [221] T. Kostakis, R. Ettelaie, and B. S. Murray, "Enhancement of stability of bubbles to disproportionation using hydrophilic silica particles mixed with surfactants or proteins," *Food colloids: Self-assembly and material science*, p. 357e368, 2007.
- [222] G. N. Sethumadhavan, A. Nikolov, and D. Wasan, "Film stratification in the presence of colloidal particles," *Langmuir*, vol. 17, pp. 2059-2062, 2001.
- [223] B. P. Binks, A. Desforges, and D. G. Duff, "Synergistic stabilization of emulsions by a mixture of surface-active nanoparticles and surfactant," *Langmuir*, vol. 23, pp. 1098-1106, 2007.
- [224] H. Schubert, R. Engel, and L. Kempa, "CHAPTER 1 - Principles of Structured Food Emulsions: Novel Formulations and Trends," in *Global Issues in Food Science and Technology*, G. Barbosa-Cánovas, A. Mortimer, D. Lineback, W. Spiess, K. Buckle, and P. Colonna, Eds., ed San Diego: Academic Press, 2009, pp. 3-19.
- [225] C. Liu, H. Tanaka, L. Zhang, J. Zhang, X. Huang, J. Ma, *et al.*, "Fouling and structural changes of Shirasu porous glass (SPG) membrane used in aerobic wastewater treatment process for microbubble aeration," *Journal of membrane science*, vol. 421, pp. 225-231, 2012.
- [226] A. Trentin, M. Ferrando, F. López, and C. Güell, "Premix membrane O/W emulsification: Effect of fouling when using BSA as emulsifier," *Desalination*, vol. 245, pp. 388-395, 2009.
- [227] M. Đ. Carić, S. D. Milanović, D. M. Krstić, and M. N. Tekić, "Fouling of inorganic membranes by adsorption of whey proteins," *Journal of membrane science*, vol. 165, pp. 83-88, 2000.
- [228] R. Takagi and M. Nakagaki, "Membrane charge of microporous glass membrane determined by the membrane potential method and its pore size dependency," *Journal of membrane science*, vol. 111, pp. 19-26, 1996.
- [229] K. Nakamura and K. Matsumoto, "Protein adsorption properties on a microfiltration membrane: a comparison between static and dynamic adsorption methods," *Journal of membrane science*, vol. 285, pp. 126-136, 2006.
- [230] K. Nakamura and K. Matsumoto, "Adsorption behavior of BSA in microfiltration with porous glass membrane," *Journal of membrane science*, vol. 145, pp. 119-128, 1998.
- [231] K. Boussu, A. Belpaire, A. Volodin, C. Van Haesendonck, P. Van der Meer, C. Vandecasteele, *et al.*, "Influence of membrane and colloid characteristics on fouling of nanofiltration membranes," *Journal of Membrane Science*, vol. 289, pp. 220-230, 2/15/ 2007.

- [232] K. Kandori, "Applications of microporous glass membranes: membrane emulsification," *Food Processing: Recent Developments*, pp. 113-142, 1995.
- [233] P. Guo, J. Huang, Y. Zhao, C. R. Martin, R. N. Zare, and M. A. Moses, "Nanomaterial Preparation by Extrusion through Nanoporous Membranes," *Small*, vol. 14, p. 1703493, 2018.
- [234] F. Leal-Calderon, V. Schmitt, and J. Bibette, *Emulsion science: basic principles*: Springer Science & Business Media, 2007.
- [235] G. T. Vladislavljevic and H. Schubert, "Preparation and analysis of oil-in-water emulsions with a narrow droplet size distribution using Shirasu-porous-glass (SPG) membranes," *Desalination*, vol. 144, pp. 167-172, 2002.
- [236] G. T. Vladislavljević, U. Lambrich, M. Nakajima, and H. Schubert, "Production of O/W emulsions using SPG membranes, ceramic α -aluminium oxide membranes, microfluidizer and a silicon microchannel plate—a comparative study," *Colloids and Surfaces A: Physicochemical and Engineering Aspects*, vol. 232, pp. 199-207, 2004.
- [237] M. S. Manga and D. W. York, "Production of Concentrated Pickering Emulsions with Narrow Size Distributions Using Stirred Cell Membrane Emulsification," *Langmuir*, vol. 33, pp. 9050-9056, 2017.
- [238] D.-X. Hao, F.-L. Gong, G.-H. Hu, Y.-J. Zhao, G.-P. Lian, G.-H. Ma, *et al.*, "Controlling factors on droplets uniformity in membrane emulsification: experiment and modeling analysis," *Industrial & Engineering Chemistry Research*, vol. 47, pp. 6418-6425, 2008.
- [239] I. Kobayashi, T. Takano, R. Maeda, Y. Wada, K. Uemura, and M. Nakajima, "Straight-through microchannel devices for generating monodisperse emulsion droplets several microns in size," *Microfluidics and nanofluidics*, vol. 4, pp. 167-177, 2008.
- [240] T. Nisisako and T. Torii, "Microfluidic large-scale integration on a chip for mass production of monodisperse droplets and particles," *Lab on a Chip*, vol. 8, pp. 287-293, 2008.
- [241] W. Sutherland, "LXXV. A dynamical theory of diffusion for non-electrolytes and the molecular mass of albumin," *The London, Edinburgh, and Dublin Philosophical Magazine and Journal of Science*, vol. 9, pp. 781-785, 1905.
- [242] C. Charcosset, "Preparation of emulsions and particles by membrane emulsification for the food processing industry," *Journal of food engineering*, vol. 92, pp. 241-249, 2009.
- [243] M. Rayner, "Scales and Forces in Emulsification," *Engineering Aspects of Food Emulsification and Homogenisation*, pp. 3-32, 2015.
- [244] N. Thapar, "Liquid-liquid dispersions from in-line rotor-stator mixers," 2004.
- [245] J. Shi, S. Xu, H. Qin, Y. Liu, W. Li, and J. Zhang, "Single-pass emulsification processes in two different inline high shear mixers," *Industrial & Engineering Chemistry Research*, vol. 52, pp. 14463-14471, 2013.
- [246] T. S. Horozov and B. P. Binks, "Particle-Stabilized Emulsions: A Bilayer or a Bridging Monolayer?," *Angewandte Chemie*, vol. 118, pp. 787-790, 2006.
- [247] B. Binks and S. Lumsdon, "Stability of oil-in-water emulsions stabilised by silica particles," *Physical Chemistry Chemical Physics*, vol. 1, pp. 3007-3016, 1999.
- [248] R. Pichot, "Stability and Characterisation of Emulsions in the presence of Colloidal Particles and Surfactants," The University of Birmingham, 2010.

- [249] S. van der Graaf, C. Schroën, and R. Boom, "Preparation of double emulsions by membrane emulsification—a review," *Journal of Membrane Science*, vol. 251, pp. 7-15, 2005.
- [250] E. Dickinson, "Emulsion gels: The structuring of soft solids with protein-stabilized oil droplets," *Food hydrocolloids*, vol. 28, pp. 224-241, 2012.